964

PRESSURE DISTRIBUTION IN EXTRUSION CONTAINERS

By

DİNÇER MUTLU

APRIL 1980

A Thesis submitted for the degree of Doctor of Philosophy of the University of London and for the Diploma of the Imperial College

Mechanical Engineering Dept.,
Imperial College,
London SW7 2BX

SYNOPSIS

In recent years a great deal of effort has been made to develop design criteria for high pressure vessels subjected to cyclic stresses. By far the largest group of pressure vessels under very high cyclic loading in practical use are conventional extrusion containers. The difficulties of design are that stress distribution in the wall of a conventional extrusion container change in a complex pattern; it is a function of container geometry, the position of the extrusion plunger and the pressure on the inside wall of the container. The latter itself depends on the properties of the deforming material, on extrusion ratio, on lubrication conditions, on the geometry of the die etc.

In this thesis alternative methods are presented to evaluate pressure distribution in extrusion containers, which provide new information for container design by taking into account actual, practical conditions.

Strain distributions on the outside diameter of the containers are measured by strain gauge methods under a number of conditions, both in direct and indirect extrusions, which are then compared with theoretical predictions.

In one alternative, a kinematically admissible velocity field is proposed, in another a semi-empirical approach is used together with the method of weighted residuals, to compute the predicted velocity, strain, strain rate and stress fields in the deformation zone. The stress distribution inside the container wall is then used, together with an elastic finite element computer programme, to calculate strains on the outside diameter of the extrusion container, which are then compared with the experimentally obtained values.

The results indicate good agreement between predictions and experiments, which proves that either of the two theoretical methods are useful to provide pressure distribution on the container wall in practical cases, as a basic information for container design.

ACKNOWLEDGEMENTS

My sincere thanks go to Dr. B. LENGYEL for suggesting this project and for his advice and encouragement while supervising this work.

I gratefully acknowledge Professor J.M. ALEXANDER'S for his kind permission to use the facilities of the Metalworking Laboratory.

The assistance given by all the members of the staff of the Metalworking Laboratory is also gratefully acknowledged. In particular, I wish to thank Mr. J. PLUMB and Mr. R. BAXTER for their help in assembling the apparatus and the late Mr. S.C. PRIDHAM for the preparation of the split billets and other technical assistance.

Finally, my thanks are due to Miss R. CARPENTER for typing this manuscript.

D. MUTLU

April, 1980

CONTENTS

		Page
Synopsis		2
Acknowledgements		4
List of Illustrations		10
Notations		16
Chapter 1	INTRODUCTION	21
1.1	Preface	21
1.2	A Review of the Literature on Evaluating the Normal Pressure and the Coefficient of Friction.	23
1.2.1	Theoretical Studies.	24
1.2.2	Experimental Studies.	29
1.3	Scope of the Present Work.	38
Chapter 2	BASIC CONCEPTS OF CONTINUUM MECHANICS.	41
2.1	Introduction.	41
2.2	The Concept of Stress.	42
2.2.1	Stress Components at a Point.	45
2.2.2	Stress Functions.	47
2.3	Strains and Strain Rates.	48
2.3.1	Stream Function.	51
2.4	A Basic Assumption of the Mathematical Theory of Plasticity.	53
2.4.1	Yield Criteria.	53
2.5	Stress Strain Relationships.	55
2.6	Haar - Von Kármán Hypothesis.	58
2.7	The Effect of Strain Hardening.	59
2.8	Power of Plastic Deformation.	59

		Page
Chapter 3	NUMERICAL METHODS	62
3.1	A Relatively Simple Treatment of Classical Problems.	62
3.2	The Method of Weighted Residuals.	62
3.3	Different Forms of the MWR.	65
3.3.1	Collocation.	65
3.3.2	Subdomain Method.	66
3.3.3	Galerkins's Method.	66
3.3.4	Least Squares Method.	67
3.4	Selection of Trail Functions.	67
3.5	Approximation within the Family of Trail Solutions.	69
3.5.1	Collocation.	72
3.5.2	Subdomain Method.	72
3.5.3	Galerkin's Method.	73
3.5.4	Method of Least Squares.	73
Chapter 4	EXPERIMENTAL WORK.	77
4.1	Introduction.	77
4.2	The Apparatus.	77
4.2.1	The Extrusion Assemblies.	78
4.2.2	The Calibration Assembly.	87
4.2.3	Instrumentation.	94
4.3	Calibration of the Apparatus.	100
4.4	Calibration Results.	104
4.5	The Experiments.	132

		Page
Chapter 5	THEORETICAL CONSIDERATIONS.	136
5.1	Semi-empirical Method.	136
5.1.1	Introduction.	136
5.1.2	Billet Design.	137
5.1.3	Grid Preparation and Measurement.	138
5.1.4	Derivation of the Solution.	141
5.1.5	The Flow Function.	143
5.1.6	Mesh for Computer Calculations.	143
5.1.7	Subroutine DATARD.	145
5.1.8	Subroutine MESH.	145
5.1.9	Subroutine FLOW.	149
5.1.10	Smoothing Procedure.	150
5.1.11	Subroutine SMOOTH.	150
5.1.12	Subroutine SMOTHZ.	151
5.1.13	Subroutine SMOTHR.	152
5.1.14	Subroutine STRATE.	153
5.1.15	Subroutines DIFFZ and DIFFR.	154
5.1.16	Effective Strain Rate and Effective Strain.	154
5.1.17	Stresses.	155
5.1.18	The Error Functions.	156
5.1.19	Normal and Shear Stresses on Boundary.	161
5.2	A Solution by Weighted Residuals.	162
5.3	A Study on Upper-bound Solution of Axi-Symmetric Extrusion Through a Conical Die.	168
5.3.1	Introduction.	168

		Page
5.3.2	Kinematically Admissible Velocity Field.	173
5.3.3	Upper Bound Solution.	179
5.3.4	Strain Distribution in the Product.	180
5.3.5	Power Involved in the Deformation of the Billet.	183
5.4	A Method to Determine Stress Field.	193
5.4.1	Derivation of the Solution.	193
5.4.2	Description of the Computer Program.	195
5.4.3	Main Program.	195
5.4.4	Subroutine MESH.	196
5.4.5	Subroutine STRESS.	197
5.4.6	Stress Field in the Solid Billet.	197
5.5	Elastic Stresses in Open-ended Cylinders under Internal Pressure.	205
5.5.1	Introduction.	205
5.5.2	Finite-element Analysis of Containers.	208
Chapter 6	RESULTS AND DISCUSSION.	212
6.1	Results for Forward Extrusion.	212
6.1.1	Velocity, Strain Rate, Strain and Stress Fields Computed from Semi-empirical Method.	212
6.1.2	Velocity, Strain Rate, Strain and Stress Fields Computed from the Assumed Velocity Field.	221
6.1.3	Pressure Distributions in the Forward Extrusion Container.	236
6.1.4	Further Experimental Results of Forward Extrusion.	252
6.2	Experimental Results of Backward Extrusion.	273

		Page
Chapter 7	CONCLUSIONS	290
7.1	Forward Extrusion.	290
7.2	Backward Extrusion.	295
REFERENCES		298
APPENDIX A		309
A1.	Symbols used in the computer programs. (Semi-empirical method and assumed velocity field).	309
A2.	Symbols used in the finite element program.	311
APPENDIX B		317
B1.	Listing of the computer program for the semi-empirical method.	317
B2.	Listing of the computer program for the assumed velocity field.	340
B3.	Listing of the finite element program.	347
APPENDIX C	Pressure distribution and friction in extrusion containers. Proceedings of the 19th (1978) MTDR Conference, UMIST.	357

LIST OF ILLUSTRATIONS

2.1	Stress components referred to cylindrical coordinates.
2.2	Stress at a generical point.
2.3	Empirical relation to stress-strain curve of commerically pure aluminium (Published in Johnson and Mellor {63}).
3.1	Voigt model.
3.2	Comparison of errors in approximate solutions.
4.1a	The forward extrusion assembly.
4.1b	The backward extrusion assembly.
4.1c	General view of the forward extrusion rig.
4.1d	General view of the backward extrusion rig.
4.2	The extrusion containers.
4.3	The extrusion dies and punch inserts.
4.3b	General view of the extrusion dies and punch inserts.
4.4	The extrusion punches.
4.5a	Calibration assembly.
4.5b	General view of the calibration assembly.
4.6	The extension blocks.
4.7	The calibration components.
4.8	The extrusion components.
4.9	Circuit connections.
4.10	Bridge circuit connections for container strain gauges.
4.11	Extrusion products.
4.4.1	Calibration of the displacement transducer.
4.4.2	Calibration of the die load cell.
4.4.3	Calibration of the load cell.
4.4.4	Calibration of the pad load cell.

4.4.5	Calibration of the load cell.
4.4.6	Calibration of the strain gauge No. 6.
4.4.7	Calibration of the strain gauge No. 7.
4.4.8	Calibration of the strain gauge No. 8.
4.4.9	Calibration of the strain gauge No. 9.
4.4.10	Calibration of the strain gauge No. 10.
4.4.11	Calibration of the strain gauge No. 11.
4.4.12	Calibration of the strain gauge No. 12.
4.4.13	Calibration of the strain gauge No. 13.
4.4.14	Calibration of the strain gauge No. 6L.
4.4.15	Calibration of the strain gauge No. 7L.
4.4.16	Calibration of the strain gauge No. 8L.
4.4.17	Calibration of the strain gauge No. 9L.
4.4.18	Calibration of the strain gauge No. 10L.
4.4.19	Calibration of the strain gauge No. 11L.
4.4.20	Calibration of the strain gauge No. 12L.
4.4.21	Calibration of the strain gauge No. 13L.
4.4.22	Calibration of the strain gauges.
4.4.23	Calibration of the strain gauges.
4.4.24	Calibration of the strain gauge No. 5.
4.4.25	Calibration of the strain gauges.
4.4.26	Calibration of the strain gauges.
5.1.1	Aluminium billet under direct lighting.
5.1.2	Mesh for computations.
5.1.3	Input data.
5.1.4	Smoothing by method of means.
5.2.1	Mesh and boundary surfaces.

5.2.2 Iterative procedure {76}.

5.3.1 Kinematically admissible velocity field and its associated hodograph.

5.3.2 Assumed mode of strain deformation on the velocity discontinuity curve.

5.3.3 Admissible velocity field.

5.4.1 Mesh for computation.

5.4.2 Flow chart, the whole sequence of operations.

5.5.1 Finite element meshes for containers.

6.1.1 Absolute velocity distribution in the deformation zone, aluminium, R = 2, die semi-angle of 25°, constant-friction factor Q = 0.12.

6.1.2 Effective strain rate distribution in the deformation zone, aluminium, R = 2, die semi-angle of 25°, constant-friction factor Q = 0.12.

6.1.3 Effective strain distribution in the deformation zone, aluminium, R = 2, die semi-angle of 25°, constant-friction factor Q = 0.12.

6.1.4 Effective stress distribution in the deformation zone, aluminium, R = 2, die semi-angle of 25°, constant-friction factor Q = 0.12.

6.1.5 Absolute velocity distribution in the deformation zone, aluminium, R = 2, die semi-angle of 25°, constant-friction factor Q = 0.12.

6.1.6 Effective strain rate distribution in the deformation zone, aluminium, R = 2, die semi-angle of 25°, constant-friction factor Q = 0.12.

6.1.7 Effective strain distribution in the deformation zone, aluminium, R = 2, die semi-angle of 25°, constant-friction factor Q = 0.12.

6.1.8 Effective stress distribution in the deformation zone, aluminium, R = 2, die semi-angle of 25°, constant-friction factor Q = 0.12.

6.1.9 Absolute velocity distribution in the deformation zone, lead, R = 3, die semi-angle of 30°, constant-friction factor Q = 0.75.

6.1.10 Effective strain rate distribution in the deformation zone, lead R = 3, die semi-angle of 30^{o}, constant-friction factor Q = 0.75 .

6.1.11 Effective strain distribution in the deformation zone, lead,R = 3, die semi-angle of 30^{o}, constant-friction factor Q = 0.75 .

6.1.12 Effective stress distribution in the deformation zone, lead, R = 3, die semi-angle of 30^{o}, constant-friction factor Q = 0.75 .

6.1.13 Absolute velocoty distribution in the deformation zone, lead, R = 4, die semi-angle of 35^{o}, constant-friction factor Q = 0.75 .

6.1.14 Effective strain rate distribution in the deformation zone, lead, R = 4, die semi-angle of 35^{o}, constant-friction factor Q = 0.75 .

6.1.15 Effective strain distribution in the deformation zone, lead, R = 4, die semi-angle of 35^{o}, constant-friction factor Q = 0.75 .

6.1.16 Effective stress distribution in the deformation zone, lead, R = 4, die semi-angle of 35^{o}, constant-friction factor Q = 0.75 .

6.1.17 Normal (σ) and frictional shear (τ) stresses in the bore of the forward extrusion container.

6.1.18 Hoop strains and pressure distributions on the container wall in the forward extrusion of lead (After 20 mm punch travel).

6.1.19 Hoop strains and pressure distributions on the container wall in the forward extrusion of lead (After 20 mm punch travel).

6.1.20 Hoop strains and pressure distributions on the container wall in the forward extrusion of lead (After 20 mm punch travel).

6.1.21 Hoop strains and pressure distributions on the container wall in the forward extrusion of aluminium (After 20 mm punch travel).

6.1.22 Axial strain distributions on the container wall in the forward extrusion of lead.

6.1.23 Axial strain distributions on the container wall in the forward extrusion of lead.

6.1.24 Axial strain distributions on the container wall in the forward extrusion of lead.

6.1.25 Axial strain distributions on the container wall in the forward extrusion of lead.

6.1.25/A Axial strain distributions on the container wall in the forward extrusion of aluminium.

6.1.26 Load on the pressure pad in the forward extrusion of lead.

6.1.27 Load on the die in the forward extrusion of lead.

6.1.28 Load on the pressure pad and die in the forward extrusion of lead.

6.1.29 Load on the pressure pad and die in the forward extrusion of aluminium.

6.1.30 Hoop and axial strain distributions.

6.1.31 Hoop and axial strain distributions.

6.1.32 Hoop and axial strain distributions.

6.1.33 Hoop and axial strain distributions.

6.1.34 Hoop and axial strain distributions.

6.1.35 Hoop and axial strain distributions.

6.1.36 Hoop and axial strain distributions.

6.1.37 Hoop and axial strain distributions.

6.1.38 Hoop and axial strain distributions.

6.1.39 Hoop and axial strain distributions.

6.1.40 Hoop and axial strain distributions.

6.1.41 Hoop strains on the container wall in the forward extrusion (After 10 mm punch travel).

6.2.1 Load on the pressure pad and punch in the backward extrusion of lead.

6.2.2 Load on the pressure pad and punch in the backward extrusion of aluminium.

6.2.3 Load on the pressure pad and punch in the backward extrusion of aluminium.

6.2.4 Hoop strain distributions.

6.2.5 Hoop and axial strain distributions.

6.2.6 Hoop and axial strain distributions.

6.2.7 Hoop and axial strain distributions.

6.2.8 Hoop and axial strain distributions.

6.2.9 Hoop and axial strain distributions.

6.2.10 Hoop and axial strain distributions.

6.2.11 Hoop and axial strain distributions.

6.2.12 Hoop and axial strain distributions.

6.2.13 Hoop and axial strain distributions.

6.2.14 Hoop strains on the container wall in the backward extrusion (After 10 mm punch travel).

NOTATIONS

a	Initial radius of the billet.
A	Apparent area.
A_i, $A_{i\dot{J}}$	Parameters of trial function.
A_o	Initial section of the billet.
A_r	The real area of contact.
b	Final radius of the product.
B_{mn}	Parameters of trial function.
c	Constant for the stress-strain curve.
C_{pq}	Parameters of trial function.
d_1, d_2	Parameters for the geometry of the flow lines.
$\dot{E}_{12}$, $\dot{E}_{23}$, $\dot{E}_{14}$	Energy-dissipation rates along the boundaries
$\dot{E}_{1234}$	Energy-dssipation rate in the deformation zone.
f	Yield function.
f	Flow function.
F	Total extrusion load.
F_c	Axial force acting along the cylinder wall.
F_d	Axial force acting along the die surface.
g_1, g_2, g_3, g_4	Weighting factors.
$G_{\dot{J}}$ G_m	Weighting factors.
i	Index.
I_1, I_2, I_3	Invariants of the strain rate tensor.
j	Index.
J_1, J_2, J_3	Invariants of the stress tensor.
J_1', J_2', J_3'	Invariants of the deviatoric stress tensor.
k	Shear yield stress of the material.

L	The length of the container
m	Index.
n	Index.
n	Parameter for the admissible velocity field.
p	Index.
p	Parameter for the admissible velocity field.
P	Total extrusion pressure.
P_1, P_2, P_3, P_4	Pressure components.
P_e	True extrusion pressure.
P_W	Wall pressure.
q	Index.
q	Parameter for the admissible velocity field.
Q	Constant friction factor.
r	Coordinate in the r-direction.
r_k	Parameter for the stream function.
R_j^*	Error functions.
R_k	Parameter for the stream function.
$R_{1n}, R_{2n}, R_{3n}, R_{4n}$	Error functions in the deformation zone and the die/billet boundary.
R_T	Total residual.
s	Parameter for the admissible velocity field.
t	Parameter for the admissible velocity field.
t	Time.
T_j^*	Generical stress.
T'	Deviatoric stress tensor.
u_i	Displacement vector.
v_{abs}	Absolute velocity.
v_F	Final velocity of the product.
v_I	Initial velocity of the billet.

v_{mag}	Magnitude of velocity.
v_s	Velocity field.
v_r	Radial velocity.
v_z	Axial velocity.
v_θ	Circumferential velocity.
W	Plastic work.
$W_{\dot{J}}$	Weighting function.
$\dot{W}$	Power dissipated in the deformation zone.
$\dot{W}_a$	Actual external work.
x	Parameter for the velocity field.
$X_{i\dot{J}}$	Coefficients of free parameters in the trail function.
Y	Tensile yield stress.
y	Parameter for the velocity field.
z	Coordinate in the z-direction.
z_{23}, z_{14}	Curves for the exit and entry boundaries.
α	Die semi-angle.
β	Semi-angle of the exit boundary.
γ	Semi-angle of the entry boundary.
r_1, r_2, r_3	Boundary surfaces of the deformation zone.
δ	Angle of inclination of a stream line.
δ_{iJ}	Kronecker delta.
$\bar{\varepsilon}$	Equivalent strain.
ε_d	Strain in the deformation zone.
$\varepsilon_{i\dot{J}}$	Strain tensor component.
ε_θ	Hoop strain.
ε_r	Radial strain.

ε_z	Axial strain.
ε_{rz}	Shear strain.
ε_{s_1}, ε_{s_2}	Strains along the entry and exit boundaries.
ε^P_{ij}	Plastic strain.
$\dot{\varepsilon}^P_{ij}$	Plastic strain rate.
$\dot{\varepsilon}_{RR}$, $\dot{\varepsilon}_{\psi\psi}$, $\dot{\varepsilon}_{\theta\theta}$, $\dot{\varepsilon}_{R\theta}$, $\dot{\varepsilon}_{\theta\psi}$, $\dot{\varepsilon}_{R\psi}$	Strain rate components in spherical coordinate system.
$\dot{\varepsilon}_r$, $\dot{\varepsilon}_\theta$, $\dot{\varepsilon}_z$, $\dot{\varepsilon}_{rz}$	Strain rate components in cylindrical coordinate system.
$\dot{\bar{\varepsilon}}$	Equivalent strain rate.
$\dot{\varepsilon}_m$	Hydrostatic strain rate component.
$\dot{\varepsilon}_{ij}$	Strain rate tensor component.
$\dot{\varepsilon}'_{ij}$	Deviatoric strain rate component.
η	Form of a stream line.
λ	Work-hardening exponent.
$\dot{\lambda}$	Constant in Levy-Mises flow rule.
μ	Coefficient of friction.
ν	Volume or domain.
ρ	Density of the material.
τ	Shear stress.
τ_r	Rapture shear stress.
τ_{rz}	Shear stress.
τ^*	Frictional stress at the die/billet interface.
$\bar{\sigma}$	Equivalent stress.
$\bar{\sigma}$	Uniaxial yield strength.
σ_{ij}	Stress tensor component.

σ_m	Hydrostatic stress component.
σ_n	Normal stress on the boundary.
σ_θ	Hoop stress.
σ_r	Radial stress.
σ_z	Axial stress.
σ_s	Shear stress on the boundary.
σ'_{ij}	Deviatoric stress tensor component.
σ'_θ	Deviatoric hoop stress.
σ'_r	Deviatoric radial stress.
σ'_z	Deviatoric axial stress.
ϕ_1, ϕ_2	Stress functions.
ψ	Stream or flow function.

1. INTRODUCTION

1.1 PREFACE

A great deal of attention has been focused in recent years on developing design criteria for high pressure vessels subjected to cyclic stresses. By far the largest group of pressure vessels under very high cyclic loading in practical use are conventional extrusion containers.

It has been realised that experiments using cyclic bore pressures and static or cylic supporting pressures on monobloc open-ended cylinders offer a convenient way of investigating the effect of the various stress components in container fatigue, and that such experiments might yield results on which the design of compound vessels for cyclic pressures could be based {1}. Investigations have therefore been commenced both to establish fatigue design criteria for pre-stressed compound vessels and to prove the usefulness of the fluid support principle in vessels for high cyclic pressures.

In earlier experiments monobloc cylinders with closed ends have been subjected to cyclic bore pressures and the results analysed with reference to the Lamé stresses in the bore {2}, {3}. It was found that the bore shear-stress range primarily determined the fatigue life {4}, {5}, {6} . Other work {7} established that while the axial tensile

stress remained the intermediate principal stress, it had no effect on the life of thick-walled cylinders subjected to repeated internal pressure. It is thus clear that the stresses in the cylinder wall must be known before containers could be designed against fatigue failure.

With a conventional extrusion container, the difficulty is that stresses in its wall change in a complex pattern; the stress distribution is a function of the pressure on the inside wall of the container, the position of the extrusion punch and the container geometry. The extrusion pressure depends on extrusion ratio, on the geometry of the die, on the properties of the deforming material, to mention only a few. While it is now possible to employ numerical methods to assess the effect of pressure and geometrical discontinuities on container stresses {8}, {9}, little is known about pressure distribution in the bore of extrusion containers and, apart from crude approximations, no method exists on which the calculation of bore pressure could be based in the design stage.

Furthermore, in addition to the pressure distribution, the determination of container/billet friction is becoming essential in the design of clamps for semi-continuous hydrostatic extrusion {10} and, more recently, for the various alternatives of continuous extrusion. A common feature of all these processes is that the billet is restrained

or moved towards the die by frictional forces between the clamp or container and the plastically deforming billet. Clearly, it is essential to predict these frictional forces before production equipment could be designed with any confidence, which was the aim of the work of Alexander and Said {11} relating to semi-continuous hydrostatic extrusion. A brief outline of the various friction assisted extrusion processes and a reference list were given by Lengyel and Kamyab {12}.

The present work is directed towards estimating the distribution of pressure and friction at the container/billet interface with a view to providing data for the design of extrusion containers.

1.2 A Review of the Literature on Evaluating the Normal Pressure and the Coefficient of Friction

Previous work by investigators was mainly concerned with the study of the behaviour of the billet material at the deformation zone. Several approaches using different techniques were developed, from which it was possible to evaluate the extrusion pressure, the interfacial pressure distribution and the average coefficient of friction at the metal/tool interface. These could be divided into basic categories, namely the theoretical and the experimental.

1.2.1 Theoretical Studies

The theoretical study of pressure distribution and frictional conditions at the metal/tool interface has attracted many investigators. These are two interconnected parameters and although their combined effects on the tool stresses, tool wear, the flow pattern, forming forces, surface finish and dimensional accuracy of the product are well recognised, they are not easily separable. This is mainly due to the fact that the mechanism of friction is still not completely understood.

In this approach usually one of the theories for the particular process together with the experimental value of the deforming force (e.g. roll force, extrusion or drawing force) and the true stress-strain curve for the deforming material is used. This method has obvious drawbacks since its accuracy depends on the validity of the theory.

In modern friction theories applicable to metal forming conditions, it is considered that Amontons's Law, which assumes a constant coefficient of friction independent of the normal pressure and area of contact, is not applicable. A theory proposed by Bowden and Tabor {13} suggests that the surface asperities deform to make junctions and the breaking of these junctions is the mechanism that contributes to the resistance to sliding. If A_r is the area of the junctions, τ_r is the rapture shear stress and P_m the average pressure

sustained by the deforming material at the boundary, the dry coefficient of friction is given by:

$$\mu = \frac{\tau_r \cdot A_r}{P_m \cdot A_r} = \frac{\tau_r}{P_m}$$

Shaw {14} suggested that, as the apparent interface pressure increases, the area of the junctions increases and the soft material below the junctions flows plastically in small zones. Under these conditions τ_r becomes the shear flow stress of the deforming material. Shaw also suggests that the value of P_m is the yield strength of the material under full constraint, as in a Brinell test, which would be equal to three times the unaxial yield strength ($\bar{\sigma}$). The overlapping plastic zones are initiated when the real area of contact A_r approaches the apparent area A. In this case, the dry coefficient of friction, assuming a Mises material, becomes:

$$\mu = \frac{A\bar{\sigma}/\sqrt{3}}{A_r 3\bar{\sigma}} = \frac{A}{A_r\sqrt{3}}$$

$(P_m = 3\bar{\sigma})$

and as A_r approaches A it would become

$$\mu = \frac{1}{\sqrt{3}} = .577$$

Lauterbach, Lira and Thomsen {15} have carried out detailed investigations in this field. They have evaluated the mean coefficient of friction under high pressures by pressing totally enclosed specimens of copper and aluminium by means of a hardened steel punch.

Of course the above points apply only when the surfaces are dry. In practice, researches have resorted to lubrication to overcome the ill effects of friction. With the use of lubricants friction may take place under conditions ranging from boundary lubrication to hydrodynamic lubrication. In the majority of metal forming processes, however, the friction takes place under boundary and quasi-hydrodynamic lubrication. In the boundary regime, the surfaces are lubricated either by molecular layers adsorbed on to the surfaces or by surface films formed by chemical reaction with the surface. In this way, the effective value of the interface shear stress is reduced. In the quasi-hydrodynamic regime hydrodynamic pockets are formed by entrapment of lubricant in troughs between the asperities. This reduces friction substantially mainly by preventing increase in the contact area.

The coefficient of friction in this type of lubrication is a function of the lubricant properties and also the conditions of the metal forming process itself, i.e. bulk plastic deformation, intensity of the interface

pressure and the sliding velocity over the interface. The above variables, however, are interdependent and therefore a proper study of friction in metal forming is only possible if a method is devised whereby the variables can be altered individually without affecting the other. This is, however, a difficult task and it seems that the only attempt that has been made to achieve this to any extent is by Kasuga and Yamagushi {16}. They studied frictional conditions on the flanges of aluminium cups while they were deep drawn from circular plates. By measuring the contact ratio $(\frac{A_r}{A})$ with an optical method and the frictional force with a split ring technique, they have concluded that, for the material they have tested, the frictional force is almost proportional to the area of contact, irrespective of the apparent interface pressure. On the basis of the model suggested, the frictional resistance is affected by the properties of the lubricating layer and also the pressure generated in them. They have found the latter to be related to the viscosity of the fluid.

One of the interesting studies in which the theoretical approach has been used is by Male and Cockroft {17}. They have used the method suggested by Kunogi {18} for evaluating the coefficient of friction at the metal/tool interface during forging ring specimens. They have used the theoretical analysis of Schroeder and Webster {19} for obtaining their calibration curves. Although there was

some scatter in the results, particularly at large deformations, the fact that reasonably straight lines were obtained, passing through the calibration points for full sticking-friction conditions, suggests that both the Schroeder and Webster analysis and the ring-test method are essentially correct.

The solution suggested by Alexander {20} for plane strain indentation problems has also been used by Takahashi and Alexander {21} for the evaluation of friction in this process. They showed that a considerable amount of information about the behaviour of lubricants in metal working processes could be obtained from the plane-strain compression test. Although useful results have been obtained from their tests, which were carried out under conditions of moderate cleanliness only, typical of those conditions normally found in mechanical-testing laboratories, it is clear that more care must be taken if a precise understanding of frictional phenomena is to be obtained. They show that it may be possible to obtain a reliable quantitative value of the coefficient of friction from the test.

Another interesting study is by Evans and Avitzur {22}. They evaluated the average coefficient of friction in wire drawing and hydrostatic extrusion by finding the optimum die angle experimentally and using it in the equation for coefficient of friction derived from Avitzur's {23} upper bound solution.

1.2.2 Experimental Studies

Several attempts have been made in the past to obtain experimental pressure distribution in conventional extrusion containers. Following the principle of early investigations into the determination of roll pressures {24}, pins were embedded in the container wall and loads on them measured {25}, {26}, {27}. This technique was first used by Siebel and Lueg {24} for the determination of normal pressure distribution along the arc of contact during rolling. In this technique, a small weighbar or pin, fitted radially into the roll and flush with the roll surface, makes contact with some type of pressure transducer which provides a measure of the load on the pin as the metal is rolled.

Frisch and Thomsen {25} used the same technique in studies of the die-wall pressures in extrusion. In their work, the wall pressure was measured with a special pressure gauge. The pressure-sensitive element of the gauge was a small piston having a reduced section on which strain gauges are mounted. This piston was in contact with a load pin, which was guided in the extrusion chamber wall and kept flush during testing with the inner wall surface of the chamber. They found that the wall pressure, as measured by a pressure gauge, increased almost linearly with the extrusion speed and the mean pressure within the metal could not be recorded by a simple wall pressure gauge whose response depended on

elastic deformation of a pressure-sensitive element. They {25} also showed that the mean pressure calculated from stress analysis using the experimental flow pattern agreed approximately with the measured mean pressure.

Frisch {26} later attempted to determine the mean pressure and radial wall stresses by using again the pressure-sensitive pin technique during the indirect extrusion of commercially pure lead at room temperature. He measured wall pressure at two points along the container length as extrusion proceeded. According to his conclusions, the size of the gauge pins inserted in the wall of the extrusion cylinder has a definite influence on the accuracy with which the mean pressures can be found, the smaller pins giving more accurate values. He showed that the same wall pressure was measured with different-sized gauge pins and was found to agree with the calculated values. Finally, the applied load and wall pressure as well as the mean pressure were found to increase linearly with increasing extrusion rates.

Later van Rooyen and Backofen {27} improved on the method by using oblique pins as well, to determine the coefficient of friction in the arc of contact in rolling. They showed that the usefulness of the oblique-radial pin technique for studying tool/metal interface friction was clearly limited by the accuracy and reliability with which measurements could be made. The fundamental behaviour of pins for measuring pressure between roll and strip, therefore,

was an especially important consideration. Their conclusions are that both the radial-oblique pin and the surface reference marker techniques were useful tools for exploring frictional conditions along the arc of contact. In addition to that, a high accuracy of measurement was found to be necessary in the use of oblique and radial pins. In particular, although the above techniques have not been refined to such an extent that they would allow the highly accurate measurements of the friction coefficient, it is felt that they have great potential and with refinement will yield results of greater precision.

The prime purpose of El-behery, Lamble and Johnson's work {28} was to measure the normal and tangential stresses and the coefficient of friction at the container wall/billet interface in a direct axi-symmetric extrusion process.

In their work, a development of the compression pin used by Frisch and Thomsen {25} was used for wall pressure measurement in direct extrusion. They measured normal pressure at six points along the container length as extrusion proceeded. Their apparatus designed to measure the normal pressure distribution at various positions along the container wall was later modified to measure the frictional stress between the billet and the container wall at a fixed position above the die face. In the measurement of the coefficient of friction, by using an inclined pin in conjunction with a pin normal to the wall, it was possible to deduce the coefficient of friction at the wall/billet interface; this method is

originally due to van Rooyen and Backofen {27}.

El-behery et al concluded that in making investigations on stronger materials, Perspex pins may not be robust enough and under large stresses it is likely that the material would creep. They state that in the extrusion process the plastic deformation of a relatively long billet and its reduction to the required size is accomplished in the immediate vicinity of the die. Between this zone and the punch, the material is not deformed and is substantially rigid. It follows that, if σ_r denotes the radial stress and σ_z the axial stress on an element in this rigid region then, because deformation does not take place, $\sigma_z - \sigma_r \leq Y$. (Y is the compressive yield stress of the billet material). Now, $\sigma_z \cong P_e$ and $\sigma_r \cong P_w$, so that $P_e - P_w < Y$ (where P_e is true extrusion pressure and P_w is wall pressure).

The experimental results also showed the greatest wall pressures to occur quite near the die face reaching 93% of the extrusion pressure for all reductions. The measured coefficient of friction was between 0.09 and 0.26 for steady state slow speed axi-symmetric extrusion, consistent with those deduced in earlier plane strain tests on lead {29}, {30}.

However, their results {28} could not be used to determine strain and thus stress distribution along the container wall without assuming a certain pressure distribution.

The pressure sensitive pin technique has also been used by Pearsall and Backofen {31} and recently by Nagamatsu, Murota and Jimma {32} for measuring the distribution of normal pressure and coefficient of friction at the tool-metal interface during the upsetting of aluminium discs.

Although this is a very effective method of determining the normal pressure and coefficient of friction at the tool/metal interface, it has certain drawbacks and sources of errors. In particular, because the gap between the pin and the tool should be made as small as possible to prevent the extrusion of the deforming material into it, the friction between the two could be quite substantial and the possibility of sticking exists. This is so, if the tool were to undergo large hoop strains as is the case in unlubricated conventional extrusion especially with comparatively thin containers. There might not always be enough space available to accommodate the pins and the holes that are required and to house the pins would weaken the container substantially. Also the oblique pin would be rather sensitve to small amounts of recession or protrusion.

Kudo {33} determined the mean container bore pressure by measuring the change of resistance of a wire wound on to the outside diameter of the container. He constructed an experimental apparatus to measure the average internal pressure on the container and the average normal

pressure on the die projection during extrusion-forging or coining. His compound container ring was made of hardened tool steel. A thick wire having known electric resistance was wound onto the outer surface of the container ring. His experimental results lead to the conclusion that the average container pressure is less than the mean extrusion pressure when the reduction is high or when the billet is long. This is in agreement with the findings of Frisch and Thomsen {25}, Thomsen {34}.

The normal pressure and the coefficient of friction could be evaluated indirectly from the measured values of other process variables which are more easily measured. An example of this approach is the work of Whitton and Ford {35} who evaluated the coefficient of friction in strip rolling. The coefficient of friction is assumed to be constant over the arc of contact.

A classical work using an indirect approach in the wire drawing process was carried out by Wistreich {36} who used the "split die" technique suggested by MacLellan {37} to investigate the mean coefficient of friction and the die pressure. While the method is simple in principle, the preparation of the die set requires great care and skill. The method was improved by Yang {38} who restrained the split die in a large ring and measured the hoop strain in the ring which gave a direct measure of the die separating force in wire drawing.

Majors {30} evaluated the normal pressure on the die by measuring the hoop strain at one point on the outer circumference of the die. The die was calibrated by applying hydraulic pressure to the inside of the die with the help of a specially designed closing plug. The same method has also been used by Blazynski and Cole {39} in the calibration of plug drawing dies and Parsons, Bretherton and Cole {40} for calibrating a hydrostatic extrusion die.

A further alternative is when foil strain gauges are bonded to the external diameter of the tool, they are calibrated and the pressure distribution is obtained experimentally, or by a combination of experimental and numerical methods {11}, {41}, {42}. Kamyab and Alexander {41} used foil strain gauges to determine the pressure distribution and the average coefficient of friction at the die/billet interface in hydrostatic extrusion. They achieved this by measuring the hoop strains on the outside surface of the die and interpreted the results by means of an analysis of the strain field in the die. In their technique, the pressure distribution on the conical part of the die was assumed to have the form of a polynomial of the fourth order to relate it directly to the circumferential strain distribution on the outer surface of the die. The influences of the die-land pressure and its corresponding frictional stress were obtained by assuming a uniform pressure on the die-land equal to the yield stress of the material being extruded. They also used the finite

element method to get the pressure distribution and found that the two methods were in good agreement.

Alexander and Said {11} used the foil strain gauge method to find the pressure distribution and the average coefficient of friction at the clamp/billet interface to enable a more complete analysis of the clamp to be made for semi-continuous hydrostatic extrusion. Using Lame's equations and a simplified equlibrium equation for an element along the clamp length, it was possible to estimate the interfacial pressure distribution and the average coefficient of friction.

They concluded that the measured values of circumferential strains at the top end of the clamp were insufficient to make a correct judgement of the pressure profile and it is unsafe to depend on the values obtained from the one gauge which was in operation at that end.

In order to check the experimental results obtained from the calibration of the strain gauges, a finite element analysis of the clamp was carried out. The results were compared with those obtained from Lame's equations for the same tube with free ends and found almost identical.

Recently, Lengyel and Musuva {42} again used a foil strain gauge method and presented hoop strains and approximate pressure distributions on a container wall during the direct (forward) extrusion of lead roads at room temperature at slow speeds, at various extrusion ratios and lubrication conditions.

Their results show that in container design it would be necessary to consider conditions along the full length of the container, since the average extrusion pressure alone could not give sufficient information relating to the most critical cross section, because the wall pressure near the die could be significantly higher than elsewhere. The critical cross section could be anywhere along the container length, depending on extrusion conditions.

Photoelasticity has been tried for evaluating the pressure distribution and coefficient of friction in plane strain drawing dies. Although, the method is an interesting one, its application is limited to non-metals and is only practicable for plane strain. Cook and Wistreich {43} first used this method for measuring the die pressure and coefficient of friction in plane strain drawing of lead through a die made of photoelastic material. Ohashi and Nishitani {44} have developed the method for the study of deformation in the work-piece made of a photoelastic material. The method was also used by El-behery and Lamble {45} to determine the stress distribution in an axi-symmetric extrusion container.

Finally, the visioplasticity method has been used to evaluate the die pressure and coefficient of friction. In this method a billet, split and gridded on one of its meridional planes, was deformed. A flow function was then defined from the shape of the flow lines from which, by numerical differentiation, the velocities and the strain

rates can be found. The total strains can then be used together with the equilibrium equations and the stress-strain curve for the deforming material to give the stress field in the deforming zone.

The method was first suggested by Thomsen and Lapsley {46} and Thomsen, Yang and Bierbower {47}, and programmed for digital computers by Shabaik and Kobayashi {48}. Shabaik and Thomsen {49} have also used this method to find the variation of normal die pressure and coefficient of friction along the die/billet interface in conventional extrusion. They have shown that the coefficient of friction can vary along the die/billet interface. However, judging by the surface appearance of some partially extruded billets, it seems that the coefficient of friction can vary circumferentially around the periphery of the interface as well. Therefore, the study of the frictional conditions of the boundary of one meridional plane (as in visioplasticity) might not give a true picture of the overall frictional conditions at the boundary. However, Dunn {50} who used this method in hydrostatic extrusion, has found the stresses to be quite erratic near the boundary and has expressed doubts about their accuracy in this region.

1.3 Scope of the Present Work

The basic aim of the work described in this thesis is to establish a method of evaluating pressure distribution

and the coefficient of friction at the container/metal interface in conventional extrusion processes, which could then be used in the design of containers.

It is proposed to examine numerically the stress field by the direct integration of the Prandtl-Reuss non-linear tensorial equations describing the plastic state in the deforming zone, particularly at the die/metal interface. It is hoped that this information will eventually lead to a better approximation of the pressure distribution on the container wall during forward extrusion.

Two computer programs have been developed and discussed in Chapter 5.

In order to check the computed results, two test rigs have been built and conventional extrusion experiments have been carried out at room temperature, at slow speeds, at various extrusion ratios and lubrication conditions, using commericial purity aluminium and pure lead specimens.

The specimens were extruded into rods by forward extrusion and into cans by backward extrusion, while loads at both ends of the billet, together with hoop and axial strains on the outside diameter of the containers were recorded simultaneously.

The pressure distribution on the containers can be evaluated by relating it to the measured values of hoop strain on their outside surfaces. The average coefficient

of friction can also be evaluated by considering equilibrium of the forces acting on the billet.

2 BASIC CONCEPTS OF CONTINUUM MECHANICS

2.1 Introduction

It is advisable to begin this work by reviewing some of the basic concepts and definitions of the elements of continuum mechanics and theories of plasticity which will be required later, in order to describe the deformation process of most of the materials commonly used in engineering. Among other principal applications of the continuum mechanics is the determination of stresses, strains and displacements of a solid subjected to external forces. In a general case, these theories are based on experimental studies of the relationships between stresses and strains of polycrystalline aggregates and hence their development was, to some extent, independent of the knowledge of the structure of matter.

In a continuum mechanics formulation, the configuration of a body is described by a continuous mathematical model whose geometrical points are identified by the position of the material particles of this body. When the configuration is changed, due to some form of physical action, assumption is made that this change is continuous, that is, that particles lying near to each other before the change remain near to each other after deformation.

In most cases, exact solutions to the partial differential equations, linear or non-linear which exist in the applications of continuum mechanics, are impossible to obtain

and often not even in an approximate form. Difficulties arise from the fact that boundary conditions involve restrictions arbitrarily imposed, not always easy to introduce in the governing equations of the process. In general, constitutive equations in the theory of plasticity add a non-linear behaviour to the governing equations which makes it impossible to obtain exact solutions for most of the problems. In some cases where the difficulties can be overcome and solutions obtained, such solutions do not necessarily represent the true stresses and strains.

2.2 The Concept of Stress

Let us consider the stresses acting on a cylindrical element as in Fig. 2.1. The stress distribution will be analysed by means of Cauchy's stress tensor σ_{ij} {51}, {52}, {53}, {54}, {55}; its representative matrix in a Cartesian system of coordinates $X_i (i = 1, 2, 3)$ is

$$\sigma_{ij} = \begin{bmatrix} \sigma_{11} & \sigma_{12} & \sigma_{13} \\ \sigma_{21} & \sigma_{22} & \sigma_{23} \\ \sigma_{31} & \sigma_{32} & \sigma_{33} \end{bmatrix} \qquad (2.1)$$

This second order tensor is symmetric and has the property

$$\sigma_{ij} = \sigma_{ji} \tag{2.2}$$

Since the principal stresses characterize the physical state of stress at a point - they are independent of any coordinates of reference. The coefficients J_1, J_2, J_3 are the invariants of the stress tensor

$$\begin{aligned} J_1 &= \sigma_{ii} \\ J_2 &= \frac{1}{2}\sigma_{ii}\sigma_{jj} - \frac{1}{2}\sigma_{ij}\sigma_{ij} \\ J_3 &= \det [\sigma_{ij}] \end{aligned} \tag{2.3}$$

It is convenient in plasticity theory to split the stress tensor into two parts, the spherical or hydrostatic stress tensor and the stress deviatior tensor. These components are:

$$\sigma_{ij} = \acute{\sigma}_{ij} + \sigma_m \delta_{ij} \tag{2.4}$$

where $\acute{\sigma}_{ij}$ is the deviatoric stress tensor, σ_m is the mean stress and δ_{ij} is the Kronecker delta.

Consequently, the deviatoric stress tensor is

$$\acute{\sigma}_{ij} = \sigma_{ij} - \sigma_m \delta_{ij} \tag{2.5}$$

whose principal invariants are

$$J_1' = \sigma_{ii}' = 0$$

$$J_2' = \frac{1}{2}\sigma_{ij}'\sigma_{ij}' \qquad (2.6)$$

$$J_3' = \det [\sigma_{ij}']$$

One advantage of using the stress deviator tensor is now apparent. The first invariant of this tensor is always zero. In a cylindrical coordinate system (r, θ, z) for the element as in Fig 2.1

$$\sigma_{ij}' = \begin{bmatrix} \sigma_r & 0 & \tau_{rz} \\ 0 & \sigma_\theta & 0 \\ \tau_{zr} & 0 & \sigma_z \end{bmatrix} \qquad (2.7)$$

Due to axial symmetry

$$\tau_{r\theta} = \tau_{\theta r} = \tau_{z\theta} = \tau_{\theta z} = 0$$

and the second principal invariant has the form

$$J_2' = -(\sigma_r'\sigma_\theta' + \sigma_\theta'\sigma_z' + \sigma_z'\sigma_r') + \tau_{rz}^2 \qquad (2.8)$$

The equivalent stress $\bar{\sigma}$ is defined by the expression {55}

$$\bar{\sigma} = \sqrt{3J_2'} = \sqrt{\frac{3}{2}\sigma_{ij}'\sigma_{ij}'} \qquad (2.9)$$

2.2.1 Stress Components at a Point {56}

If we are given the six components of stress at a general point with respect to a cylindrical coordinate system (r, θ, z), we can determine the stresses acting on any plane through this point.

Consider now rotation of the coordinate axes r, z by an angle α to the new coordinate axes $\bar{n}$, $\bar{z}'$. This rotation at point P_i is illustrated in Fig 2.2. The stress components at a generical point on that surface (z' axis) are

$$S_i = \sigma_{ij} n_j \tag{2.10}$$

where $\bar{n}$ is a normal vector and given by

$\bar{n} = (\cos\alpha, 0, -\sin\alpha)$

In this particular case

$$\begin{aligned} S_r &= \sigma_r \cos\alpha - \tau_{rz} \sin\alpha \\ S_\theta &= 0 \\ S_z &= \tau_{rz} \cos\alpha - \sigma_z \sin\alpha \end{aligned} \tag{2.11}$$

The stress component tangent to that surface is

$$\tau_\alpha = \frac{\sigma_r - \sigma_z}{2} \sin 2\alpha + \tau_{rz} \cos 2\alpha \tag{2.12}$$

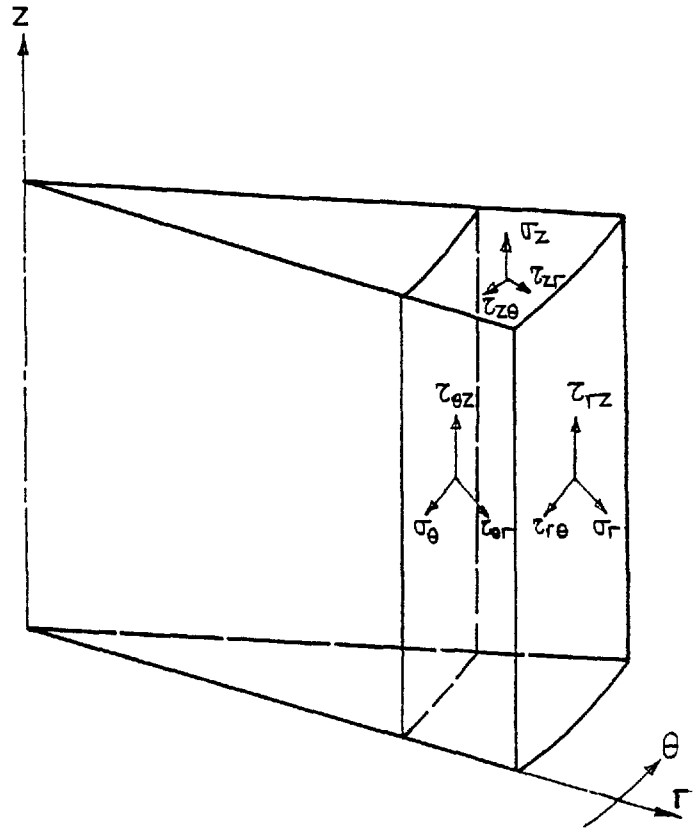


Fig. 2.1 Stress components referred to cylindrical coordinates.

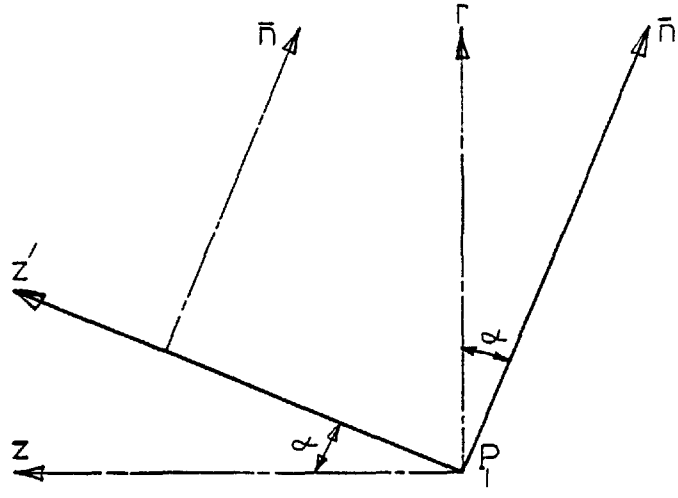


Fig. 2.2 Stress at a generical point.

2.2.2 Stress Functions

The equilibrium condition in terms of stress is given by

$$\frac{\partial \sigma_{ij}}{\partial X_j} + \rho f_j = 0 \qquad \begin{matrix} i = 1, 2, 3 \\ j = 1, 2, 3 \end{matrix} \qquad (2.13)$$

where f_j is the body force per unit mass, ρ is the density and X_j is a generical coordinate.

Assuming that no body forces are operative, eq. (2.13) becomes

$$\frac{\partial \sigma_{ij}}{\partial X_j} = 0 \qquad (2.14)$$

In the case of cylindrical coordinates and axisymmetric conditions, the following equilibrium equations can be derived from eq. (2.14)

$$\frac{\partial \sigma_r}{\partial r} + \frac{\partial \tau_{rz}}{\partial z} + \frac{\sigma_r - \sigma_\theta}{r} = 0 \qquad (2.15)$$

$$\frac{\partial \sigma_\theta}{\partial \Theta} = 0 \qquad (2.15)$$

$$\frac{\partial \tau_{rz}}{\partial r} + \frac{\partial \sigma_z}{\partial z} + \frac{\tau_{rz}}{r} = 0$$

To determine the stress components, two free functions called "stress functions" ϕ_1 and ϕ_2 are needed since in (2.15) there are three equations with four unknowns. The stress components are calculated from stress functions ϕ_1 and ϕ_2 {53} as

$$\sigma_r = \frac{1}{r}\frac{\partial^2\phi_1}{\partial z^2} + \frac{\phi_2}{r}$$

$$\sigma_\theta = \frac{\partial\phi_2}{\partial r}$$

$$\sigma_z = \frac{1}{r}\frac{\partial^2\phi_1}{\partial r^2} \qquad (2.16)$$

$$\tau_{rz} = -\frac{1}{r}\frac{\partial^2\phi_1}{\partial r\partial z}$$

where $\phi_1 = \phi_1(r, z)$ and $\phi_2 = \phi_2(r, z)$.

2.3 Strains and Strain Rates {53}, {54}

If we introduce the displacement vector u with components

$$u_i = x_i - a_i \qquad i = 1, 2, 3$$

where a_i is a system of coordinates of a body at a certain instant of time and X_i is the new coordinate system at a later instant of time.

If the components of displacement U_i are such that their first derivatives are so small that the squares and products of the partial derivatives of U_i are negligible, then Cauchy's infinitesimal strain tensor is obtained as

$$\varepsilon_{ij} = \frac{1}{2}\left(\frac{\partial U_j}{\partial X_i} + \frac{\partial U_i}{\partial X_j}\right) \tag{2.17}$$

In cylindrical coordinates and in a case of axial symmetry

$$\varepsilon_{ij} = \begin{bmatrix} \varepsilon_r & 0 & \varepsilon_{rz} \\ 0 & \varepsilon_\theta & 0 \\ \varepsilon_{rz} & 0 & \varepsilon_z \end{bmatrix} \tag{2.18}$$

The strain rate tensor is defined as

$$\dot{\varepsilon}_{ij} = \frac{\partial \varepsilon_{ij}}{\partial t} \tag{2.19}$$

where t is the time and, in terms of velocities of displacements V_{ij}, as

$$\dot{\varepsilon}_{ij} = \frac{1}{2}\left(\frac{\partial V_j}{\partial X_i} + \frac{\partial V_i}{\partial X_j}\right) \tag{2.20}$$

The assumption that the material is incompressible leads to $\dot{\varepsilon}_{ii} = 0$ (2.21)

As in the case of the stress tensor, the strain rate tensor can be separated into two parts, a spherical or hydrostatic part $\dot{\varepsilon}_m \delta_{ij}$ and deviatoric part ε'_{ij} as

$$\dot{\varepsilon}_{ij} = \dot{\varepsilon}'_{ij} + \dot{\varepsilon}_m \delta_{ij} \tag{2.22}$$

where $\dot{\varepsilon}_m = \frac{1}{3}\dot{\varepsilon}_{ii}$

Consequently, the deviatoric strain rate tensor then becomes

$$\dot{\varepsilon}'_{ij} = \dot{\varepsilon}_{ij} - \dot{\varepsilon}_m \delta_{ij} \tag{2.23}$$

whose principal invariants are

$$I_1 = \dot{\varepsilon}'_{ii} = 0$$

$$I_2 = \frac{1}{2} \dot{\varepsilon}'_{ij} \dot{\varepsilon}'_{ij} \tag{2.24}$$

$$I_3 = \det [\dot{\varepsilon}'_{ij}]$$

In axisymmetry

$$I_2 = -(\dot{\varepsilon}'_r \dot{\varepsilon}'_\theta + \dot{\varepsilon}'_\theta \dot{\varepsilon}'_z + \dot{\varepsilon}'_z \dot{\varepsilon}'_r) + \dot{\varepsilon}^2_{rz} \tag{2.25}$$

The equivalent strain rate {54} is defined by

$$\dot{\bar{\varepsilon}} = \frac{2}{\sqrt{3}} \sqrt{I_2} = \frac{2}{\sqrt{3}} \sqrt{\frac{1}{2} \dot{\varepsilon}_{ij} \dot{\varepsilon}_{ij}} \qquad (2.26)$$

$\dot{\bar{\varepsilon}}$ is an accepted measure of the combined effect of the components of strain rates. It provides a means of comparison between different modes of straining.

Equivalent strain {57}, {58} is obtained from eq. (2.26) as

$$\bar{\varepsilon} = \frac{2}{\sqrt{3}} \int_{t=o}^{t} \sqrt{I_2}\, dt \quad \text{or} \quad d\bar{\varepsilon} = \sqrt{\frac{2}{\sqrt{3}} d\varepsilon_{ij} d\varepsilon_{ij}} \qquad (2.27)$$

2.3.1 Stream Function

The continuity equation must be satisfied for any strain rate field $\dot{\varepsilon}_{ij}$ derived from a kinematically admissible velocity field.

In the case of cylindrical coordinates (r, θ, z) eq. (2.20) $\dot{\varepsilon}_{ij} = 0$ becomes

$$\frac{\partial v_r}{\partial r} + \frac{1}{r} \frac{\partial v_\theta}{\partial \theta} + \frac{v_r}{r} + \frac{\partial v_z}{\partial z} = 0 \qquad (2.28)$$

or from incompressibility for axial symmetry

$$\frac{\partial v_r}{\partial r} + \frac{v_r}{r} + \frac{\partial v_z}{\partial z} = 0 \tag{2.29}$$

If it is possible to choose a stream function $\psi = \Psi(r, z)$ such that

$$v_r = \frac{1}{r}\frac{\partial \psi}{\partial z}$$

$$v_z = -\frac{1}{r}\frac{\partial \Psi}{\partial r} \tag{2.30}$$

the continuity eq. (2.29) will be automatically satisfied.

Eq. (2.26) satisfied by eq. (2.30) will be developed for the case of cylindrical coordinates in order to obtain strain rate components. These are:

$$\dot{\varepsilon}_r = \frac{\partial}{\partial r}\left(\frac{1}{r}\frac{\partial \psi}{\partial z}\right) = \frac{\partial v_r}{\partial r}$$

$$\dot{\varepsilon}_\theta = \frac{1}{r^2}\frac{\partial \Psi}{\partial z} = \frac{v_r}{r}$$

$$\dot{\varepsilon}_z = -\frac{\partial}{\partial z}\left(\frac{1}{r}\frac{\partial \psi}{\partial r}\right) = -\frac{\partial v_z}{\partial z}$$

$$\dot{\varepsilon}_{rz} = \frac{\partial}{\partial z}\left(\frac{1}{r}\frac{\partial \psi}{\partial z}\right) - \frac{\partial}{\partial_r}\left(\frac{1}{r}\frac{\partial \psi}{\partial r}\right) = \frac{\partial v_r}{\partial z} + \frac{\partial v_z}{\partial r}$$

$$\dot{\varepsilon}_{r\theta} = \dot{\varepsilon}_{\theta z} = 0 \qquad (2.31)$$

In the case of a spherical coordinate system (R, ψ, θ) the corresponding strain rate field under axisymmetric conditions is described by

$$\dot{\varepsilon}_{RR} = \frac{\partial v_R}{\partial R}$$

$$\dot{\varepsilon}_{\psi\psi} = \frac{v_R}{R}$$

$$\dot{\varepsilon}_{\theta\theta} = \frac{v_R}{R} = -\left(\dot{\varepsilon}_{RR} + \dot{\varepsilon}_{\psi\psi}\right) \qquad (2.32)$$

$$\dot{\varepsilon}_{R\theta} = \frac{1}{2R}\frac{\partial v_R}{\partial \theta}$$

$$\dot{\varepsilon}_{\theta\psi} = \varepsilon_{R\psi} = 0$$

2.4 A BASIC ASSUMPTION OF THE MATHEMATICAL THEORY OF PLASTICITY {59}, {60}

2.4.1 Yield Criteria

Numerous criteria have been proposed to describe the yielding of solids, going as far back as Coulomb in 1773. Many of these were originally suggested as criteria

for failure of brittle materials and were later adopted as yield criteria for ductile materials.

A material is said to be isotropic if there is no orientation effect in the material. If the yield function f depends only on the invariants (with respect to rotation of coordinates) of stress, strain, and strain history, then the plastic characteristics of the material are isotropic. If the yield function f is an isotropic function of the stress (the scalar function σ_{ij}) alone, then the theory of plasticity is called an isotropic stress theory. In such theories, f can be expressed in terms of the principal invariants of σ_{ij} as

$$f(\sigma_{ij}) = f(J_1, J_2, J_3) \tag{2.33}$$

Let J_2' and J_3' be the second and third invariants of the stress deviation σ_{ij}'. By assuming constancy of volume, eq. (2.33) has the form

$$f = f(J_2', J_3') \tag{2.34}$$

Von Mises took the simplest of such functions, assuming further that J_3' is equal to 0, and in this way obtained his famous criterion $f = J_2' - \text{constant} = 0$

or

$$f = J_2' - k^2 = 0 \tag{2.35}$$

where $J_2' = \frac{1}{2}\sigma_{ij}'\sigma_{ij}'$ and k is a scalar function depending on plastic strain history.

Tresca suggested that the decisive factor for yielding is the maximum shear stress in the material during plastic flow. To express Tresca's idea analytically, it is the simplest to use the principal stresses $\sigma_{11}, \sigma_{22}, \sigma_{33}$. If it is known that $\sigma_{11} \geq \sigma_{22} \geq \sigma_{33}$, then Tresca's yield condition is

$$f = \sigma_{11} - \sigma_{33} - 2k = 0 \tag{2.36}$$

The yield criterion of Von Mises will be used throughout this work.

2.5 Stress Strain Relationships {57}, {58}, {61}

In elasto-plastic theory, the total strain components can be expressed in terms of a purely elastic and a purely plastic component as

$$\varepsilon_{ij} = \overset{E}{\varepsilon}_{ij} + \overset{P}{\varepsilon}_{ij} \quad \text{or} \quad \dot{\varepsilon}_{ij} = \overset{E}{\dot{\varepsilon}}_{ij} + \overset{P}{\dot{\varepsilon}}_{ij} \tag{2.37}$$

where ε_{ij}^{E} is the elastic component and ε_{ij}^{P} is the plastic component.

However, if the plastic strains are larger than the elastic strains, the elastic component in relation to the plastic component may be neglected and then

$$\varepsilon_{ij} = \varepsilon_{ij}^{P} \quad \text{or} \quad \dot{\varepsilon}_{ij}^{P} = \dot{\varepsilon}_{ij} \tag{2.38}$$

The expression for the plastic stress-strain relationship for a material that hardens isotropically is

$$d\varepsilon_{ij}^{P} = G \frac{\partial F}{\partial \sigma_{ij}} dF \tag{2.39}$$

where G is a scalar function depending on stresses, strains and loading history.

Prandtl-Reuss assumed that the plastic strain increment at any instant of the loading is proportional to the instantaneous stress deviation as

$$d\varepsilon_{ij}^{P} = \frac{\partial F}{\partial \sigma_{ij}} d\lambda \tag{2.40}$$

where $d\lambda = GdF$

For the yield condition of Von Mises , eq.(2.35), eq. (2.40) becomes

$$d\varepsilon_{ij}^{P} = \sigma_{ij} d\lambda \tag{2.41}$$

or in terms of strain rates

$$\dot{\varepsilon}^{P}_{ij} = \Delta \sigma'_{ij} \tag{2.42}$$

where $\Delta = \frac{d\lambda}{dt} = G \frac{\partial F}{\partial t} = \frac{\sqrt{I_2}}{k}$

Thus, we obtain the Prandtl-Reuss relationship as

$$\sigma'_{ij} = \frac{k}{\sqrt{I_2}} \dot{\varepsilon}^{P}_{ij} = \frac{k}{\sqrt{\frac{1}{2}\dot{\varepsilon}^{P}_{ij}\dot{\varepsilon}^{P}_{ij}}} \dot{\varepsilon}^{P}_{ij} \tag{2.43}$$

or, by means of symbolic notation

$$T' = \frac{k}{\sqrt{I_2}} v_s \tag{2.44}$$

where $T' = \sigma'_{ij}$, I_2 is the second principal invariant of the strain rate tensor and v_s is the strain rate tensor.

Eq. (2.44) is the form to be used throughout this work.

2.6 Haar-Von Kármán Hypothesis

As the following eq. (2.6.2) shows, if the radial and hoop strain rates are the same at any point, then the radial and hoop stresses will also be the same. The assumption that the hoop stress is a principal stress and is equal to the radial stress is often made in analysing axisymmetric deformation problems.

Von Mises yield criterion (eq. (2.35)) and flow rule (eq. (2.42)) can be written for

$$\bar{\sigma}^2 = \frac{1}{2}\left[(\sigma_r - \sigma_\theta)^2 + (\sigma_\theta - \sigma_z)^2 + (\sigma_z - \sigma_r)^2\right] + 3\tau_{rz}^2 \qquad (2.6.1)$$

$$\dot{\lambda} = \frac{\dot{\varepsilon}_r}{\sigma_r + \sigma_m} = \frac{\dot{\varepsilon}_\theta}{\sigma_\theta + \sigma_m} = \frac{\dot{\varepsilon}_z}{\sigma_z + \sigma_m} = \frac{\dot{\varepsilon}_{rz}}{2\tau_{rz}} = \frac{3}{2}\frac{\dot{\bar{\varepsilon}}}{\bar{\sigma}}$$

where $\sigma_m = -\frac{1}{3}(\sigma_r + \sigma_m + \sigma_z)$

From eq. (2.6.1)

$$\dot{\varepsilon}_r = \dot{\lambda}(\sigma_r + \sigma_m)$$
$$\dot{\varepsilon}_\theta = \dot{\lambda}(\sigma_\theta + \sigma_m)$$
$$\dot{\varepsilon}_z = \dot{\lambda}(\sigma_z + \sigma_m)$$

therefore

$$\sigma_r = \sigma_z + \frac{\dot{\varepsilon}_r - \dot{\varepsilon}_z}{\dot{\lambda}}$$
$$\sigma_\theta = \sigma_z + \frac{\dot{\varepsilon}_\theta - \dot{\varepsilon}_z}{\dot{\lambda}} \qquad (2.6.2)$$

2.7 The Effect of Strain Hardening

It is useful to employ an empirical equation for the strain-hardening characteristic. The one to be used here is $\bar{\sigma} = A\ (B + \bar{\varepsilon})^{\lambda}$ suggested by Swift {62}. A is some measure of the basic strength of the material, independent of its initial state, B gives an indication of the initial state of the material and λ is a measure of the rate of hardening with strain.

The most widely used equation to represent a stress-strain curve is of the form

$$\bar{\sigma} = c\,\bar{\varepsilon}^{\lambda} \tag{2.45}$$

where c and λ are constants for a particular material.

The value of the constant λ depends on the degree of initial work-hardening, small values indicating a cold-worked material.

To fit of this empirical relation to commerically pure aluminium is shown graphically in Fig. 2.3. Using the Von Mises yield criterion, the current yield shear stress k is given by

$$k = \frac{\bar{\sigma}}{\sqrt{3}} = \frac{Y}{\sqrt{3}} \tag{2.46}$$

where Y is the current tensile yield stress.

2.8 Power of Plastic Deformation {54}

The power developed by the plastic deformation of a material volume ν is

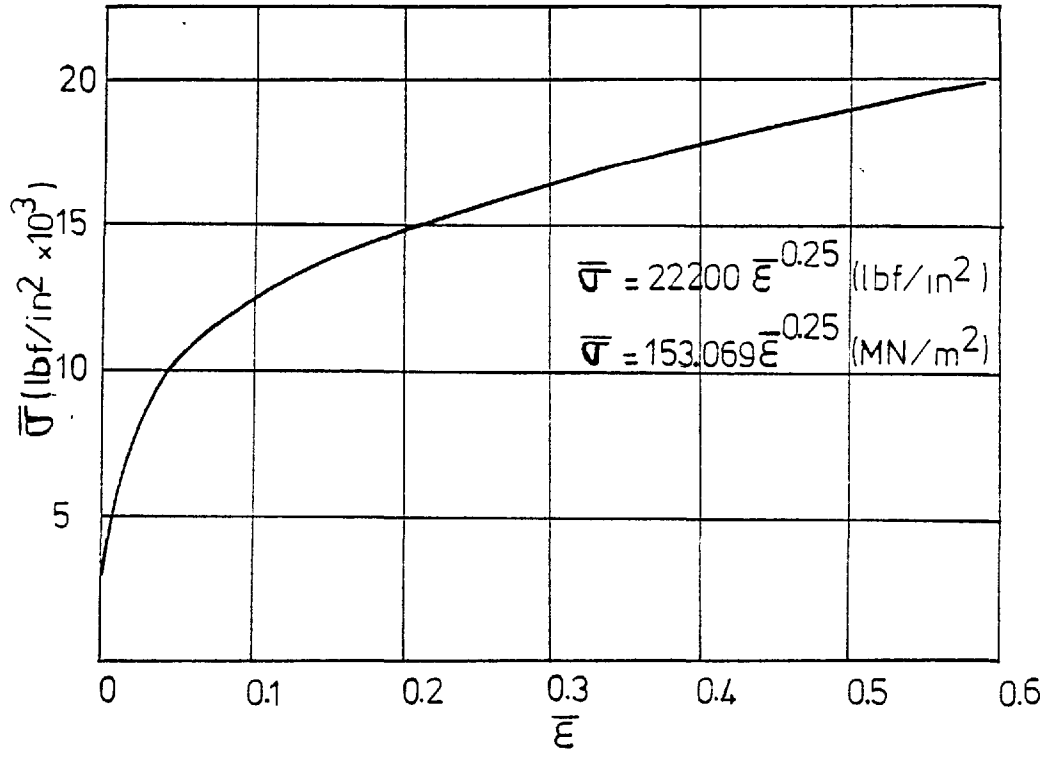


Fig. 2.3 Empirical relation to stress-strain curve of commercially pure aluminium
(Published in Johnson and Mellor {63}).

$$\dot{W} = \int_{\nu} \sigma_{ij}' \dot{\varepsilon}_{ij} \, d\nu \tag{2.47}$$

For a material obeying the Prandtl-Reuss relationship it is

$$\sigma_{ij}' = \frac{k}{\sqrt{I_2}} \dot{\varepsilon}^P_{ij}$$

and, consequently, expression (2.47) rewrites as

$$\dot{W} = \int_{\nu} \frac{k}{\sqrt{I_2}} \dot{\varepsilon}^P_{ij} \dot{\varepsilon}^P_{ij} \, d\nu = \int_{\nu} 2k \sqrt{I_2} \, d\nu \tag{2.48}$$

since $I_2 = \frac{1}{2} \dot{\varepsilon}^P_{ij} \dot{\varepsilon}^P_{ij}$

If k has a constant value all over ν and the material does not exhibit strain hardening, eq. (2.48) can be written as

$$\dot{W} = 2k \int_{\nu} \sqrt{I_2} \, d\nu = \frac{2}{\sqrt{3}} \bar{\sigma} \int_{\nu} \left(\frac{1}{2} \dot{\varepsilon}^P_{ij} \dot{\varepsilon}^P_{ij} \right)^{1/2} d\nu \tag{2.49}$$

The work per unit volume is obtained by integrating the power with respect to time as follows

$$W = \int_{t} \dot{W} dt = 2 \int_{t.} k \sqrt{\frac{1}{2} \dot{\varepsilon}^P_{ij} \dot{\varepsilon}^P_{ij}} \, dt \tag{2.50}$$

3. NUMERICAL METHODS

3.1 A Relatively Simple Treatment of Classical Problems

Approximate solutions of differential equations satisfy only part of the conditions of the problems: for example the differential equation may be satisfied only at a few positions, rather than at each point. Usually, solutions are proposed in the form of a set of known functions with arbitrary parameters which are then determined so as to satisfy the equations as closely as required. There are several methods by which approximate solutions can be obtained {64}. Methods like finite elements are necessary to be identified with variational calculus where a function is derived mathematically and then minimised. In some cases such variational principle does not exist {65} and direct approaches are necessary.

3.2 The Method of Weighted Residuals

The method of weighted residuals (henceforth abbreviated as MWR) is a general method of finding approximate solutions to the equations of change of distributed systems.

The applications of the MWR to solve a single scalar differential equation is discussed by Crandall {64} and Kantorovich and Krylov {66}. A generalization of this procedure to the integration of vector differential equations

and systems of differential equations is considered by Finlayson and Scriven in {67} and by Finlayson in {68}.

As the method is basically proposing a solution in the form of a series, it is inherently capable of converging to an exact solution if a sufficient number of terms are included in the series. The approximate solution is expanded in a set of trial functions with arbitrary parameters.

Briefly, the procedure consists of assuming an approximate solution in the form of a linear combination of known trial functions with unknown coefficients. This proposed solution, when substituted in the governing equation, results in a "residual" or "error" function. The free parameters are then determined by forcing this residual function to vanish. As the solutions obtained by the MWR are of analytical form, they are more useful than those obtained by numerical integration and usually require much less computing time {64}.

Let us consider a differential equation {67}

$$N(U) - \frac{\partial U}{\partial t} = 0 \qquad X \in \nu_D \tag{3.1}$$

where $u = u(X,t)$, $N(U)$ denotes a generical differential operator involving spatial derivatives of "u". ν_D is a

three dimensional domain with a boundary B and t is the time. The initial and boundary conditions may have the form

$$u(x,o) = u_o(X) \qquad X \in \nu_D \tag{3.2}$$

$$u(x,t) = f_B(x,t) \qquad X \in B \tag{3.3}$$

Assume a trial solution

$$U^*(x,t) = U_B(x,t) + \sum_{i=1}^{m} A_i(t)\, U_i(x,t) \tag{3.4}$$

where the approximating functions, U_i are required to satisfy the boundary condition

$$U_B(x,t) = f_B(x,t) \quad \text{and} \quad U_i(x,t) = 0 \quad X \in B \tag{3.5}$$

and $A_i(t)$ are the parameters to be determined.

For simplicity, the trial solution is usually chosen to be linear on the A_i parameters. By substituting expression (3.4) in the differential eq. (3.1), we obtain the residual function of the differential equation.

$$R(U^*) = N(U^*) - \frac{\partial U^*}{\partial t} \neq 0 \tag{3.6}$$

According to the requirements of a specific problem, if the assumed trial functions were the exact solution, then the residual function will be zero. In all assumed trial functions, we focus our attention on achieving to force the residual to vanish in an average sense over the entire domain of interest. A set of weighting functions W_j which are orthogonal to the residual functions can be selected in such a way that the residual is forced to be zero in an average sense {69}. The weighted integrals of the residual are set to zero as

$$\int_{\nu} W_j R_j d\nu = 0 \qquad (3.7)$$

where $< W_j R_j > = 0$ and $j = 1,2, \ldots, M$

3.3 Different Forms of the MWR

In the general process, the weighting functions can be chosen in many ways and each choice corresponds to a different criterion of MWR. Some of the well-known widely used approximation methods are:

3.3.1 Collocation

In this criterion, the weighting functions are chosen to be the displaced Dirac delta function

$$W_j = \delta (X - X_j)$$

which has the property that

$$\int W_j R \, d\nu = R \Big|_{X_j} = 0 \tag{3.8}$$

Thus, the residual is zero at M specified collocation points j. We select as many locations as there are free parameters until the residual vanishes at these locations {70}. As M increases, the residual is zero at more and more points and presumably approaches zero everywhere.

3.3.2 Subdomain Method

The domain ν_D is divided into as many subdomains ν_j as there are adjustable parameters and the weighting functions are selected as

$$W_j = \begin{cases} 1 & X \in \nu_j \\ 0 & X \notin \nu_j \end{cases}$$

and

$$\int_{\nu_j} W_j R \, d\nu = 0 \tag{3.9}$$

3.3.3 Galerkins's Method

In this method, the weighting functions are chosen to be trial functions, $W_j = A_j$ and

$$\int_{\nu} A_J^{\cdot} \, R \, d\nu = 0 \tag{3.10}$$

Here the trial functions must be selected as members of a complete set of functions. A set of functions $[w_i]$ is complete if any function of a given class can be expanded in terms of the set, $f = \Sigma \, a_i w_i$.

3.3.4 Least Squares Method

The weighting function is $\frac{\partial R}{\partial A_J^{\cdot}}$ so that

$$\frac{\partial}{\partial A_J^{\cdot}} \int_{\nu} R^2 \, d\nu = 0 \tag{3.11}$$

is minimized with respect to the free parameters $A_J^{\cdot}$, over the desired interval.

An analysis of these four methods for the selection of trial families will be considered on a simple problem further in section 3.5.

3.4 Selection of Trial Functions

As the purpose of these methods is merely to choose the "best" approximation of a given family, good results cannot be obtained if good approximations are not included within the family. The choice of trial functions is somewhat arbitrary. Since a polynomial is probably the easiest form for computation, it is frequent to adopt it

as trial solutions. Theoretically, polynomials with sufficient number of terms are a complete set in as much as any continuous function can be expanded in terms of polynomials. They are also easy to handle. In numerical calculations, the trial functions must be linearly independent. Although the property of completeness of a set of functions ensures that, if sufficient number of terms are used, we can represent the exact solution. Otherwise, the successive approximations might converge to something which is not the solution {68}.

The trial functions must be selected to satisfy the governing equation and the largest possible number of boundary conditions, independently of the values taken by the set of free parameters. Unfortunately, satifying all the boundary conditions in one set of trial functions is not always possible, or at least, not for all the prescribed boundary conditions. In these circumstances, it is more convenient to have separate error functions for the boundary conditions and the total weighted residual function will be the sum of individual weighted residual functions arising from separation, as

$$G_1 \int_{\nu} w_J^* \, R d\nu + G_2 \int_{B} w_J^* \, R \, dB = 0 \qquad (3.12)$$

Where G_1 and G_2 are constants known as "weighting factors", R are the error functions corresponding to the governing

equation and the boundary condition respectively. The integral form (3.12) associated with the boundary condition is calculated only at boundary points. The weighting factors are particularly useful when in the domain of interest only a small proportion of points lie on the boundary. If expression (3.12) represents a linear system of equations, the unknown parameters used for the trial solutions will be obtained by means of any of the standard methods. Otherwise, a non-linear system would be obtained which in general is more difficult to solve by computer methods. Any symmetry conditions that may exist in the problem must also be satisfied by the trial functions.

Apart from satisfying these requirements, the selection of approximating functions is yet somewhat dependent on the user's intuition and experience, and this is often regarded as a major disadvantage of this method. However, some guidelines of general application may be outlined. Together with the use of the trial functions based on the simplified analytical solutions to related problems and a large number of parameters with a finer net, a better accuracy is obtained, but the computing time and the rounding error increases very rapidly, so a compromise situation must be found between these factors.

3.5 Approximation within the Family of Trial Solutions

Let us consider the Voigt Model {51} for the

viscoelastic solid in order to compare the four approaches with respect to the amount of computational labour. As shown in Fig. 3.1 the Voigt model is composed of combinations of a linear spring with spring constant μ and a dashpot with coefficient of viscosity η.

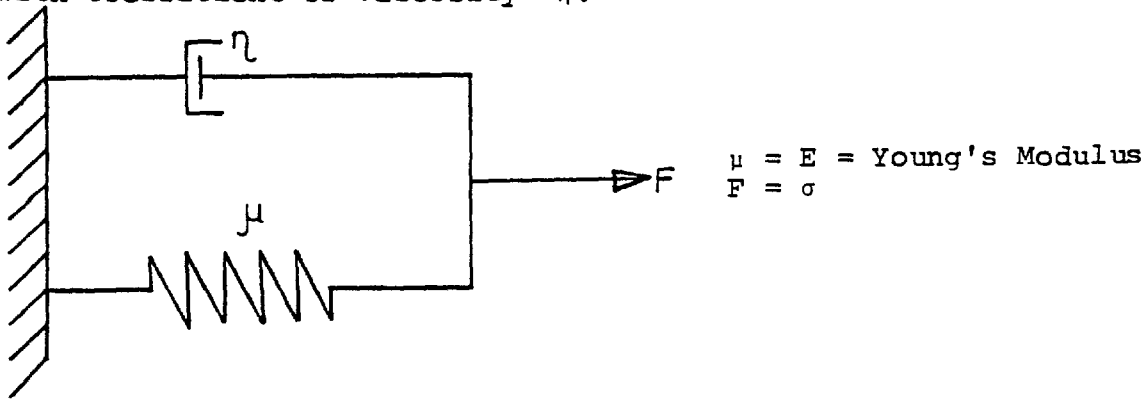


Fig. 3.1 Voigt Model.

The load-deflection relationship for this model is

$$F = \mu u + \eta \dot{u} \quad \text{or} \quad \sigma = E\varepsilon + \eta \dot{\varepsilon} \tag{3.13}$$

where F is the force at time t and u is the total elongation of the viscoelastic solid.

The exact solution can be easily derived by solving eq. (3.13) for $\varepsilon(t)$ when $\sigma(t)$ is a unit-step function σ. That is

$$\varepsilon(t) = \frac{1}{E}\left[1 - e^{-(E/\eta)t}\right]\sigma \tag{3.14}$$

Finally, the governing differential equation is

$$\eta \frac{d\varepsilon}{dt} + E\varepsilon(t) - \sigma = 0 \qquad (3.15)$$

with the boundary condition

$$\varepsilon(t) = 0 \qquad t = 0 \qquad (3.16)$$

in the time interval $0 \leq t \leq 1$.

The first and most important step in the application of the method is to adopt a trial family of approximate solution. For this particular case we choose

$$\varepsilon(t) = \sum_{i=1}^{n} A_i t^i \qquad (3.17)$$

where A_i are the free parameters to be determined.

By substituting function (3.17) in the differential equation (3.15) we obtain the expression of the residual R(t) as follows:

$$R(t) = \left[\sum_{i=1}^{n} (\eta i t^{i-1} + E t^i) A_i \right] - \sigma \neq 0 \qquad (3.18)$$

or

$$R(t) = (\eta + Et)A_1 + (2\eta t + Et^2)A_2 + \cdots + (n\eta t^{n-1} + Et^n) - \sigma$$

The next step requires the adoption of a criterion for selecting the best approximation within the family.

3.5.1 Collocation

Having in this case 'n' free parameters of the domain $0 < t < 1$, we choose 'n' number of collocation points within equal intervals of $\frac{1}{n+1}$. Consequently, applying the criterion (3.3.1) we have Dirac delta function $w_j = \delta(t - t_j)$ and

$$R_j = \left[\sum_{i=1}^{n} (\eta i t_j^{i-1} + E t_j^{i}) A_i \right] - \sigma = 0$$

$$\text{for} \qquad t_j = \frac{1}{n+1} \left(\frac{1}{n+1}\right) \frac{n}{n+1} \tag{3.19}$$

The free parameters can now be determined by solving this system of equations.

3.5.2 Subdomain Method

We divide the subdomain $0 < t < 1$ into equally spaced subdomains of $\frac{1}{n}$. Applying the criterion (3.3.2) we establish that

$$w_j = \begin{cases} 1 & t \in j \\ 0 & t \notin j \end{cases}$$

$$R_j = \int_{t_{j-1}}^{t_j} \left[\sum_{i=1}^{n} (\eta i t^{i-1} + E t^{i}) A_i - \sigma \right] dt = 0$$

$$= \sum_{i=1}^{n} \left\{ \eta (t_j^{i} - t_{j-1}^{i}) + E \left(\frac{t_j^{i+1} - t_{j-1}^{i+1}}{i+1} \right) \right\} A_i - \sigma (t_j - t_{j-1}) = 0$$

$$\text{for} \quad t_{\dot{J}} = \frac{1}{n}\,(\tfrac{1}{n})1 \qquad (3.20)$$

This system of equations can now be solved to determine the free parameters.

3.5.3 Galerkin's Method

This criterion (3.3.3) requires that:

$$w_{\dot{J}} = t_{\dot{J}}$$

and

$$R_{\dot{J}} = \int_0^1 \left[\sum_{i=1}^{n} (\eta_i t^{i-1} + E t^{i}) A_i - \sigma \right] t^{\dot{J}}\, dt = 0$$

$$R_{\dot{J}} = \sum_{i=1}^{n} \left(\frac{\eta_i}{i + \dot{J}} + \frac{E}{i + \dot{J} + 1} \right) A_i - \frac{\sigma}{\dot{J} + 1} = 0$$

$$\text{for} \quad \dot{J} = 1(1)n \qquad (3.21)$$

where A_i are the free parameters to be determined.

3.5.4 Method of Least Squares

Applying criterion (3.3.4) we set

$$R_{\dot{J}} = \frac{\partial}{\partial A_{\dot{J}}} \int_0^1 R^2\, dt = 2 \int_0^1 R\, \frac{\partial R}{\partial A_{\dot{J}}}\, dt$$

$$R_{\dot{J}} = 2\int_0^1 \left[\sum_{i=1}^{n} (\eta i t^{i-1} + E t^{i})A_i - \sigma\right] \cdot \left[\sum_{i=1}^{n} (\eta \dot{J} t^{\dot{J}-1} + E t^{\dot{J}})\right] dt = 0$$

$$= \left[\sum_{i=1}^{n} \left(\frac{\eta^2 i\dot{j}}{i + \dot{J} - 1} + E\eta + \frac{E^2}{i + \dot{J} + 1}\right)A_i\right] - \sigma\left(\eta + \frac{E}{\dot{J} + 1}\right) = 0$$

for $\dot{J} = 1(1)n$ (3.22)

We have just obtained four slightly different approximate solutions to (3.15), all within the trial family (3.17). Solutions to equations (3.19) to (3.22) are represented graphically in Fig. 3.2 for n = 2. We note that in every case we have a set of simultaneous equations to solve. The only difference is in the way the coefficients are derived from the residual. It is clearly seen that all of them rapidly converge to exact solutions, the choice of weighting function is not critical as long as sufficiently high order expansions are used in the trial function. Collocation is most direct, requiring only evaluations of the residual, whereas the other three methods require integrations. These integrations are least awkward for the subdomain method and most awkward in the method of least squares. It is observed that the error of approximation is more uniformly distributed in the least square method. The maximum error of the worst case (collocation) is more or less twice the maximum error of the best (least squares).

As a conclusion, the method of least squares can be selected to be used throughout the MWR, because of providing the most uniform distribution of the error as seen in Fig. 3.2 and also the mean square residual in the method of least squares has theoretical significance as error bounds can sometimes be determined in terms of the residual. Even when error bounds can not be determined, the mean square residual can be regarded as a measure of the accuracy of the solution.

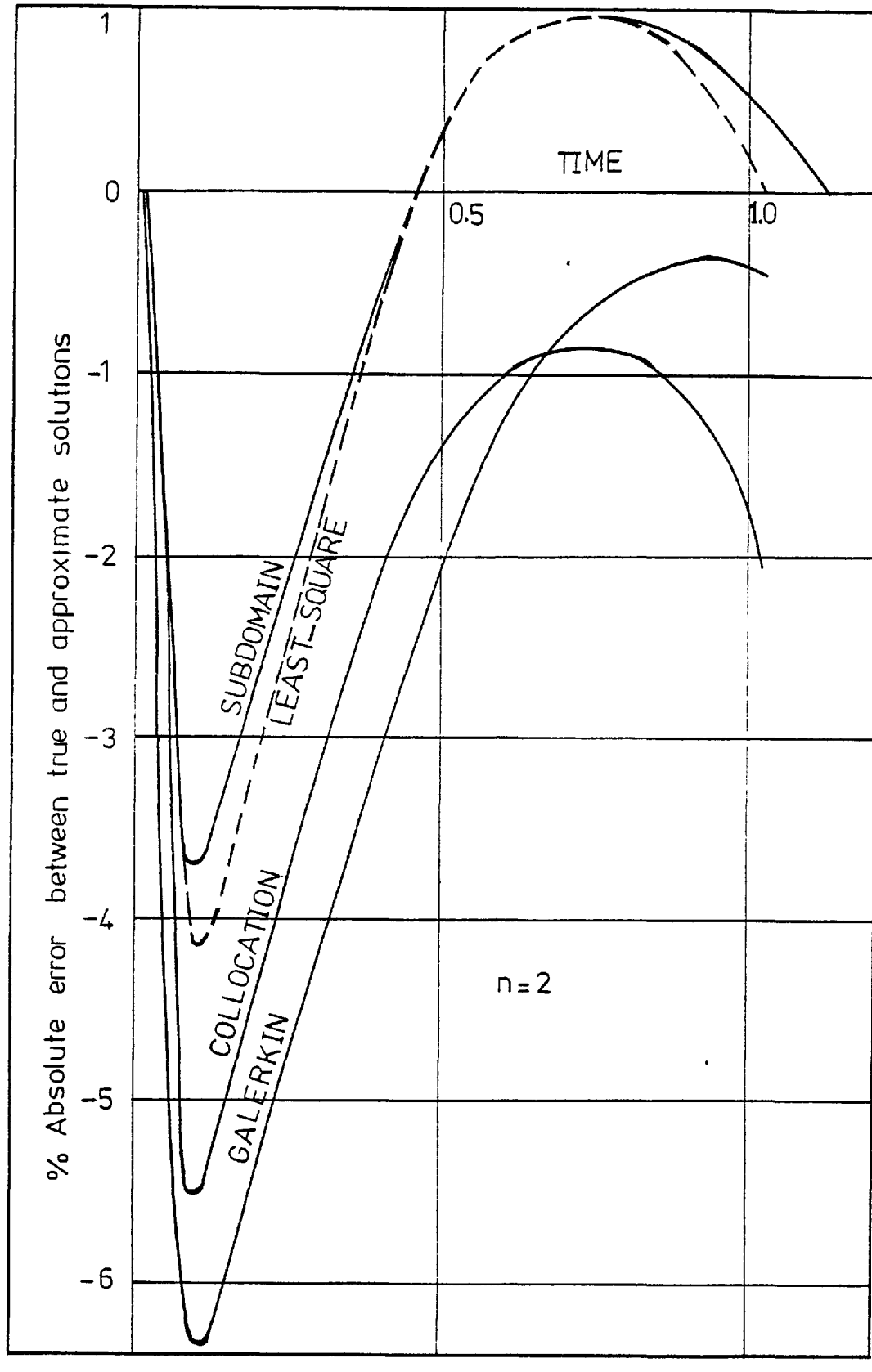


Fig. 3.2 Comparison of errors in approximate solutions.

4. EXPERIMENTAL WORK

4.1 Introduction

The main aim of this experimental work is to develop apparatus to be used in the measurement of the strain distribution on the container outer surface, and from these recorded strains to evaluate the stress distribution inside the container wall, and then to compare these experimental results in theoretically evaluated pressure distributions in extrusion containers.

The general purpose of these experiments is to extrude lead and aluminium specimens by forward and backward extrusion, while punch and die loads are recorded simultaneously by strain gauge load cells. Most of the experiments have been carried out with commerically pure lead and pure aluminium at various extrusion ratios and lubricants to determine the effect of these on the strain and pressure distributions.

4.2 The Apparatus

The experimental apparatus which was designed and built for the conventional forward and backward extrusions of commerically pure lead and aluminium for extrusion pressures of up to 28 tons/in^2 ($\sim$ 462 MN/m^2) will be described below in three sections, namely, the extrusion assemblies; the calibration assembly; and the instrumentation of measuring and recording the experimental data.

4.2.1 The Extrusion Assemblies

The general views of the full assemblies for forward and backward extrusion can be seen in Figs 4.1a and 4.1b and both consist of the extrusion container, the extrusion dies, the punch, the pressure pad, support plates for the container, together with the die and punch load cells (see also Figs 4.1c and 4.1d).

The design of these assemblies were based on the mean extrusion pressure obtained from an experimental formula proposed by Hirst and Ursell {71}. Another method for obtaining extrusion pressure given by Alexander and Lengyel {72} was also used, and the pressures calculated by the two methods were compared with those tabulated in {73} so as to obtain a satisfactory result. Finally, the design pressure of these assemblies was decided to be 28 tonf/in^2 ($\sim$ 462 MN/m^2), so as to ensure that the containers, described in detail in the next paragraphs, would remain elastic throughout the experiments.

The containers were monobloc cylinders of 30 mm internal diameters and 48 mm external diameters machined from thick walled steel tubes with a K-ratio of 1.60. The inside and outside of the containers (Fig. 4.2) were machined to a very good surface finish to lessen friction at the deforming material and container interface. The inside of the short container near the base was machined to accommodate dies supported by a load cell as seen in Fig. 4.1a. This design

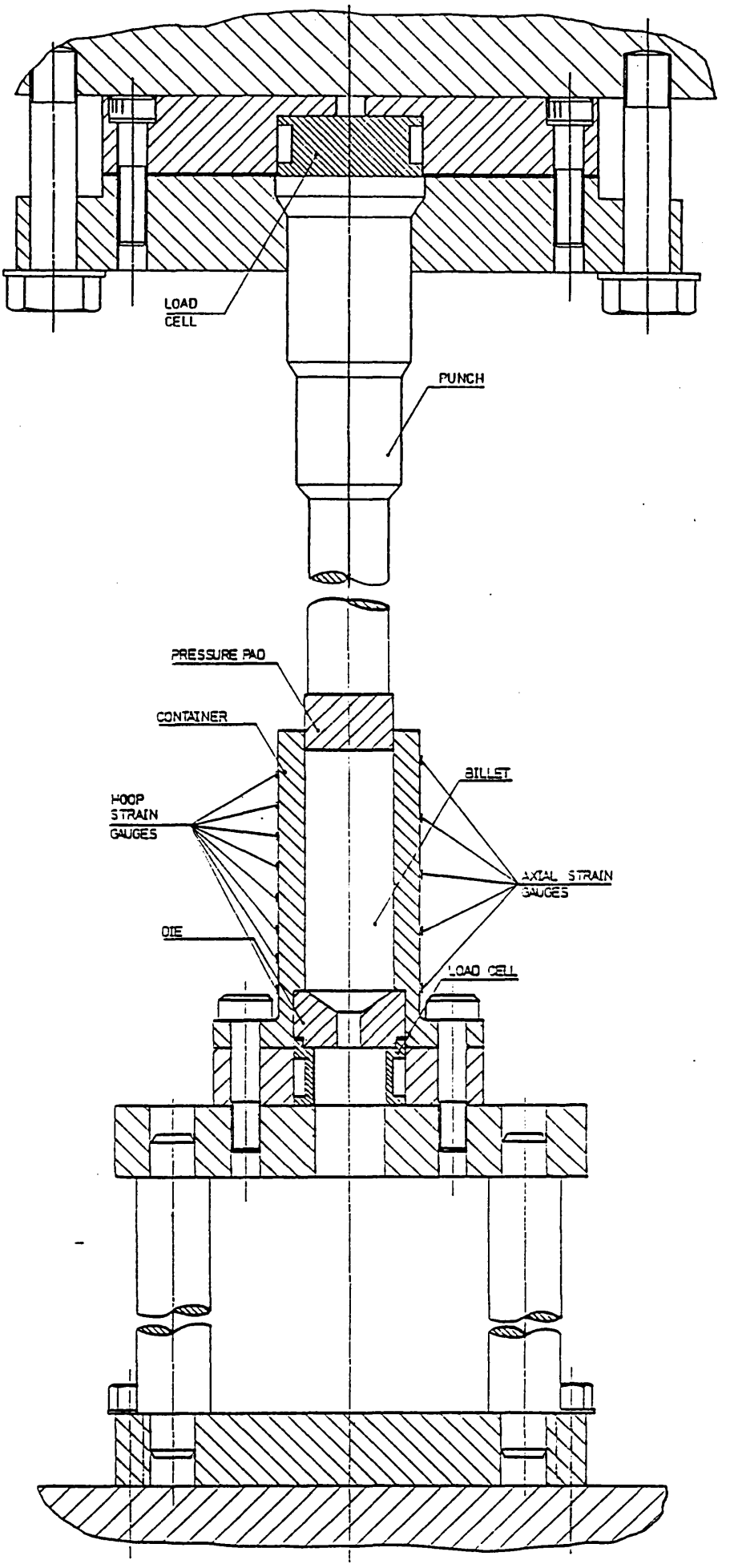


Fig. 4.1a The Forward Extrusion Assembly.

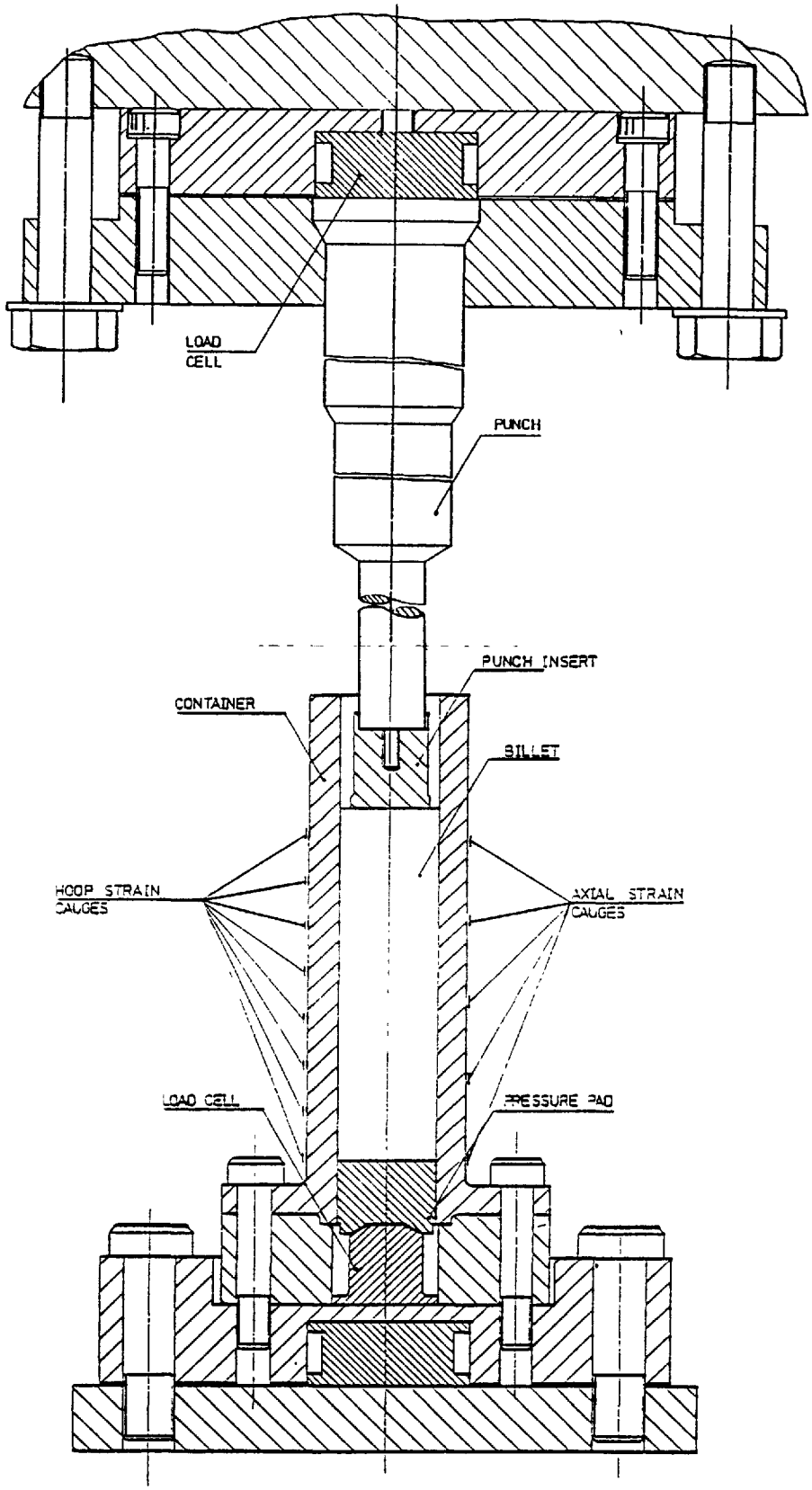


Fig. 4.1b The Backward Extrusion Assembly.

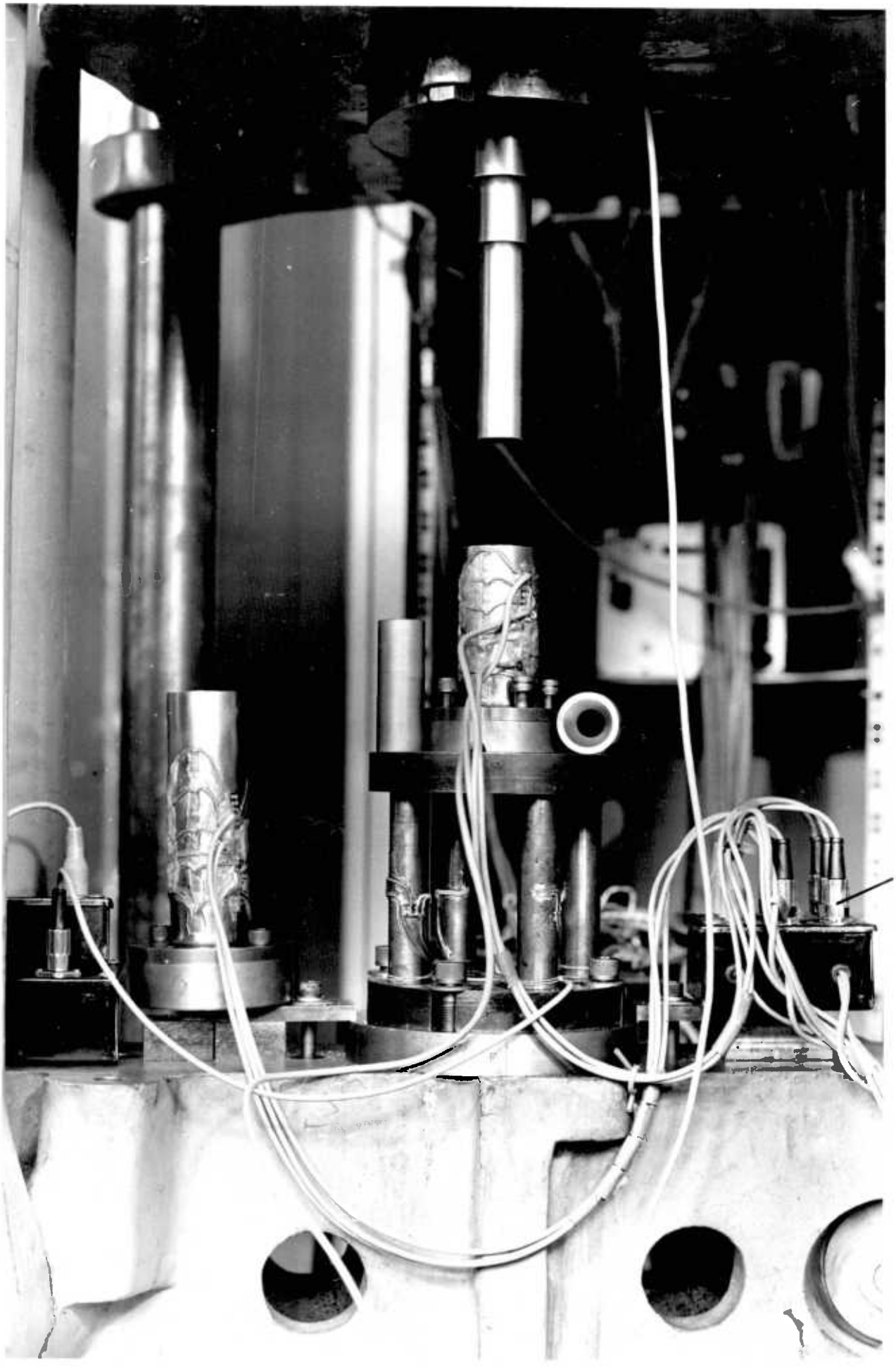


Fig. 4.1c General view of the forward extrusion rig.

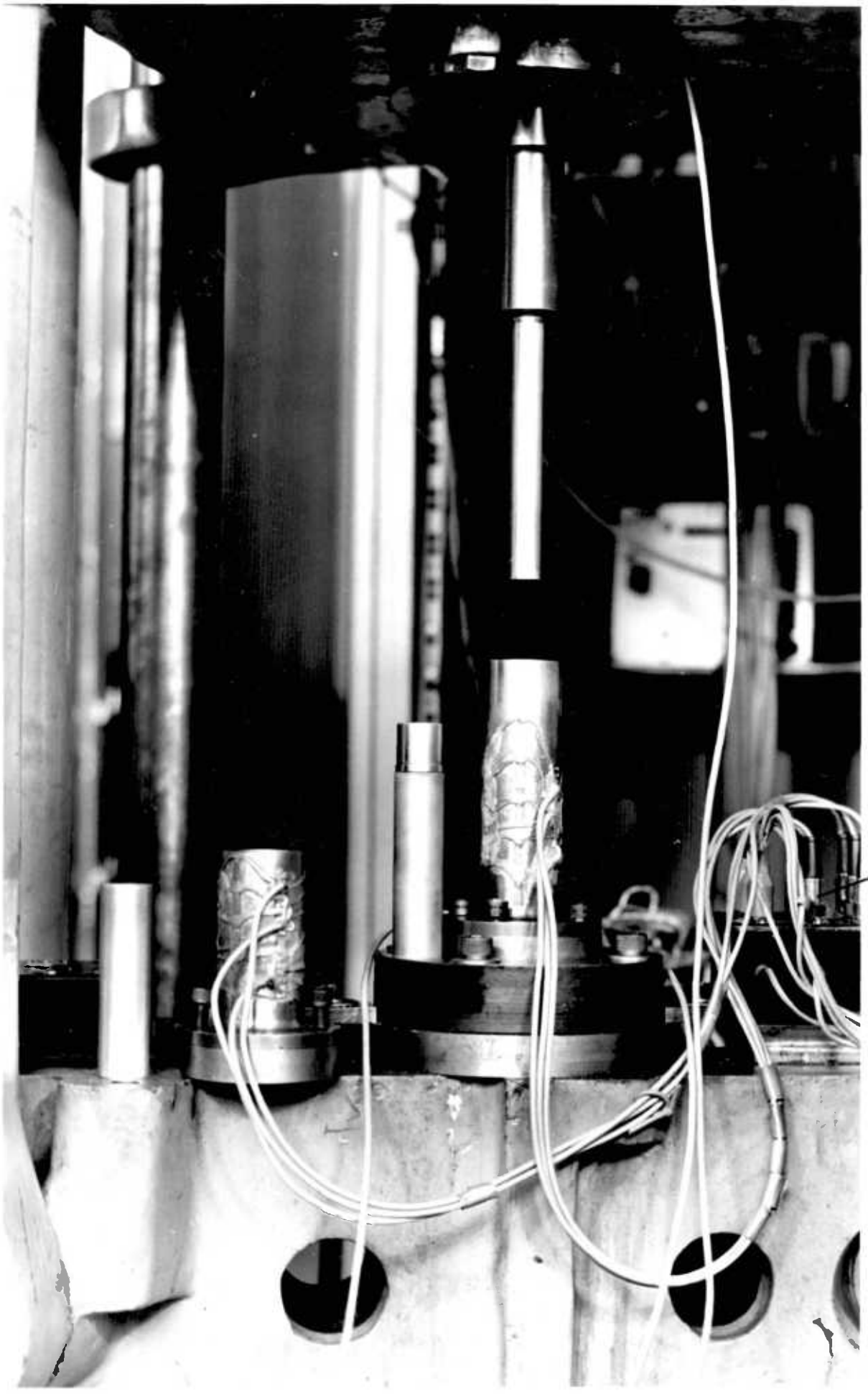


Fig. 4.1d General view of the backward extrusion rig.

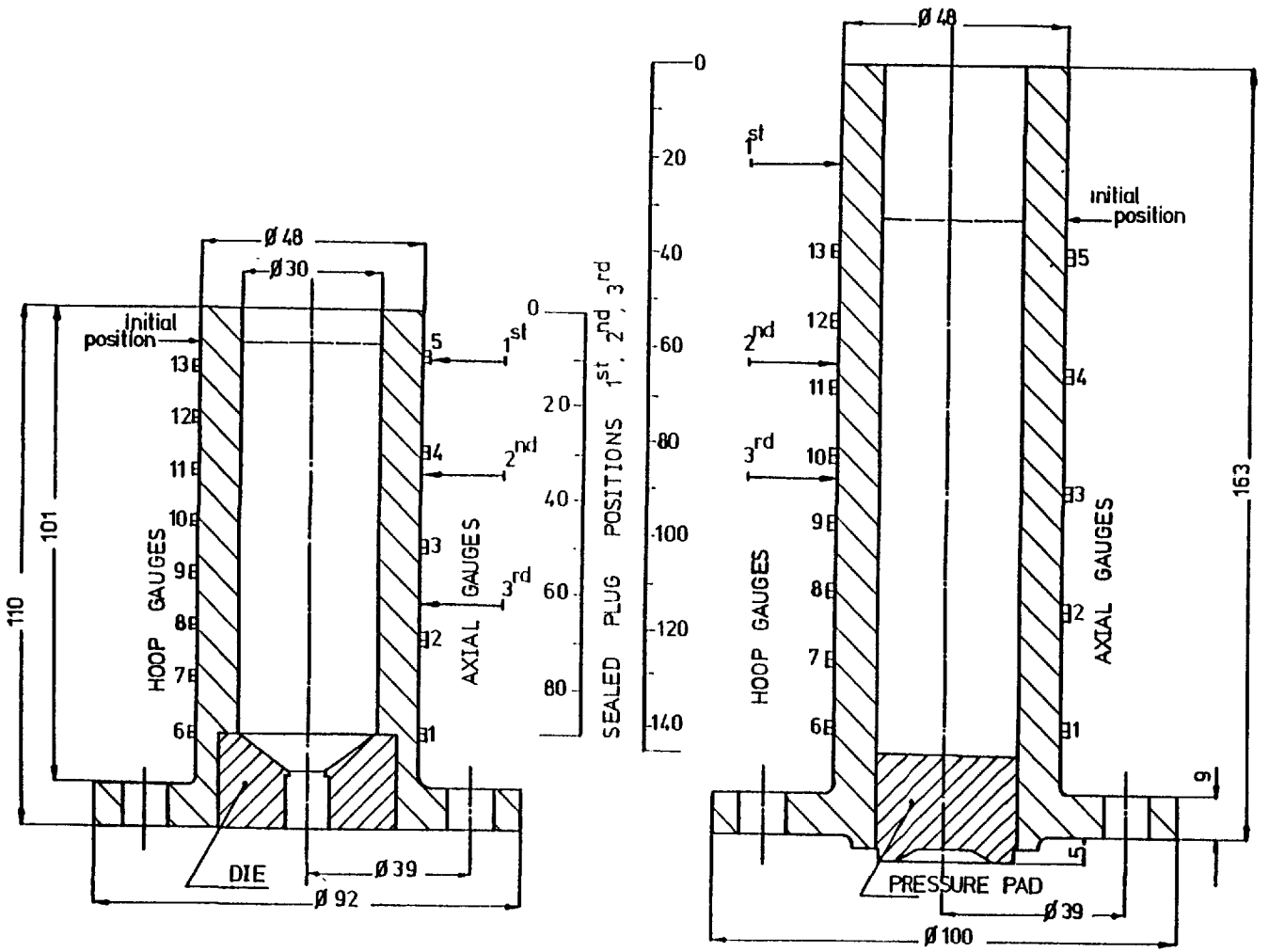


Fig. 4.2 The Extrusion Containers.

was highly satisfactory because flash formation in extrusion and leaking of the fluid during calibration were prevented. Four 10 mm diameter holes were drilled in each container base for bolting down the containers to the supporting plates.

The extrusion containers were made from 4½ % Ni - CHROME-MOYBDENUM (EN30B) alloy steel, heat-treated to 47 RC hardness.

The containers were made longer so that longer billets could be extruded in order to study frictional effects along the length of the container wall during the process. The design ensured accessibility of the container surface from the open end to the die face (forward extrusion), and from the open end to the pressure pad face (backward extrusion) for attaching strain gauges and the containers had a low K-ratio so that strains could be easily measured on the outside but yielding never occured at the bore.

The extrusion dies were made from tool steel (C 1.55 %, Cr 12 %, Mo 0.85 % and V 0.28 %) and machined as shown in Figs 4.3a and 4.3b. They were ground to 10 - 15 MICRO-INCH CLA (∿ 0.25 - 0.38 μm) surface finish, while the container-die contact surfaces in forward extrusion were polished to 3 - 5 MICRO-INCH CLA (∿ 0.076 - 0.127 μm). Five conical dies were made to extrusion ratios (R) of 2, 3, 4, 9 and 16 for semi-angles of 25°, 30°, 35°, 45° and 51° and two dies to extrusion ratios of 4 and 16 with a semi-angle

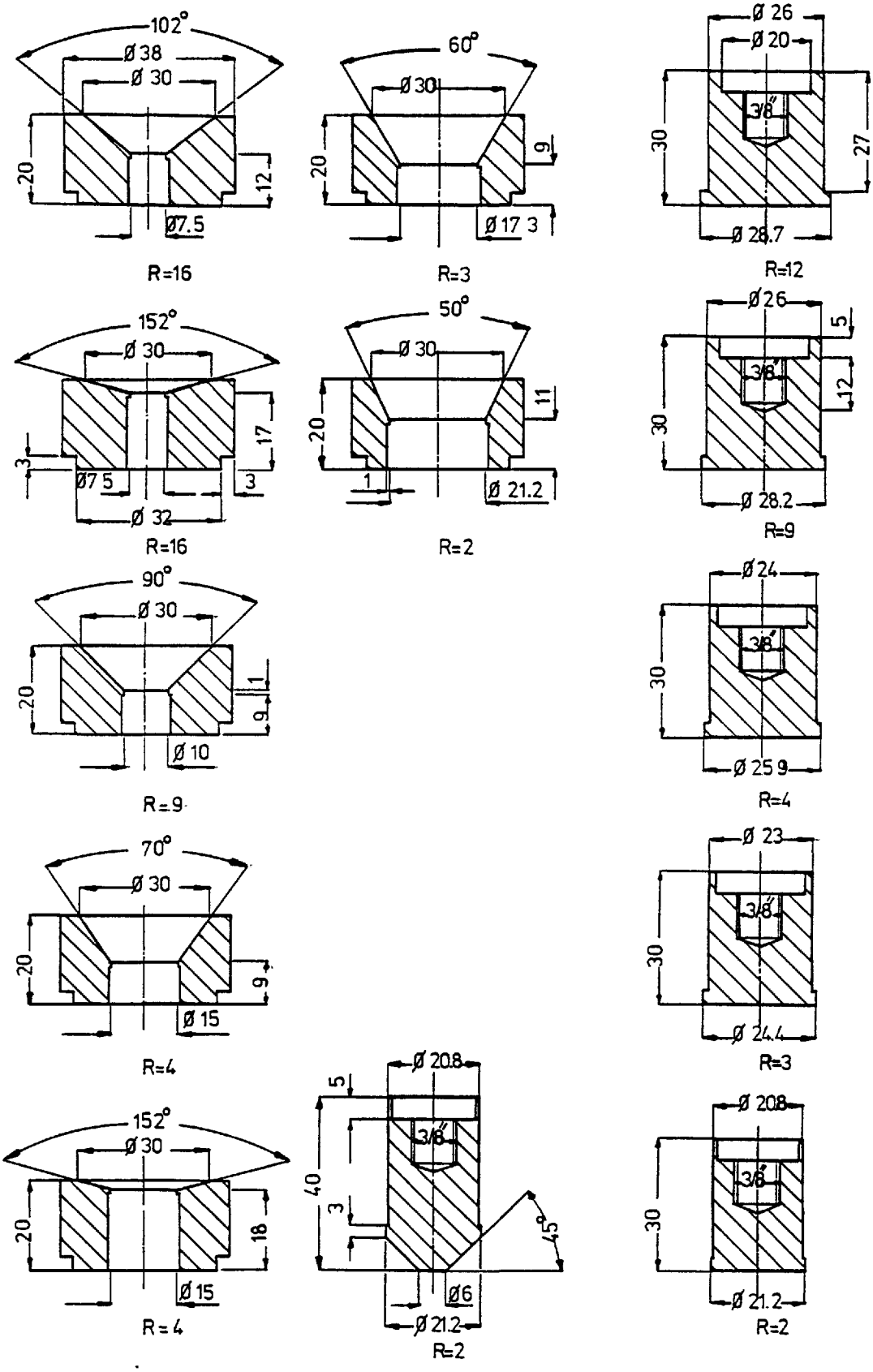


Fig. 4.3a The Extrusion Dies and Punch Inserts.



Fig. 4.3b General view of the extrusion dies and punch inserts.

of 76°. For backward extrusion, five square punch inserts were machined to extrusion ratios, R of 2, 3, 4, 9 and 12 and one conical punch insert with a semi-angle of 45°. All dies and punch inserts were heat treated to about 55 RC hardness.

The extrusion punches were machined to diameters somewhat smaller than the internal diameters of the containers, as shown in Fig. 4.4. The top of the punches was machined to fit into a supporting plate bolted to the top crosshead of a DENISON 50 tonf (∿ 498 kN) hydraulic compression testing machine. Both punches were heat-treated to 55 RC hardness and designed against buckling.

The pressure pads were steel blocks of 30 mm diameter and 20 mm long and machined to a sliding fit in the container bore. The main aim of using pressure pads was to take up any misalignment between the punch and the container axes in forward extrusion and between the load cell and pad axes in backward extrusion. The bottom of the pressure pad for backward extrusion was machined to a conical shape to be supported by the load cell, as shown in Fig. 4.1b.

4.2.2 The Calibration Assembly

The main purpose of this assembly was to calibrate the strain gauges against known internal fluid pressures applied to the bore of the containers.

As the general view of the assembly shows (Figs 4.5a and 4.5b) it is basically a supporting frame for the

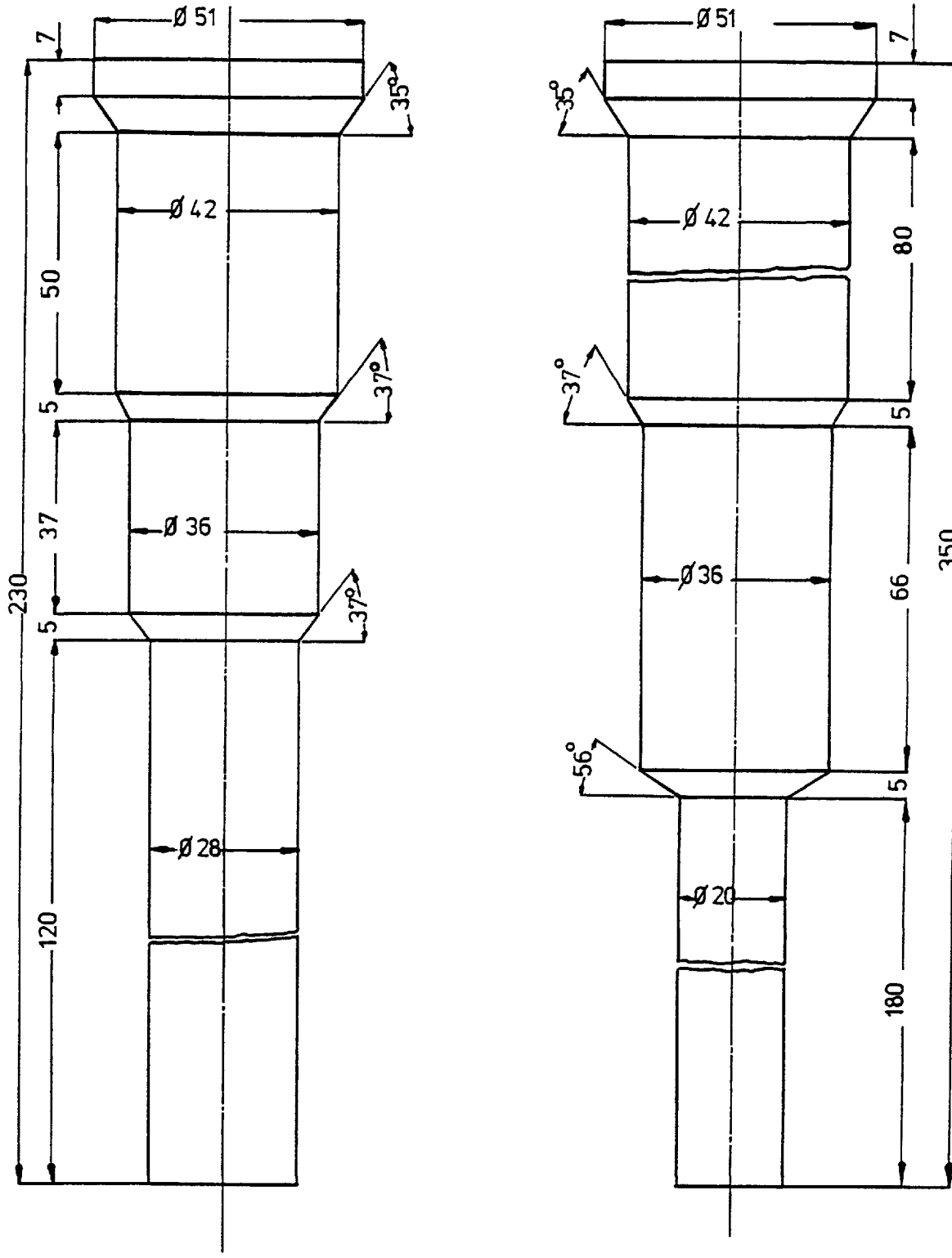


Fig. 4.4 The Extrusion Punches.

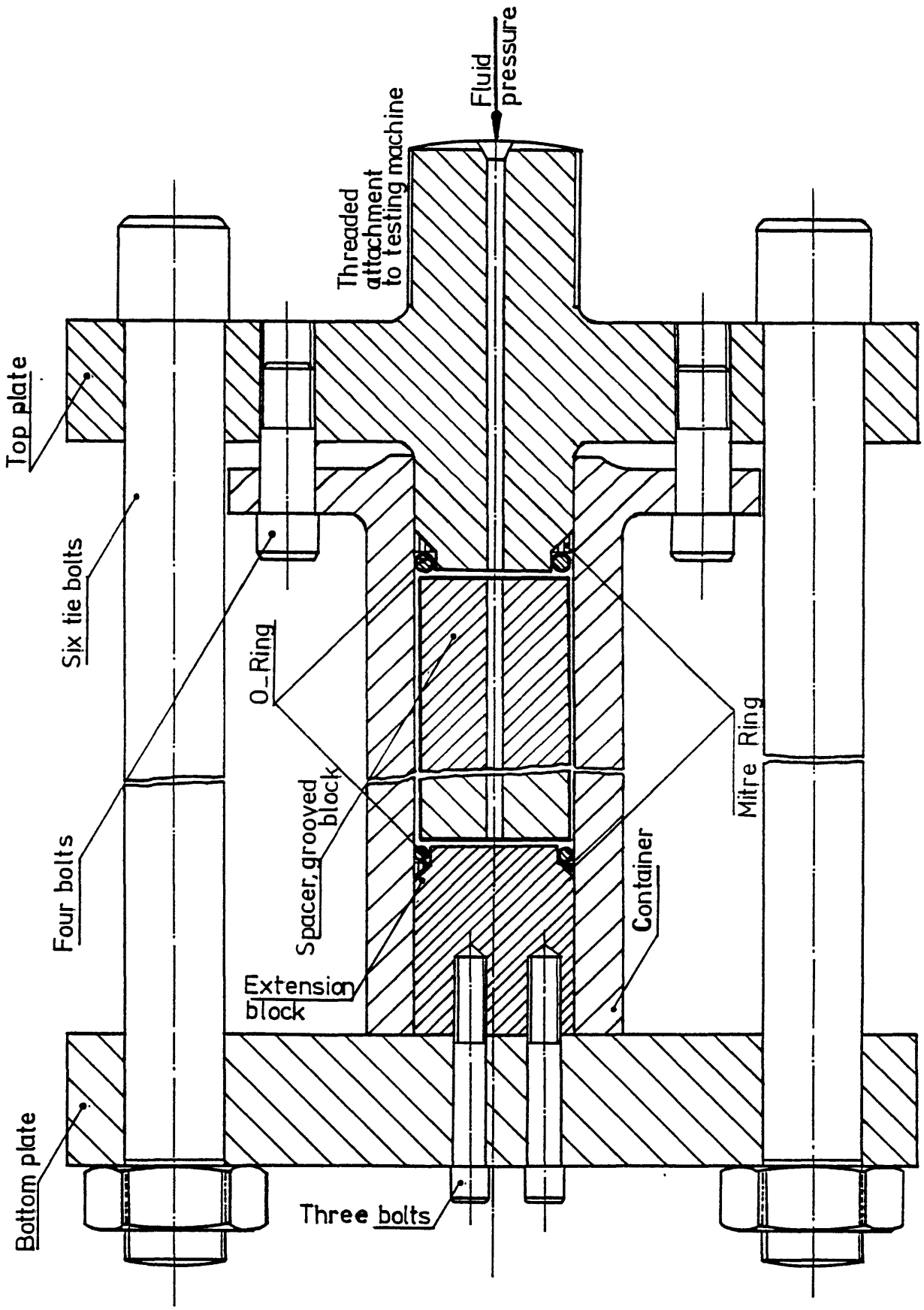


Fig. 4.5a The Calibration Assembly.

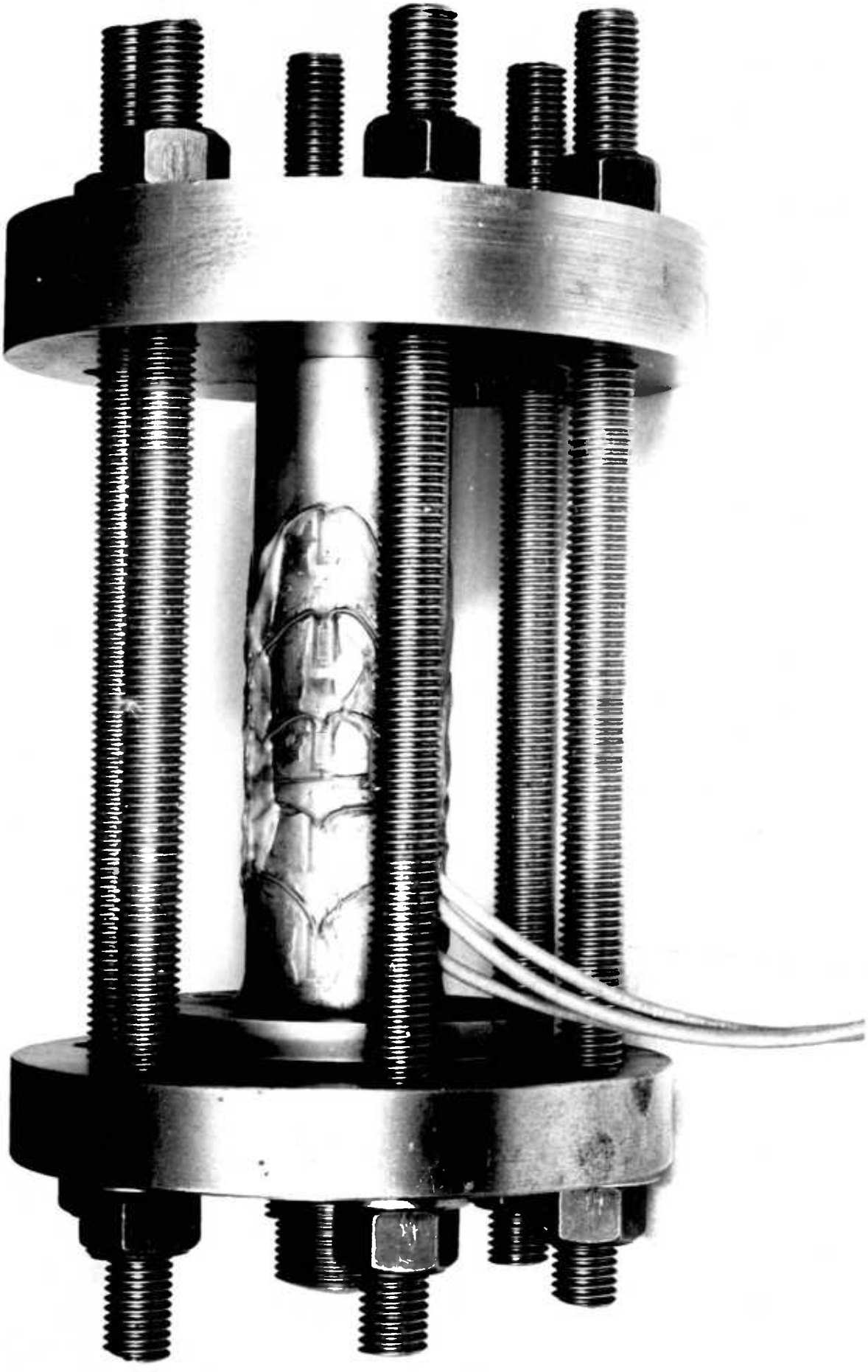


Fig. 4.5b General view of the calibration assembly.

container for calibration in a Harwood Controlled Clearance Piston Gauge (dead weight tester).

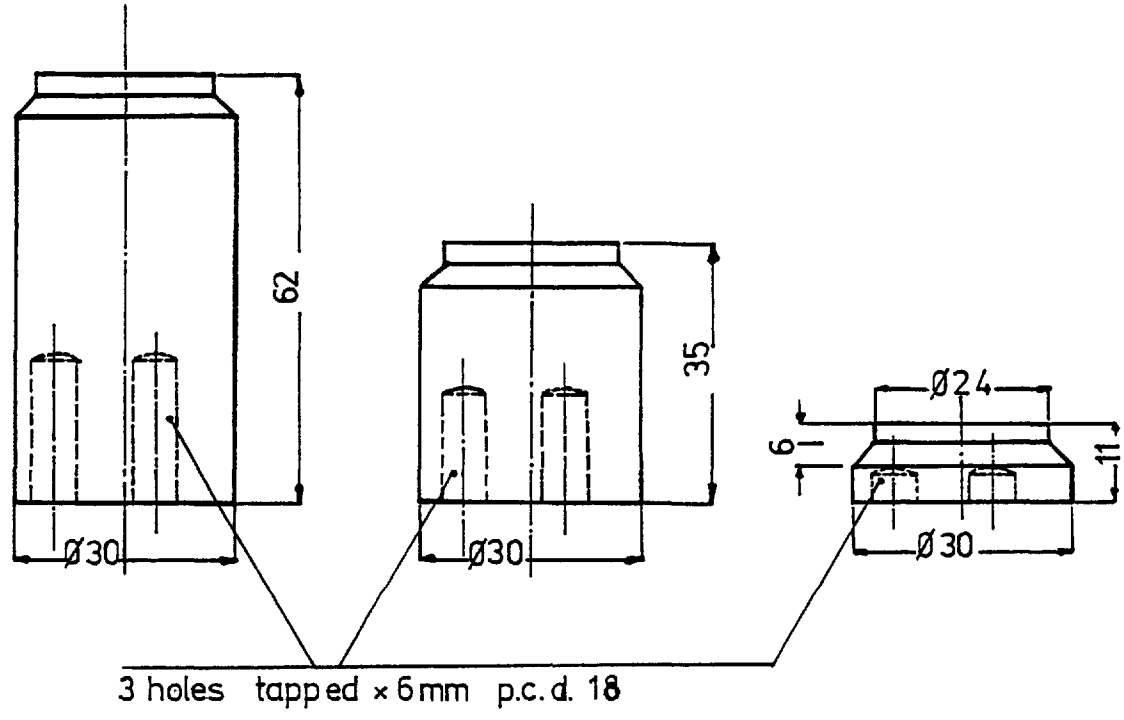
The bottom and top plates were machined from mild steel to 160 mm diameter and 25 mm thickness. Six 20 mm diameter holes were drilled through the bottom plate equidistant on a 120 mm pitch circle diameter for the six bolts of the frame, and three holes, 1/8" (3.17 mm) diameter on 18 mm pitch circle diameter were also drilled through the plate so that extension blocks could be attached to simulate punch travel during calibration.

The upper side of the top plate was threaded into the Harwood dead-weight tester (Fig. 4.5a), while the projection on the bottom plate fitted into the bore of the container, with a standard O-ring and anti-extrusion mitre ring to seal the fluid.

Tie rods supported the load on the end plates due to fluid pressure.

Six adaptors (Fig. 4.6) of various lengths have been used to find the effect of different seal and punch positions on the strain gauge readings during calibration. Filler blocks (Fig. 4.7) were used for reducing the quantity of fluid in the containers to a minimum for safety, with longitudinal grooves around their circumference, and also on their end faces, to ensure the free circulation of fluid.

A die shaped adaptor with a seal was used in the calibration of the forward extrusion container (Fig. 4.7).



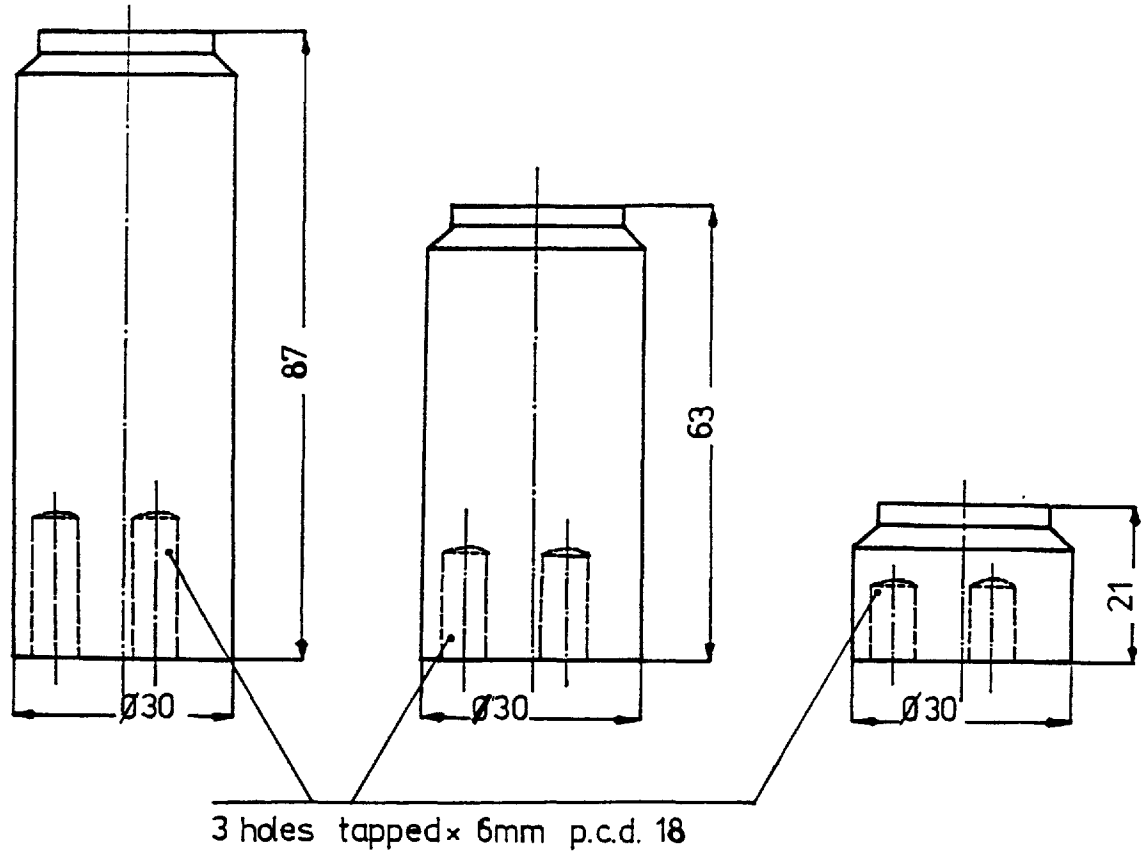
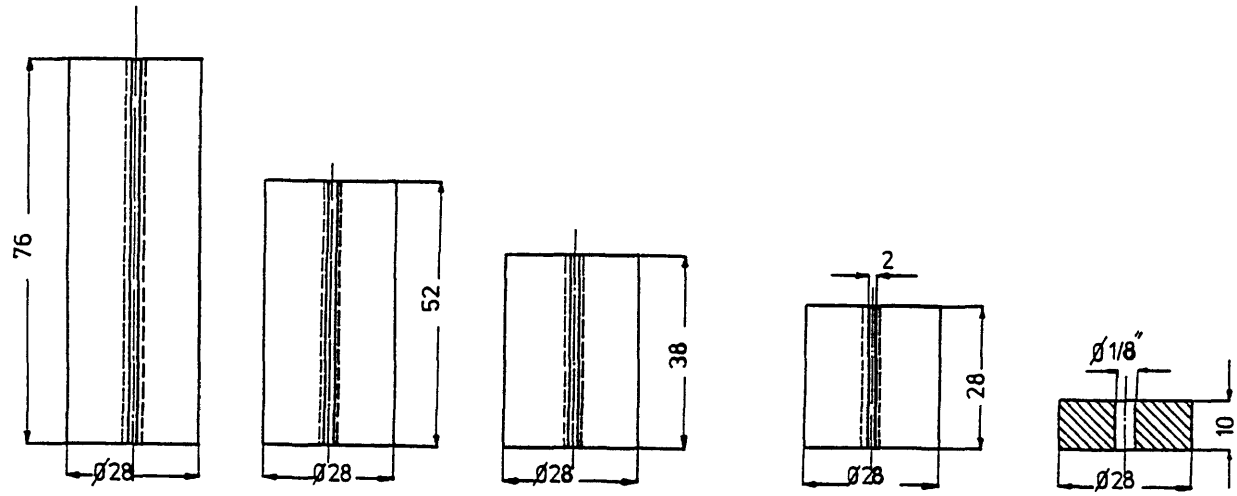
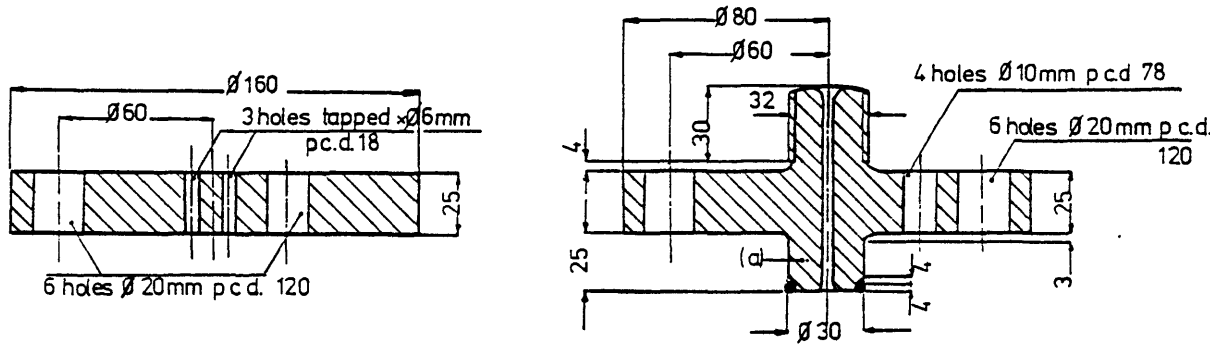


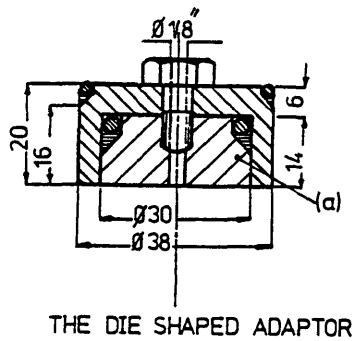
Fig. 4.6 The Extrusion Blocks.



THE GROOVED BLOCKS (or SPACERS)



THE BOTTOM AND TOP PLATES OF CALIBRATION ASSEMBLY (Scale. 1/2)



THE DIE SHAPED ADAPTOR

Fig. 4.7 The Calibration Components.

4.2.3 Instrumentation

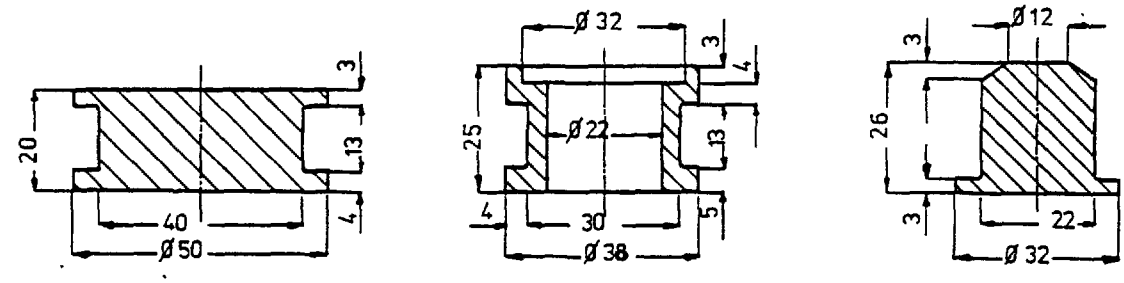
The apparatus for measuring and recording the experimental data includes container strain gauges, strain gauge load cells to measure loads on the pressure pads and dies and a variable resistance type displacement transducer to measure punch displacement. All strain gauges and the displacement transducer were connected to a SOLARTRON LP 1029 Digital Data Recorder to record the output data.

Five strain gauge load cells (Fig. 4.8) were made, four solid steel cylinders, one thin-walled steel tube.

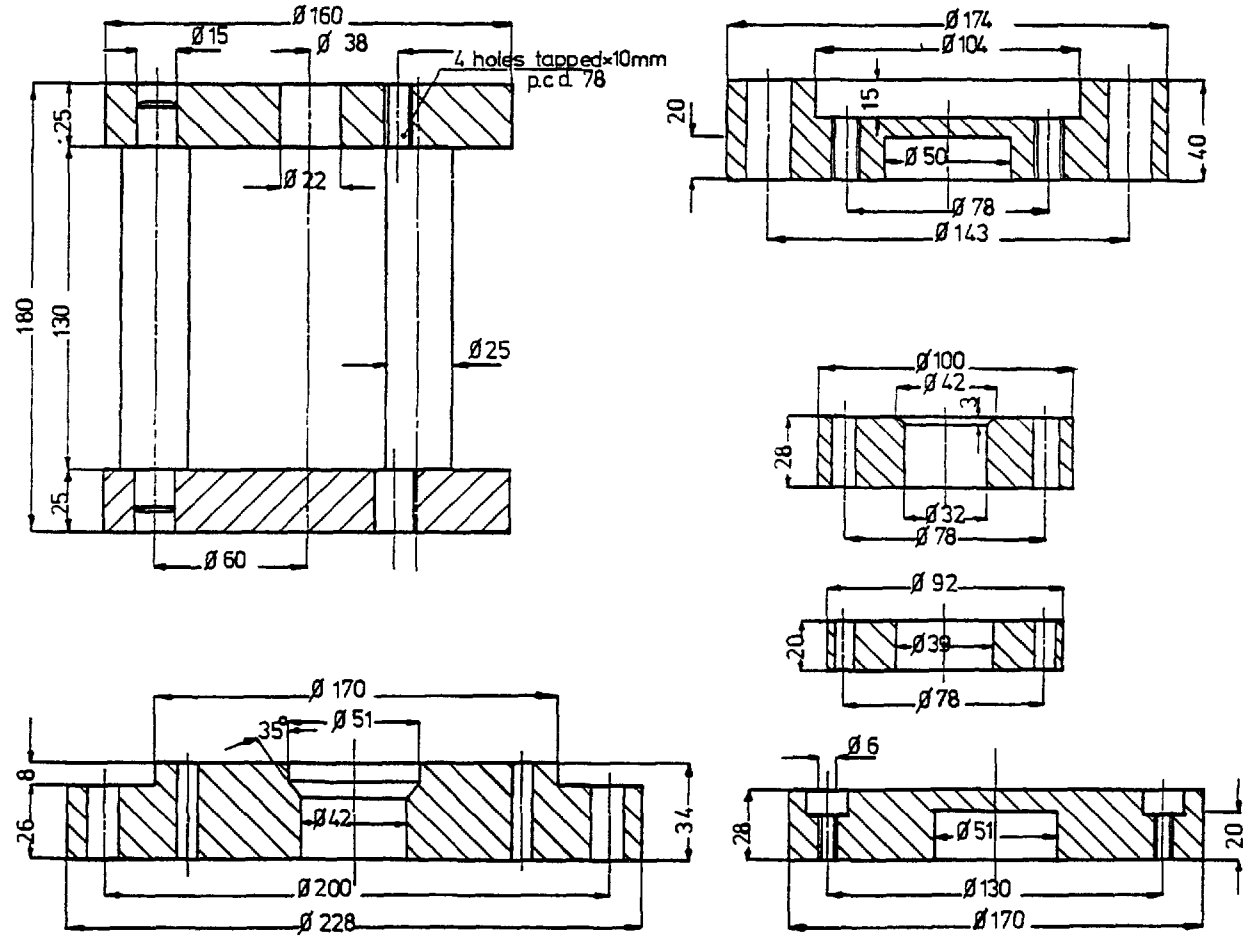
The load cell used behind the pressure pad in forward extrusion and under the punch insert in backward extrusion was made from EN24 steel and heat-treated to 45 RC hardness. Four strain gauges were attached to it, two in the hoop and two in the axial directions, equidistant and alternating around the circumference. They were wired according to Fig. 4.9 and then connected to the digital data recorder.

The die load cell in forward extrusion was also made from EN24 steel, with a central hole for the extrusion product to pass through it during extrusion. It was heat-treated and wired as the load cell described in the preceeding paragraph.

A die load cell in forward extrusion was used for two main purposes; to support the forward extrusion container and to measure the die load to compare it with the readings of



THE STRAIN GAUGE LOAD CELLS



THE SUPPORT PLATES (Scale 1/2)

Fig. 4.8 The Extrusion Components.

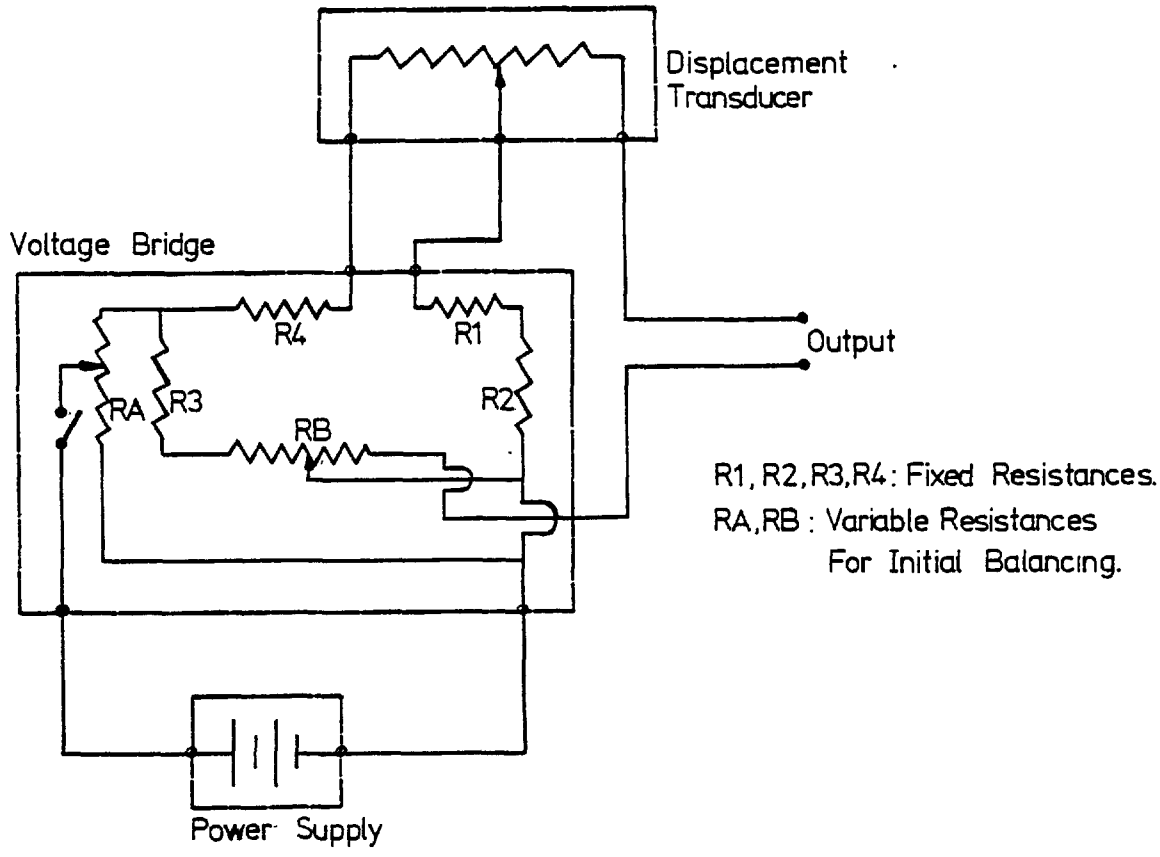
the punch load cell. It was made from EN24 steel, with two plates and four tie rods (Fig 4.1a) and heat-treated. Eight strain gauges were attached to it, one in the hoop and one in the axial directions on each tie rod and wired as described before.

The pressure pad load cell in backward extrusion was also made from EN24 steel, with a reduced diameter at the top for supporting the pressure pad. It was heat-treated and wired as Fig. 4.9.

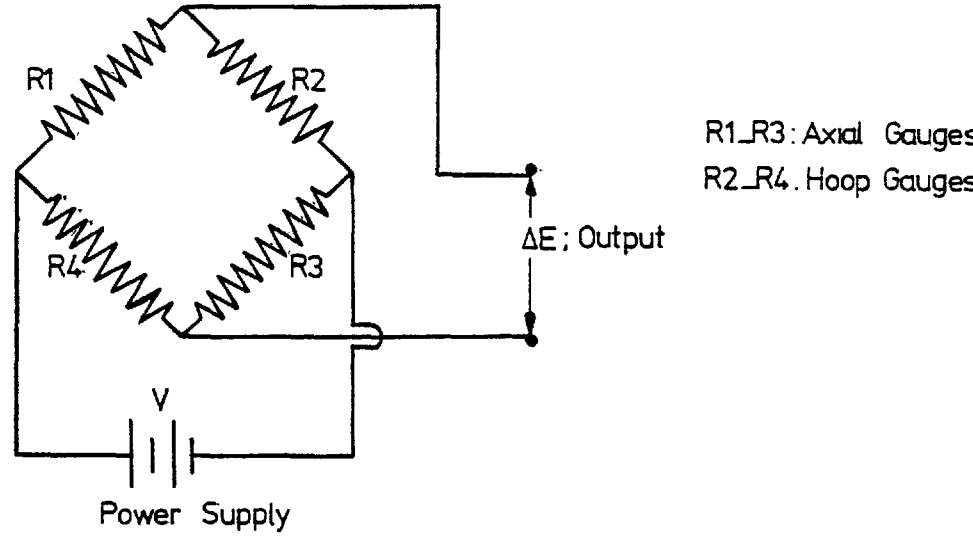
The displacement transducer was a variable resistance type and its wiring is shown in Fig. 4.9 . It was fixed to the crossheads of the testing machine. A voltage bridge was used for initial balancing.

Thirteen strain gauges were bonded onto the outside diameter of each container, eight to measure hoop strains and five for axial strains. The gauge positions can be seen in Fig. 4.2.

The strain gauges were supplied by Micro-Measurements Inc. together with the M-Bond 200 bonding kit. The hoop strain gauges of type EA-06-19CDK-120 were long and narrow (1.9" (48.26 mm) gauge length and 0.028" (0.71 mm) grid width) to provide a good average measurement of the hoop strain. The axial gauges were of the type EA-06-250BG-120 with 1/8" (3.175 mm) gauge length. The gauge factor (dimensionless and used in the calculation of strains in Section 4.4)for



DISPLACEMENT TRANSDUCER WIRING DIAGRAM.



THE WHEATSTONE BRIDGE ARRANGEMENT FOR LOAD CELLS.

Fig. 4.9 Circuit connections.

the hoop and axial gauges were 2.09 ± 0.5 % and 2.06 ± 0.5 %, at 75° F (24° C), with cross-sensitivity factors of - 0.5 % and + 0.5 % respectively. The small value of cross sensitivity was particularly useful for minimising the effect of strain across the gauges.

All gauges were temperature compensated for use on steel and had a resistance of 120.0 ± 15 % ohms.

The gauges were stuck onto the container following the instructions of the gauge manufacturers and wired according to Fig. 4.10. They were covered with a protective coating of Arøldite adhesive hardener to protect them during experiments and connected to the strain gauge bridge of the recorder.

The active and compensating circumferential and axial gauges formed 13 half bridges which were energised simultaneously by the supply voltage. The 13 junctions connecting the active and compensating gauges in each bridge, together with the two common wires carrying the constant supply voltage across all the bridges, were taken out of the containers through miniature plugs (Fig. 4.1d). The 13 half bridges were connected to 13 channels in a 100 channel data recorder, each of which constitute the other half of the bridge. The connection between each of the two half bridges were made externally through two junction boxes, one for the dummy gauges and the other for the active ones.

The Solarton LP 1029 Digital Data Recorder can scan the output data in sequence at speeds varying between 10 samples

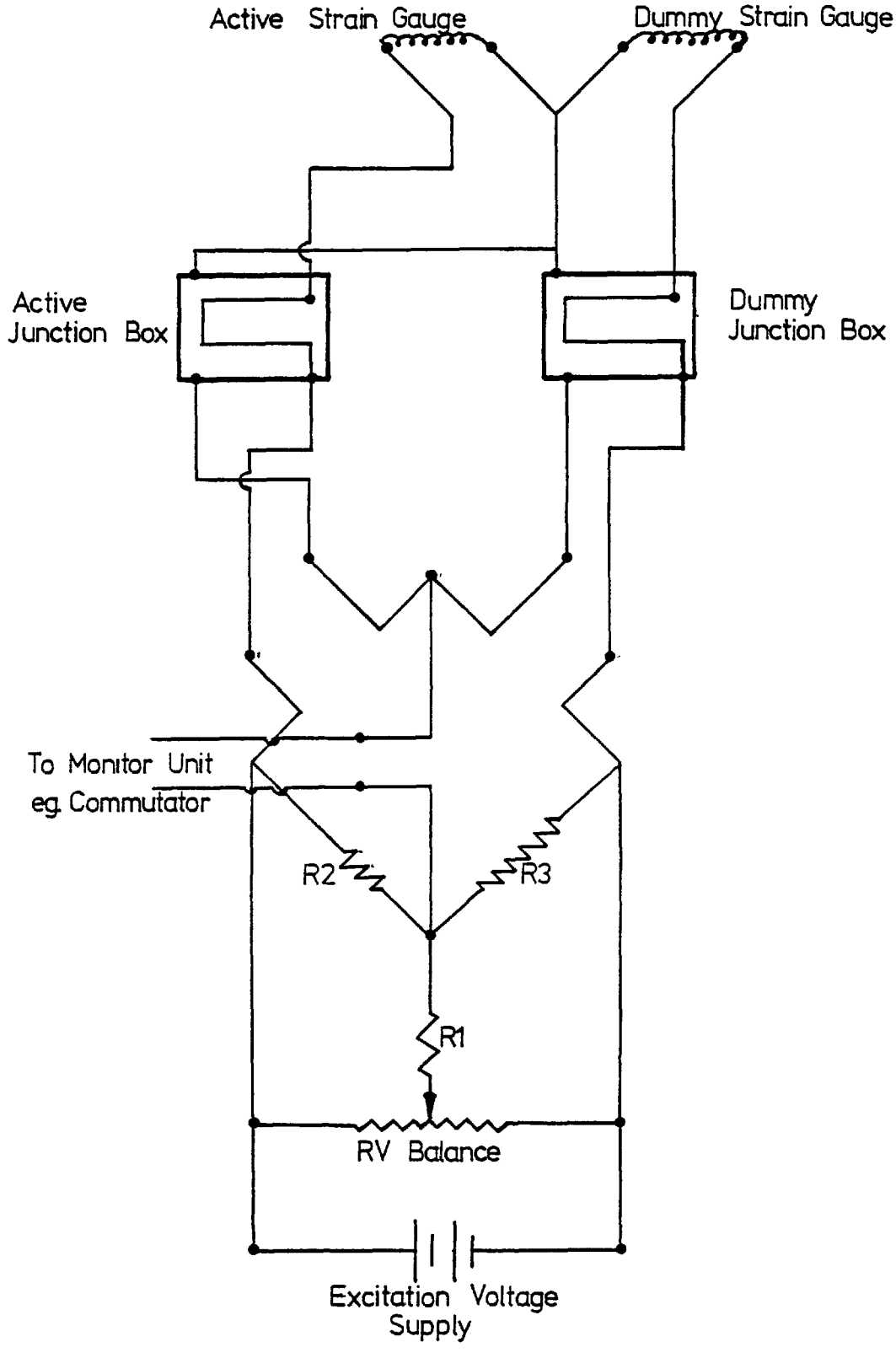


Fig. 4.10 BRIDGE CIRCUIT CONNECTIONS FOR CONTAINER STRAIN GAUGES.

per second and one sample in every four seconds. Thus, at low extrusion speeds a single scan of the seventeen channels (13 channels for container strain gauges, one for the displacement transducer and three channels for the load cells) used in the experiments could be regarded as the simultaneous recording of all data.

The digital logging machine was used for recording the experimental data from the strain gauge load cells, the displacement transducer and the container strain gauges. The analogue signals were converted into digital form and their values printed on a paper strip using an electronic printer or they could be punched onto a paper tape. The digital values could also be observed on an in-line illuminated display unit.

4.3 Calibration of the Apparatus

The strain gauge load cells and displacement transducer were calibrated in a high precision testing machine, while known pressures were applied to the bore of the containers in a Harwood Controlled Clearance Piston Gauge when calibrating the container strain gauges.

In the calibration of the strain gauge load cells, displacement transducer and container strain gauges, the Solartron Data Recorder was set at a scanning speed of four channels per second, a constant bridge supply voltage of 6 volts and a print out position of voltmeter of x 100 mV

(an incremental strain-induced output for the bridge in milli-volts). The supply voltage of the displacement transducer was set at 25 volts (Fig. 4.9) . This setting provided consistent readings with good accuracy throughout the calibration and thus proved very satisfactory.

The strain gauge load cells were calibrated against known compressive loads using the 120,000 lbf (∿ 534 kN) high precision Tinius Olsen testing machine. The load cells were stress-cycled by applying maximum loads of between 35,000 lbf (∿ 156 kN) and 60,000 lbf (∿ 267 kN) several times until the output of each load cell was constant for those loads.

Each load cell was then loaded in steps of 5,000 lbf (∿ 22 kN) up to a predetermined maximum load of the load cell, recording the output with the Solartron Recorder. This was repeated for each load cell until constant readings were achieved and calibration curves of loads against output in millivolts were drawn.

The displacement transducer was calibrated in conjunction with the Solartron Recorder. Readings were taken at different positions of the punch and the calibration curve of punch travel against the printout of the machine was then drawn.

The calibration assembly as seen in Fig. 4.5a was used for calibrating the container strain gauges. The hoop

and axial strain gauges were calibrated against known internal fluid pressures applied to the extrusion containers using the Harwood deadweight testing machine. The whole calibration equipment was set up by first assembling the calibration unit and then securely attaching the unit to the testing machine. At the second step, the apparatus was tested for leaks and then each container was stress-cycled by applying a fluid pressure of 30,000 lbf/in^2 ($\sim$ 207 MN/m^2) several times until all the strain gauge readings were found to be consistent.

The strain gauge readings were adjusted to zero before pressure was applied, using the balancing points of the strain gauge bridge of the Data Recorder. In steps of 3,000 lbf/in^2 ($\sim$ 21 MN/m^2) pressure was then applied up to a maximum of 30,000 lbf/in^2 ($\sim$ 207 MN/m^2) and all the strain gauge readings recorded and repeated several times until they remained constant for particular internal pressures. The 11 mm long adaptor (Fig. 4.6) was set in position in the first calibration of the forward extrusion container, simulating a punch travel of 11 mm from the open end. A second and third set of calibrations of the strain gauges of this container were then carried out at "punch travels" of 35 mm and 62 mm respectively, by using adaptors of the appropriate length.

The calibration of the strain gauges of the backward extrusion container was carried out in the same manner. In the first, second and third set of calibrations of the strain gauges the adaptors positioned in the container were of 21 mm,

63 mm and 87 mm length. In all calibrations, one of the containers was used as a dummy container.

The strain gauge readings were then plotted against internal pressures applied to the bore of the containers for each set of calibrations at various adaptor (punch) positions. It was found that these were straight lines but their slopes (pressures per millivolt) change. Two types of calibration curve for each hoop strain gauge were plotted.

a) Internal applied pressure against hoop strains for each position of the punch in the container.

b) For each applied internal pressure, punch (adaptor) position against hoop strains.

Some of the gauges gave slightly different results from the others. Slight (although repeatable) non-linear behaviour of some of the gauges was also noticed. These variations were attributed to minor misalignments of the gauges in the circumferential and axial directions and to variation in cement thickness.

4.4 Calibration Results

The strain gauge load cells, displacement transducer and the container strain gauges were calibrated in a high precision testing machine, in situ and in a Harwood Controlled Piston Gauge respectively as described.

Fig. 4.4.1 shows the calibration curve for the displacement transducer, a straight line with a slope of 2.35 mm/mV change in output voltage recorded by the Solartron data recorder.

The calibration results for the strain gauge load cells as shown in Figs 4.4.2 to Fig 4.4.5 are straight lines with slopes of 9.09 kN/mV, 29.28kN/mV, 11.11 kN/mV and 44.44 kN/mV respectively.

The milli-volt readings recorded by the data recorder from the output of the container strain gauges were transformed to strains using the formula described by Murray and Stein {74}

$$\varepsilon_R = \frac{4 \cdot 10^3}{(GF)} \frac{\Delta E}{V}$$

where (GF) = Gauge factor supplied by manufacturers (given in 4.2.3)

ΔE = Millivolt output representing the resultant strain ε_R

V = Bridge supply voltage in volts

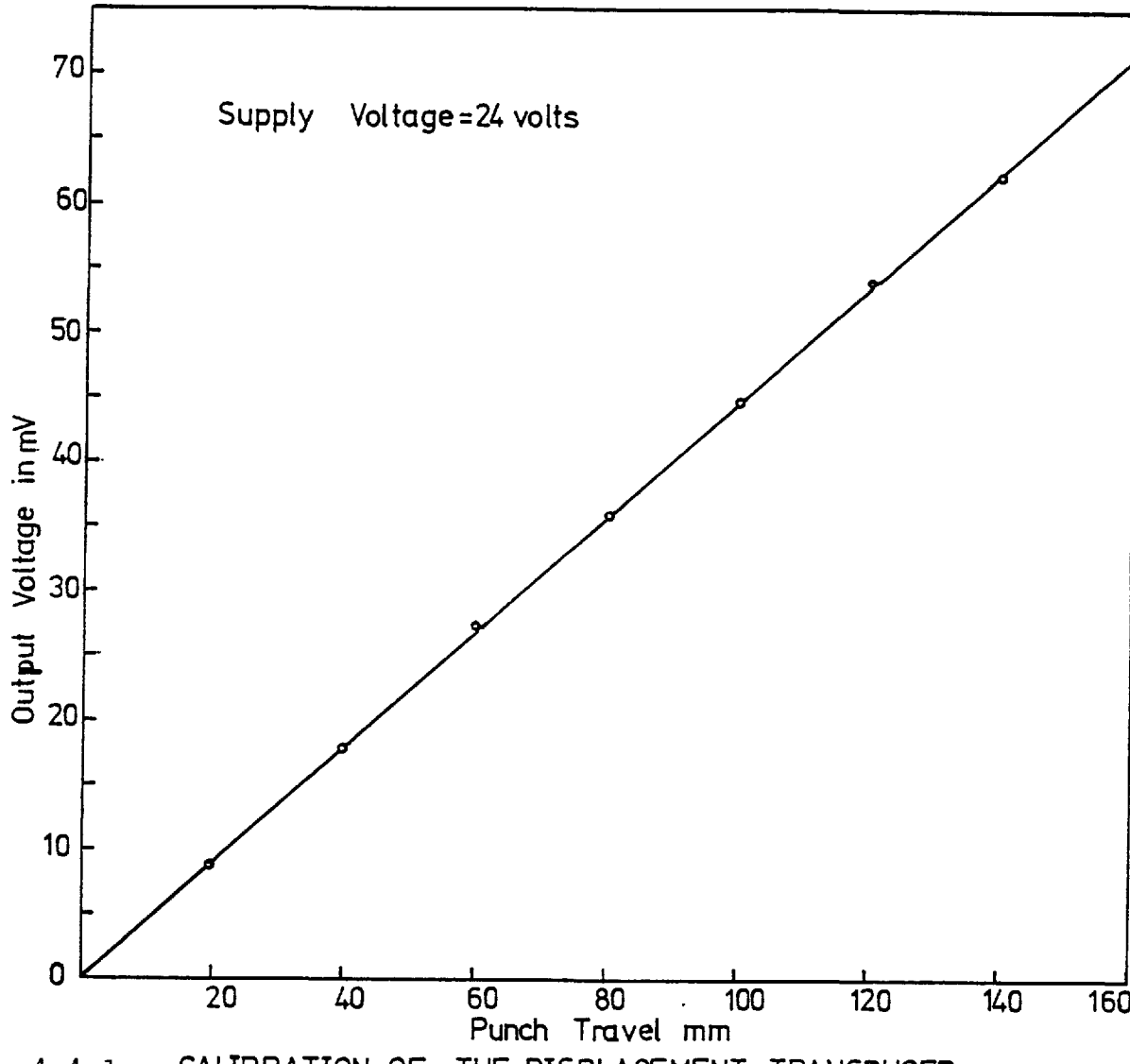


Fig. 4.4.1 CALIBRATION OF THE DISPLACEMENT TRANSDUCER.

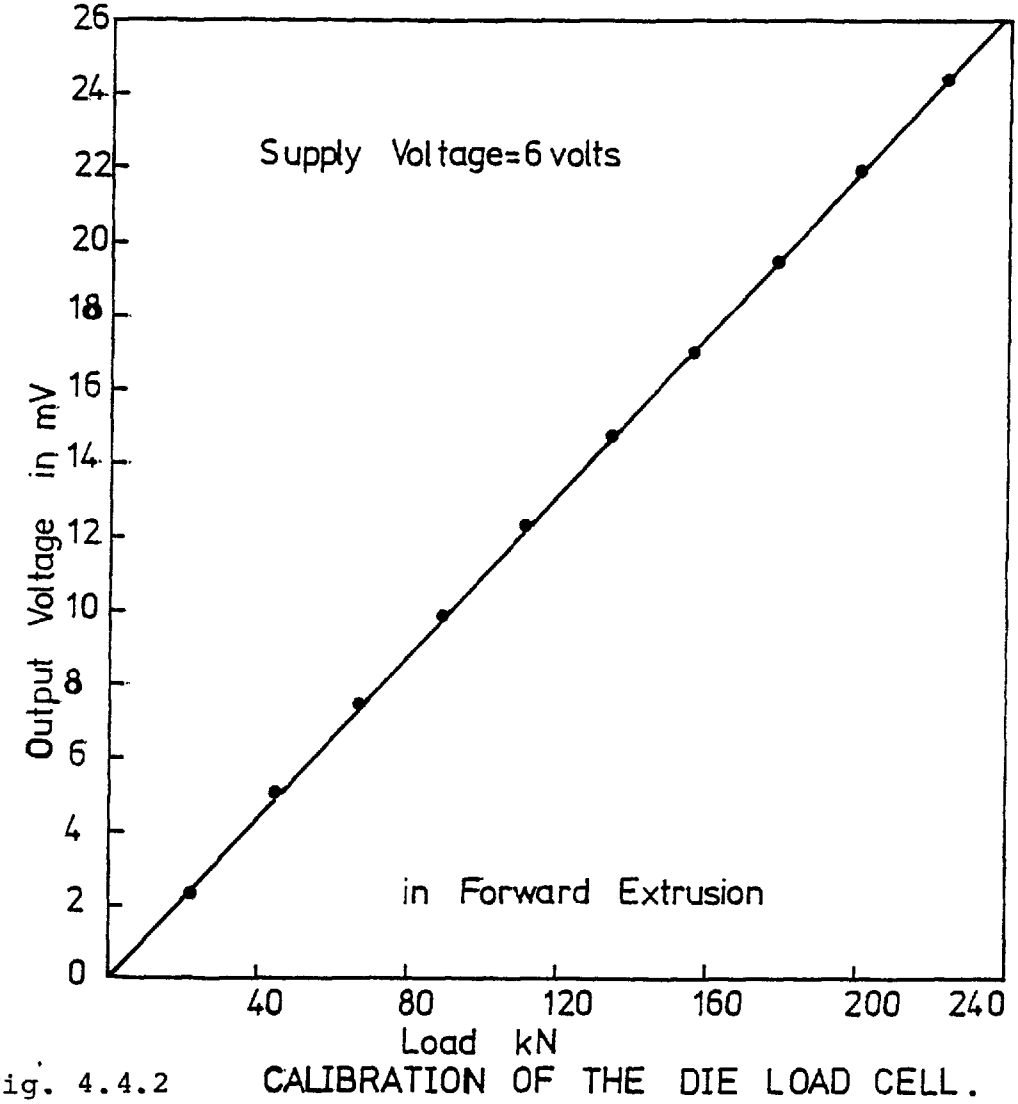


Fig. 4.4.2 CALIBRATION OF THE DIE LOAD CELL.

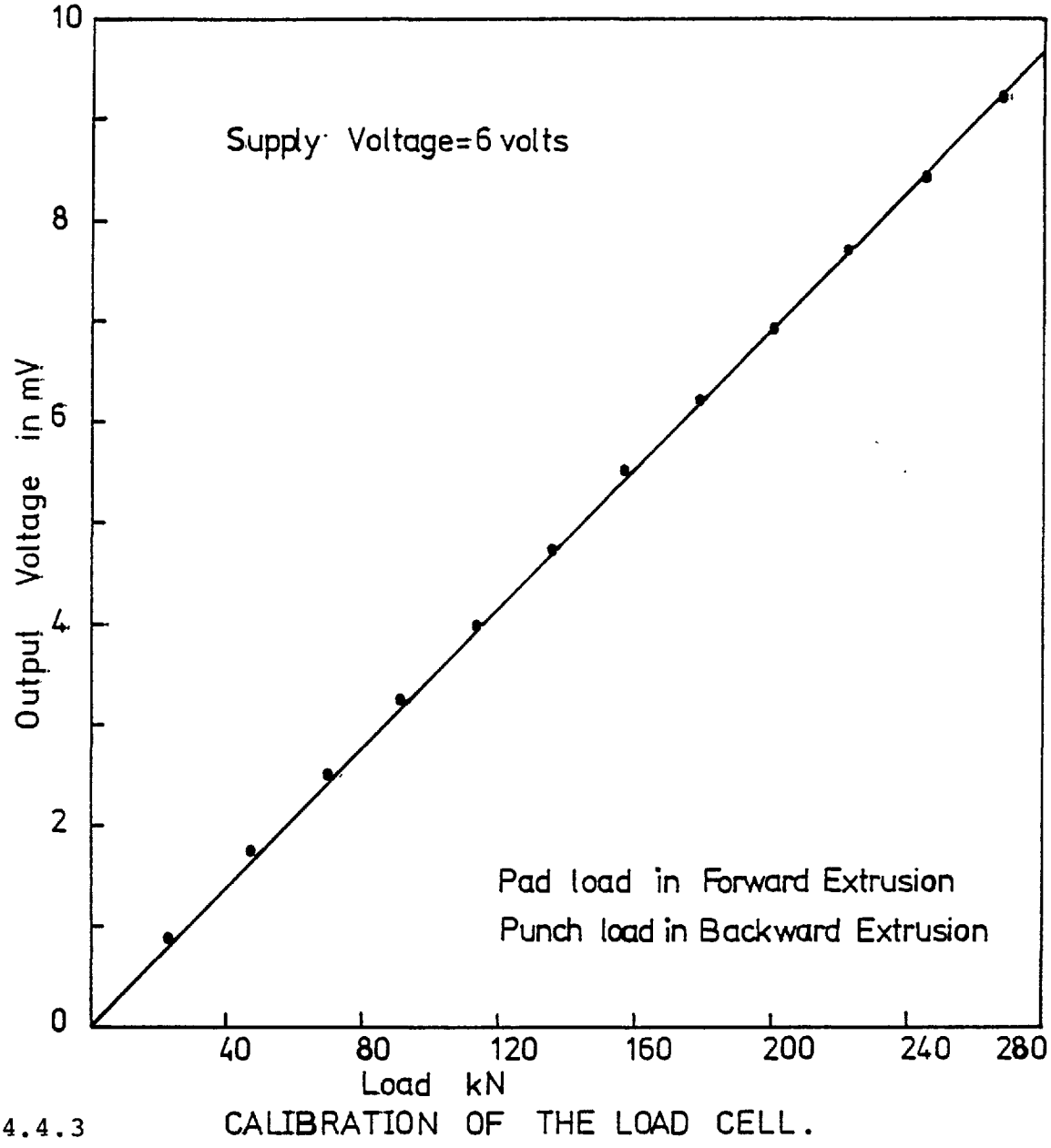


Fig. 4.4.3 CALIBRATION OF THE LOAD CELL.

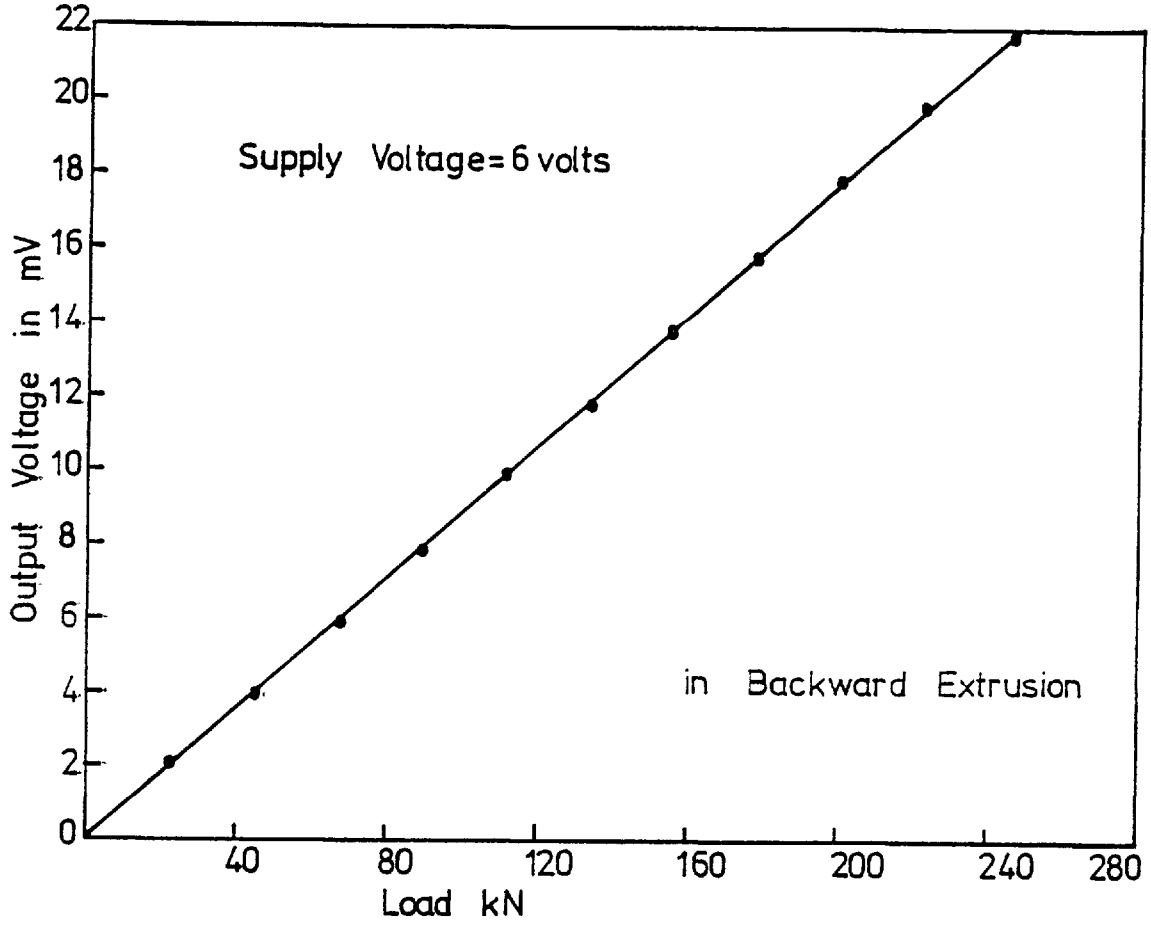


Fig. 4.4.4 CALIBRATION OF THE PAD LOAD CELL.

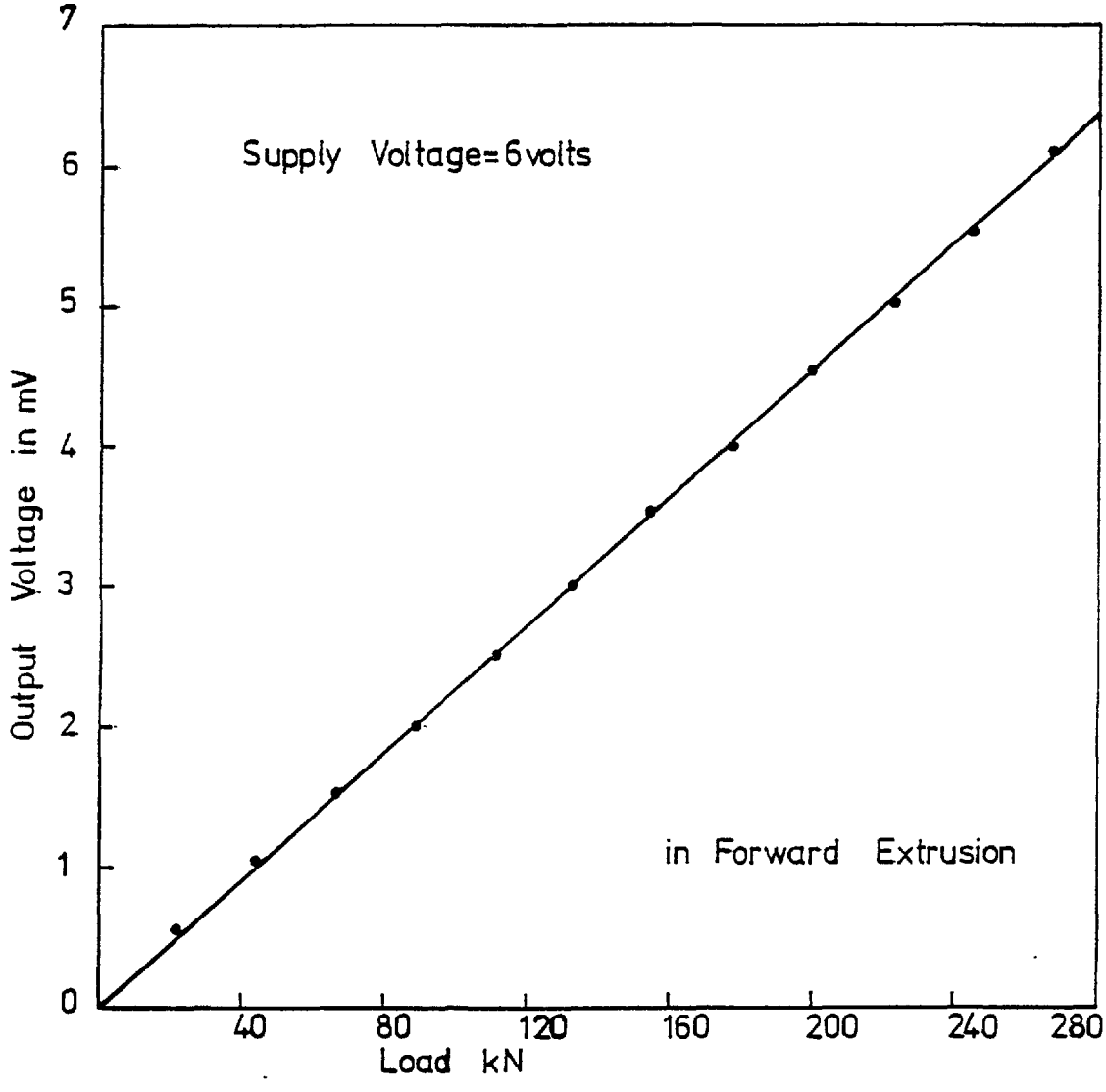


Fig. 4.4.5 Calibration of the Load Cell.

Thus for a gauge factor of 2.09 of the hoop strain gauges, one 2.06 for the axial gauges and a constant bridge supply voltage of 6 volts, the resultant strains are

$$\varepsilon_R(\text{hoop}) = \frac{4.10^3}{2.09}\,\frac{\Delta E}{6} = 3.189.10^2\ \Delta E \text{ micro strain}$$

and $$\varepsilon_R(\text{axial}) = \frac{4.10^3}{2.06}\,\frac{\Delta E}{6} = 3.236.10^2\ \Delta E \text{ micro strain}$$

Two sets of calibration curves for each hoop strain gauge of the containers are shown in Figs 4.4.6 to 4.4.21. The calibration results of each axial strain gauges are also plotted in Figs 4.4.22 to 4.4.26 which are straight lines but their slopes (pressure per millivolt) change.

On the whole the calibration results were consistent except that the axial strain gauges as well as the hoop strain gauges at the seals or near the seals gave slightly varied readings.

The calibration results obtained from the circumferential and axial strain gauges were compared with the results obtained from Lame's equations and the finite element analysis as described in Chapter 5.5.

Six of the eight hoop strain gauges gave similar results to those obtained from Lame's equations and the finite element analysis, and the other two (in the seal region) gave slightly different results within 8% of the theoretical ones.

The axial strains measured along the length of the containers had a magnitude of about 15% smaller than that obtained from the finite element analysis.

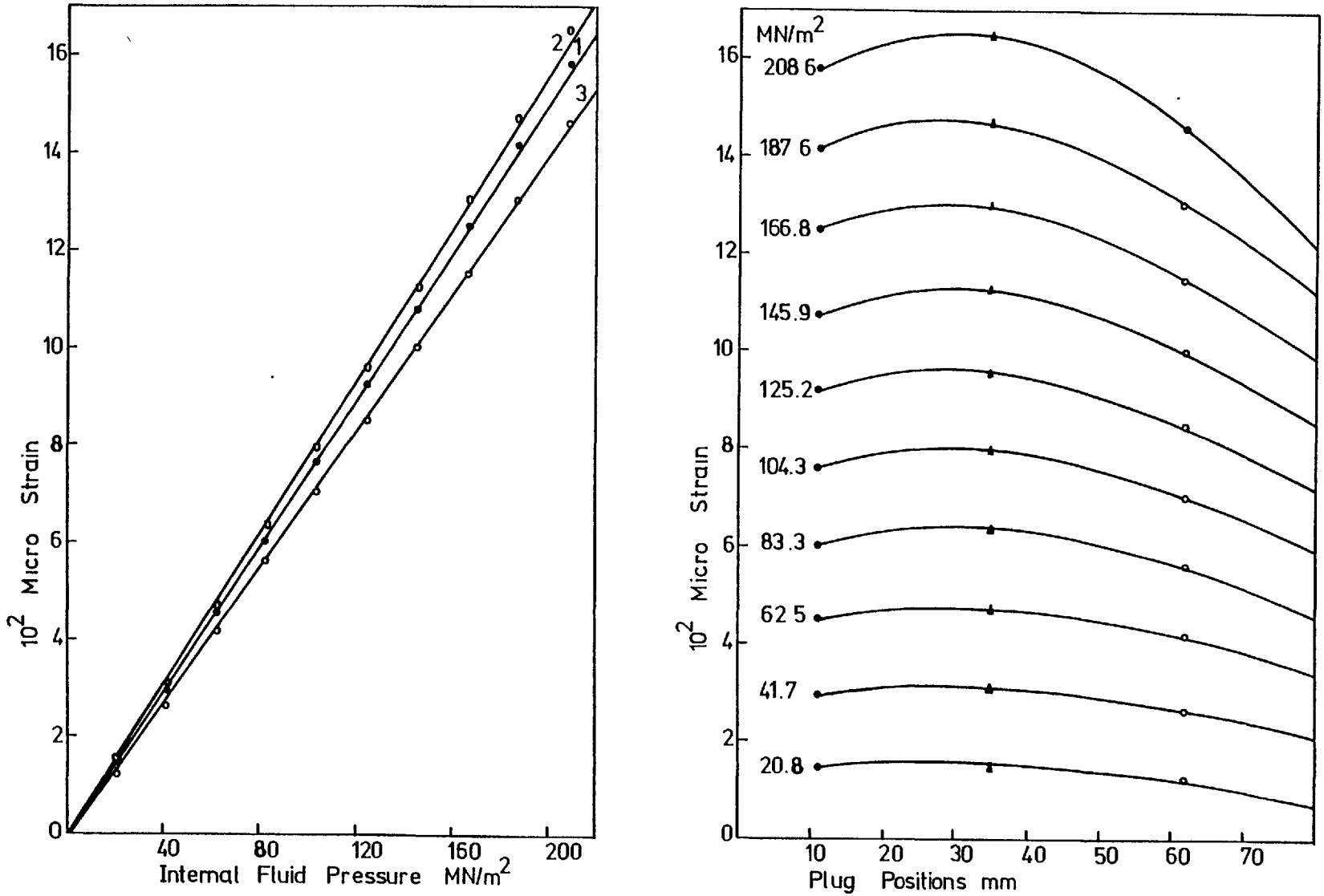


Fig. 4.4.6 Calibration of the Strain Gauge No. 6.

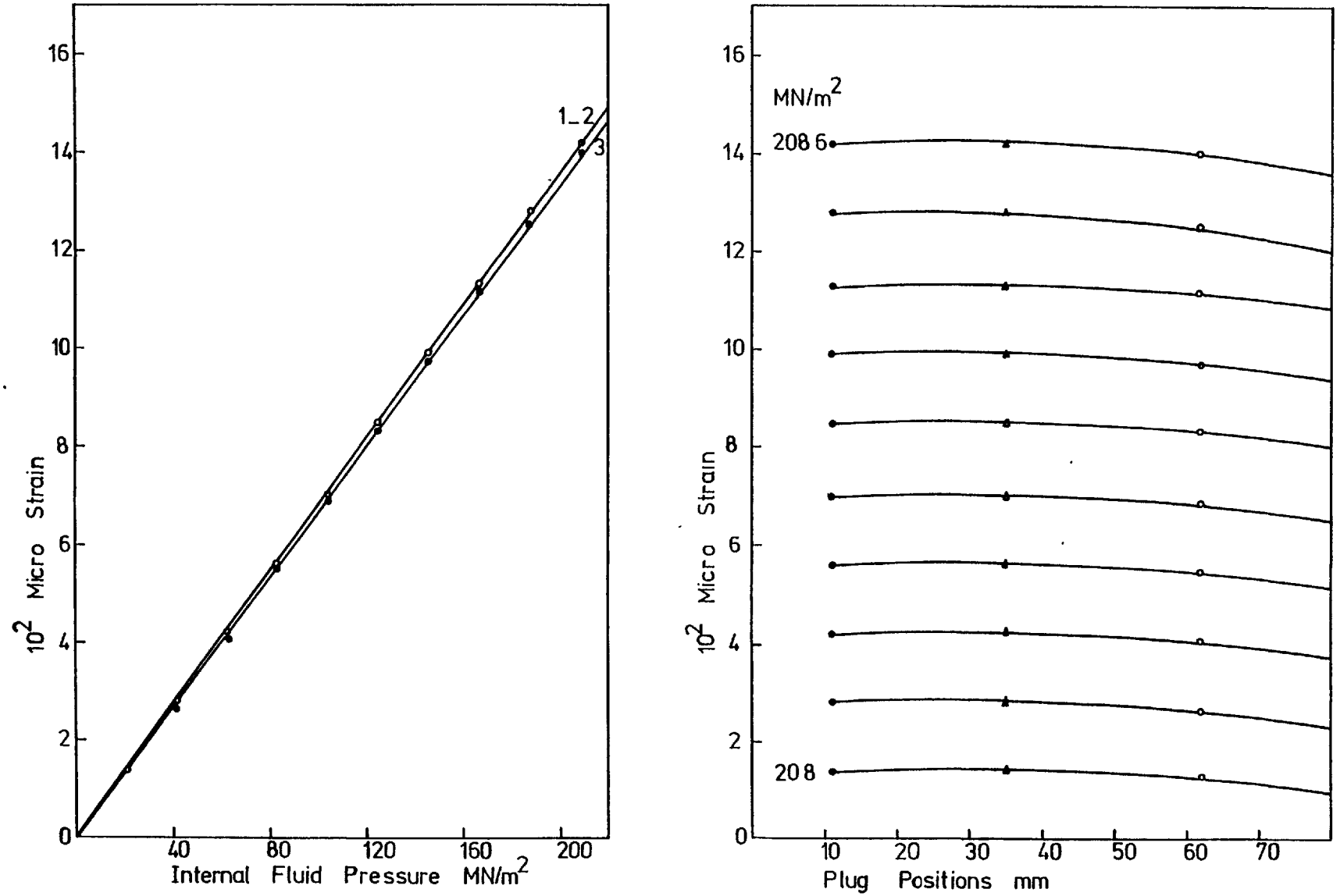


Fig. 4.4.7 Calibration of the Starin Gauge No. 7.

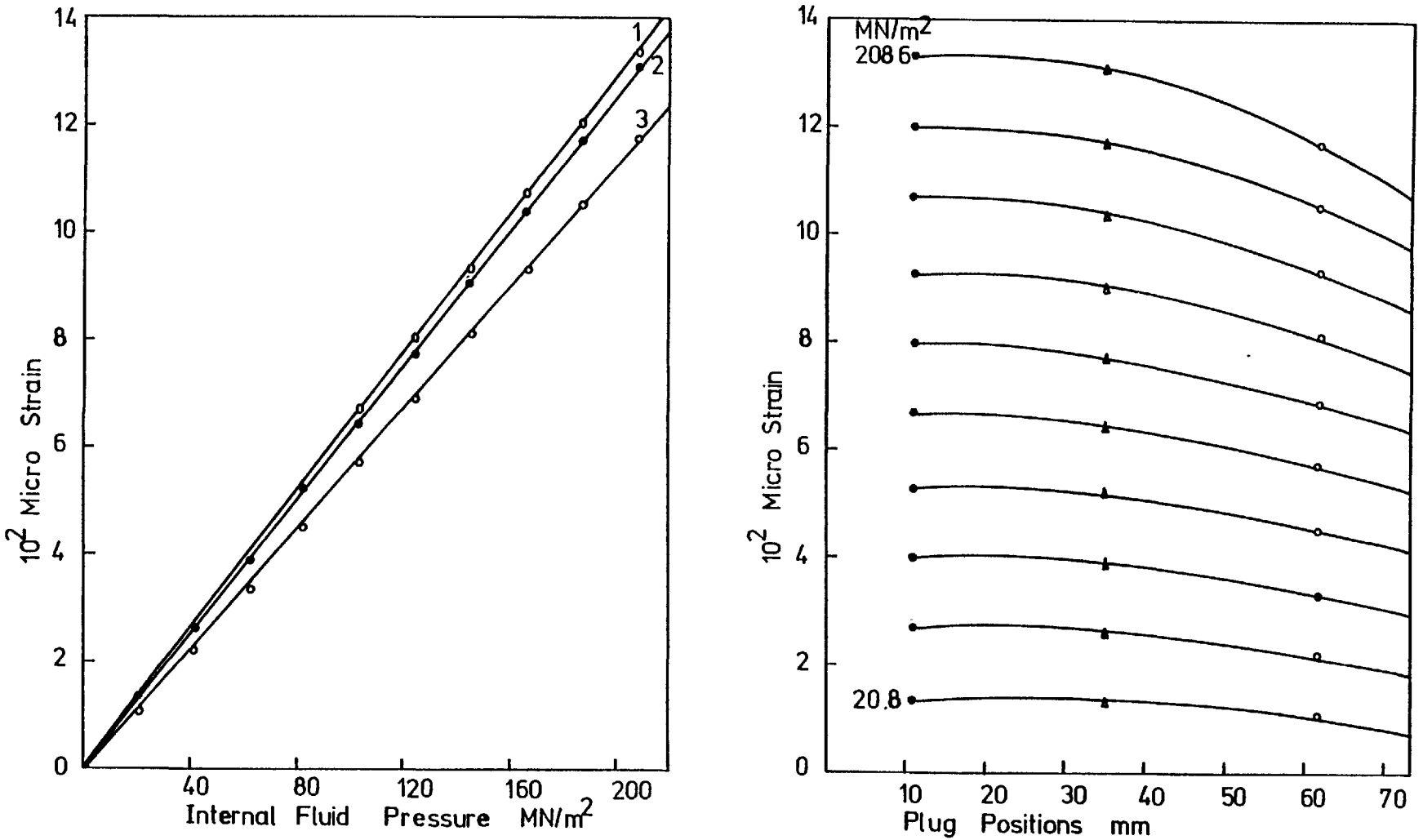


Fig. 4.4.8 Calibration of the Strain Gauge No. 8.

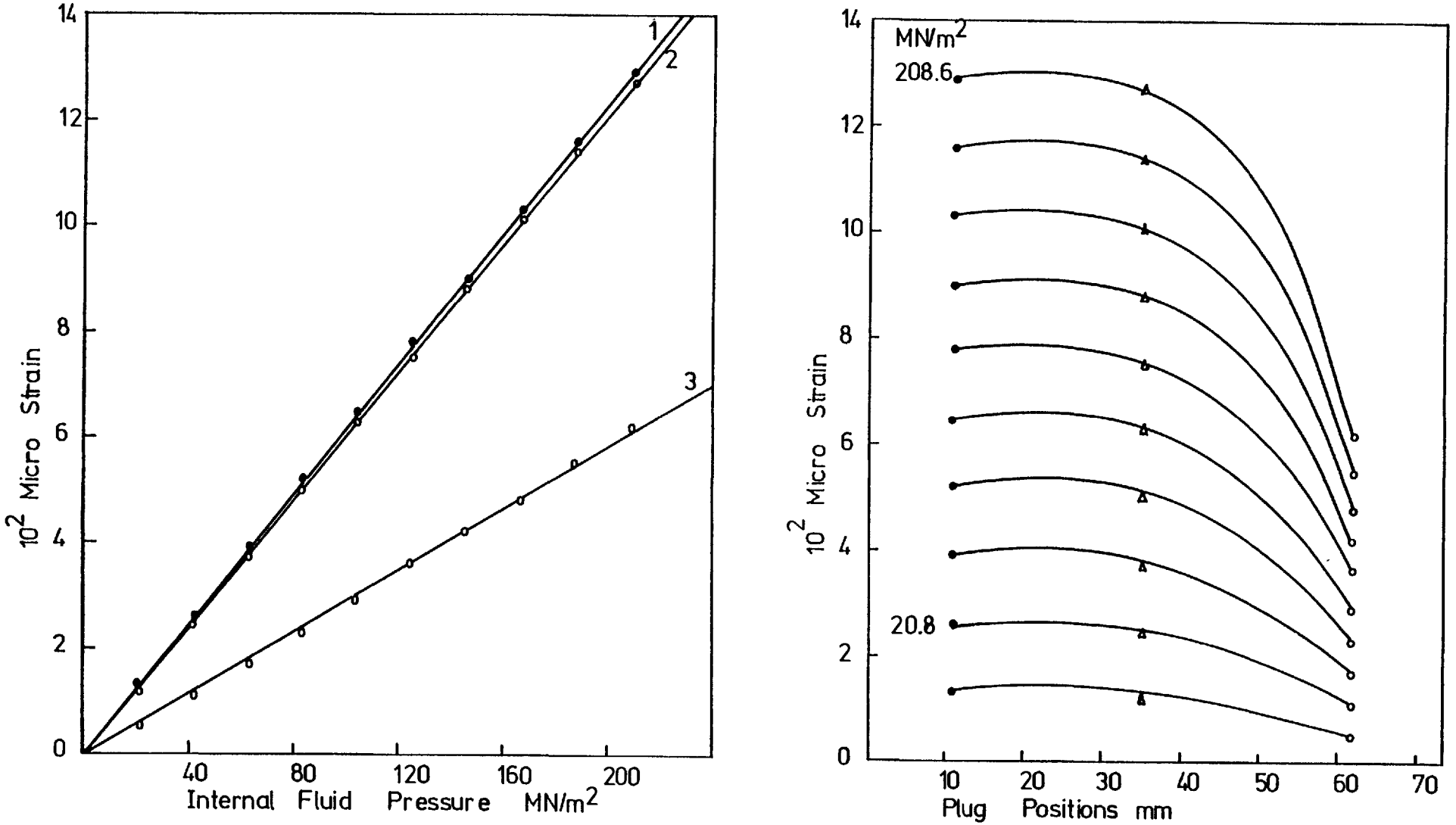
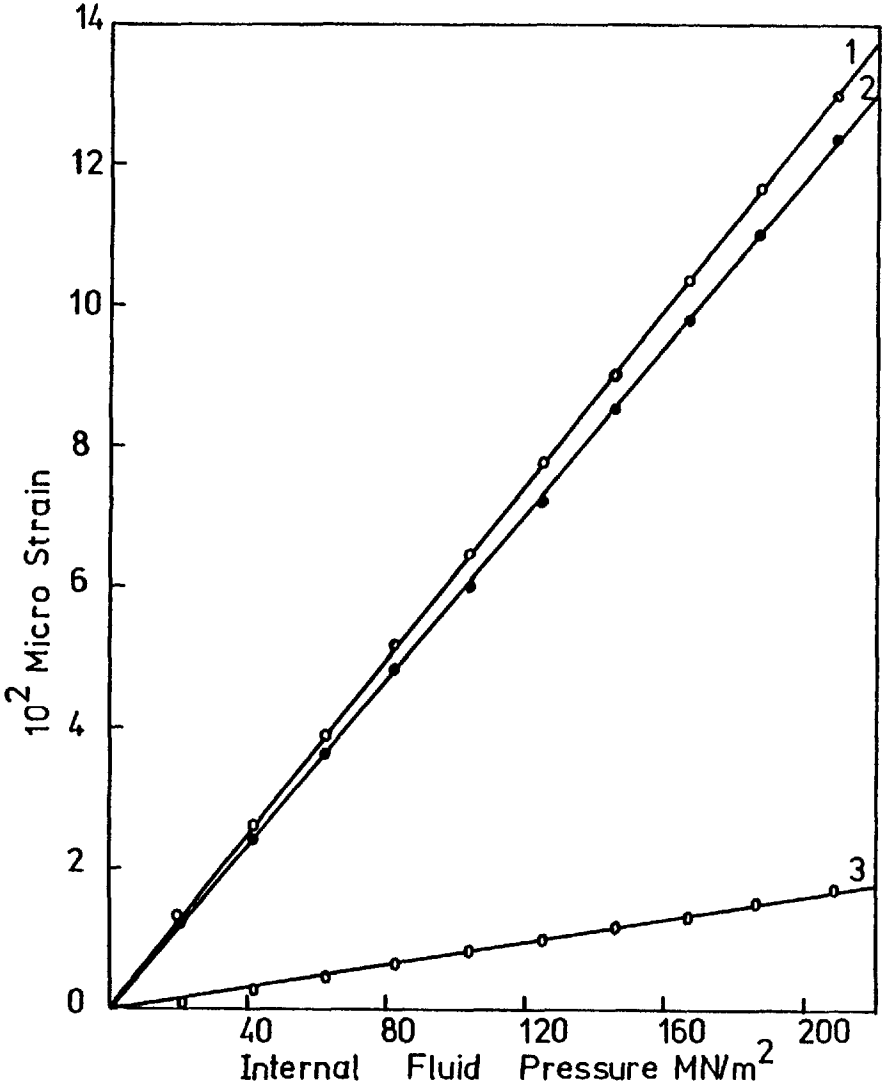


Fig. 4.4.9 Calibration of the Strain Gauge No. 9.



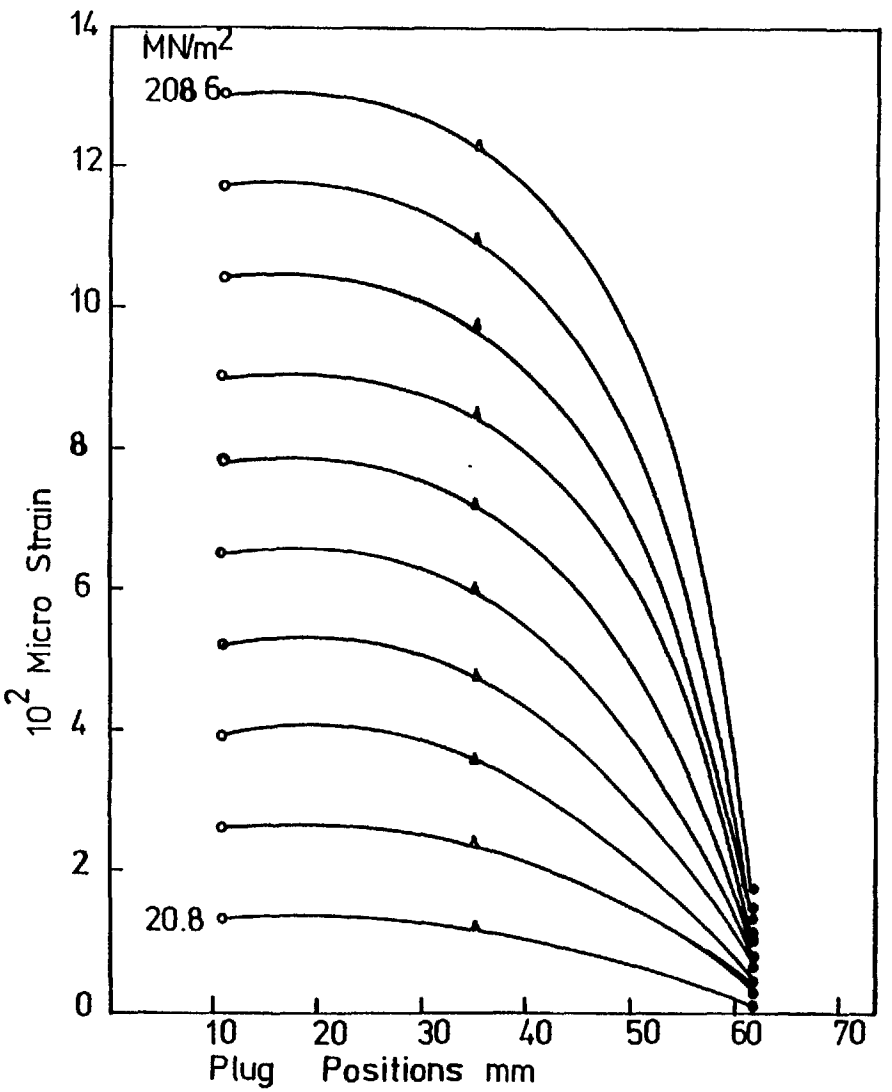
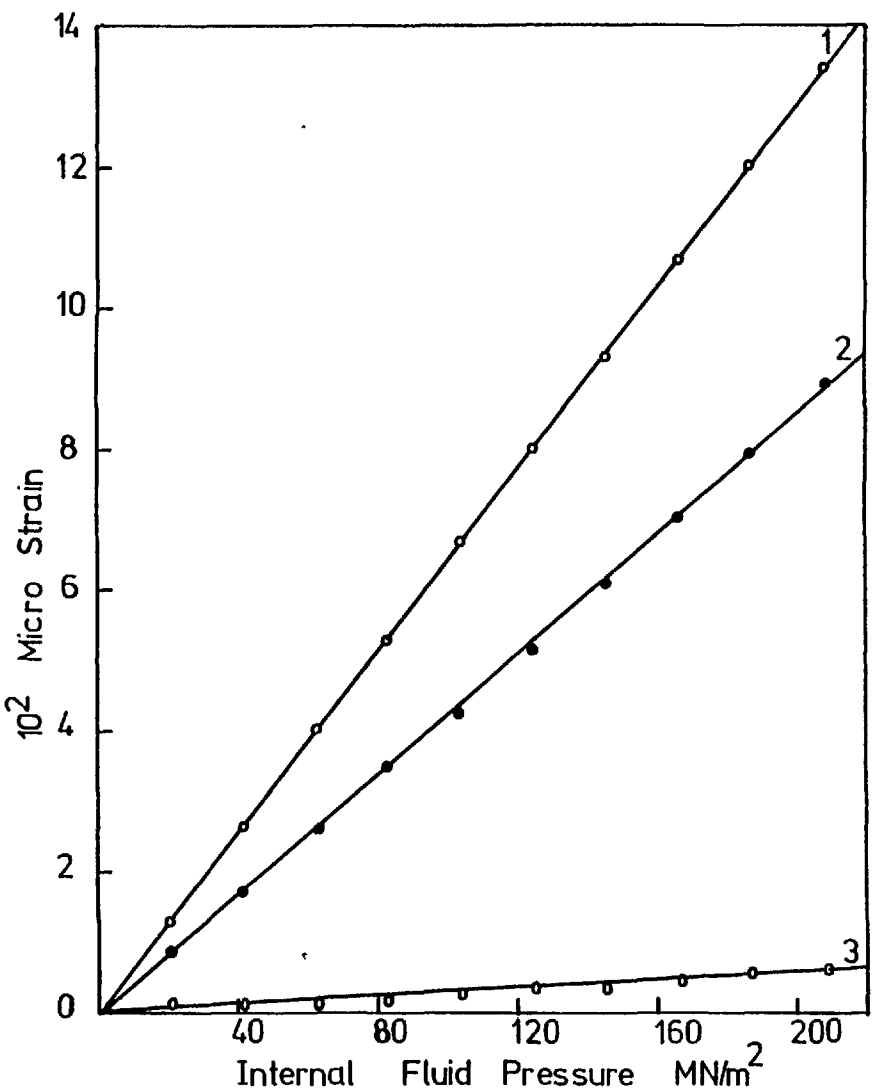


Fig. 4.4.10 Calibration of the Strain Gauge No. 10.



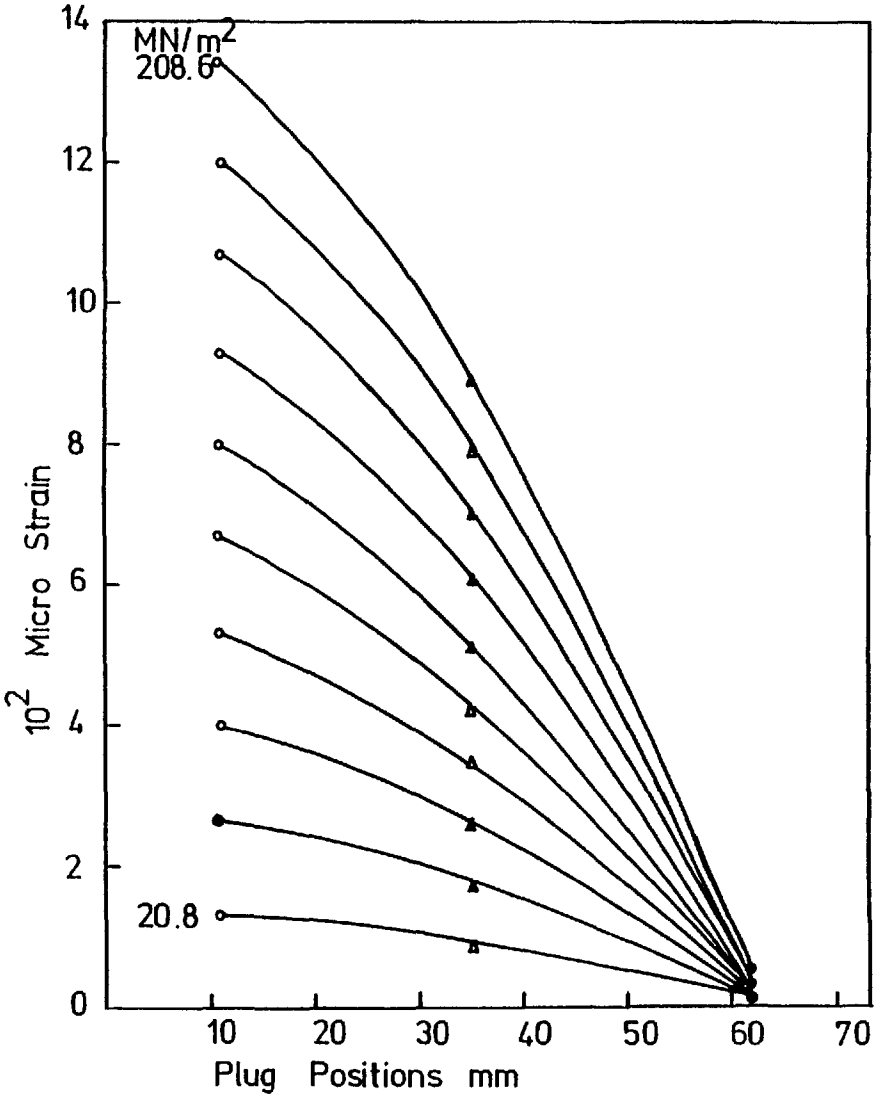


Fig. 4.4.11 Calibration of the Strain Gauge No. 11 .

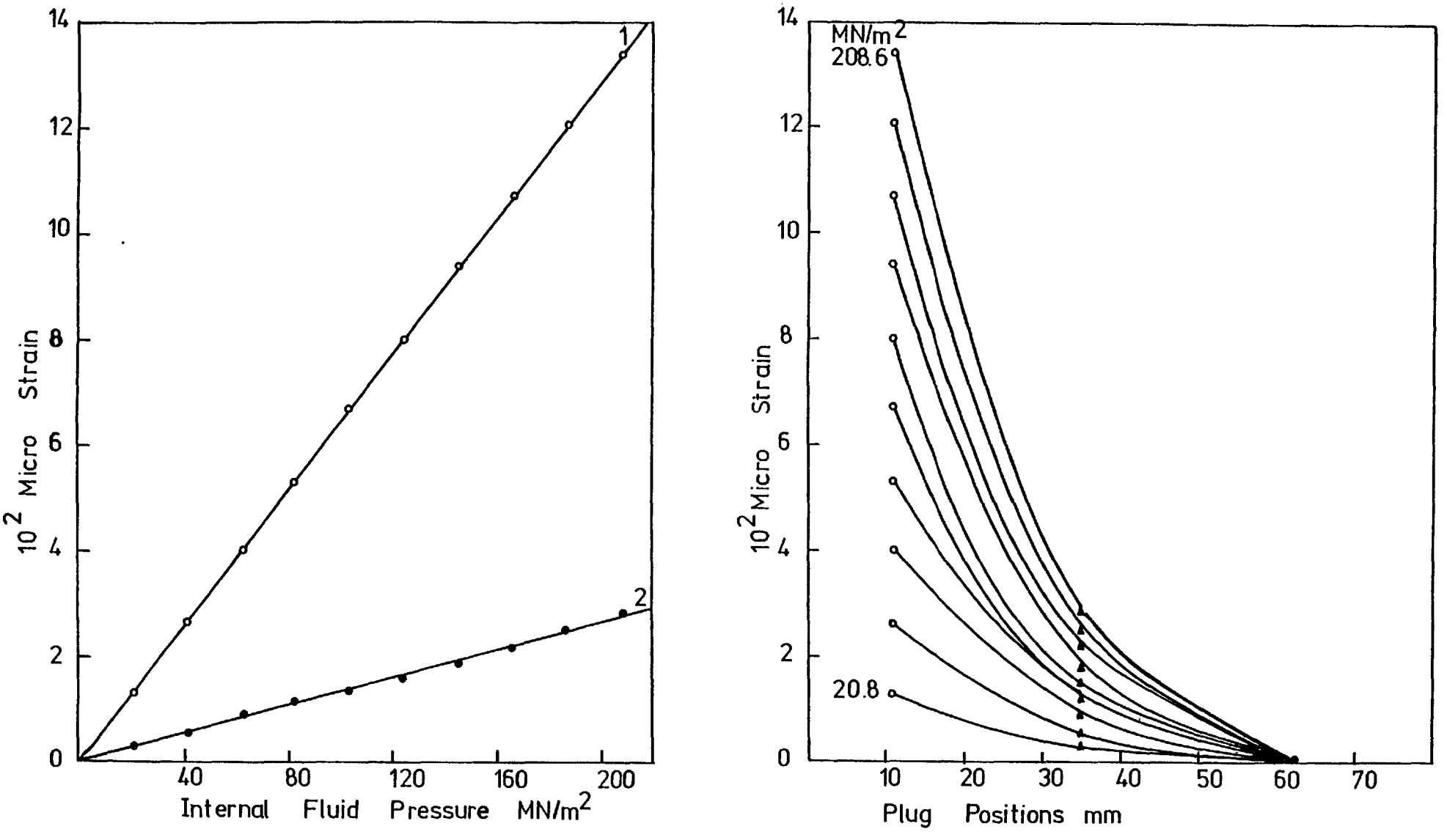
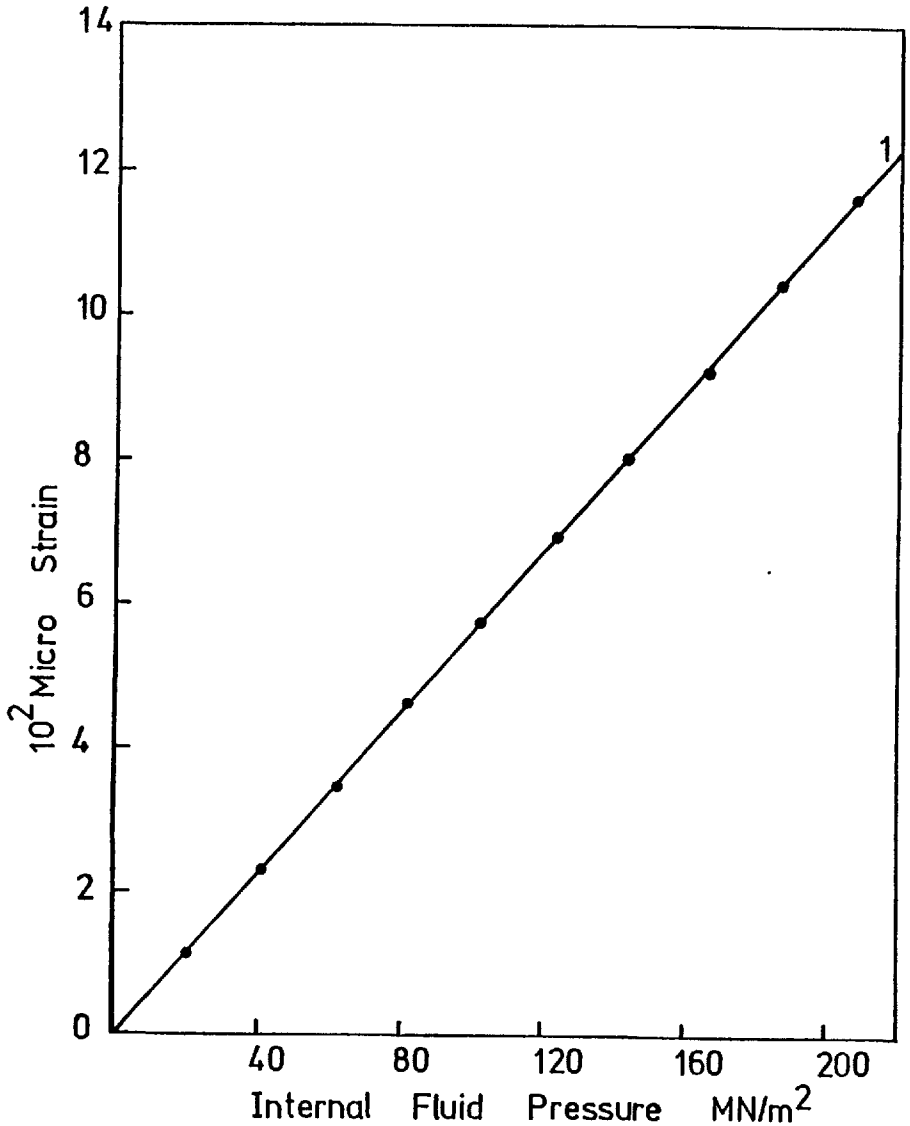


Fig. 4.4.12 Calibration of the Strain Gauge No. 12 .



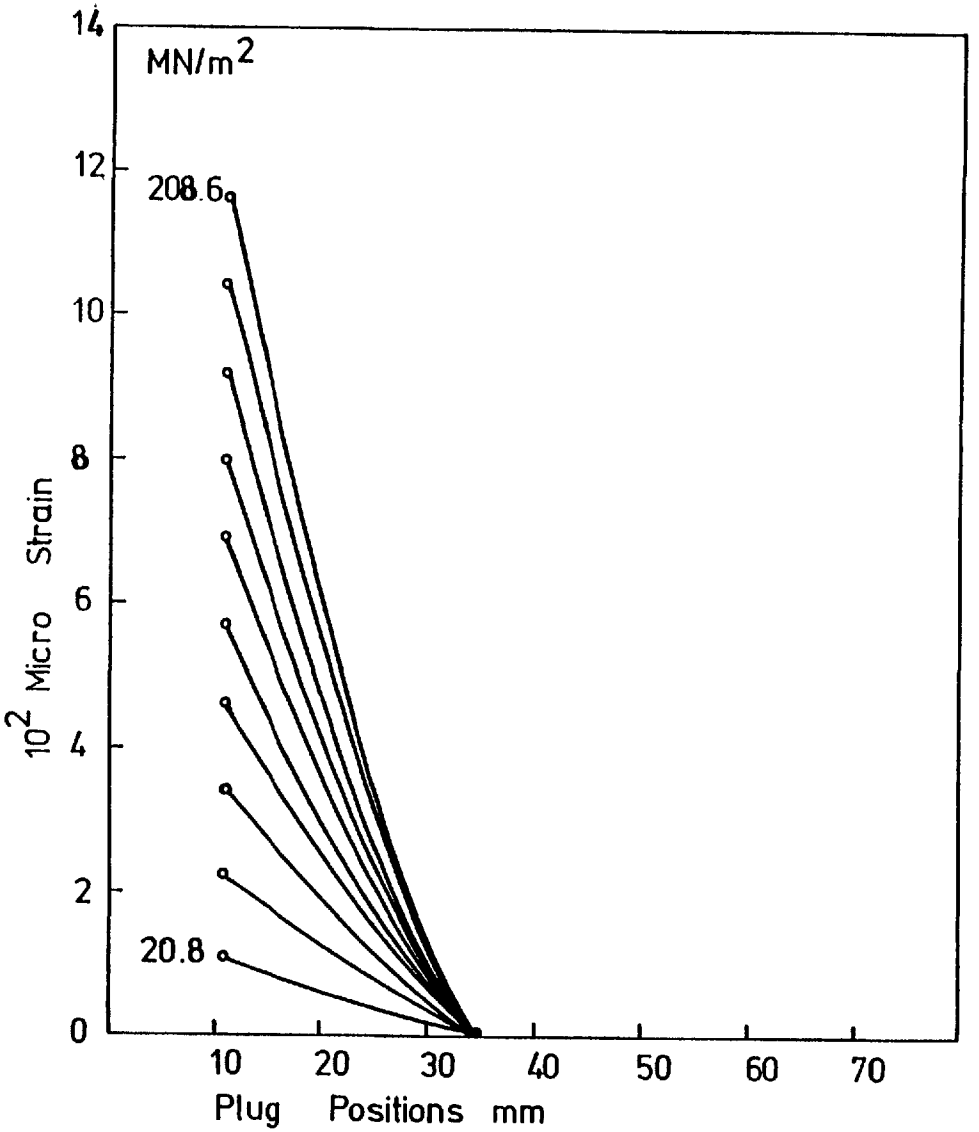
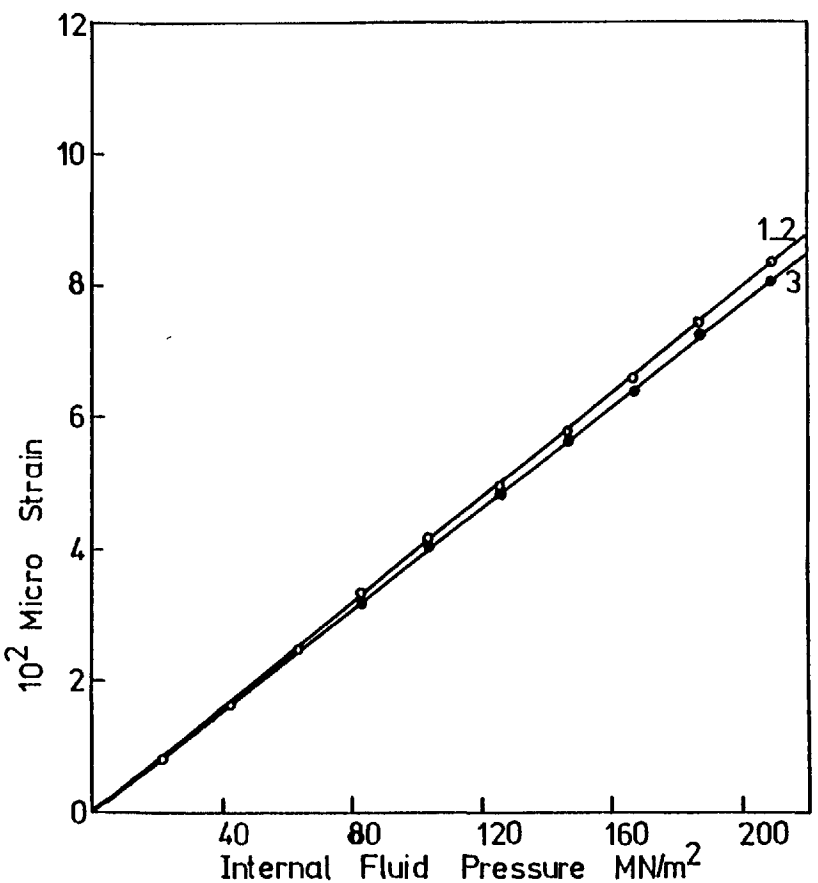


Fig. 4.4.13 Calibration of the Strain Gauge No. 13 .



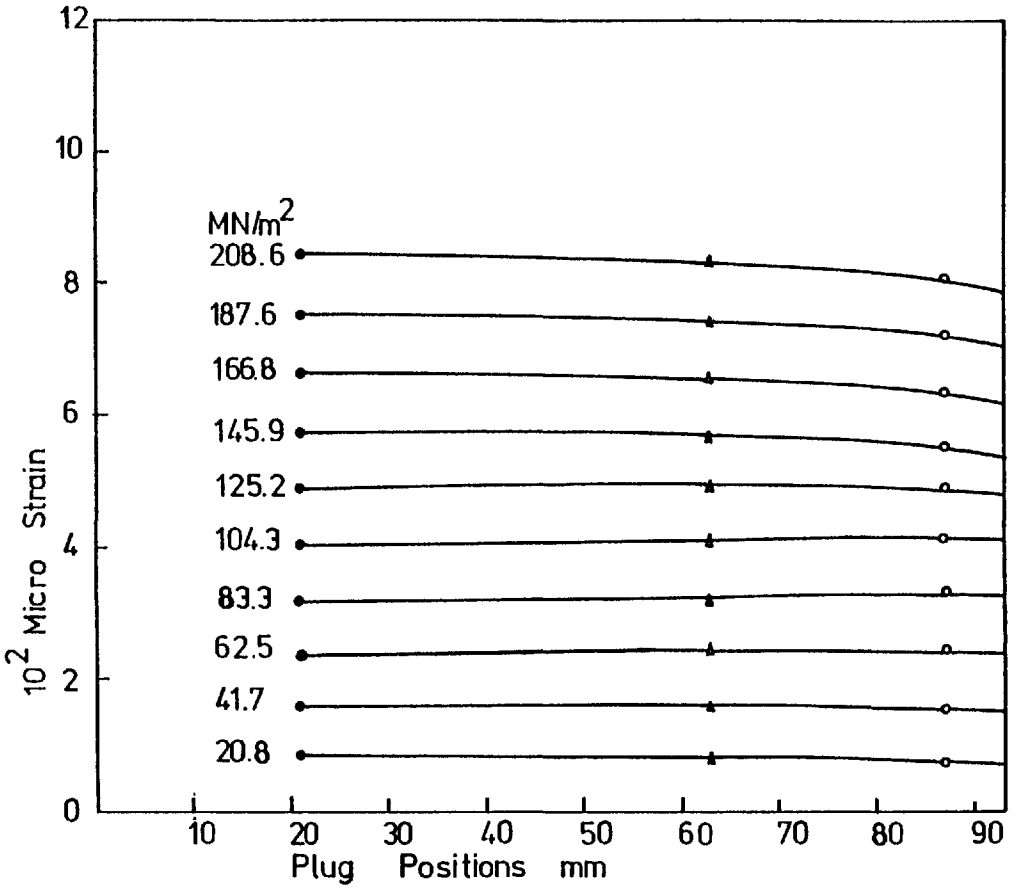


Fig. 4.4.14 Calibration of the Strain Gauge No. 6L .

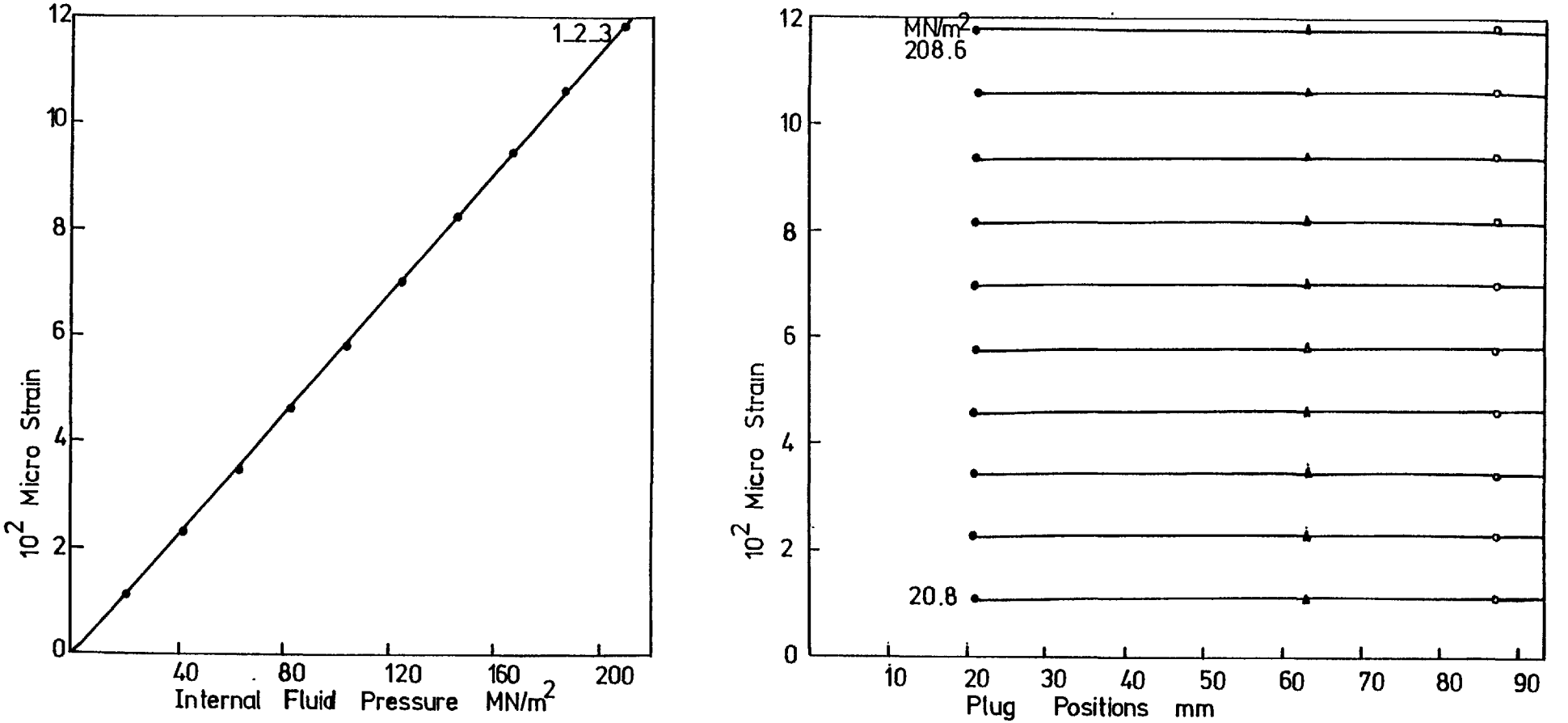


Fig. 4.4.15 Calibration of the Strain Gauge No. 7L .

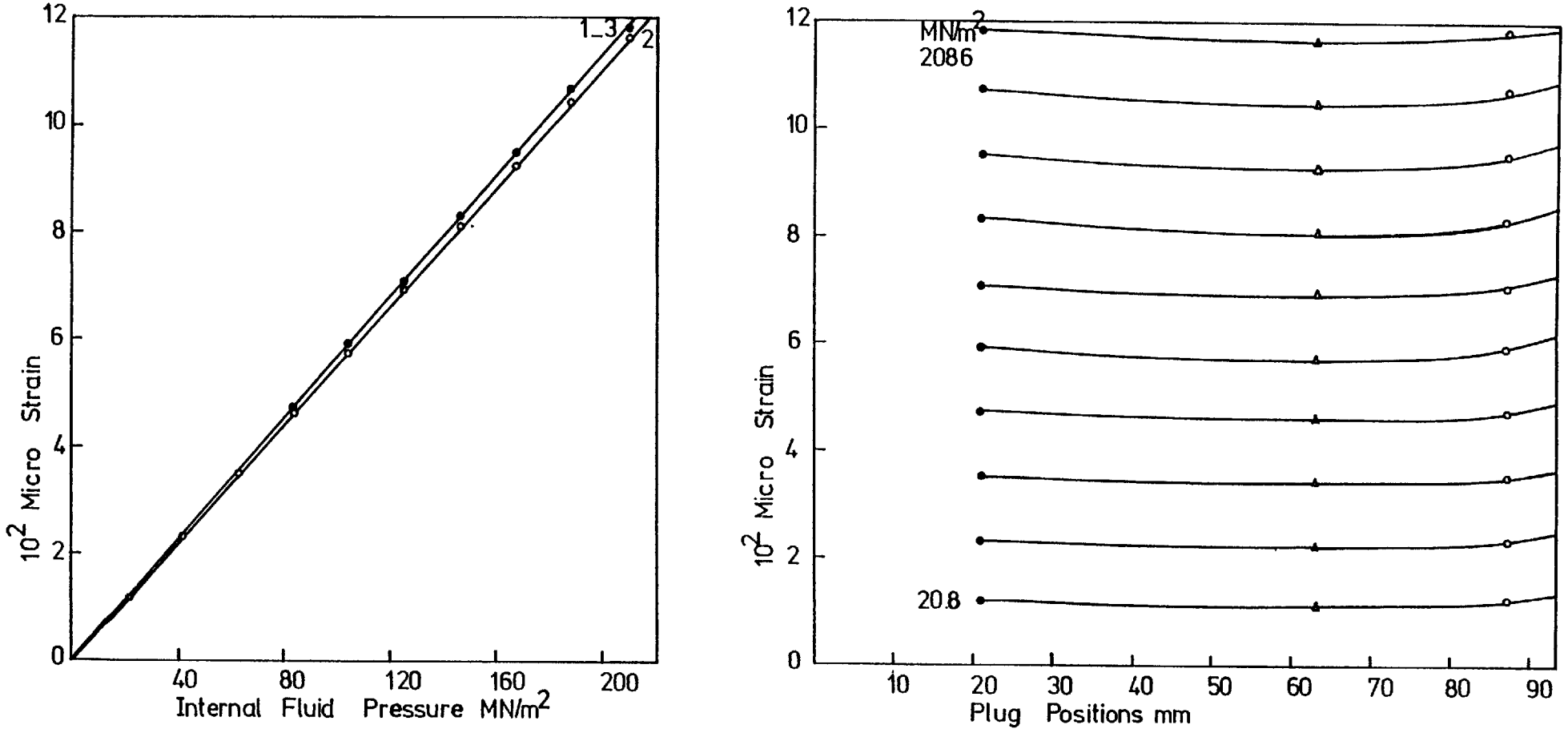
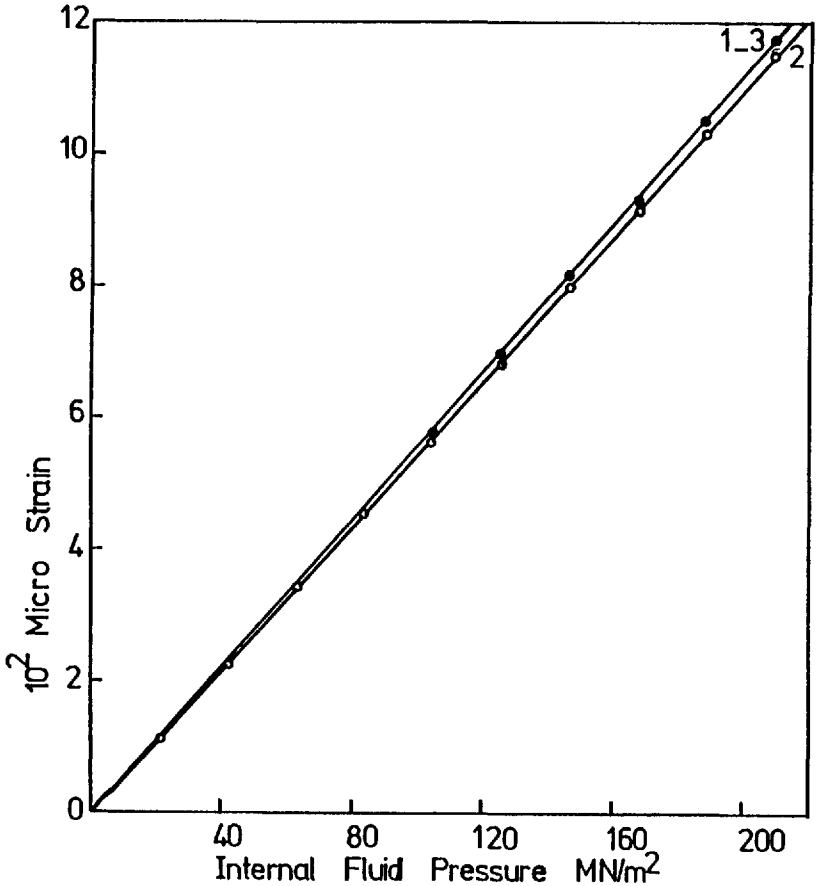


Fig. 4.4.16 Calibration of the Strain Gauge No. 8L.



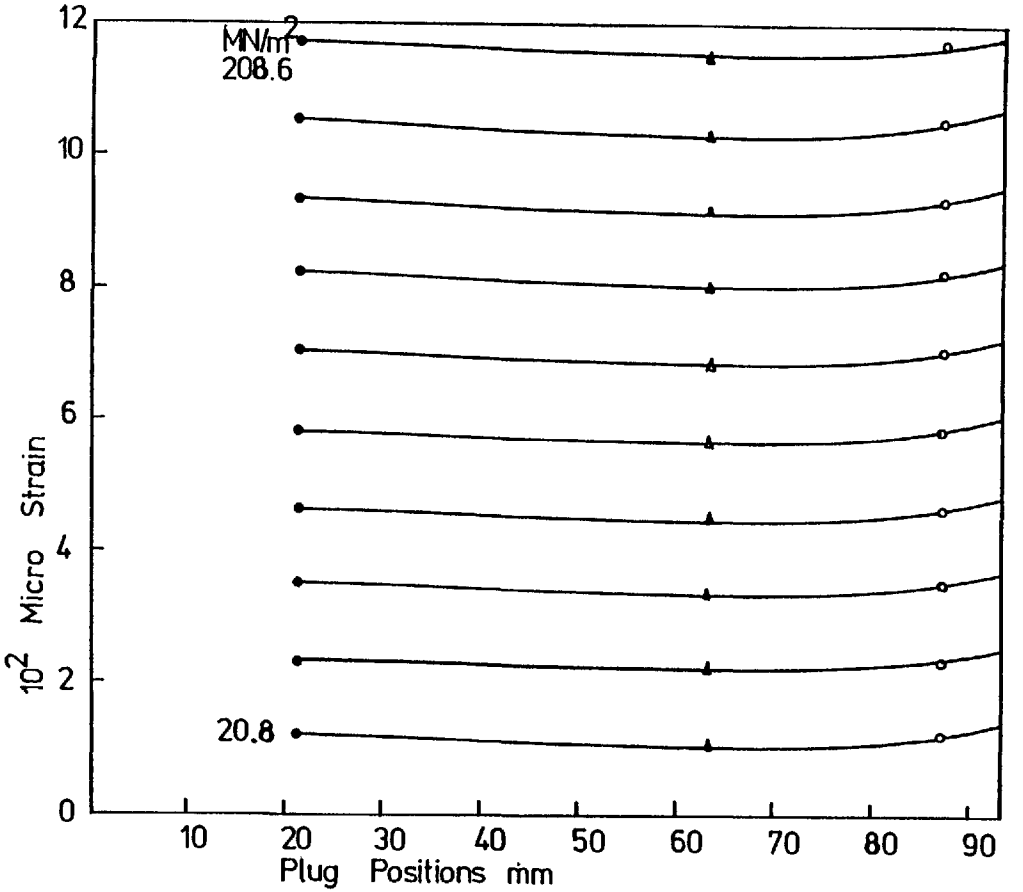


Fig. 4.4.17 Calibration of the Strain Gauge No. 9L .

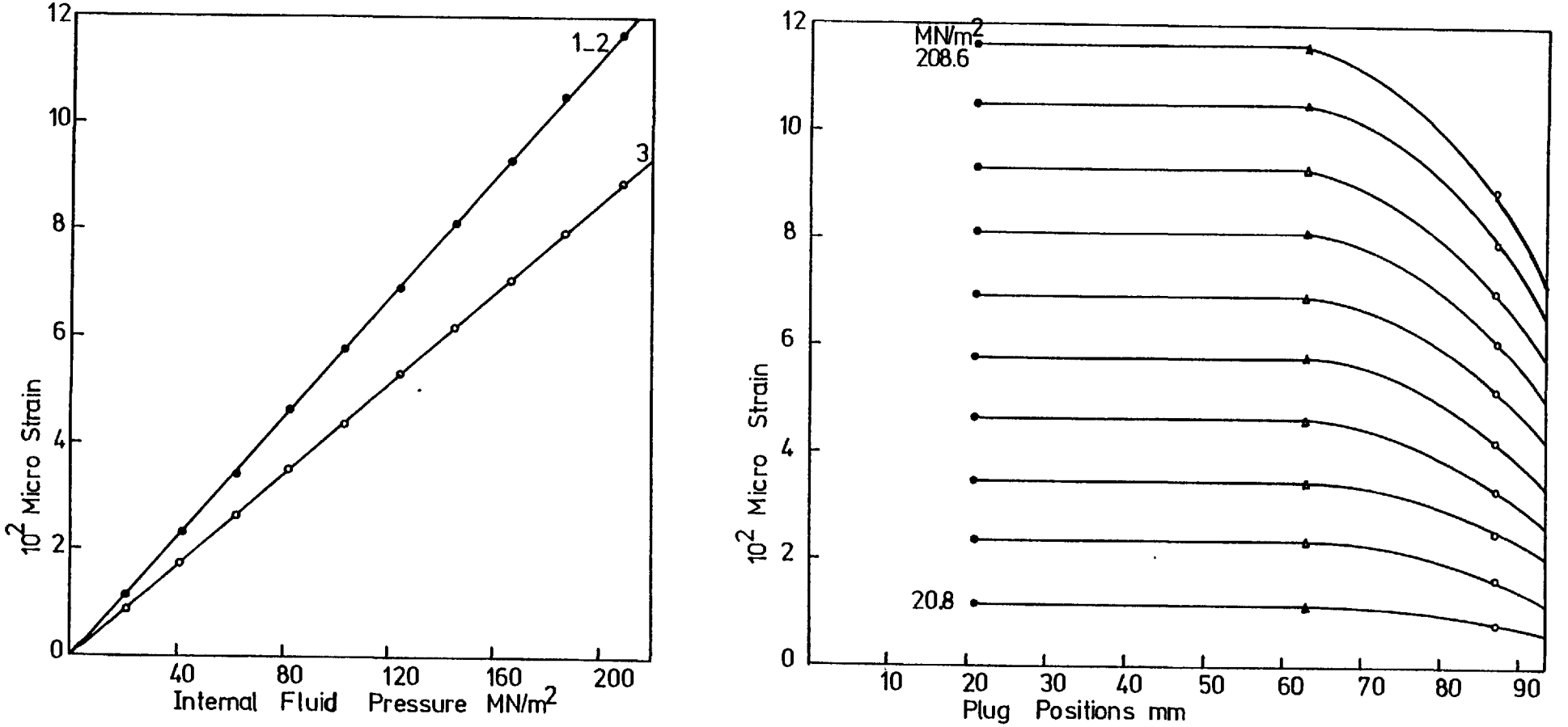


Fig. 4.4.18 Calibration of the Strain Gauge No. 10 L .

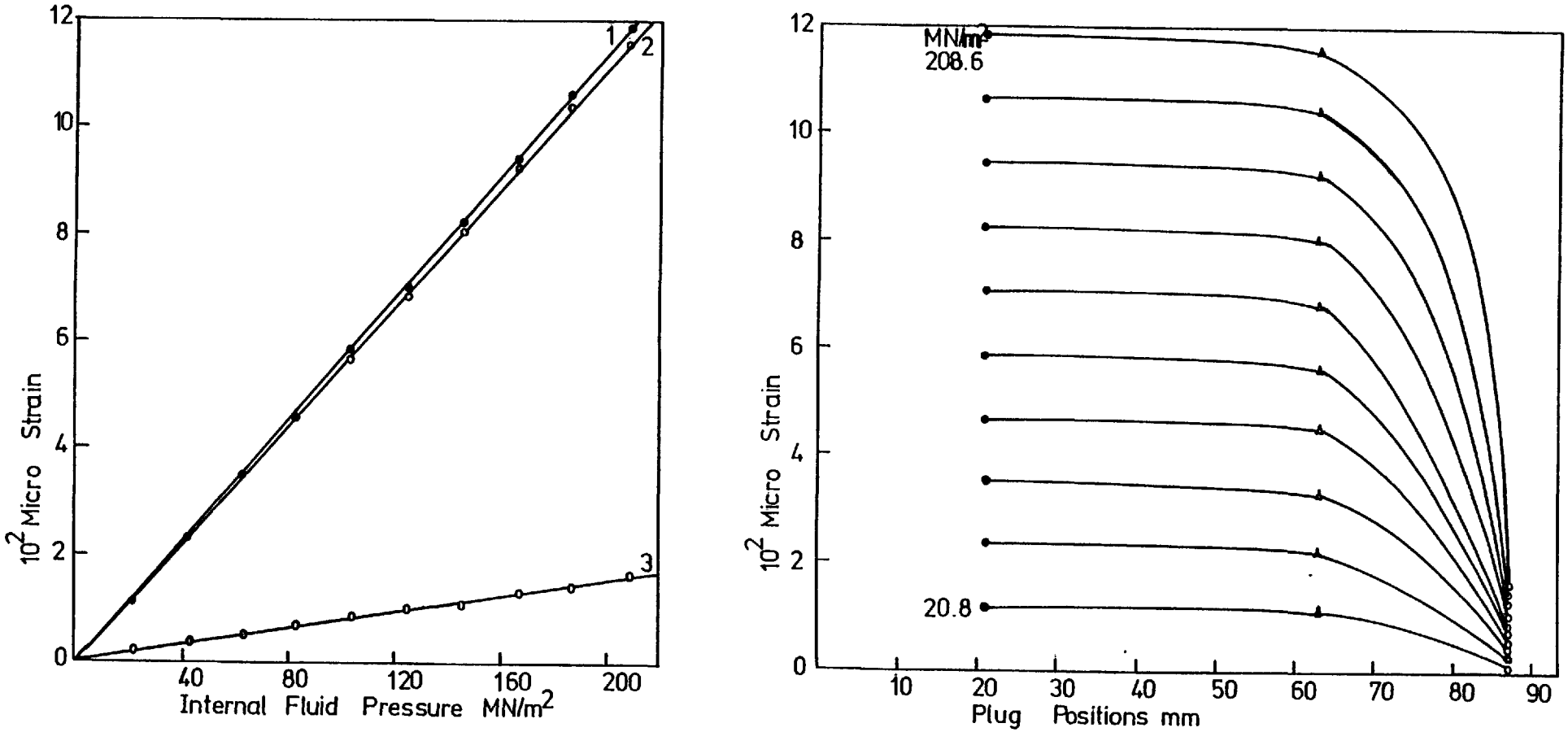


Fig. 4.4.19 Calibration of the Strain Gauge No. 11L .

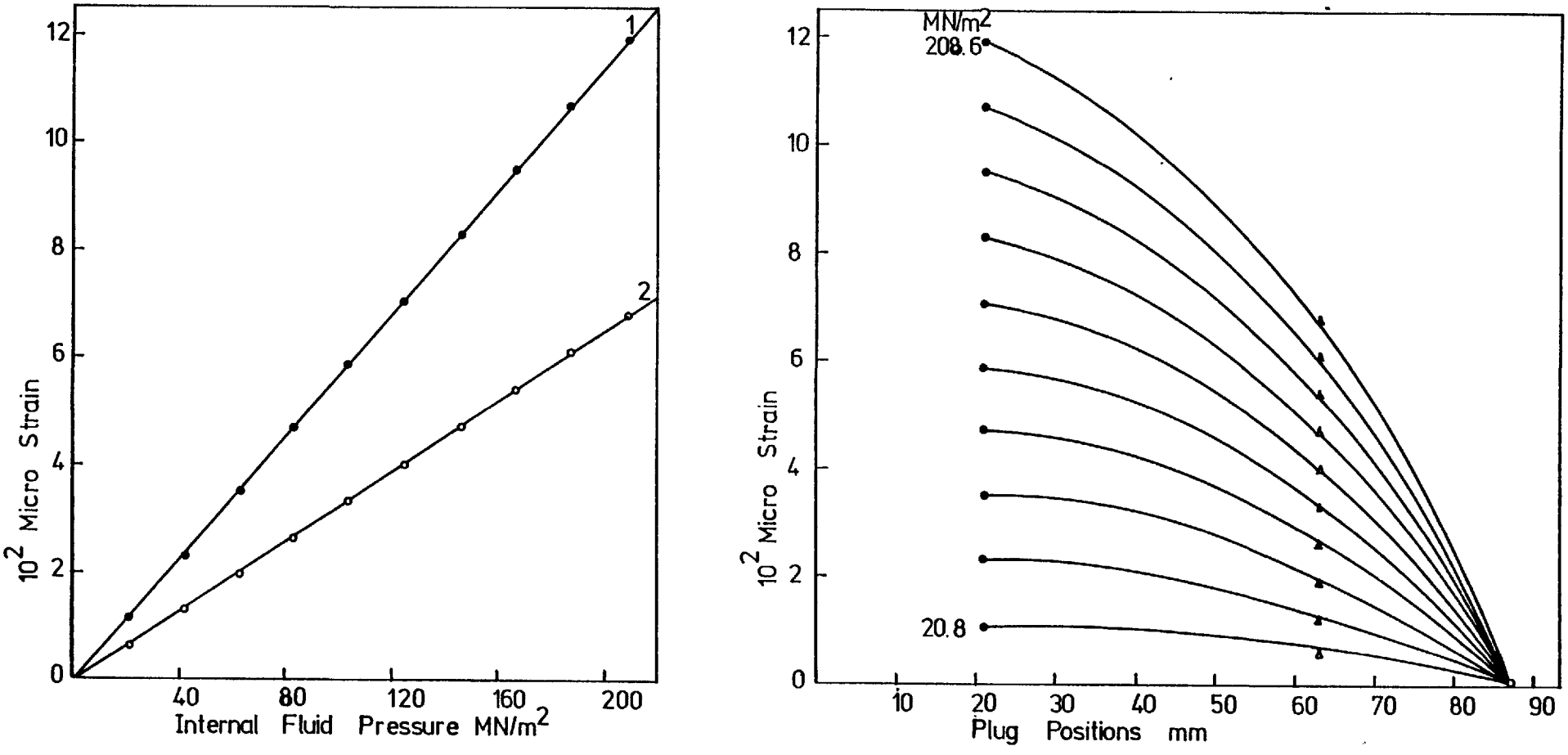
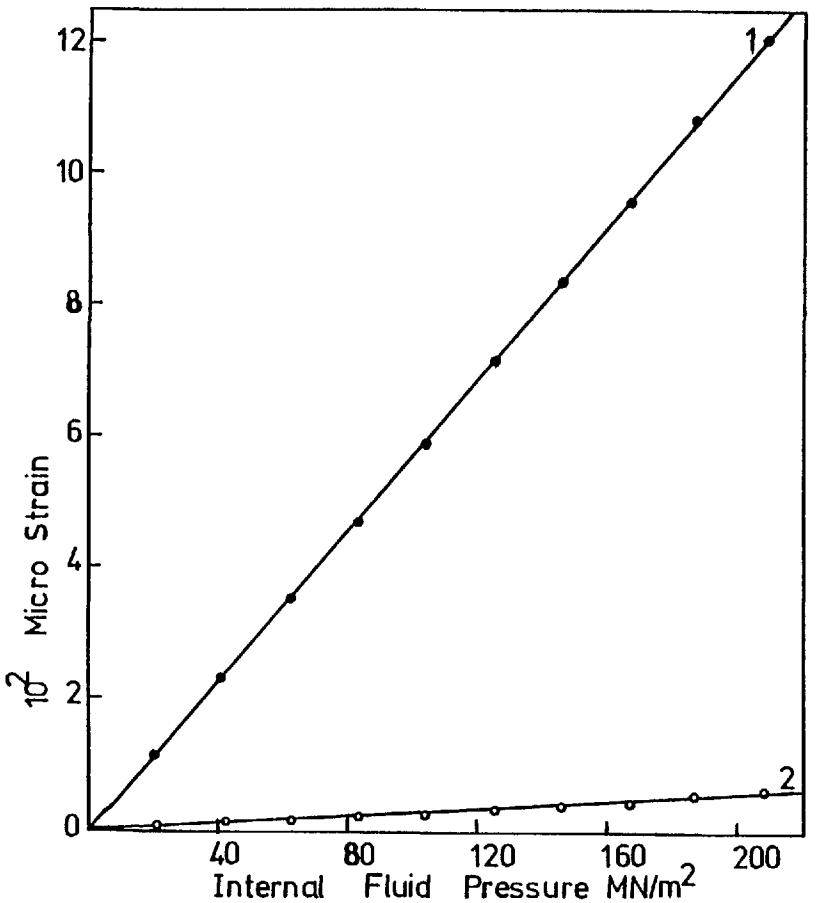


Fig. 4.4.20 Calibration of the Strain Gauge No. 12L .



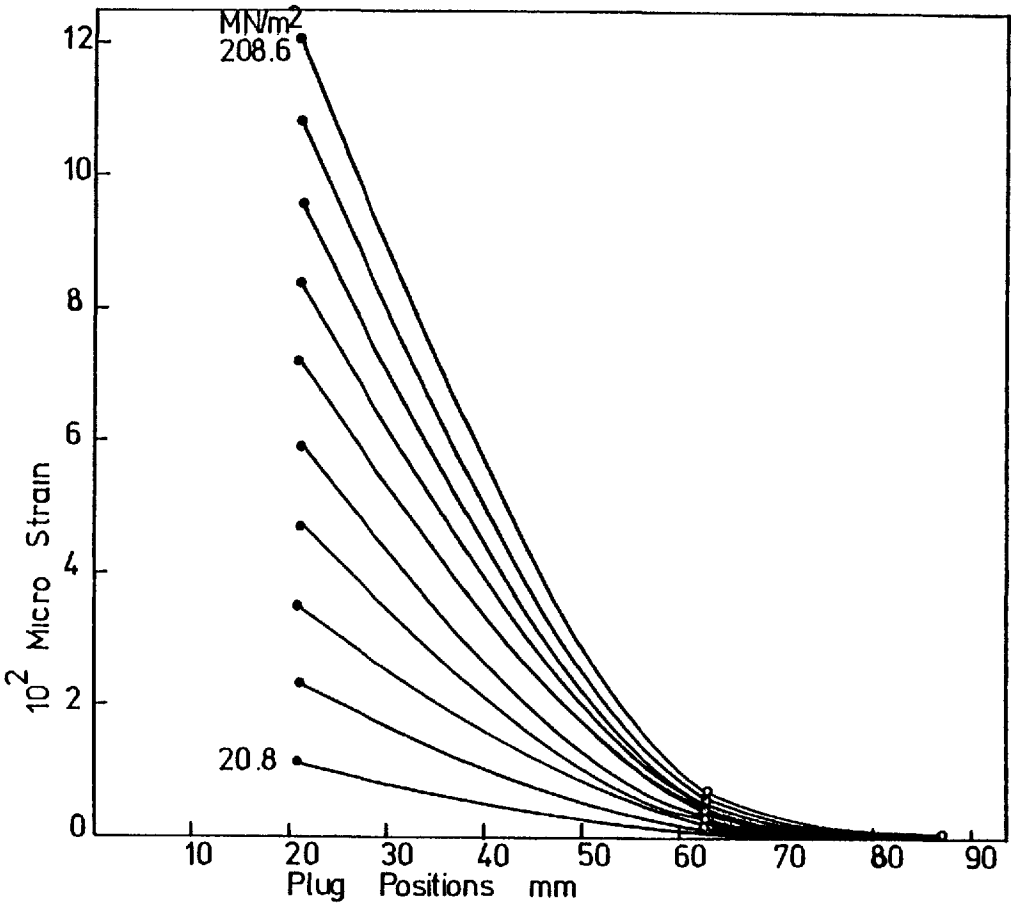
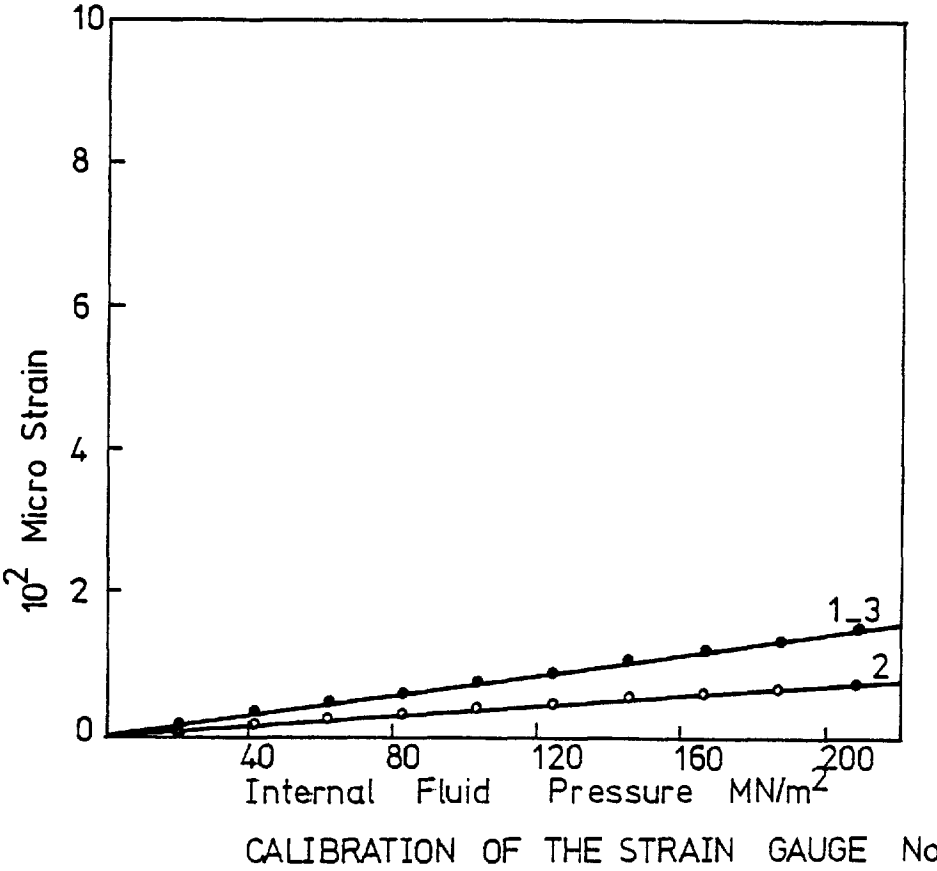
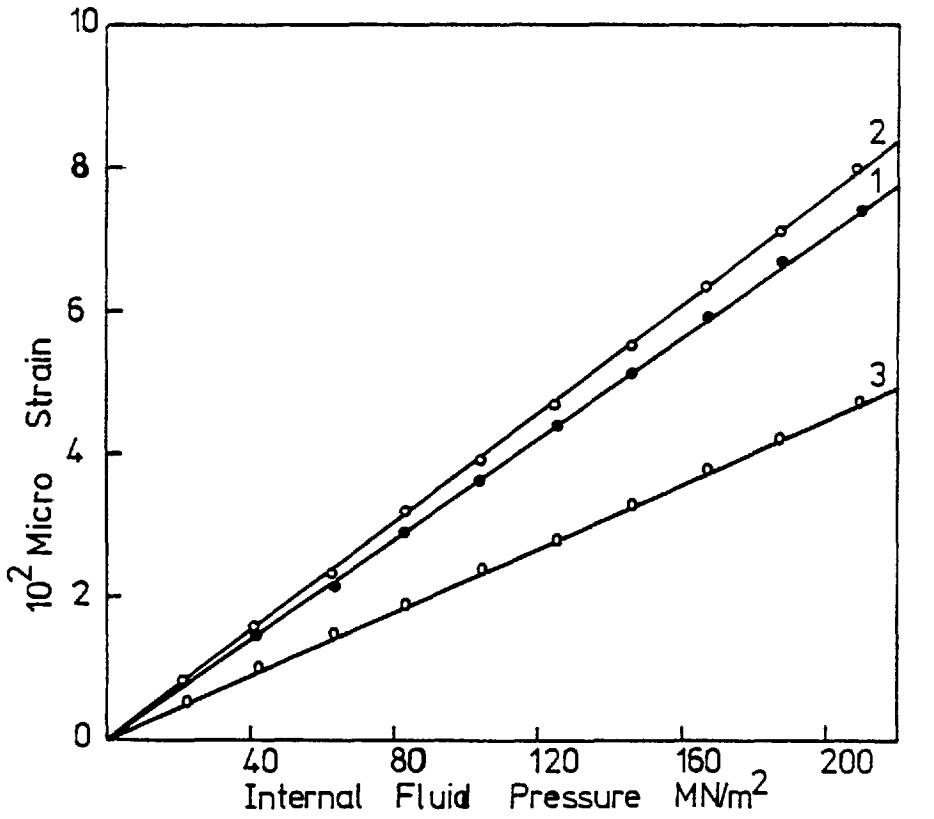


Fig. 4.4.21 Calibration of the Strain Gauge No. 13L .

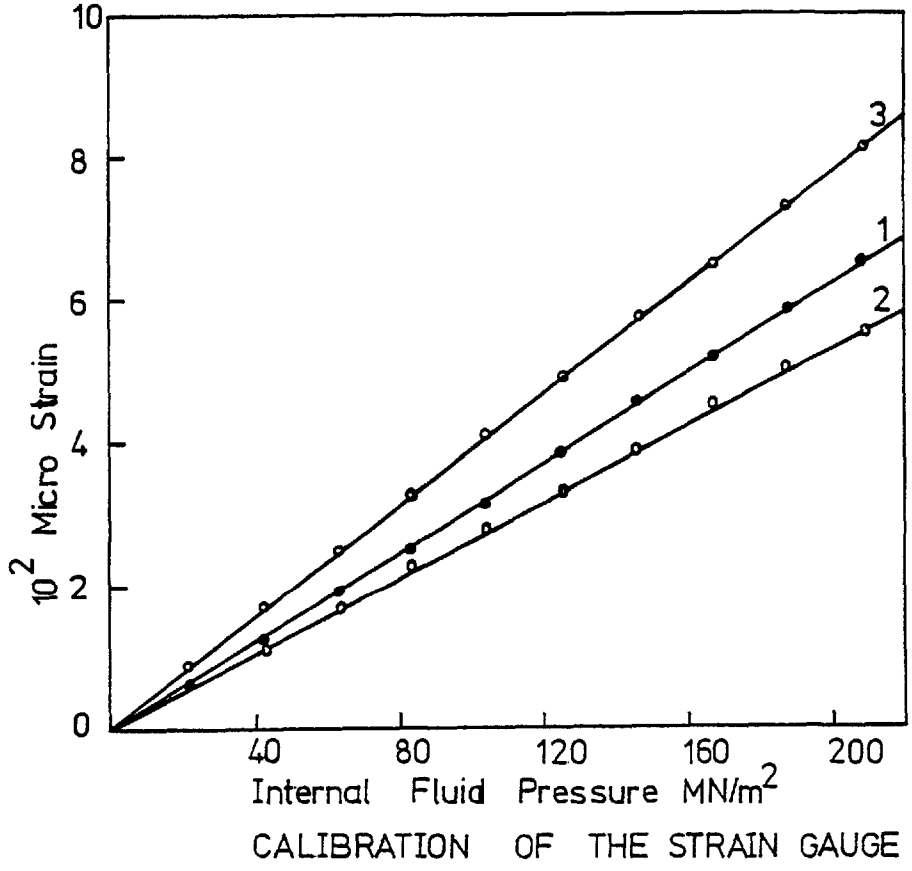


CALIBRATION OF THE STRAIN GAUGE No.1



CALIBRATION OF THE STRAIN GAUGE No.2

Fig. 4.4.22 Calibration of the strain gauges.



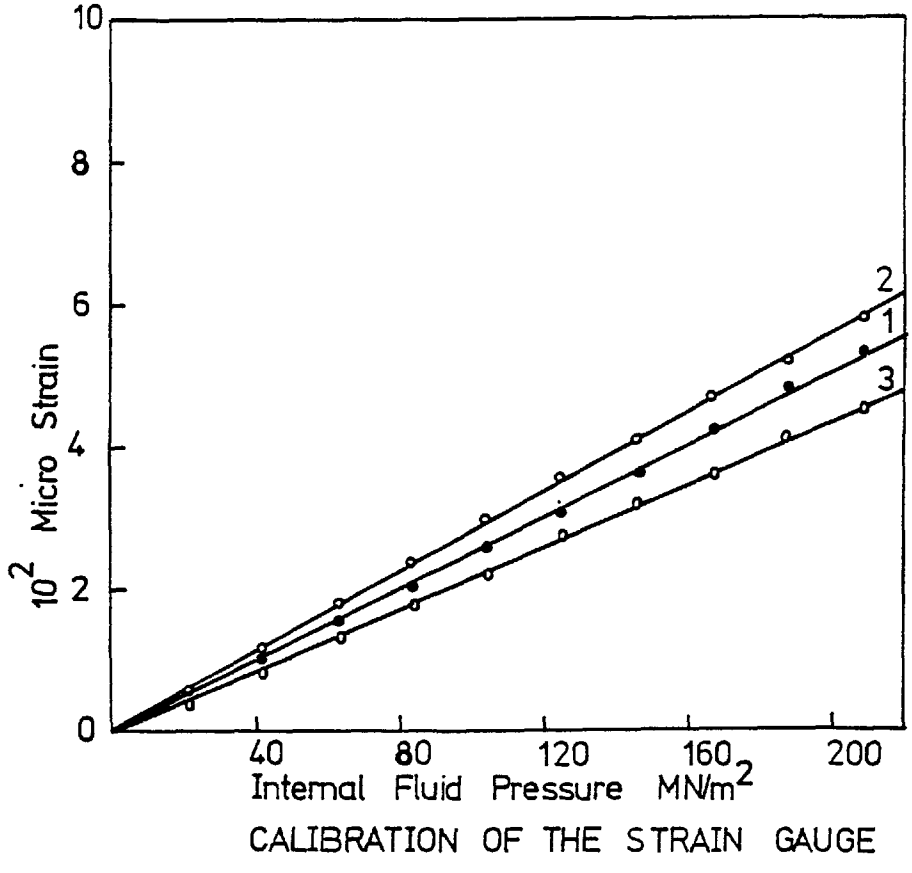


Fig. 4.4.23 Calibration of the strain gauges.

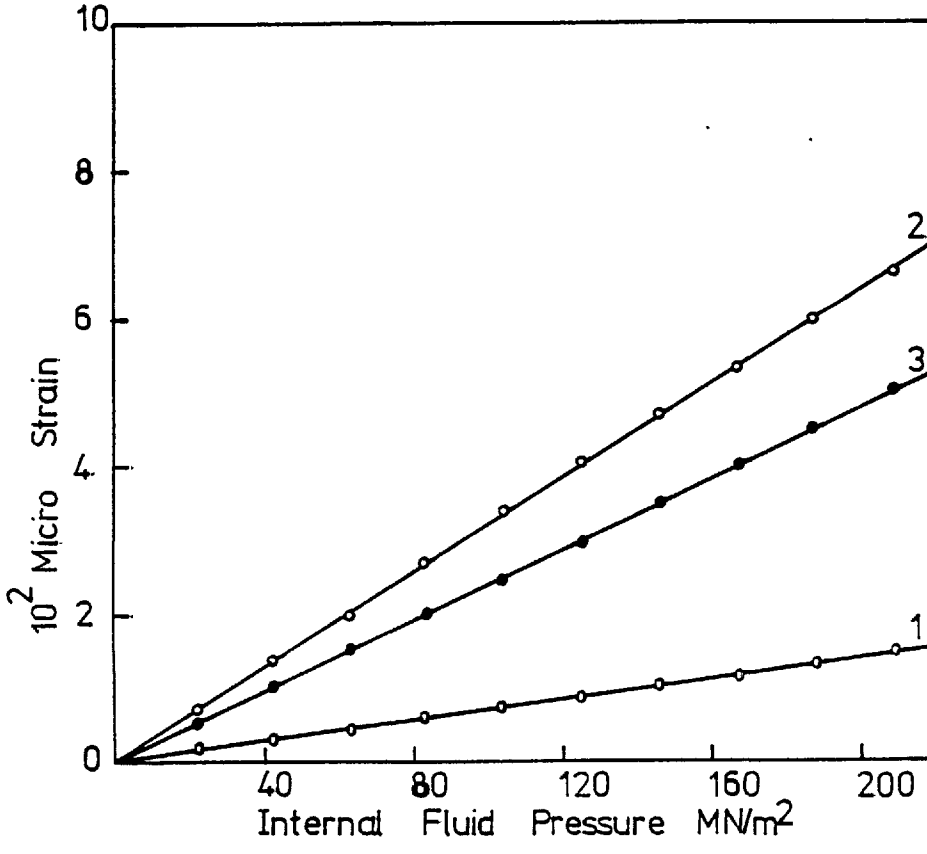
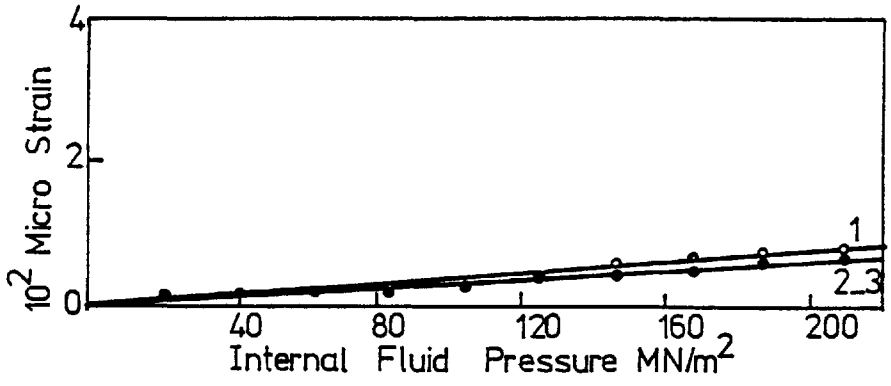
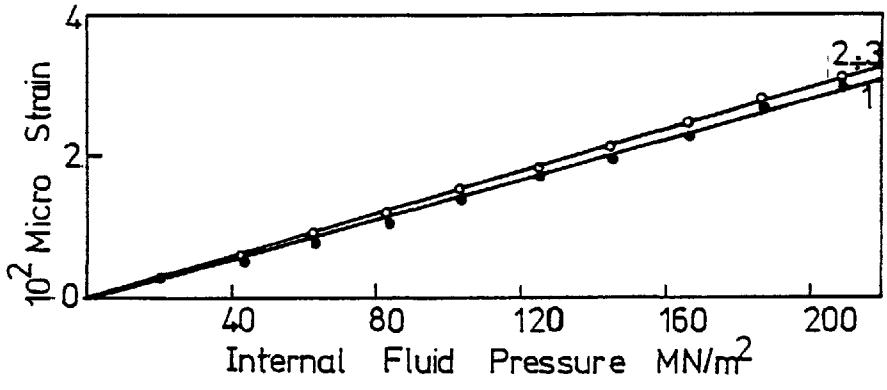


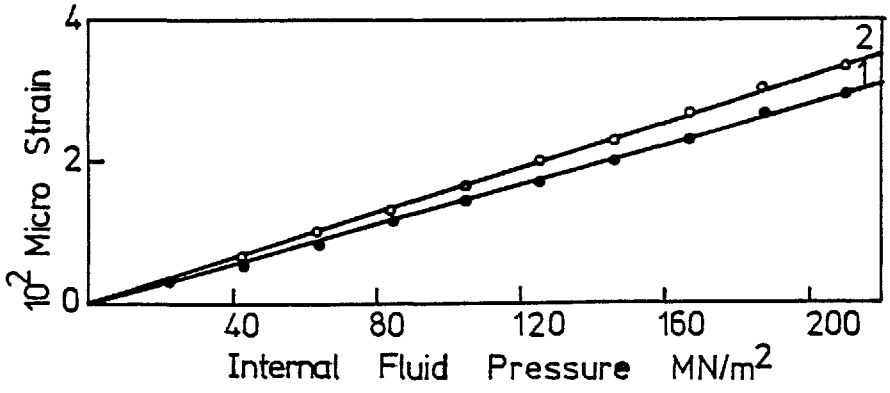
Fig. 4.4.24 Calibration of the Strain Gauge No. 5 .



CALIBRATION OF THE STRAIN GAUGE No.1L

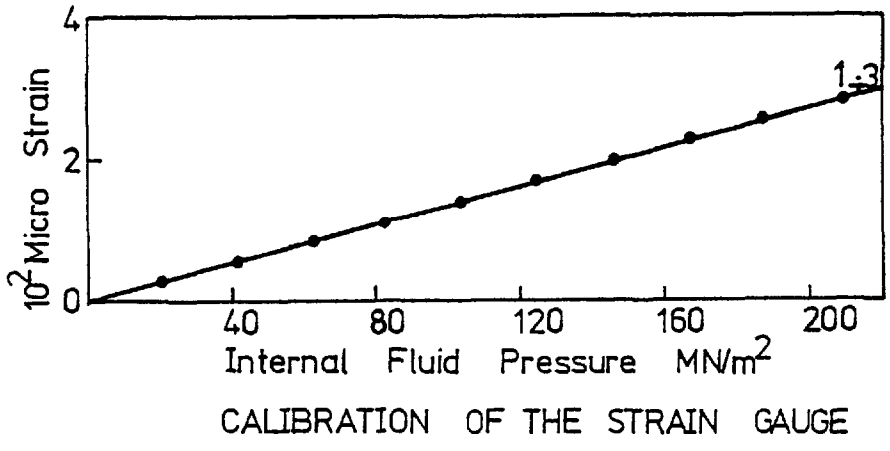


CALIBRATION OF THE STRAIN GAUGE No.2L

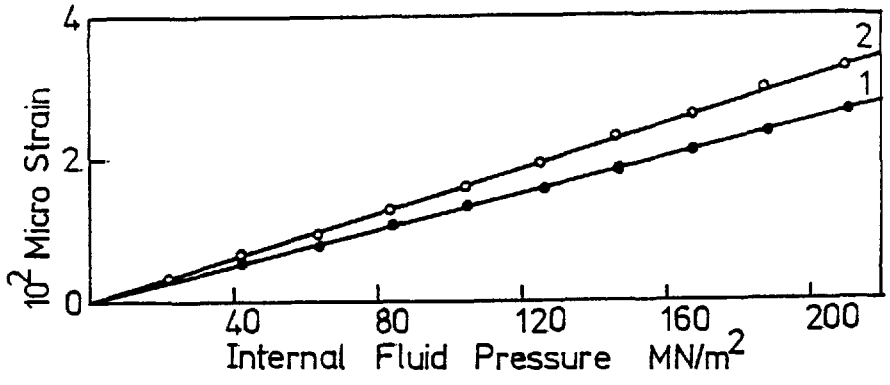


CALIBRATION OF THE STRAIN GAUGE No.3L

Fig. 4.4.25 Calibration of the strain gauges.



CALIBRATION OF THE STRAIN GAUGE No. 4L



CALIBRATION OF THE STRAIN GAUGE No. 5L

Fig. 4.4.26 Calibration of the strain gauges.

4.5 The Experiments

Commercially pure lead and aluminium specimens were extruded into rods by forward extrusion and into cans by backward extrusion (Fig. 4.11), while loads at both ends of the billet, together with hoop and axial strains on the outside diameter of the containers were recorded simultaneously.

30 mm diameter billets with 83 mm and 110 mm initial lengths were used for forward and backward extrusion respectively. Specimens of commercially pure aluminium were machined from cold drawn bars and lead billets were made by casting and machining. Care was taken to machine them to about the same surface finish. The aluminium specimens were annealed at 360^{o} C for one hour in vacuo.

The experiments were carried out either in the dry condition, or the billets and tools were lubricated with molybdenum disulphide in solution or with castor oil. Before each unlubricated test, the tools and billets were carefully cleaned with trichloroethylene to ensure good repeatability of the results. Tests on the lubricated extrusion of aluminium specimens were performed only at a low extrusion ratio so as to limit the container pressure.

The tools were first assembled for the forward extrusion of commerically pure lead with a die of extrusion ratio 2. After the data recorder had been left on for sometime to stabilise, all the strain gauge readings were adjusted to zero using the balancing points of the strain gauge bridge. All the wiring connections of the load cells were checked and the billet, previously cleaned by using trichloroethylene, was then loaded into the container.



Fig. 4.11 Extrusion products.

The electronic printer was switched on and started scanning all 17 channels repeatedly and continually at a speed of four channels per second. At the end of the extrusion, the electronic printer was switched off and the printed data on a paper strip was cut off and labelled.

A load of between 2 and 4 tonf ($\sim$ 20 kN and $\sim$ 40 kN) depending on the extrusion ratio was required to press out the discard from the container, the higher load was needed when flash was present.

For the latter case, the experiment was repeated until at least two similar sets of results were obtained with negligible or no flash. After each extrusion test the container bore, the die and the pressure pad were thoroughly cleaned with trichloroethylene to remove any traces of lead or other contaminants and to ensure that they were clean and perfectly dry.

The whole procedure was repeated for extrusion ratios of 3, 4, 9 and 16 and similarly a set of the best consistent results were chosen.

Similar extrusion experiments were performed on the lubricated extrusion of lead specimens. The billet, the container bore, the die, and the pressure pad were first cleaned using trichloroethylene and then smeared with the appropriate lubricant. The extrusion experiment was then carried out and each time the best consistent set of results were selected.

For lubricated extrusion, it was found that the the discard was easily removed from the container, using very little force.

After having carried out the forward extrusion of lead, the backward extrusion assembly was fitted. A similar procedure as previously described for forward extrusion was repeated for the backward extrusion of lead for ratios of 2, 3, 4 and 9.

Forward and backward extrusion experiments of aluminium at an extrusion ratio of 2 were carried out in the lubricated condition. It was found that significant forces were needed for the ejection of the extruded can.

Tests on the lubricated extrusion of aluminium were not performed at higher extrusion ratios because the strain readings near the die were high, indicating stresses close to the yield point of the container material.

5. THEORETICAL CONSIDERATIONS

5.1 Semi-empirical Method

5.1.1 Introduction

This method consists of obtaining the velocity field experimentally and calculating the complete strain rate, strain and stress fields {46}, {47}, {48}, {49}, {50}.

In spite of the fact that this method offers the possibility of obtaining useful information on the detailed mechanics in various forming operations, it has been applied to only a few problems. This is mainly because the calculations involved are time consuming, and graphical differentiations and integrations are unavoidable. When applying numerical differentiations to the experimental data, the results obtained usually were not smooth. Therefore, the development of a proper smoothing procedure became a critical problem in the application of a computer to this method.

Two kinds of analysis were used here for the solution of the detailed mechanics of the forward extrusion. One is based on the flow field observed experimentally, and the other on the method of weighted residuals.

For steady state axisymmetric deformation processes, a pattern of flow lines on a meridian plane at any distance in the steady state is sufficient for deriving a complete solution. For rod direct extrusion, this is achieved by

partially extruding cylindrical specimens split into halves along a meridian plane on which grid lines are printed, and by examining the resulting distortion of the grid lines. The coordinates of a total of 23 points along each flow line were recorded, and the data were punched on IBM cards. Using the coordinates as input data, the flow function ψ was calculated along the flow lines; the calculations were based on the fact that the value of the flow function is constant along a flow line.

5.1.2 Billet Design

A certain number of solid commercial purity aluminium billets were manufactured for testing the apparatus. After machining to a fine, turned finish and annealing, the billets were cleaned with grade 600 emery paper.

Several different methods for the manufacture of split billets were tried before a satisfactory approach was formulated. The final method, described below, resulted in specimens with the split on their mid-plane to within 0.0015 cm and no tendency for the two halves to bow apart.

Firstly, two rectangular pieces of material were fly-cut until they were accurately of the same thickness. These were then held in a four-jaw chuck to be turned. On first attempts to turn the composite bar between centres, it

was found there was a tendency for the centre to separate the two halves. Therefore, jubilee clips were used at each end of the billet and only the central portion was turned. The billet was then transferred to a collet where the ends were turned down. This was sufficiently accurate for the end portions, as no measurements are actually taken in these regions.

After machining, the billets had to be annealed. During annealing, the billets were again clamped together by jubilee clips, the billet surface being protected by copper sheet. Thus, no bowing could take place during stress relieving.

5.1.3 Grid Preparation and Measurement

The surfaces of the annealed two halves were cleaned by abrasion on 600 grade wet and dry paper. They were then polished with 6 μ diamond paste on a flat polishing table. After polishing, an etching procedure specially recommended for very high purity aluminium was applied to the two halves and final polishing with with 6 μ diamond paste, using a slowly rotating wheel was carried out. After these treatment, the surfaces were highly reflective.

Full grids were drawn on one of the two halves. This grid comprised of a set of lines parallel to the billet axis, called flow lines, and a set initially perpendicular to the first, called transverse lines. However, only flow

lines were needed as input data for the computer program. These lines were scribed on the surface using a Société Genevoise Universal measuring machine. Grid lines as thin as 0.01 mm could be discerned after extrusion but only with difficulty. It was more practical to use lines about 0.03 mm thick. The accuracy of measurement was still greater than this figure as the centre of the line could be estimated under the microscope.

Using a 50 tonf (500 kN) Dennison hydraulic compression testing machine, the two halves of a cylindrical specimen were put together and partially extruded through a conical die of a semi-angle of 25° with an extrusion ratio of 2. The extrusion was stopped after the punch had travelled approximately 1/2", with a speed of 0.2 mm/sec (12 mm/min), and the steady-state flow pattern was photographed Fig. 5.1.1 shows a photograph taken under direct lighting.

It can be clearly seen here that the surface of the split is no longer flat. The same figure also illustrates that the flow lines are still clearly visible, their path has, in places, been distorted by the cross flow on the meridian plane.

Although sophisticated measuring techniques are now being developed for finding the coordinates of the lines after extrusion, two different methods were used. The first method was to look at the steady-state flow lines through an optical

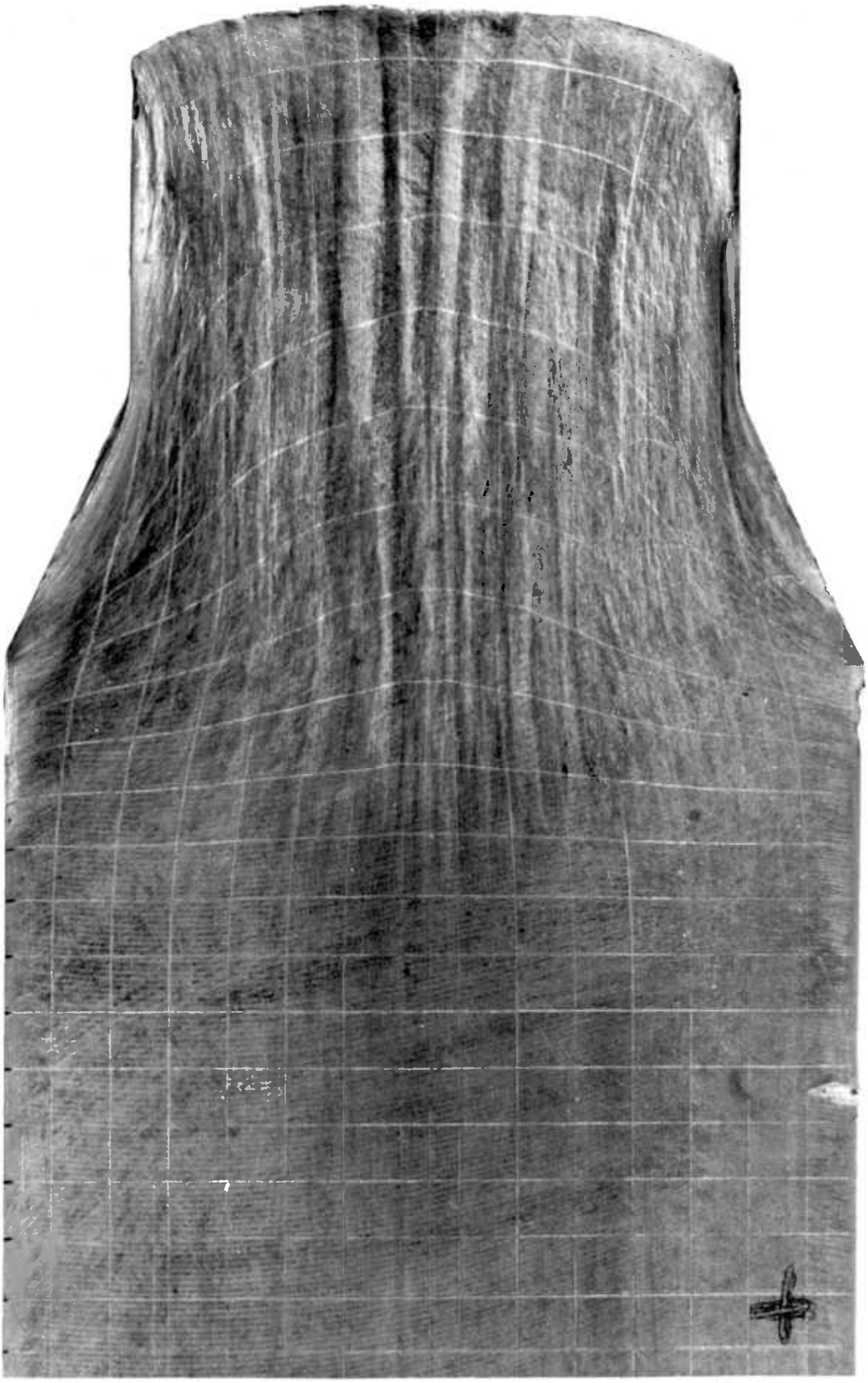


Fig. 5.1.1 Aluminium billet under direct lighting.

projector and the second was to use the measuring machine again. The former was less fatiguing than looking through the microscope but, because of difficulties with illumination, the measurement was less accurate and repeatability was worse. Therefore, the measuring machine was used throughout.

To estimate the accuracy of measurement several points were measured repeatedly, approaching them from different directions. The coordinates never varied by more than 0.004 mm for any one point, so this can be taken to be the measuring error.

5.1.4 Derivation of the Solution

As is usually the case in problems of large plastic deformation, the elastic strains are ignored throughout the analysis and the material is assumed work hardening.

For each flow line a flow function is specified, from the condition in the rigid region, as

$$\psi_L = \pi r_L^2 |v_I| \qquad (5.1.1)$$

This function is now constant along each line through the deformation region.

From the flow function, the axial and radial velocities, from eq.(2.30), as follows

$$v_z = -\frac{1}{2\pi r}\frac{\partial \psi}{\partial r}$$

(5.1.2)

$$v_r = \frac{1}{2\pi r}\frac{\partial \psi}{\partial z}$$

In turn, the strain rates are calculated from the velocity field according to the eq. (2.31).

Assuming the flow to be incompressible, we have eq. (2.21) as

$$\dot{\varepsilon}_r + \dot{\varepsilon}_\theta + \dot{\varepsilon}_z = 0 \qquad (5.1.3)$$

This condition is automatically satisfied by the system of eq. (2.31) with (5.12), viz

$$\frac{\partial v_r}{\partial r} + \frac{v_r}{r} + \frac{\partial v_z}{\partial z} = 0.$$

or (5.1.4)

$$\frac{\partial}{\partial r}\left(\frac{1}{2\pi r}\frac{\partial \psi}{\partial z}\right) + \frac{1}{2\pi r^2}\frac{\partial \psi}{\partial z} - \frac{\partial}{\partial z}\left(\frac{1}{2\pi r}\frac{\partial \Psi}{\partial r}\right) = 0$$

Once the values of the strain rates have been calculated in the three coordinate directions, along with the only non-zero shear strain rate $\dot{\varepsilon}_{rz}$, the mean effective strain rate can be calculated from eq. (2.26).

The total strain values are next found by integrating the effective strain rate, with respect to time, along each flow line.

The strain rate and total strain fields are now known for the whole deformation zone and can be used with the method of weighted residuals to give the stress field.

5.1.5 The Flow Function

Values of the function are found in the zone before deformation starts from eq.(5.1.1). This defines the function along each flow line. However, to carry out the numerical differentiations, the flow function must be evaluated at mesh points, which cover the field of deformation, by a numerical procedure which is now described.

5.1.6 Mesh for Computer Calculations

Previous applications found in the literature on such semi-empirical methods have used rectangular or square meshes for the calculations. This is standard procedure as the difference quotients, estimating the differentials can be calculated using standard formulae. Here, the choice of a rectangular mesh, such that mesh points lie on the die-workpiece interface, produces greater step length in the axial than in the radial direction. While this problem could easily be solved by decreasing the step length in the axial direction by a factor of 2 or 3 and not having the maximum radius at each

section on the bounding flow line, there are still other problems.

In conventional extrusion, the observed flow lines (as seen in Fig. 5.1.1) indicate that deformation can start before the billet reaches the die, by the build-up of pressure. If the present method is to be successful in predicting the surface conditions then this effect can not be overruled by enforcing a sharp change of slope on the surface of the billet at contact with the die. This is especially true if the conditions are favourable for the build-up of lubrication over the die surface.

Further, if the step length in the radial direction is chosen to give a reasonable number of steps in the billet, it is not usually possible to arrange for one of the mesh points to correspond with the product surface. This is desirable in the calculations.

For these reasons, it was decided that a mesh with constant step length in the axial direction but variable step length in the radial direction would be used. This type of mesh is shown in Fig. 5.1.2. Input data to the program gives the number of mesh points in the radial direction both in the billet and the product. A mesh is then chosen with equal spacing up to the product diameter. After this radius has been reached another step length is chosen so that the mesh continues, with equal spacing, until the radius corresponds to the billet radius. The mesh is stopped if the radius at

any K section exceeds that of the bounding flow line. The radius is then set equal to this value and the corresponding I value stored in an array IMAX.

One further array is used to characterise the mesh. This is the array KMIN, in which the minimum K value is stored, for each I section. The radial and axial coordinates of each mesh point (I,K) are stored in two arrays, R(I,K) and z(I,K).

5.1.7 Subroutine DATARD

The calculations to give the four arrays R,Z,IMAX and KMIN which define the mesh, can only be carried out after the input data has been transformed so that the radius of each flow line is known at each K section.

Data is first read in by DATARD giving the die angle, initial velocity of the process, the coordinates of 23 points along each flow line and the coordinates of the plane where deformation ends and so that all radial values are positive.

5.1.8 Subroutine MESH

First the radius of each flow line at each K section RPSI (L,K) was calculated from the input data. The K sections are chosen so that the plane K = 2 coincides with the end of deformation and so that the step length is (for notation see Appendix A1).

XKDIV = (DBIL - DPROD)/(FLOAT(NKK - 2) • TAN(ALPHA).2)

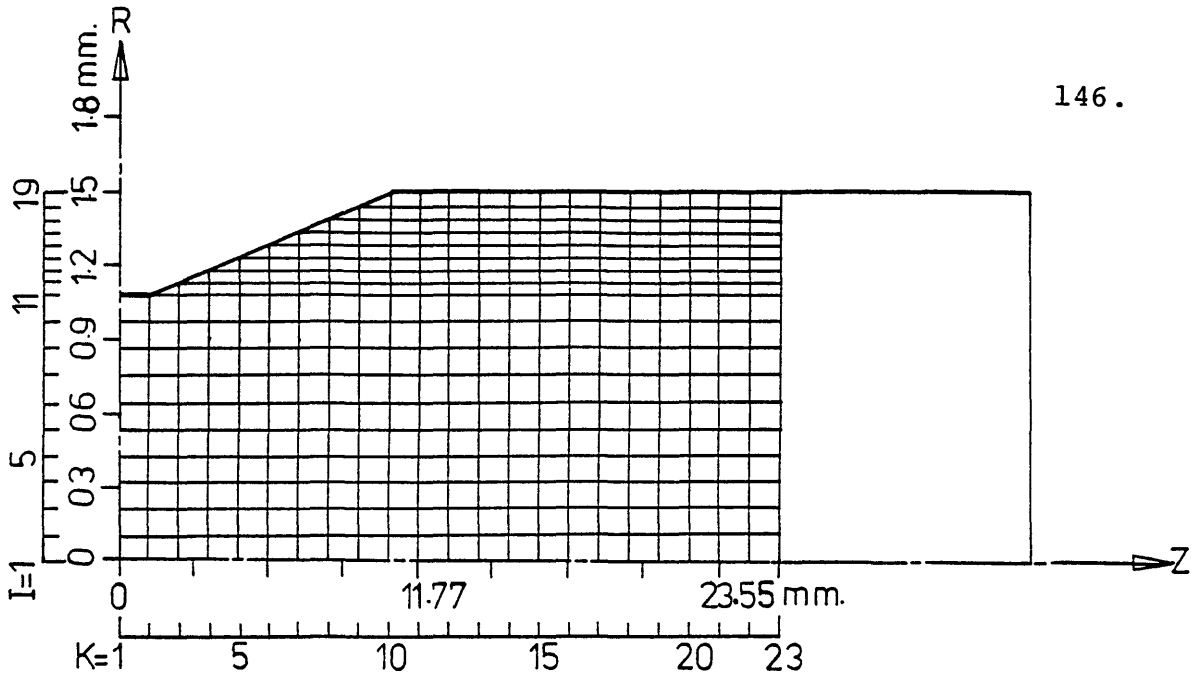


Fig. 5.1.2 Mesh for computations.

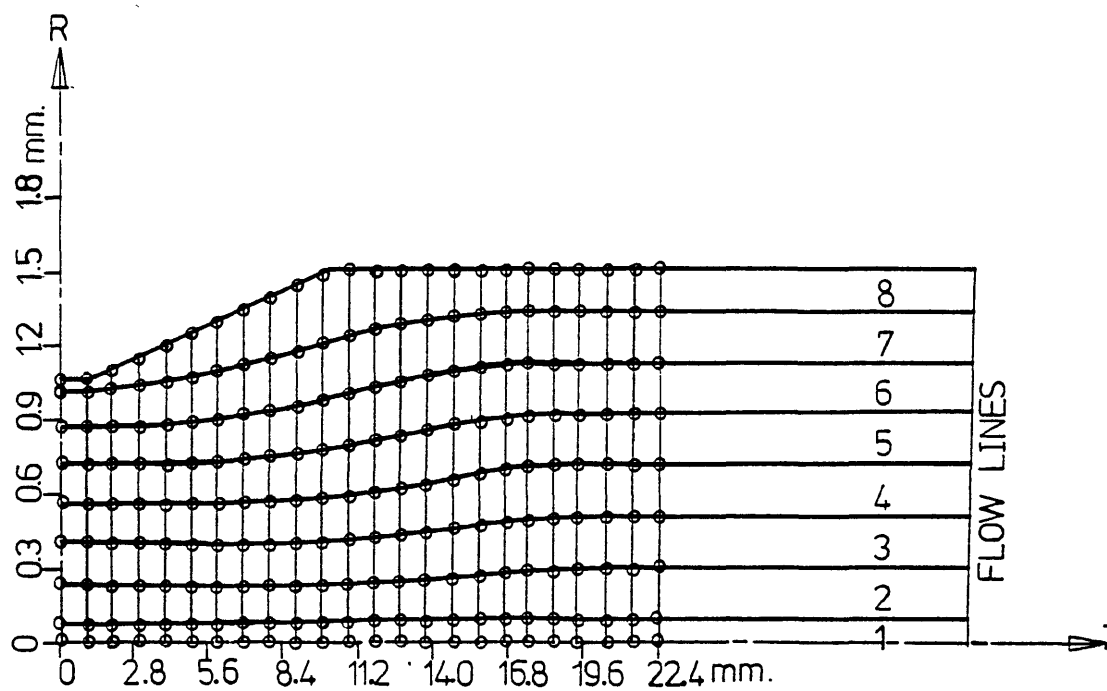


Fig. 5.1.3 Input data.

As illustrated in Fig. 5.1.2, the spacing in the z direction is assigned such that the boundary mesh point will fall on the surface.

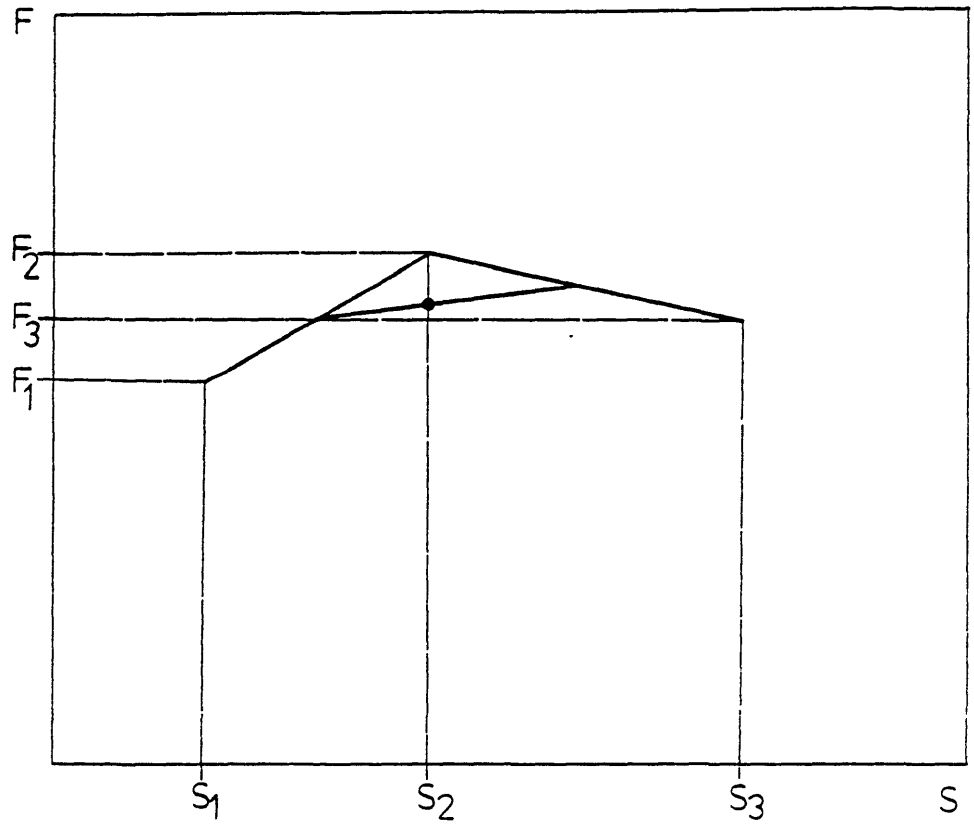
The method used for finding the values of RPSI was a polynomial least mean squares fit to the experimental data. This was carried out by means of two NAG library routines (in I.C. computer) E02ADF and E02AEF. E02ADF computes weighted least-squares polynomial approximations to an arbitrary set of data points. Each polynomial is represented in Chebyshev-series form. Subsequent evaluation of the Chebyshev-series representations of the polynomial approximations should be carried out using E02AEF.

After some trials, it was found that a 7th order polynomial worked satisfactorily. None of the features of the lines were lost and there was no tendency to give a high frequency ripple to the line.

The flow lines were then smoothed using the method of means. In this method, as shown in Fig. 5.1.4, the smoothed value of RPSI (L,K) is estimated by

$$(RPSI(1,K-1) + 2. \times RPSI(L,K) + RPSI(1,K+1))/4$$

Smoothing the flow lines once in this way produced no measurable difference in the velocity and strain rates calculated later but it did make the total strain results



Smoothed value of F_2 is :

$$\frac{F_1 + F_2}{2} + \left(\frac{F_3 - F_1}{2}\right) \cdot \left(\frac{S_2 - S_1}{2}\right) / \left(\frac{S_3 - S_1}{2}\right)$$

Fig. 5.1.4 Smoothing by method of means.

smoother, as these were found by integration along each flow line.

5.1.9 Subroutine FLOW

The values of the flow function can now be calculated at each mesh point defined by R(I,K), Z(I,K). To do this, a polynomial least mean squares curve fitting was tried.

If the billet were deforming uniformly, that is with plane sections remaining plane, then the curve of flow function against radius would be a quadratic. The change of slope is therefore greatest near the centre of the billet and a polynomial least squares fit consistently estimates values here. For use in the radial direction, it was found that a polynomial of the type

$$\psi = C_1 + C_2R^2 + C_3R^4 + C_4R^6 + C_5R^8 \qquad (5.1.5)$$

was most suitable. The theory on which the coefficients are defined is not given here. As the library routine could only deal with polynomials in which all the coefficients are defined a further routine, POLFIT, was written. The linear simultaneous equations which are formulated are solved using the library subroutine F04ATF. This routine calculates the accurate solution of a set of real linear equations with a single right hand-side AX = B, by Crout's factorisation

method. Given a set of linear equations, AX = B, the routine uses Crout's method with partial pivoting to decompose A into triangular form A = LU, where L is lower triangular and U is unit upper triangular. This polynomial least squares curve fitting method was used throughout to define the flow function, CPSI(I,K), at each mesh point.

5.1.10 Smoothing Procedure

Smoothing of the flow function is necessary for deriving the complete solution from the experimental flow pattern. To ensure that the difference quotient estimates of the differentials are smooth, the flow function is smoothed and checked along the boundaries, where its value is known. Therefore, it would be simpler to smooth the calculated velocities and then the strain rates. Because of this method could not ensure that the compressibility condition is satisfied, an alternative procedure of building up a smooth flow function is therefore adopted.

5.1.11 Subroutine SMOOTH

The purpose of this routine is to define the zone in which plastic deformation takes place. The necessary data are obtained by estimating where the steady-state flow lines deviate from straight lines in the billet and product. This can be done either on the specimen itself under the microscope or on an enlarged plot of the data produced by the computer.

The data is then smoothed and after some trials, a 5th order polynomial is fitted. Once this polynomial fitting has been made, at each K section, and hence the value of z, at which deformation starts and stops is found and stored in the arrays of KI and KF. If no data can be fed in giving the axial values at which deformation starts and stops for each flow line, then KI is set equal to (NK - 2) and KF is all equal.

The values of the flow function, in the regions where the material is rigid are known to be

$$\psi = \pi.R(I,K)^2.\ |VBIL| \quad \text{before deformation} \tag{5.1.6}$$

and

$$\psi = \pi.R(I,K)^2.\ |VPROD| \quad \text{after deformation}$$

The values of ψ at the points outside the deformation zone are examined and compared with the correct values obtained by using the incompressibility condition. If any error is found, it is linearly distributed in the z direction.

5.1.12 Subroutine SMOTHZ

This subroutine smooths the differentials with respect to z. With the present coordinate system, the radial velocity must always be negative as it is in the opposite direction to the radial coordinate, assuming non-outward flow pattern. After calling the routine DIFFZ which estimates

the differentials the routines AVZ and AVR are called to smooth the differentials twice using the method of means described previously in both the radial and axial directions.

Finally, the flow function is then built up from the smoothed differentials by calling the routine IZA. End values must be checked and if any error is found it is smoothed and added to the final values to bring them closer to the initial values.

After smoothing in this way, the flow function is checked to ensure it is monotonically decreasing in the positive z direction for constant values of R.

5.1.13 Subroutine SMOTHR

If the smoothing is carried out on the second differential, it is less likely to produce changes in the overall flow pattern, as its slope will be smaller than that of the first differential. Thus, the second difference with respect to R is smoothed by using subroutine AVR. The condition of maximum axial velocity at exit is checked and then smoothing is again applied in the R and Z directions. After these adjustments, the third differential is formed and smoothed in the R direction. The flow function is then built up from the smoothed differentials, calling the routine IRA, and its value along the boundary is checked.

5.1.14 Subroutine STRATE

From the flow function defined by experiment and the foregoing numerical procedure, the velocity components at the mesh points can be calculated by eq.(5.1.2). The strain rates are then evaluated by a numerical differentiation of the velocity components, according to eq.(2.31).

Difference quotient approximations to the differentials in eq.(2.31) are obtained by subroutines DIFFZ and DIFFR in which a polynomial fitting to 3 points is used, one on each side of the point in question. Along the die surface and cylinder wall 2 points on one-side formula of differentiation is used.

Along the centre line, the axial velocity is evaluated by fitting a quadratic to points VZ(2,K) and VZ(3,K), such that the slope of VZ with respect to R is zero at the centre line (R(I,K) = 0) whilst the radial velocity is set to zero.

The necessary additional differentiations are carried out in order to obtain the strain rates as defined in the equation given above from the velocity field. Along the centre line

$$VZ(1,K) = (4VZ(2,K) - VZ(3,K))/3$$

and $$\dot{\varepsilon}_\theta = \dot{\varepsilon}_R = \frac{\partial V_r}{\partial r}$$

5.1.15 Subroutines DIFFZ and DIFFR

The purpose of these routines is to fit a polynomial to any number of points to find the difference quotient. The linear, simultaneous equations defining the coefficients of the polynomial were set up by routine FIT and solved by a NAG library routine F04ATF.

Difficulties arose near the surface where two points could be very close together, because of the mesh defined with varying step length. In this case, the points at R(IMAX,K), R(IMAX -2,K) and so on are used, R(IMAX-1,K) being ignored. This method used throughout to define R(IMAX,K) at the surface resulted in smoother difference quotients.

5.1.16 Effective Strain Rate and Effective Strain

The effective strain rate, directly from its definition in eq.(2.26), is calculated by subroutine T STRAIN at each mesh point. Once the values of the effective strain rates have been calculated, by linear interpolation, the value of effective strain rate and at the same time, the axial component of velocity V_{ZL} (I,K) on each flow line, at each K section can be found.

From the calculations detailed above, the time taken to reach each K section, along each flow line, can be found from

$$TIME(L,K) = TIME(L,K+1)+2(Z(1,K+1)-Z(1,K))/(VZL(L,K+1)+VZL(L,K))$$

The time is taken as zero at section NK.

Total effective strain along each flow line is now calculated from eq.(2.27). Finally, the total effective strain at each mesh point is calculated from values on the flow lines by linear interpolation.

5.1.17 Stresses

For the description of an axisymmetric stress field, two stress functions are required. Let us propose the following polynomial forms as trial functions

$$\phi_1(r,z) = \sum_m \sum_n B_{mn} r^{2m+3} z^n$$
$$\phi_2(r,z) = \sum_p \sum_q C_{pq} r^{2p+1} z^q \qquad (5.1.7)$$

where B_{mn} and C_{pq} are parameters to be determined.

From the stress functions, according to expressions (2.16), the trial functions corresponding to the stress field are obtained as follows

$$\sigma_\theta = \sum_p \sum_q C_{pq}(2p+1) r^{2p} z^q$$
$$\sigma_z = \sum_m \sum_n B_{mn}(2m+3)(2m+2) r^{2m} z^n$$
$$\sigma_r = \sum_m \sum_n B_{mn} n(n-1) r^{2m+2} z^{n-2} + \sum_p \sum_q C_{pq} r^{2p} z^q \qquad (5.1.8)$$
$$\tau_{rz} = -\sum_m \sum_n B_{mn}(2m+3) n\, r^{2m+1} z^{n-1}$$

The ϕ_1 and ϕ_2 expressions have been chosen in such a way as to have a general polynomial form and, at the same time, allow the stress field to accomplish the following boundary conditions for any set of values of their free parameters:

(1) Radial stress σ_r, axial stress σ_z and tangential stress σ_θ are symmetrical across the z axis.

(2) For mesh points on the z-axis (r=0), conditions of axisymmetry require: $\tau_{rz} = \sigma_\theta = \sigma_r = 0$, $\sigma_z = f(z)$ where $f(z)$ is the expression of $\sigma_z(r,z)$ for $r = 0$.

(3) For mesh points on the entry boundary:

$$\sigma_r = \sigma_\theta = \tau_{rz} = 0 \ , \ \sigma_z \neq 0.$$

(4) The axial stress σ_z vanishes along the exit plane.

(5) The axial symmetry condition also requires that the functions σ_r, σ_θ and σ_z be even in the r variable, while τ_{rz} be odd in this variable.

5.1.18 The Error Functions

By substituting eqs(2.31) and (5.1.8) into Prandtl-Reuss's eq.(2.43), the following error functions are obtained

$$R_{1n} = \sigma_r - \sigma_m - \frac{k}{\sqrt{I_2}} \dot{\varepsilon}_r$$

$$R_{2n} = \sigma_\theta - \sigma_m - \frac{k}{\sqrt{I_2}}\dot{\varepsilon}_\theta$$

$$R_{3n} = \tau_{rz} - \frac{k}{\sqrt{I_2}}\dot{\varepsilon}_{rz} \qquad (5.1.9)$$

where n is representing a generical node point,

$$\sigma_m = \frac{1}{3}(\sigma_r+\sigma_\theta+\sigma_z) \quad \text{and} \quad I_2 = \dot{\varepsilon}_{rz}^2 - (\dot{\varepsilon}_r'\dot{\varepsilon}_\theta'+\dot{\varepsilon}_\theta'\dot{\varepsilon}_z'+\dot{\varepsilon}_r'\dot{\varepsilon}_z')$$

The expression corresponding to σ_z does not appear to constancy of volume, since $\sigma_z = -(\sigma_r + \sigma_\theta)$.

Another error function R_{4n} is obtained from the boundary condition at the billet/die interface.

The frictional stress at the die/billet interface may be expressed in terms of a fraction of the shear yield stress of the billet material, i.e.

$$\tau_\alpha = Qk \quad \text{and} \quad Q = \sqrt{3}\,\mu \text{ (assumed)} \qquad (5.1.10)$$

where Q is the friction factor and varies between 0 and 1, and μ is the coefficient of friction assumed to be 0.07 {17}, {21} (for lubricated condition).

Substituting eq.(5.1.10) into (2.12), the stresses on the conical surface corresponding to the die/billet interface

$$\frac{\sigma_r - \sigma_z}{2}\sin 2\alpha + \tau_{rz}\cos 2\alpha = Qk \qquad (5.1.11)$$

is obtained.

Consequently R_{4n} becomes

$$R_{4n} = \frac{\sigma_r - \sigma_z}{2} \sin 2\alpha + \tau_{rz} \cos 2\alpha - Qk \qquad (5.1.12)$$

where σ_r, σ_z and τ_{rz} are to be substituted by eq.(5.1.8).

Eqs(5.1.9) are to be calculated in the whole deformed volume while eq.(5.1.11) is to be considered only at the die/billet interface.

These four error functions are to be joined together in a general error function R_n, as a linear combination of them with weighting factors

$$R_n = g_1 R_{1n} + g_2 R_{2n} + g_3 R_{3n} + g_4 R_{4n} \qquad (5.1.13)$$

In this case, these are $g_1 = g_2 = g_3$ and, hence

$$R_n = g_1 (R_{1n} + R_{2n} + R_{3n}) + g_4 R_{4n} \qquad (5.1.14)$$

The values of g_1 and g_4 are adopted proportional to the number of nodal points existing in the whole deforming zone and at the die/billet interface respectively.

After all substitutions have been made, the total of the residual over the entire discretised domain in terms of the coordinates and free parameters B_{mn} and C_{pq} is obtained

$$R_T = \sum_{n=1}^{N} \sum_{m=1}^{M} G_m R_{mn}(r, z, B_{mn}, C_{pq}) \qquad (5.1.15)$$

where G_m is the weighting factor discussed previously.

The nodal points lying on the surfaces r_2 and r_3 are relatively few. The significance of boundary conditions associated with these may be lost in this solution. Therefore, the weighting factors G_m are determined as

$$G_m = N/N_m$$

N : total number of nodal points,

N_m: number of nodal points on the boundary

The total residual R_T when expanded will be the form

$$R_T = A_i X_i + C \geq 0 \quad \text{for} \quad i = 1(1)p \qquad (5.1.16)$$

where p is the total number of free parameters, A_i replaces B_{mn} and C_{pq} and C is the constant term.

The expression of the total error function is to be squared and minimised with respect to the free parameters, in the volume of the deforming zone. The corresponding sequence of calculations will be programmed in the frame of the MWR, as was already described.

Given a residual function $R = R(A_p)$, a suitable weighting function can be chosen to force the residual to be zero in an average sense over the domain of interest. Applying

the least squares method we have

$$\frac{\partial}{\partial A_p} \int_{\nu} R^2(A_p) = 0 \qquad (5.1.17)$$

In a discrete domain, this can be expressed as

$$\frac{\partial}{\partial A_p} \sum_{i=1}^{N} R_i^2 (A) = \frac{\partial R_T^2}{\partial A_p} = 0 \qquad (5.1.18)$$

where $R_T = \sum_{i=1}^{N}$

From eq. (5.1.18) we have

$$R_T = A_i X_i + C$$

$$R_T^2 = A_i A_j X_i X_j + 2CA_i X_i + C^2 \qquad (5.1.19)$$

$$\frac{\partial R_T^2}{\partial A_p} = \delta_{ip} A_j X_p X_j + \delta_{jp} A_i X_i X_p + 2CX_p$$

$$= 2A_i X_i X_p + 2CX_p = 0$$

and, finally

$$\frac{\partial R_T^2}{\partial A_p} = A_i X_i X_p + CX_p = 0 \qquad (5.1.20)$$

which is a generical equation of the system to be solved. It is interesting to point out that the coefficient matrix of the system contains the same elements $\{X_i X_p\}$ as in R_T^2, making the derivative operation unnecessary.

Once the unknown free parameters A_i are determined, the stress field can be obtained from eq.(5.1.8). The complete sequence corresponding to the computer program is given in Appendix B1.

5.1.19 Normal and Shear Stresses on Boundary

The normal and shear stresses acting on the billet in contact with the die can be found from the stress values calculated by the method of weighted residuals, by using the standard equilibrium equations

$$\sigma_n = \sigma_r \cos^2\alpha + \sigma_z \sin^2\alpha - 2\tau_{rz} \sin\alpha\cos\alpha \qquad (5.1.21)$$

and $$\sigma_s = \tau_{rz} \cos 2\alpha + (\sigma_r - \sigma_z) \sin 2\alpha/2$$

where α is the die semi-angle.

Then the local coefficient of friction can be defined at each K position along the die/billet interface simply as

$$\mu = \left| \frac{\sigma_s}{\sigma_n} \right| \qquad (5.1.22)$$

5.2 A Solution by Weighted Residuals

A discrete method of weighted residuals (least squares) is used to obtain velocity and stress field in the deformation zone of axially symmetrical forward extrusion for a work-hardening material. The formulation of the problem is discussed here.

The deformation boundary in the die as shown in Fig. 5.2.1 is approximated by

$$r^*(z) = -\tan\alpha z + 15 \qquad (5.2.1)$$

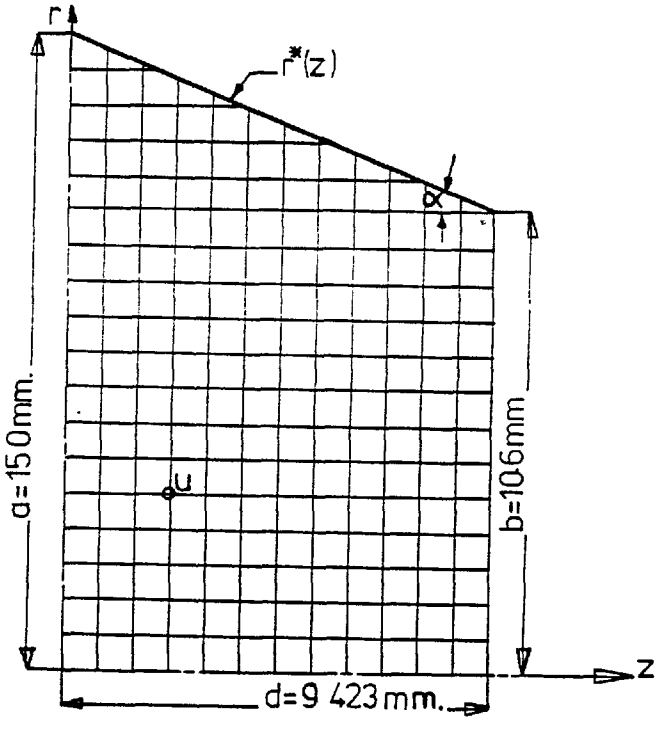


Fig. 5.2.1 Mesh and Boundary Surfaces

Stream and stress functions were proposed by Steck {75}, {76} as follows

$$\psi = \psi_o \frac{r^2}{r^{*2}(z)} + (r^2 - r^{*2}(z)) \sum^{I} \sum^{J} A_{ij} r^{2i+2} z^{j+1}$$

$$\phi_1 = \sum^{M}\sum^{N} B_{mn} r^{2m+3} z^n$$

$$\phi_2 = \sum^{P}\sum^{Q} C_{pq} r^{2p+1} z^q \qquad (5.2.2)$$

where A_{iJ} , B_{mn}, C_{pq} are unknown parameters and ψ_o is a constant. From eqs(2.31) and (2.16) the following can be obtained

$$\begin{aligned}
\dot{\varepsilon}_r &= \dot{\varepsilon}_r(r,z,A_{i\dot{J}}) \\
\dot{\varepsilon}_\theta &= \dot{\varepsilon}_\theta(r,z,A_{i\dot{J}}) \\
\dot{\varepsilon}_z &= \dot{\varepsilon}_z(r,z,A_{i\dot{J}}) \\
\dot{\varepsilon}_{rz} &= \dot{\varepsilon}_{rz}(r,z,A_{i\dot{J}}) \\
I_2 &= I_2(r,z,A_{i\dot{J}}) \\
\sigma_r &= \sigma_r(r,z,B_{mn},C_{pq}) \\
\sigma_\theta &= \sigma_\theta(r,z,C_{pq}) \\
\sigma_z &= \sigma_z(r,z,B_{mn}) \\
\tau_{rz} &= \tau_{rz}(r,z,B_{mn}) \\
\sigma_m &= \sigma_m(r,z,B_{mn},C_{pq})
\end{aligned} \qquad (5.2.3)$$

Applying stress strain relationship eq.(2.43), the following error functions were obtained

$$R_{1u} = \sigma_r(r_u,z_u,B_{mn},C_{pq}) - \sigma_m(r_u,z_u,B_{mn},C_{pq}) - \frac{k}{\sqrt{I_2(r_u,z_u,A_{i\dot{J}})}}\dot{\varepsilon}_r(r_u,z_u,A_{i\dot{J}})$$

(5.2.4)

If these errors are calculated and their squares are added up for various points of the deformation zone, at the intersection points of the rectangular grid as shown in Fig. 5.2.1, then one obtains the error function in terms of free parameters as

$$R_1(A_{i\dot{J}}, B_{mn}, C_{pq}) = \sum^{U} (R_{1u})^2 > 0 \qquad (5.2.5)$$

Similarly, constancy of volume was assumed and the two remaining independent error functions R_2 and R_3 were also obtained from eq.(5.2.3). Applying the following boundary condition for the die/billet interface one more error function R_4 was obtained

$$R_4(B_{mn}, C_{pq}) = \sum^{U} (R_{4u})^2 = \sum^{U} \left[\tau_{rz}(r_u, z_u, B_{mn}, C_{pq}) - \tau^*_{rz}\right]^2 \geq 0 \qquad (5.2.6)$$

where $\tau_{rz} = \tau^*_{rz} = -k/2$

Consequently, the total error

$R_T = \sum^{J} G_{\dot{J}} R_{\dot{J}}$ formed by adding the individual error functions, eventually multiplied by weight function $G_{\dot{J}}$.

From the condition, that the total error must be minimum, according to eq.(3.11) one obtains a system of equations from which the values of $A_{i\dot{J}}$, B_{mn}, and C_{pq} can be determined. As these equations are non-linear, an iterative procedure illustrated in Fig. 5.2.2 was employed.

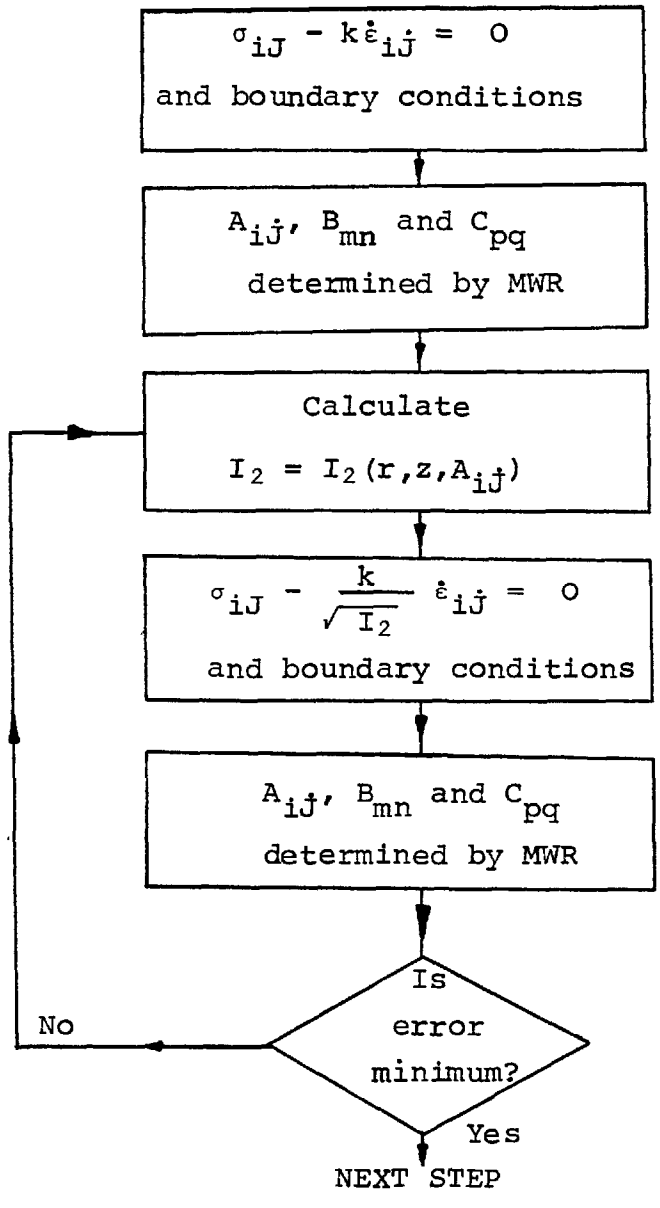


Fig 5.2.2 Iterative procedure {76}

Considerable time and effort was spent in trying to produce the results obtained by Steck {76}. A computer programme was developed following the iterative procedure illustrated in Fig 5.2.2 and did not converge to solution.

In a first approach, it was assumed that eq.(2.43) may be written as

by means of symbolic notation $T' = kV_s$.

In the next step, the error functions were recalculated with $\frac{k}{\sqrt{I_2^{(1)}}}$ instead of only k in order to find a "better" set of parameters after the first step of iteration where I_2 is assumed to be equal to unity and the system is equivalent to viscous fluid with viscosity $\eta = k/2$. This may be considered as sufficient proof that there are no programming errors. The programme was tried for various geometry and friction conditions and in no case could meaningful results be obtained.

The results obtained from the iterative procedure and seemed unreasonable have now been discarded as being unreliable on account of the following explanation:

It is observed that this formulation of the problem is not satisfactory. Eq.(5.2.4) is not the same as the residual function, eq.(3.6). It indicates as though two sets of approximating functions with unknown parameters were proposed for the same quantity and then the parameters were determined minimising the difference between these two sets of approximating functions. This formulation of the problem can be expressed as follows

$$\lambda\{A\}\{X\} - \{B\}\{Y\} = 0 \qquad (5.2.7)$$

where $\lambda = \lambda(A)$.

Here, it is possible to determine several sets of A and B satisfying the requirements with given X and Y values. Mathematically, there is no reason why any of these solutions should be considered unique unless a criterion with a physical meaning is established. Therefore, it would seem that this approach is not very sound. It is possible to get around this difficulty by obtaining strain rate field through a predetermined velocity field obtained by using some other technique discussed in section 5.3 and construct residual functions of the form

$$\sigma_{ij}(r,z,B_{mn},C_{pq}) - \frac{k}{\sqrt{I_2(r,z)}}\dot{\varepsilon}_{ij} = R \neq 0 \qquad (5.2.8)$$

5.3 A Study on Upper-bound Solution of Axisymmetric Extrusion Through a Conical Die

5.3.1 Introduction

Mathematically exact solutions to metal forming problems are difficult to obtain, so extremum principles are being increasingly used. The solution proposed here is derived from the limit theorems first put forward by Hill {77} and independently by Drucker, Greenberg and Prager {78} which may be stated as: "The yield point loads, determined by equating the external work to the internal work done in a deformation zone, satisfying the displacement boundary conditions by that stress distribution needed to enforce it at each point, are not less than the actual yield-point loads. The stress distribution need not be in equilibrium and is only defined where the strain rate is non zero".

Prager {79} also states the fundamental limit analysis theorem for upper bound as follows: "in a rigid, perfectly plastic continuum, plastic flow must occur under loads for which an unstable, kinematically admissible velocity field can be found".

The analytical expression of the theorem for a solid obeying von Mises yield criterion and characterised as an isotropic rigid-perfectly plastic material is {54}

$$W = \frac{2}{\sqrt{3}} Y \int_{\nu} \left[\frac{1}{2} \dot{\varepsilon}^{P}_{iJ} \dot{\varepsilon}^{P}_{iJ} \right]^{1/2} d\nu + \int_{S_r} \tau^* |\Delta V| dS_r - \int_{S_t} T_J V_J dS_t \quad (5.3.1)$$

where v is the deformed volume, S_r represents velocity discontinuities and S_t is the portion of the outer surface where external stresses T_j are applied. According to the sign convention, in equation (5.3.1) T_j^* denotes tractions. $\dot{\varepsilon}_{ij}^{P*}$ is the strain rate field derived from the velocity field V_j^*. If V_j^* is kinematically admissible so is $\dot{\varepsilon}_{ij}^{P*}$.

Numerous applications of the upper bound method to the analysis of axisymmetric extrusion through conical dies have appeared in the literature in recent years {54}. Johnson {80} suggested first an expression for an upper-bound. He considered a simplified slip-line field, composed of a series of appropriate straight lines, in which the metal was subjected to velocity discontinuities along these lines but moves between them as a rigid body. An upper-bound extrusion load was calculated by evaluating the shear deformation along the slip lines.

Kudo {81} introduced the concept of a unit rectangular deforming region in plane-strain problems and considered several types of admissible velocity fields in the deforming regions in order to find a better upper-bound solution. Of his velocity fields, it appears that the rigid-triangle velocity field lends itself best to the analysis of plane-strain forming processes in which deformation zones are bounded by straight lines. Kudo extended the concept

of the unit rectangular deforming region to the analysis of axisymmetric forming problems. He used it to solve rod, can, rod-rod and can-can extrusion problems as well as the compression of a cylindrical billet between flat platens. He also considered cavity formation during each of the above extrusion operations. Kudo examined a method for allowing for Coulomb friction which does not give a true upper bound {82} but is not likely to underestimate the working pressure if realistic values of friction coefficient are used.

Kobayashi {83} assumed curved surface discontinuities for the admissible velocity fields, which yield better upper-bound solutions for the forming pressure than the Kudo velocity fields. Kobayashi {84} also derived an upper bound solution for drawing and extrusion through conical dies using triangular deforming regions. This solution is similar to Alexander's {85} in that the stream lines run parallel to the die. In this work, his calculation of the upper bound was later shown to be incorrect since the effect of the shear strain rate $\dot{\varepsilon}_{rz}$ had been ignored {86}.

Kobayashi and Thomsen {87} discussed a method of approach to bounding solutions and in particular discuss a way of modifying an admissible stress field in two dimensions to one in three dimensions. They obtained upper and lower bounds for compressing a cylinder between rough platens, and frictionless extrusion through square and conical dies. Their upper bound for extrusion through square dies showed a slight improvement

on Kudo's solution. They also compared their results for extrusion through conical dies with a 60° semi-angle with Avitzur's {23} solution. The radial flow field {23} gives lower upper bounds for small reductions but for larger reductions Kobayashi's solution is better.

Upper and lower bounds for flange extrusion were obtained by Alexander and Lengyel {88} using a homogeneous velocity field for the upper bound, and a similar stress field to that used by Kobayashi and Thomsen for extrusion through square dies.

Halling and Mitchell {89} used a double triangle arrangement of velocity discontinuities similar to the solutions of Alexander {85} and Kobayashi but allowed a dead metal zone to form if this gave a lower upper bound. Their solution agrees well with that of Kobayashi and Thomsen {87} for reductions up to 70%, but for higher reductions Kobayashi and Thomsen's solution gives lower upper bounds. The Halling and Mitchell method of representing the velocity field in the form of a hodograph offers a very convenient means of solving axisymmetric problems using solid billets but cannot be used for problems such as tube extrusion from a hollow billet. They extended their solution to incorporate the effects of strain hardening, though this does not give a true upper bound as pointed out by Haddow {90}.

Lange and Steck {91} obtained an upper bound solution for tube extrusion through conical dies by setting the axial and radial velocities equal to functions of r and z. Some of the constants in the functions were determined by the boundary conditions and the remainder were arbitrary. Thus, the rate of internal energy dissipation could be optimised with respect to the arbitrary constants describing the velocity field.

Radial flow fields with two (entry and exit) velocity discontinuity lines were used by Stepanskii {92}, Avitzur {23}, Zimerman and Avitzur {93}, Pugh {94}, and more recently Osakada and Niimi {95}.

Lambert and Kobayashi produced a theory on the mechanics of axisymmetric extrusion through conical dies {96}. Their upper bound approach is based on the development of an admissible velocity field without discontinuities, obtained by superposition of basic flow patterns.

The radial flow field with spherical boundaries has often been used because of its simplicity. However, it is known that a field with spherical boundaries gives a higher upper bound value of extrusion pressure than some other fields do for large die angles. An attempt {97} has been made to improve the shapes of the velocity discontinuity surfaces of the radial flow field in order to achieve a lower upper bound value.

Avitzur {54} and others {98}, {99}, {100} have presented upper bound solutions to the axisymmetric extrusion using

generalized velocity fields for the plastic zone.

Essential to the formulation of a general upper bound solution is the selection of a general kinematically admissible velocity field applicable to the problem. In this work, an approach is outlined for obtaining such a velocity field.

5.3.2 Kinematically Admissible Velocity Field

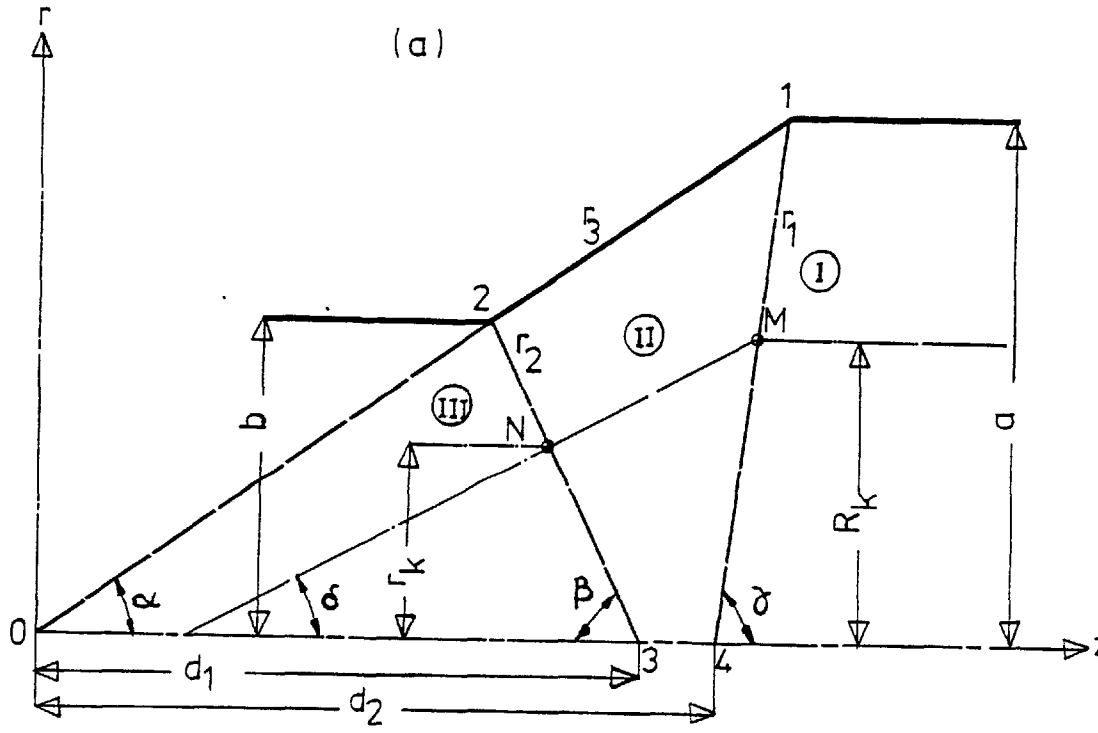
Consider the flow of a work-hardening material through a conical die as shown in Fig. 5.3.1. The flow is axisymmetric, and the deformation takes place in the zone enclosed by 1-2-3-4 and along the velocity discontinuities 1-4 and 2-3. The specimen is divided into three zones in which the velocity field is continuous. In zone I and III the velocity is uniform and has an axial component only.

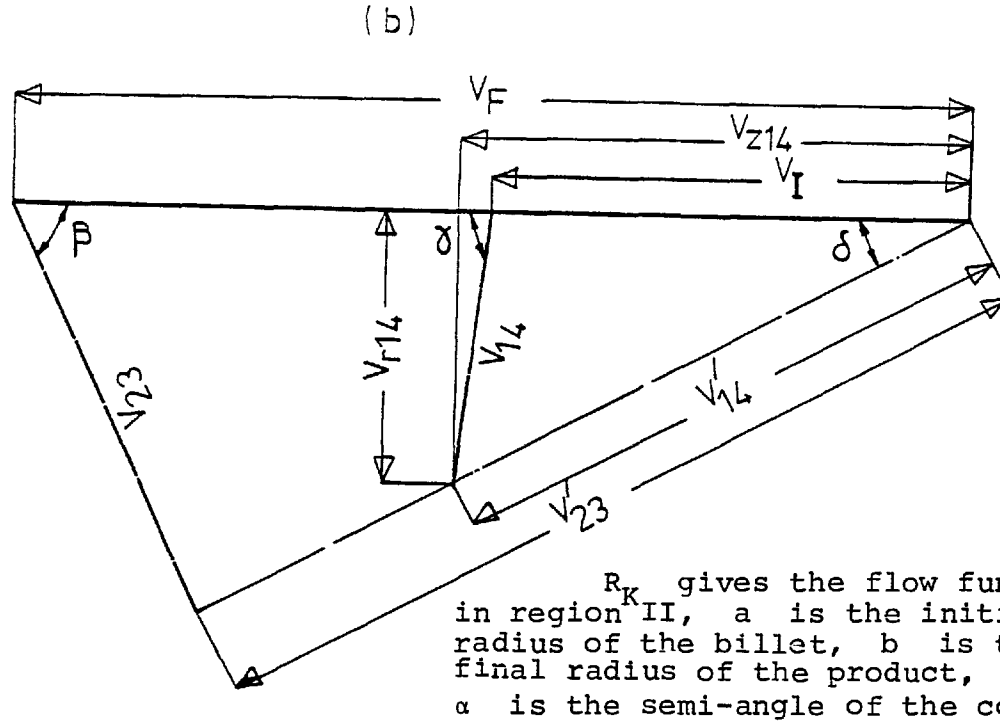
In zone I deformation has not yet began. Deformation starts when the incoming specimen crosses the boundary surface r_1 and ends at surface r_2.

In any upper-bound solution, the assumed strain rate field and therefore the velocity field must satisfy incompressibility and velocity boundary conditions.

In Fig. 5.3.1 (b) it is seen that the velocity components in zones I and III are given by

$$\begin{aligned} &\text{zone I} \quad v_r = 0 , \quad v_z = v_I \\ &\text{zone III} \quad v_r = 0 , \quad v_z = v_F \end{aligned} \tag{5.3.2}$$





R_K gives the flow function in region II, a is the initial radius of the billet, b is the final radius of the product, α is the semi-angle of the converging die and d_1 and d_2 are the coordinates which determine the geometry of the flow lines.

Fig. 5.3.1 Kinematically admissible velocity field and its associated hodograph.

The equation for the curves of velocity discontinuities 14 and 23 can be found from the requirement that the normal velocity component must be continuous across these curves. The velocity components along the discontinuity curve 14 in Fig. 5.3.1 (b), for example, must satisfy the equation

$$\frac{dz_{14}}{dr} = \frac{v_{z_2} - v_{z_1}}{v_{r_2} - v_{r_1}} \tag{5.3.3}$$

where v_{z_1}, v_{r_1}, v_{z_2} and v_{r_2} are the velocity components in zone I and II respectively.

From the hodograph associated with the pattern of the flow the streamline directions are as shown in Fig. 5.3.1 and the velocity components

$$v_{r_1} = 0, \quad v_{z_1} = v_I$$

$$v_{r_2} = v_{r_{14}} = v_{14} \sin\delta \ , \ v_{z_2} = v_{z_{14}} = v'_{14} \cos\delta \tag{5.3.4}$$

where $v_{14} = \dfrac{v_I \sin\delta}{\sin(\gamma - \delta)}$ and $v'_{14} = \dfrac{v_I \sin\gamma}{\sin(\gamma - \delta)}$.

Substituting the values v_{z_1}, v_{r_1}, v_{z_2} and v_{r_2} from eq. (5.3.4) into eq. (5.3.3), one obtains

$$z_{14} = \cot\gamma r + c \tag{5.3.5}$$

where c is a constant determined by the use of one of the boundary conditions given by

$$z_{14} = d_2 \quad \text{at} \quad r = 0 \quad \text{and} \quad z_{14} = a\cot\alpha \quad \text{at} \quad r = a$$

Thus the equation for the curve 14 becomes

$z_{14} = \cot\gamma r + d_2$. Similarly $z_{23} = -\cot\beta r + d_1$

In zone II the flow lines are

$$z = c_1 r + c_2 \tag{5.3.7}$$

where coefficients c_1 and c_2 are determined for each flow line for given velocity discontinuity curves formed in eq. (5.3.6). From the conditions at points M and N in Fig. 5.3.1 (a) the flow lines in zone II are then given by:

$$z = \frac{1}{q}\left[(p + \frac{t}{R_k})r - (nR_k + s)\right] \tag{5.3.8}$$

where $q = 1 - \frac{b}{a}$, $p = \cot\gamma + \frac{b}{a}\cot\beta$, $t = d_2 - d_1$, $n = \frac{b}{a}(\cot\gamma + \cot\beta)$ and $s = \frac{b}{a} d_2 - d_1$. The solution of eq. (5.3.8) for R_k gives the flow function in zone II.

Thus R_k becomes

$$R_k = \frac{1}{2n}\left[(pr - qz - s) + ((pr - qz - s)^2 + 4tnr)^{1/2}\right] \tag{5.3.9}$$

where p, q, n, s and t are defined in eq.(5.3.8).

A velocity field {100} which satisfies the incompressibility eq. (2.29) and the form of streamlines given by equation $\eta(r, z)$ = Constant is of the general form

$$\begin{aligned} v_r &= -\frac{1}{r} f'(\eta) \frac{\partial \eta}{\partial z} \\ v_z &= \frac{1}{r} f'(\eta) \frac{\partial \eta}{\partial r} \end{aligned} \tag{5.3.10}$$

where $f(\eta) = \psi$ (flow function) and $f'(\eta) = df(\eta)/d\eta$. From continuity across entry boundary r_1, eq. (5.3.3) solved for $f'(\eta)$ becomes, on simplication,

$$f'(\eta)\Big|_{(r,z)=(R_k,z_k)} = -v_I R_k \frac{dR_k}{dn_1} \tag{5.3.11}$$

similarly, satisfying continuity across exit boundary r_2 yields

$$f'(\eta)\Big|_{(r,z)=(r_k,\,z_k)} = -v_F r_k \frac{dr_k}{d\eta_2} \tag{5.3.12}$$

Equations (5.3.11) and (5.3.12) are admissibility conditions on $f'(\eta)$. Appropriate form for $f'(\eta)$ which satisfies these admissibility conditions is {100}

$$f'(\eta) = -v_F r_k \frac{dr_k}{d\eta} = -v_I R_k \frac{dR_k}{d\eta}$$

or (5.3.13)

$$f(\eta) = \psi = -v_F \frac{r_k^2}{2} + c = -v_I \frac{R_k^2}{2} + c \quad \{100\}$$

where ψ is flow function, c is a constant and r_k and R_k are defined in Fig. (5.3.1). Substituting eq. (5.3.13) in eq. (2.30) and an inspection of the incompressibility equation and velocity boundary conditions, the following equation for a velocity field is obtained

$$v_r = \frac{v_I b^{1/2}}{4n^2 r z \tan\alpha}\, y \left(\frac{\partial y}{\partial z} - \frac{y}{2z}\right)$$

$$v_z = -\frac{v_I b^{1/2}}{4n^2 r z \tan\alpha}\, y \frac{\partial y}{\partial r} \tag{5.3.14}$$

where $y = (pr - qz - s) + ((pr - qz - s)^2 + 4tnr)^{1/2}$

$$\frac{\partial y}{\partial z} = -q\left(1 + \frac{(pr - qz - s)}{\left[(pr - qz - s)^2 + 4tnr\right]^{\frac{1}{2}}}\right)$$

$$\frac{\partial y}{\partial r} = p + \frac{p(pr - qz - s) + 2tn}{\left[(pr - qz - s)^2 + 4tnr\right]^{\frac{1}{2}}}$$

and p, q, s, n and t are defined in eq. (5.3.8).

The strain rates in the deformation zone are

$$\dot{\varepsilon}_r = \frac{\partial v_r}{\partial r} = \frac{v_I b^{1/2}}{4n^2 rz\tan\alpha}\left\{\frac{y}{r}\frac{\partial y}{\partial z} + \frac{\partial y}{\partial z}\frac{\partial y}{\partial z} + y\frac{\partial}{\partial r}\left(\frac{\partial y}{\partial z}\right) + \frac{y^2}{2zr} - \frac{y}{z}\frac{\partial y}{\partial r}\right\}$$

$$\dot{\varepsilon}_z = \frac{\partial v_z}{\partial z} = \frac{v_I b^{1/2}}{4n^2 rz\tan\alpha}\left\{\frac{\partial y}{\partial z}\frac{\partial y}{\partial r} + y\frac{\partial}{\partial z}\left(\frac{\partial y}{\partial r}\right) - \frac{y}{z}\frac{\partial y}{\partial r}\right\}$$

$$\dot{\varepsilon}_\theta = \frac{v_r}{r} = \frac{v_I b^{1/2}}{4n^2 r^2\tan\alpha}\, y\left(\frac{\partial y}{\partial z} - \frac{y}{2z}\right) \qquad (5.3.15)$$

$$\dot{\varepsilon}_{rz} = \frac{1}{2}\left(\frac{\partial v_r}{\partial z} + \frac{\partial v_z}{\partial r}\right) = \frac{1}{2}\cdot\frac{v_I b^{1/2}}{4n^2 rz\tan\alpha}\left\{-2\frac{y}{z}\frac{\partial y}{\partial z} + \left(\frac{\partial y}{\partial z}\right)^2\right.$$

$$\left. + y\frac{\partial}{\partial z}\left(\frac{\partial y}{\partial z}\right) + \frac{y^2}{z^2} + \frac{y}{r}\frac{\partial y}{\partial r} - \left(\frac{\partial y}{\partial r}\right)^2 - y\frac{\partial}{\partial r}\left(\frac{\partial y}{\partial r}\right)\right\}$$

and the corresponding second principal deviatoric invariant is then calculated by means of

$$I_2 = \dot{\varepsilon}_{rz}^2 - (\dot{\varepsilon}_r\dot{\varepsilon}_\theta + \dot{\varepsilon}_r\dot{\varepsilon}_z + \dot{\varepsilon}_z\dot{\varepsilon}_\theta) \qquad (5.3.16)$$

where $$\frac{\partial}{\partial r}\left(\frac{\partial y}{\partial z}\right) = -q\left[px - \frac{\partial x}{\partial r}(pr - qz - s)\right]/x^2$$

$$\frac{\partial}{\partial z}\left(\frac{\partial y}{\partial r}\right) = -\left[pqx + \frac{\partial x}{\partial z}((pr - qz - s)p + 2tn)\right]/x^2$$

$$x = \left[(pr - qz - s)^2 + 4tnr\right]^{1/2}$$

$$\frac{\partial x}{\partial r} = \left[p(pr - qz - s) + 2tn\right]/x$$

$$\frac{\partial x}{\partial z} = -q(pr - qz - s)/x$$

$$\frac{\partial}{\partial z}\left(\frac{\partial y}{\partial z}\right) = q\left[qx + \frac{\partial x}{\partial z}(pr - qz - s)\right]/x^2$$

$$\frac{\partial}{\partial r}\left(\frac{\partial y}{\partial r}\right) = \left[p^2x - \frac{\partial x}{\partial r}(p(pr - qz - s) + 2tn)\right]/x^2$$

5.3.3 Upper Bound Solution

As an application of the velocity field discussed in the foregoing, the upper bound to the extrusion pressure through a conical die is calculated.

It can be readily shown that the extrusion pressure P is equal to the work done per unit volume of billet extruded, which is made up of four parts, namely;

(1) Work of homogeneous deformation per unit volume P_1 to change the shape of the billet into that of the product.

(2) Work per unit volume against the billet-die friction P_2.

(3) Work per unit volume against the billet-container friction P_3.

(4) Redundant work per unit volume P_4.

Assuming that the contributions of these components additive the total extrusion pressure P can be written as

$$P = P_1 + P_2 + P_3 + P_4 \qquad (5.3.17)$$

It is clear from the above that, before meeting the die, the billet can be assumed to be travelling without deformation parallel to its axis towards the die entry and within the die zone 1-2 (Fig. 5.3.1) to be undergoing homogeneous deformation and travelling along the stream lines. Some boundary, at the die entry separate these two regions. In crossing this boundary, the material is sheared to change its direction of travel and the work done constitutes the redundant work. A similar situation exists at the exit.

5.3.4 Strain Distribution in the Product

The equivalent strain distribution in the product is calculated by integrating the incremental strain along a stream line which has an angle of inclination δ to the axis in the deformation zone as seen in Fig. 5.3.1.

Before the stream lines can change from their initial axial movements as shown in Fig. 5.3.2, the work material must have been subjected to shear corresponding to a strain ε_{s_1} along the entry boundary and therefore it has undergone some work-hardening. Similarly, at the exit the work material

suffers a strain ε_{s_1} at entry to the die, a strain ε_d imposed in the deformation zone as it approaches the exit boundary, a strain ε_{s_2} at the exit from the die and a final strain ε as it emerges

$$\varepsilon = \varepsilon_{s_1} + \varepsilon_d + \varepsilon_{s_2} \qquad (5.3.18)$$

The shear strains at entry and exit constitute the redundant strains. Further, the redundant strains for the entry and exit boundaries are not the same, the work done in crossing the entry is usually much less than the exit because the flow stress is generally much smaller.

The jump in strain $\Delta\bar{\varepsilon}$ at point 1 (in Fig. 5.3.2) can be obtained from the jump in shear strain $\Delta\gamma$ at point 1

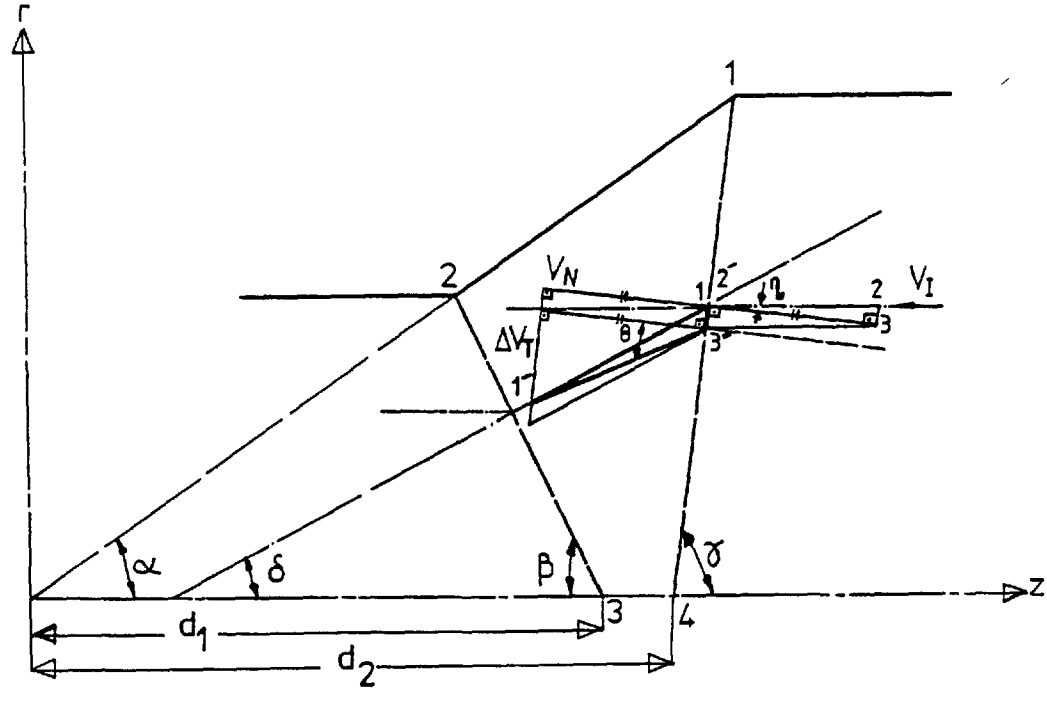


Fig. 5.3.2 Assumed mode of strain deformation on the velocity discontinuity curve.

Considering Fig. 5.3.1(b), the total velocity v_{12} along the die is calculated from its known components, and $\Delta\gamma s_1 = \frac{\Delta v_I}{v_N}$ can be obtained graphically, from which

$$\Delta\bar{\varepsilon} = \Delta\gamma s_1/\sqrt{3} \tag{5.3.19}$$

For continuity, the component of velocity of the work material normal to the boundaries, e.g. 14, must remain unchanged when the work material crosses it. It follows that the velocity components immediately to the left of M are shown in Fig. 5.3.1(b) where the velocity v_{14} is given to the work material along the tangent to the boundary. From Fig. 5.3.1(b) it follows that

$$v_{14} = \frac{v_I \sin\delta}{\sin(\gamma - \delta)}\ ,\quad v_{23} = \frac{v_F \sin\delta}{\sin(\beta + \delta)}\ ,$$
$$v'_{14} = \frac{v_I \sin\gamma}{\sin(\gamma - \delta)} \quad \text{and} \quad v'_{23} = \frac{v_F \sin\beta}{\sin(\beta + \delta)} \tag{5.3.20}$$

From the above definition, the engineering shear strain {95} γs_1 at the entry velocity discontinuity line 14 shown in Fig. 5.3.2 is

$$\gamma_{s_1} = \frac{v_{13}}{v_N} = \frac{v_{13}}{v_I \sin\gamma} = \frac{\sin\delta}{\sin\gamma\sin(\gamma - \delta)} \tag{5.3.21}$$

and the equivalent strain εs_1 from eq. (5.3.19)

$$\varepsilon_{s_1} = \frac{\sin\delta}{\sqrt{3}\,\sin\gamma\sin(\gamma - \delta)}\ .$$

similarly $$\varepsilon_{s_2} = \frac{\sin\delta}{\sqrt{3}\,\sin\beta\sin(\beta + \delta)} \qquad (5.3.22)$$

The strain imposed in the deformation zone is expressed by

$$\varepsilon_d = \int d\varepsilon = -\int_{r_k}^{R_k} \frac{d\varepsilon}{dt}\,\frac{dt}{dr}\,dr = -\int_{r_k}^{R_k} \dot{\varepsilon}\,\frac{dr}{\frac{dr}{dt}} = -\int_{r_k}^{R_k} \dot{\varepsilon}\,\frac{dr}{v_r} \qquad (5.3.23)$$

where $\dot{\varepsilon} = \frac{2}{\sqrt{3}}\sqrt{I_2}$ and I_2 is given in eq. (5.3.16).

Finally the equivalent strain of the material in the product which has passed along a stream line with an angle of inclination δ to the axis is

$$\bar{\varepsilon} = \frac{\sin\delta}{\sqrt{3}}\left(\frac{1}{\sin\gamma\sin(\gamma - \delta)} + \frac{1}{\sin\beta\sin(\beta + \delta)}\right) + \varepsilon_d \qquad (5.3.24)$$

5.3.5 Power involved in the Deformation of the Billet

In relation to the deformation process of the billet, two different kinds of power are identified: dissipative and active powers.

The sources of dissipation or consumption of energy for the billet are:

1. Dissipation on the surfaces of discontinuities, while the active power is due to the punch pressure of extrusion. Surfaces r_1 and r_2 are surfaces where discontinuities exits in the velocity field. Such discontinuities parallel

to the surfaces have values given in eq. (5.3.6).

The energy-dissipation rate due to shear along the line 14 in Fig. 5.3.1(a) is expressed as

$$\dot{E}_{13} = \int_0^a \frac{\bar{\sigma}}{\sqrt{3}} |v_{14}| 2\pi r \frac{dr}{\sin\gamma} \tag{5.3.25}$$

similarly, the energy-dissipation rate along the line 23 is obtained as

$$\dot{E}_{23} = \int_0^b \frac{\bar{\sigma}}{\sqrt{3}} |v_{23}| 2\pi r \frac{dr}{\sin\beta} \tag{5.3.26}$$

where γ and β are the angles between the z-axis and the lines 14 and 23 respectively, v_{14} and v_{23} are the amount of velocity discontinuities given by eq.(5.3.2), $\bar{\sigma}$ is the flow stress expressed by eq. (2.45) and a and b defined in Fig. 5.3.1 are the limits of the integrals. Substitution of eqs (2.45) and (5.3.22) into equations (5.3.25) and (5.3.26), and integrations result in

$$\dot{E}_{13} = \pi c V_I \left(\frac{\sin\delta}{\sqrt{3}\sin\gamma\sin(\gamma - \delta)}\right)^{(\lambda+1)} a^2 \tag{5.3.27}$$

$$\dot{E}_{23} = \pi c V_F \left(\frac{\sin\delta}{\sqrt{3}\sin\beta\sin(\beta + \delta)}\right)^{(\lambda+1)} b^2$$

where c and λ are defined in eq. (2.45) and their values for commercially pure aluminium given in {63}.

2. The dissipation of power due to friction at the die-billet interface can be expressed as

$$\dot{E}_{12} = \int_{r_3} \tau^* |v_{12}| 2\pi r \frac{dr}{\sin\alpha} \qquad (5.3.28)$$

where α is the half-angle of a converging die, v_{12} is the discontinuity in velocity across r_3 and τ^*, given by eq. (5.1.10), is the tangential stress developed at the die-billet interface due to friction. The absolute velocity along the die surface is

$$V_{12} = \frac{a}{r} v_I \frac{\sin\gamma}{\sin(\gamma - \alpha)} \qquad (5.3.29)$$

where a is the initial radius and α is the converging die of half-angle.

The flow stress varies along the die surface

$$\bar{\sigma}_d(r) = \bar{\sigma}(\bar{\varepsilon}_r) \qquad (5.3.30)$$

where $\bar{\varepsilon}_r = \varepsilon_{s_1} + \varepsilon_d(r)$

Substituting the values in eq. (5.3.28), the following expression is obtained

$$\dot{E}_{12} = 2\pi Q a v_I \frac{\sin\gamma}{\sin\alpha\sin(\gamma - \alpha)} \int_{r=b}^{a} k\,dr \qquad (5.3.31)$$

where k (the shear yield stress) $= \frac{\bar{\sigma}}{\sqrt{3}} = \frac{Y}{\sqrt{3}}$, Y is the tensile yield stress and Q is a friction factor between 0 and 1.

As a first approximation eq. (5.3.31) can be integrated using a mean value of k such that the dissipation of power due to friction at the die-billet interface can be expressed by

$$\dot{E}_{12} = \sqrt{3}\, k_{m_{12}} (\bar{\varepsilon}_2 - \bar{\varepsilon}_1) = \frac{c}{(\lambda + 1)} \left[\bar{\varepsilon}_2^{(\lambda+1)} - \bar{\varepsilon}_1^{(\lambda+1)} \right]$$

whence

$$\dot{E}_{12} = 2\pi Q a v_I \frac{\sin\gamma}{\sin\alpha\sin(\gamma - \alpha)} k_{m_{12}} (a - b) \qquad (5.3.32)$$

where $$k_{m_{12}} = \frac{c}{\sqrt{3}(\lambda + 1)} \left[\frac{\bar{\varepsilon}_2^{(\lambda+1)} - \bar{\varepsilon}_1^{(\lambda+1)}}{\bar{\varepsilon}_2 - \bar{\varepsilon}_1} \right] ,$$

$$\bar{\varepsilon}_1 = \frac{\sin\alpha}{\sqrt{3}\,\sin\gamma\sin(\gamma - \alpha)} , \quad \bar{\varepsilon}_2 = \frac{\sin\alpha}{\sqrt{3}\,\sin\beta\sin(\beta + \alpha)}$$

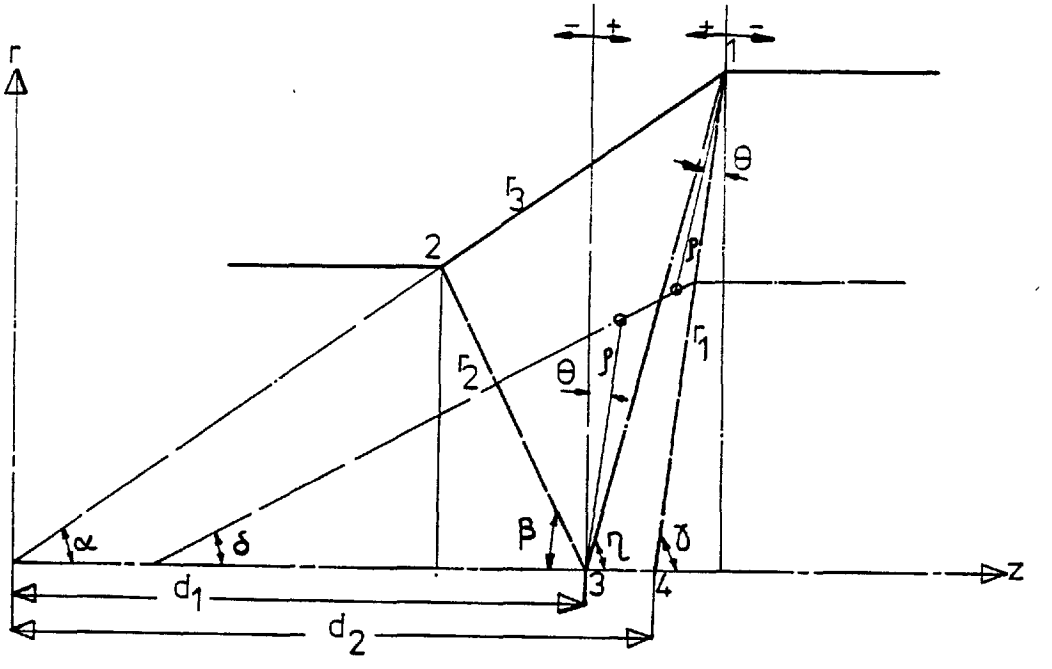
and c and λ are given in eq. (5.3.27).

3. For the continuously deforming region 1234, the energy-dissipation rate can be calculated according to

$$\dot{E}_{1234} = \iiint \bar{\bar{\sigma}}\bar{\bar{\dot{\varepsilon}}} 2\pi r dr dz \qquad (5.3.33)$$

where the integration must be performed over the total volume of deformation.

For the purpose of integration of eq. (5.3.33), the polar coordinate system (ρ,θ) is introduced on the meridian plane as shown in the following diagram.



Eq. (5.3.33) then, can be rewritten as

$$E_{1234} = \iiint_{\nu_{123}} \bar{\bar{\sigma}}\bar{\bar{\dot{\varepsilon}}} 2\pi\rho^2\cos\theta d\theta d\rho + \iiint_{\nu_{341}} \bar{\bar{\sigma}}\bar{\bar{\dot{\varepsilon}}} 2\pi\rho^2\cos\theta d\theta d\rho \qquad (5.3.34)$$

where $\nu = \nu_{123} + \nu_{341}$ is the total volume and the limits of integrations are

$$-(\frac{\pi}{2} - \beta) \leq \theta \leq (\frac{\pi}{2} - \eta)$$

$$0 \leq \rho \leq r_3 = \frac{d_1}{\cos\theta\cot\alpha - \sin\theta} \quad (r_3; \text{ expression for the die})$$

and

$$(\frac{\pi}{2} - \eta) \leq \theta \leq (\frac{\pi}{2} - \gamma)$$

$$0 \leq \rho \leq r_1 = \frac{a}{\cos\theta}$$

respectively.

Substituting the effective strain rate $\dot{\bar{\varepsilon}}$ eq.(2.26) and the flow stress $\bar{\sigma}$ eq.(2.45) into eq.(5.3.34) yields

$$\dot{E}_{1234} = \iiint_{\nu_{123}} c\bar{\varepsilon}_1^{\lambda} \frac{2}{\sqrt{3}} \sqrt{I}_2 2\pi\rho^2\cos\theta d\rho d\theta + \iiint_{\nu_{341}} c\bar{\varepsilon}_2^{\lambda} \frac{2}{\sqrt{3}} \sqrt{I}_2 \, 2\pi\rho^2\cos\theta d\rho d\theta \qquad (5.3.35)$$

$$\text{where}\quad \varepsilon_1 = -\frac{8n^2\tan\alpha}{\sqrt{3}v_I b^{1/2}} \int_{r=r_k}^{r} \sqrt{I_2}\,\frac{z\,dr}{y\left(\frac{\partial y}{\partial z} - \frac{1}{2z}y\right)} + \frac{\sin\delta}{\sqrt{3}\,\sin\beta\sin(\delta+\beta)}$$

$$\varepsilon_2 = -\frac{8n^2\tan\alpha}{\sqrt{3}v_I b^{1/2}} \int_{r=r}^{R_k} \sqrt{I_2}\,\frac{z\,dr}{y\left(\frac{\partial y}{\partial z} - \frac{1}{2z}y\right)} + \frac{\sin\delta}{\sqrt{3}\,\sin\gamma\sin(\gamma-\delta)}$$

r, R_k, β and γ are shown in Fig. 5.3.1, c and λ are given in eq.(5.3.27) and n, y and $\frac{\partial y}{\partial z}$ are defined in eq. (5.3.14).

For the numerical integration of eq. (5.3.35), the following Simpson's formula with 8-strip is performed

$$\int_{x_o}^{x_2} f(x)\,dx \doteq \frac{h}{3}(f_o + 4f_1 + 2f_2 + 4f_3 + 2f_4 + 4f_5 + 2f_6 + 4f_7 + f_8) \tag{5.3.36}$$

where $h = (x_2 - x_o)/2N$ and $2N$ is the total number of equal subintervals.

Finally, the total energy-dissipation rate of the deforming region is obtained by adding equations (5.3.27), (5.3.32) and (5.3.35), as

$$\dot{W} = \dot{E}_{14} + \dot{E}_{23} + \dot{E}_{12} + \dot{E}_{1234} \tag{5.3.37}$$

The actual external work rate $\dot{W}_a$ is expressed by

$$\dot{W}_a = pA_o|v_I| \tag{5.3.38}$$

where p is the extrusion pressure, A_o the initial section of the billet, and v_I the punch velocity.

For the pattern of Fig. 5.3.1, the plastic deformation energy rate per unit volume can be obtained by integrating along each streamline and taking into account the energy dissipation on the surfaces of discontinuities and the dissipation of power due to friction at the die/billet interface defined by eqs (5.3.27) and (5.3.32), respectively. The upper bound of the mean extrusion pressure is then calculated, in the following way, by the mean value of such computations along the various streamlines

$$\dot{W}_a \leqslant \dot{W} \tag{5.3.39}$$

Now, since all these are upper bound solutions, then the one giving the lowest extrusion pressure is the best and the others can be discarded. Such a solution can be obtained by minimizing the total energy rate eq.(5.3.37) with respect to β and γ (the arbitrary semi-angles of conical boundaries). This occurs when $\beta \cong 62^o$ and

$\gamma \doteq 83^{o}$, the mean extrusion pressure is then $\sim$ 9.52 tonf/in^2 ($\sim$ 147 MN/m^2)) (the measured pressure = 9.2 tonf/in^2($\sim$ /142 MN/m^2)) for commercially purity aluminium extruded through a conical die of semi-angle of 25^{o} with an extrusion ratio of 2.

It should be noted that the stress distribution need not be completely known in order to calculate the upper bound load.

In eq. (5.3.37), the minimization of the total energy rate with respect to β and γ (the arbitrary semi-angles of conical boundaries) was carried out using the NAG library subroutine E04CEF, which minimizes a function F(x) of N independent variables,

$$\underline{X} \quad (X_1, X_2, \ldots\ldots, X_N)^T.$$

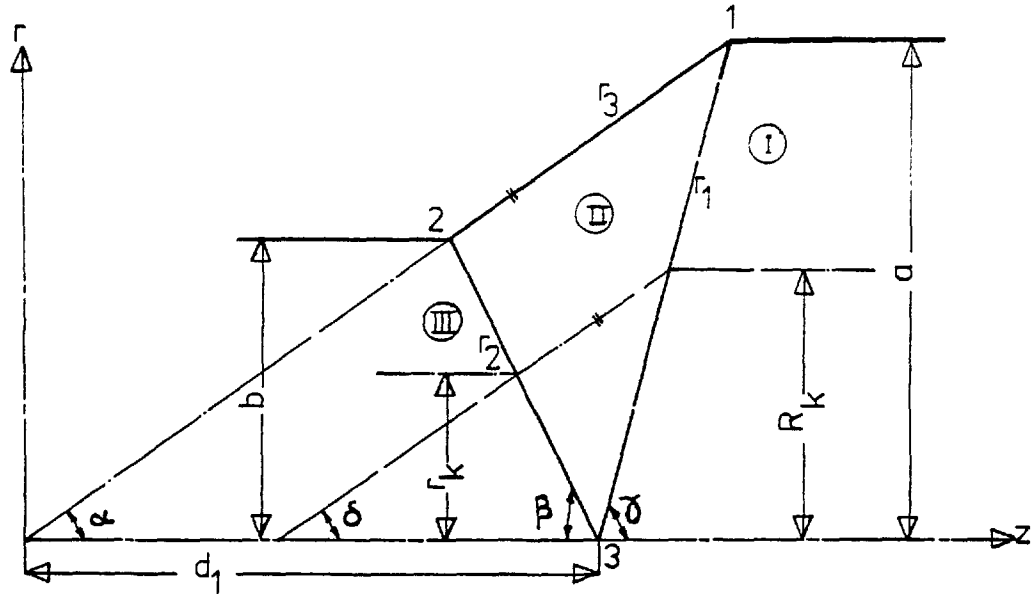
The following admissible velocity field is also selected to compare the upper bound load obtained by the previous kinematically admissible velocity field

$$v_r = -\frac{v_I(\cot\gamma + \frac{b}{a}\cot\beta)}{\frac{b^2}{a^2}(\cot\beta + \cot\gamma)^2}\left\{1 - \frac{z - d_1}{r}\left(\frac{1 - \frac{b}{a}}{\cot\gamma + \frac{b}{a}\cot\beta}\right)\right\}\cdot(1 - \frac{b}{a})$$

$$v_z = -\frac{v_I(\cot\gamma + \frac{b}{a}\cot\beta)^2}{\frac{b^2}{a^2}(\cot\beta + \cot\gamma)^2}\left\{1 - \frac{z - d_1}{r}\left(\frac{1 - \frac{b}{a}}{\cot\gamma + \frac{b}{a}\cot\beta}\right)\right\} \qquad (5.3.40)$$

where the initial velocity V_I , initial radius a, final radius b and d_1 is a parameter as seen in Fig. 5.3.3.

The total energy rate was obtained in the same way as explained above and then minimized with respect to β (the arbitrary semi-angle of conical boundary). This occurred when δ (an angle of inclination of a streamline, in this case, it is identical for all the streamlines) = α (half-angle of the die), $\beta \cong 53^\circ$ and $\gamma \cong 84{,}5^\circ$, the extrusion pressure is then 9.7 tonf/in^2 ($\sim$ 150 MN/m^2) for commercially purity aluminium extruded through a conical die of semi-angle of 25° with an extrusion ratio of 2.



where α is a converging die of half-angle d_1 is a parameter which determines the geometry of the flow lines, a and b are the initial and final radius respectively, $r_k = \frac{b}{a}R_k$ and R_k is the flow function in region II.

Fig. 5.3.3 Admissible velocity field.

5.4 A Method to Determine Stress Field

The method of weighted residuals described in Chapter 3 is now being used to calculate the stress field developed in the deforming zone during the direct (forward) extrusion of metals.

It is assumed that the pattern of deformation follows the arbitrary flow field described in 5.3 with the arbitrarily selected conical boundaries. The conditions held to be valid are:

The material is incompressible, isotropic and work hardens as in eq. (2.45). The elastic strains are small in comparison with plastic strains and can be neglected. The frictional stress at the tool/billet interface is assumed to be proportional to the shear yield stress of the material.

From the stress field, a value for the extrusion pressure is obtained, which can be compared with the experimental results.

5.4.1 Derivation of the Solution

The velocity field was described in 5.3, in a cylindrical coordinate system by the stream function

$$\psi = \frac{1}{2}V_I \frac{R_k^2 b^{1/2}}{z\tan\alpha} = \frac{1}{2}\frac{V_I b^{1/2}}{z\tan\alpha}\left[\frac{1}{2n}\left\{(pr - qz - s) + ((pr - qz - s)^2 + 4tnr)^{1/2}\right\}\right]^2 \qquad (5.4.1)$$

where V_I, R_k, p, q, n, s and t are defined in eq. (5.3.8) which gives, according to eq. (2.30), the velocity equations and the strain rate field given by eqs (5.3.14) and (5.3.15) respectively.

Hence for any nodal point the principal invariant of the strain rate tensor I_2 can be determined and k, the mean shear yield stress, is the same at all points at the beginning of deformation.

From the Prandtl-Reuss relationship (2.43), the governing equations can be written as

$$\begin{aligned}
\sigma_r - \sigma_m - \frac{k}{\sqrt{I_2}}\dot{\varepsilon}_r &= 0 \\
\sigma_\theta - \sigma_m - \frac{k}{\sqrt{I_2}}\dot{\varepsilon}_\theta &= 0 \\
\sigma_z - \sigma_m - \frac{k}{\sqrt{I_2}}\dot{\varepsilon}_z &= 0 \\
\tau_{rz} - \frac{k}{\sqrt{I_2}}\dot{\varepsilon}_{rz} &= 0
\end{aligned} \qquad (5.4.2)$$

and the boundary conditions

$$\begin{aligned}
\tau_{rz} - Qk &= 0 \qquad n \in \Gamma_3 \\
\sigma_z &= 0 \qquad n \in \Gamma_2
\end{aligned}$$

where n is any nodal point.

As constancy of volume is assumed, the equation corresponding to σ_z need not be considered.

For the description of an axisymmetric stress field which will satisfy the equilibrium conditions (2.15), two stress functions ϕ_1 and ϕ_2 given by eq. (5.1.7) are chosen.

Having satisfied all the requirements a set of residual functions could be assembled for each generic nodal point n as followed in eq. (5.1.9). The total of the residual over the entire discretised domain was given by eq. (5.1.15).

5.4.2 Description of the Computer Program

For simplicity the program was divided into a main program and subroutines MESH and STRESS. Subroutine MESH generates the coordinates of nodal points selected in the solid billet for the analysis of stress. Subroutine STRESS calculates the stress distribution, according to the method of weighted residuals already described.

The detailed sequence of operations performed during the process by each subroutine is summarised in the form of a flow chart in Fig. 5.4.1, which corresponds to the computer program given in Appendix B.

5.4.3 Main Program

The main program reads the data related to the physical and geometrical characteristics of the problem,

which are expressed as FORTRAN variables given in Appendix A. It also performs several preliminary operations which are enumarated in the corresponding flow chart presented as Fig. 5.4.1.

At the end of the input data the velocity and the strain rate fields are calculated. From the strain rate components, the strain components along the flow lines can be calculated according to the following equations

$$\begin{aligned} \varepsilon_r &= \int \dot{\varepsilon}_r \frac{dz}{v_z} \\ \varepsilon_z &= \int \dot{\varepsilon}_z \frac{dz}{v_z} \\ \varepsilon_\theta &= \int \dot{\varepsilon}_\theta \frac{dz}{v_z} \\ \varepsilon_{rz} &= \int \dot{\varepsilon}_{rz} \frac{dz}{v_z} \end{aligned} \qquad (5.4.3)$$

where v_z is the axial velocity along the flow lines.

5.4.4 Subroutine MESH

The coordinates of the nodal points are calculated with reference to a cylindrical system of coordinates (r, z), according to Fig. 5.4.2.

5.4.5 Subroutine STRESS

It performs the method of weighted residuals with the numerical values for the variables read in the main program and the coordinates generated in MESH. All these variables are contained in common declaration statements.

In order to solve the linear system of equations, this subroutine calls another subroutine F04A5F, a standard of the NAG library package. The complete sequence is summarised in the form of the flow chart in Fig. 5.4.1.

5.4.6 Stress Field in the Solid Billet

By means of the described program , the stress distribution produced during the direct (forward) extrusion process of a solid billet is obtained. This means the description of the stress tensor component fields : σ_r , σ_θ, σ_z and τ_{rz}. The strain heardening distribution in the billet, according to the adopted rule of hardening, is also described.

The numerical values selected for the physical and geometrical parameters which characterized the experiments carried out are as follows, in S.I. Units wherever relevant.

Number of flow lines	9
Number of nodes in z direction	19
Number of nodes at the die/billet interface	19
Semi-die angle	.4363E + 00
Semi-angle of entry boundary	.1448E +.01

Semi-angle of exit boundary	.1082E + 01
Radius at exit	.1060E + 01
Radius at entry	.1500E + 01
Velocity at exit	.4000E - 01
Velocity at entry	.2000E - 01
Constant Q (friction)	.1212E + 00
Constant c for the billet	.1560E + 04
Constant λ	.2500E + 00
Weighting factors (stress)	.1000E + 01
Number of error functions (stress)	4
Number of indices (stress 1)	3
Number of indices (stress 2)	3

As far as the polynomial solution is concerned, a polynomial of nine terms has been adopted for the determination of the unknown parameters in the expressions of the stress functions

$$\phi_1 = \sum_{m=1}^{3} \sum_{n=1}^{3} B_{mn} r^{2m+3} z^{n}$$

$$\phi_2 = \sum_{p=1}^{3} \sum_{q=1}^{3} C_{pq} r^{2p+1} z^{q}$$

This is achieved in the computer programme by making m = n = 3 and also p = q = 3. The calculations have also been made with higher values of indices (4, 5 and 6) and, since no significant differences with the previous results arise, the value 3 has been adopted for the final results.

The contours corresponding to the absolute velocity ($v_{abs} = v_{mag}/v_{Billet}$, $v_{mag} = \sqrt{v_r^2 + v_z^2}$ and v_r and v_z

are given in eq. (5.3.14)), the effective strain rate, the effective strain and the effective stress are given in Chapter 6.

In order to compare with the experimental results, the extrusion pressure has been calculated from the theoretical stress field. The method of weighted residuals is also used to compute the stress field for a non work-hardening material (lead) in the same way as explained above. The results of this analyses are summarised in Chapter 6.

Main Program

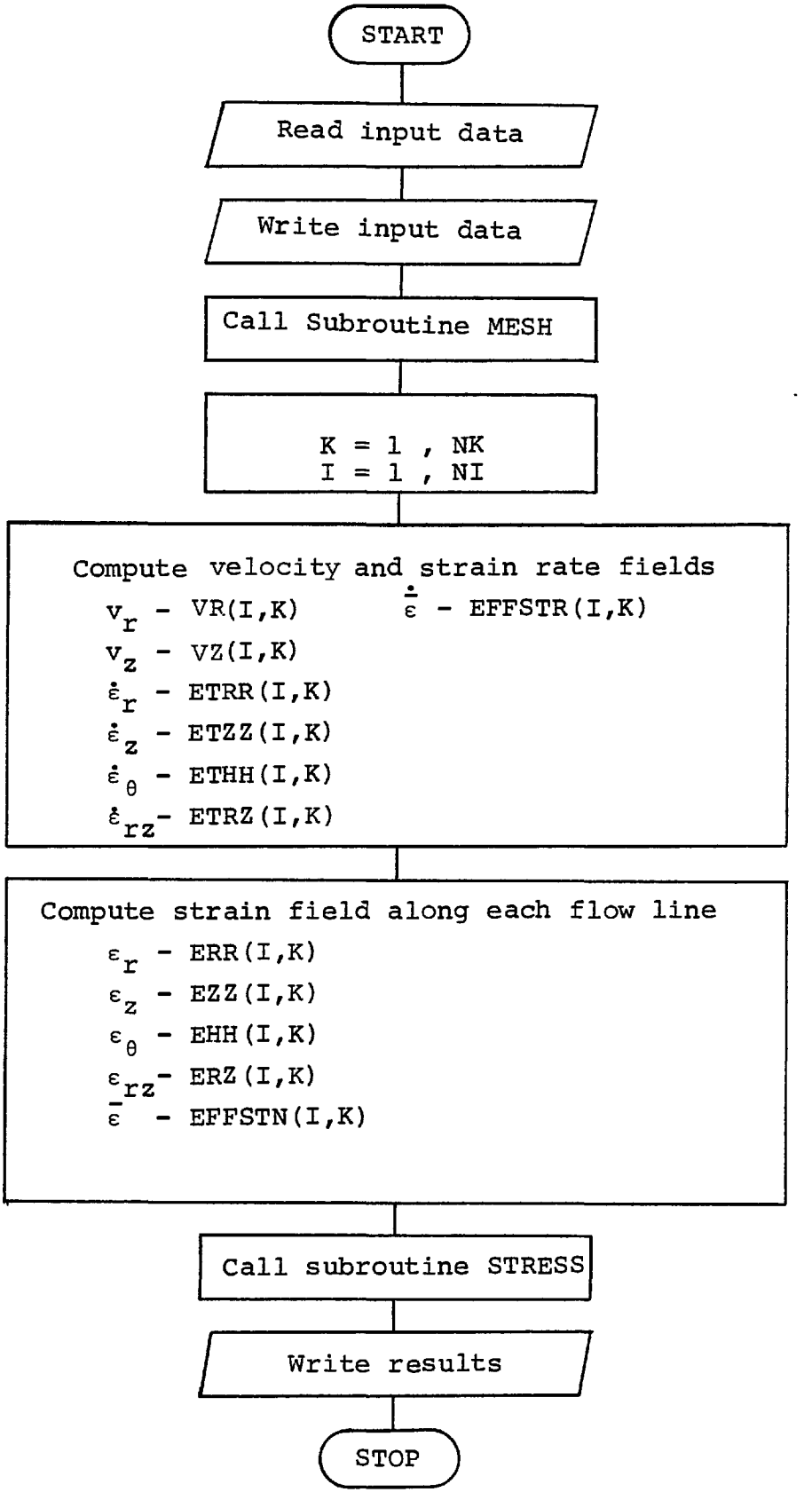
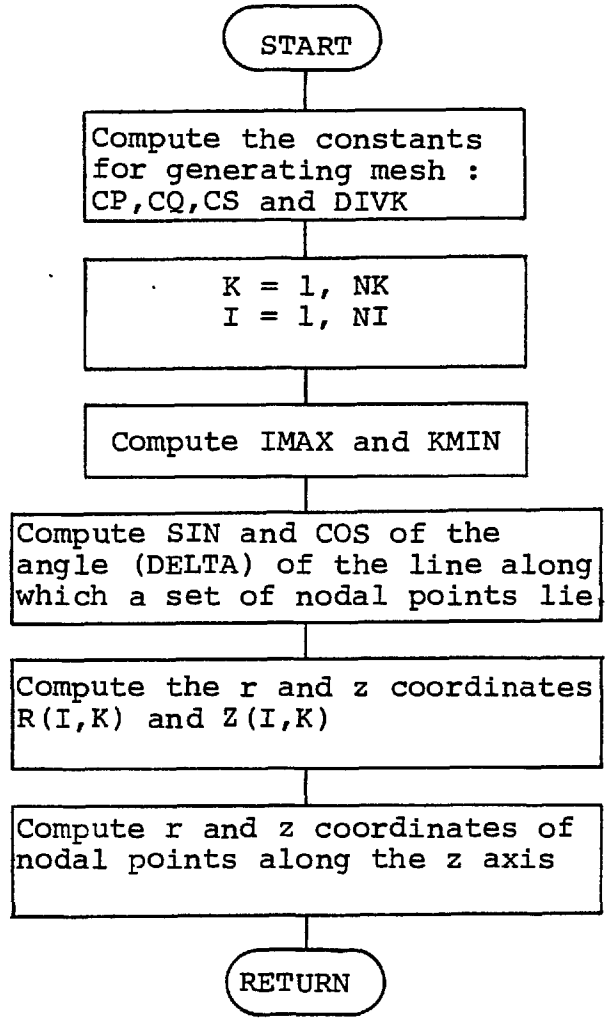


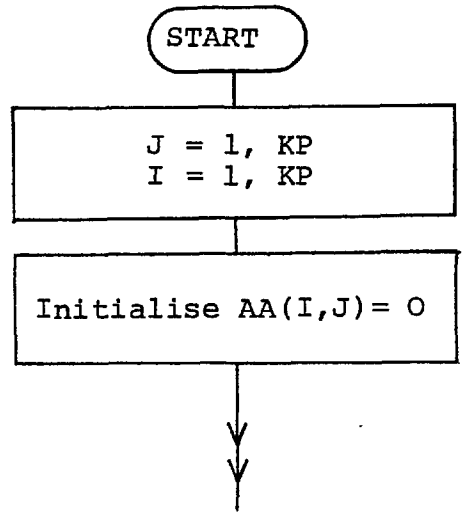
Fig. 5.4.1 Flow chart, the whole sequence of operations.

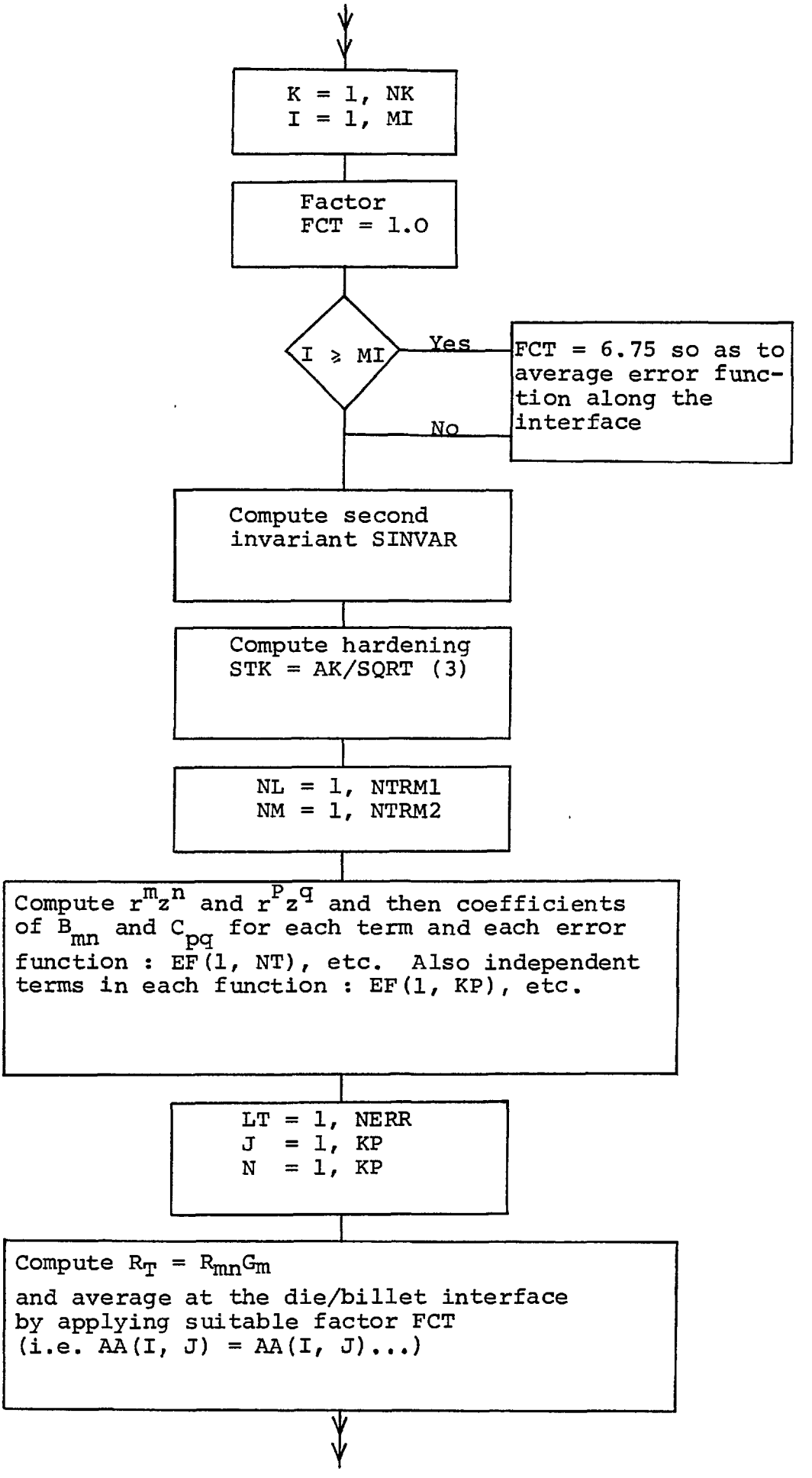
(cont.)

Subroutine MESH



Subroutine STRESS




K = 1, NK
I = 1, MI
Factor
FCT = 1.0
I ≥ MI
Yes
FCT = 6.75 so as to average error function along the interface
No
Compute second invariant SINVAR
Compute hardening
STK = AK/SQRT (3)
NL = 1, NTRM1
NM = 1, NTRM2
Compute $r^m z^n$ and $r^p z^q$ and then coefficients of B_{mn} and C_{pq} for each term and each error function : EF(1, NT), etc. Also independent terms in each function : EF(1, KP), etc.
LT = 1, NERR
J = 1, KP
N = 1, KP
Compute $R_T = R_{mn}G_m$
and average at the die/billet interface by applying suitable factor FCT
(i.e. AA(I, J) = AA(I, J)...)

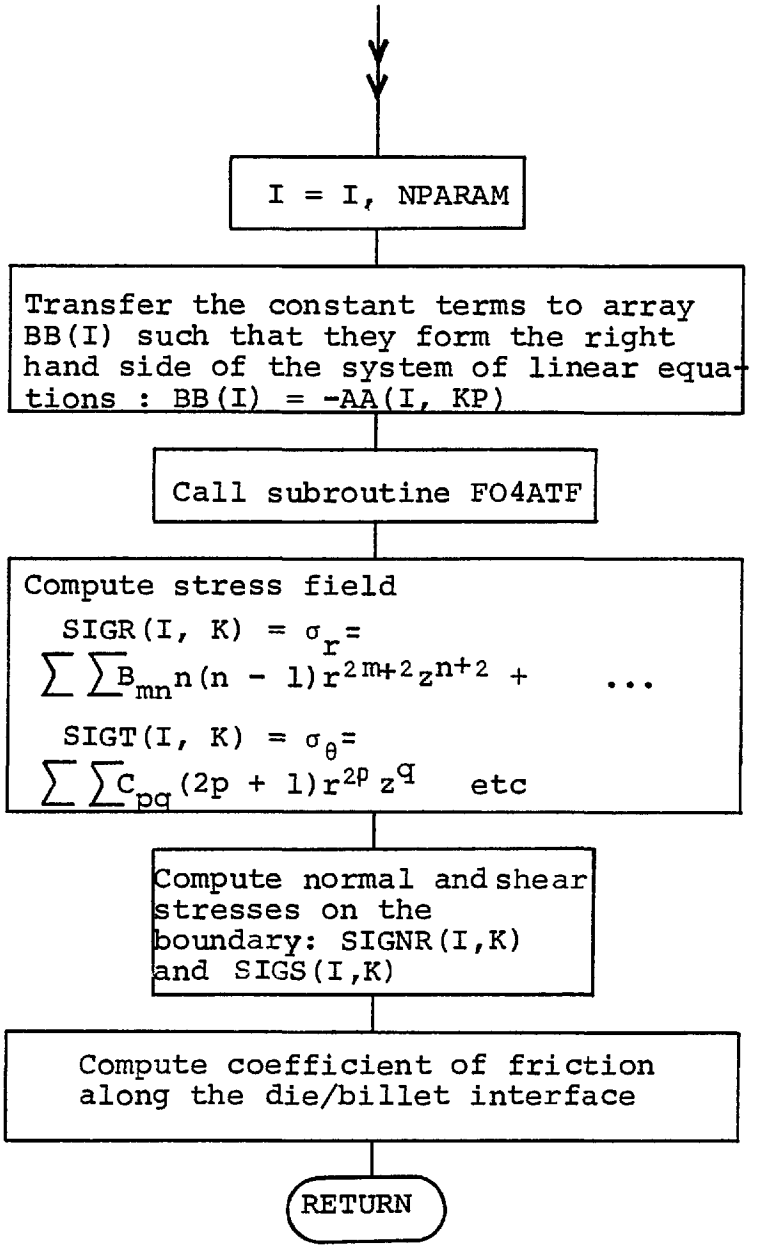


Fig. 5.4.1 Flow chart, the whole sequence of operations.

(end)

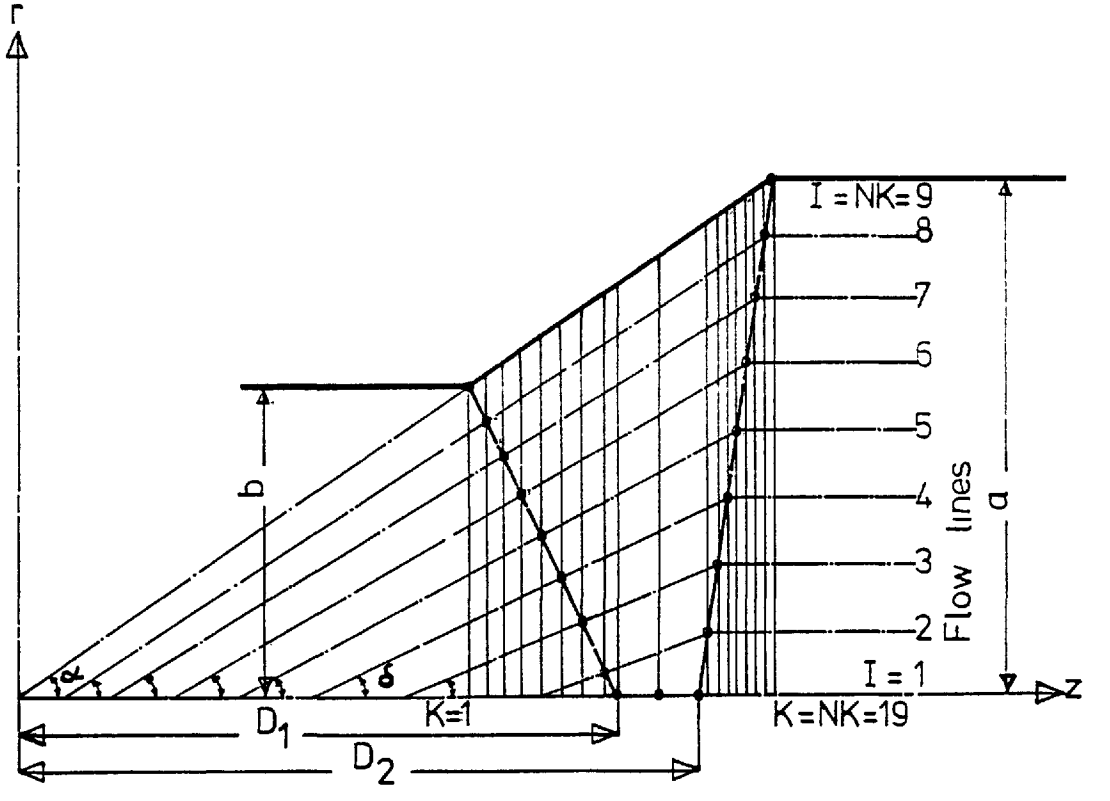


Fig. 5.4.2 Mesh for computation.

5.5 Elastic Stresses and Strains in Open-ended Cylinders under Internal Pressure

5.5.1 Introduction

In the preceeding chapters an experimental method was outlined to obtain strains on the outside diameter of the container for various extrusion conditions, while procedures to compute theoretical normal and shear stress distributions in the die, including its junction with the container wall (die corner), have also been given.

The experimental results presented in Chapter 6 indicate that, in the well lubricated forward extrusion of lead, the steady state pressure pad and die loads are identical within the accuracy of the experiments (Fig. 6.1.28, reproduced here for ease of reference). This in turn indicates low friction and constant pressure distribution along the container wall, so that the theoretically obtained stresses at the die corner could be assumed to represent the predicted container bore stresses.

To test the validity of the predictions, it is necessary to compute strains on the outside diameter of the container from the predicted bore stresses and compare them with the experimental strains.

A variety of methods are available for theoretical analysis of the discontinuity and steady stresses in a thick-walled cylinder subjected to a band of pressure. One of the most exhaustive treatments of the subject is given in the "Thick-walled Cylinder Handbook {101}" where the Fourier integral method is used to calculate

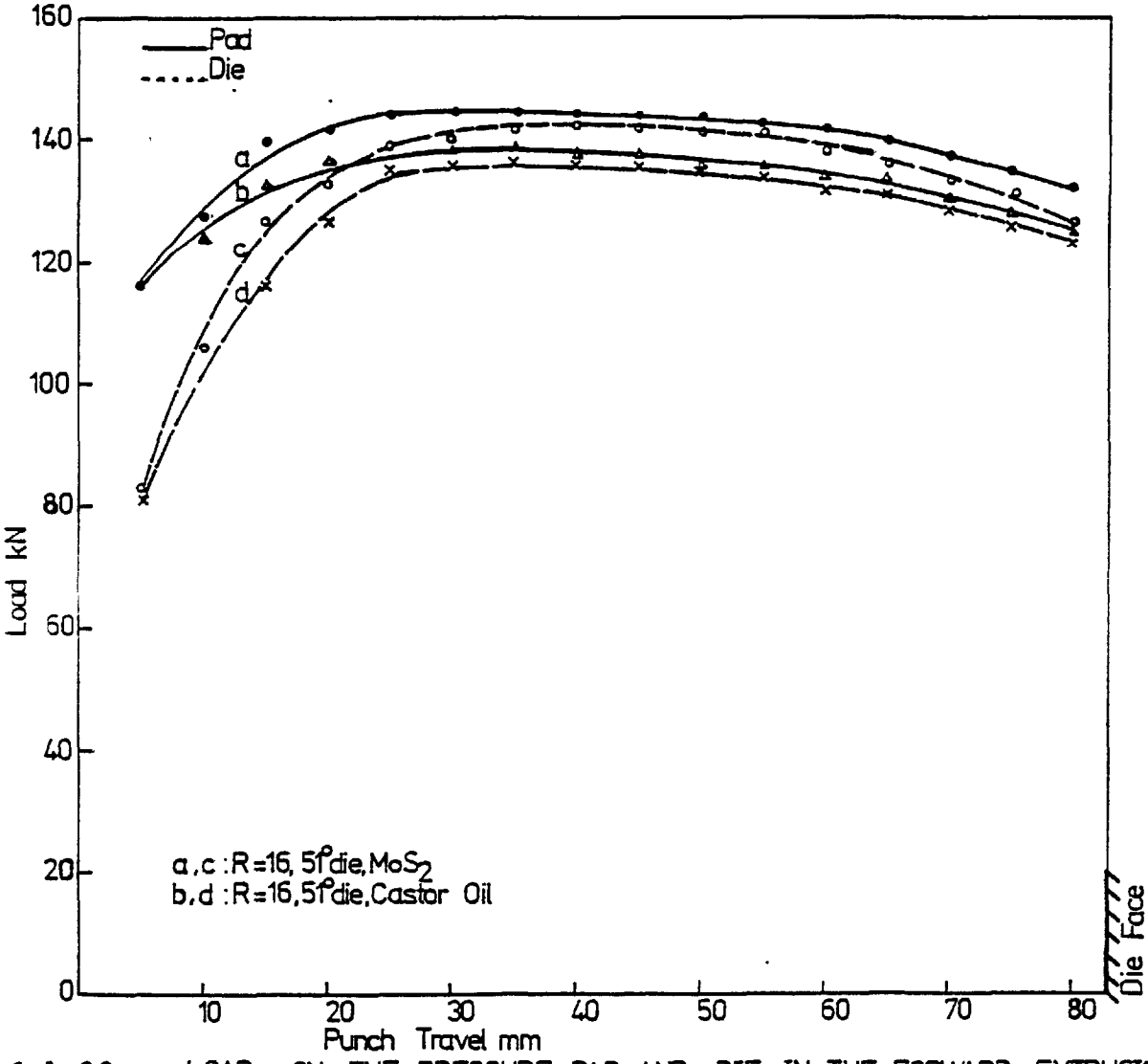


Fig. 6.1.28 LOAD ON THE PRESSURE PAD AND DIE IN THE FORWARD EXTRUSION OF LEAD

the stress distribution in plain semi-infinite cylinders with internal pressure. Similar results are produced by Timoshenko and Goodier {102} from the paper by Barton {103}. In these analyses, the pressure loading is assumed to reduce instantaneously to zero at the end of the pressure band.

Kudo and Matsubara {9} used the succesive over-relaxation method due to Southwell to calculate the stresses induced in a cylindrical die of finite length by a band of uniform internal pressure. The analysis shows that considerable constraint is provided by the pressure-free ends of the die so that hoop stresses less than the corresponding Lamé values are present in the pressurized portion of the die. Although most of the analysis assumes a rectangular or step pressure distribution, an example is given of a trapezoidal or ramp pressure distribution. This has the effect of significantly reducing the amplitude or severity of the stress discontinuities.

Thick-shell analysis has been used {104} to investigate stress distributions in a thick-walled vessel subject to equal internal and external pressures.

The numerical method of boundary-point least squares {106} was used by Simonen et al {105} to examine discontinuity stresses in a plain cylinder of $K = 2$. Internal and external pressure loadings were applied separately, and the conclusion in both cases was that the most severe shear stresses were to be found in the pressurized portion of the cylinder away from the discontinuity.

The finite-element method of stress analysis {8} was used to compute elastic stresses at the seals in plain and necked cylinders under internal and external pressures, under open-ended conditions. The analysis indicates that although tensile axial as well as hoop stresses are present at the seals, away from the seals the stress conditions are significantly more severe, so that fatigue failures due to repeated pressures would not normally be expected in the vicinity of the seals.

5.5.2 Finite-element Analysis of Containers

The finite-element method of stress analysis is today the major computer-oriented stress-analysis technique, and is rapidly gaining acceptance as an alternative to the traditional experimental techniques. The method is introduced by Argyris {107} and by Turner {108} and his associates, in the fifties, to solve problems in the stress analysis of structures. The technique is strongly related to the matrix formulation of structural analysis, and has been developed as a direct consequence of the concurrent availability of the large electronic computers it requires. The method is well explained in the available handbooks on the subject as, for instance, Zienkiewicz {109} or Desai and Abel {110}.

The technique involves the division of a structure or continuum into a number of small (finite) elements, commonly triangular in cross-section, interconnected at their corners.

These connecting points are known as nodes, an external loading is applied to the body via the nodal points. In the case of plane stress or plane strain, the elements are effectively triangular, laminae, and in the axisymmetric case are rings of triangular cross-section.

An axisymmetric finite-element stress analysis program called FLAP-5 (Imperial College, Mech. Eng. Dept.) was used to examine elastic stress-strain distributions in the extrusion containers under internal pressures. The program with triangular finite elements analyses elastically the small displacements in a loaded isotropic plane body of uniform thickness under the condition of either plane stress or plane strain.

The method of solution of the stiffness equation is the Gauss-Seidel iteration with over relaxation. A complete out-of-balance force tactic enables the program to permit all restraint conditions in which any node is either forced to be at any specified fixed point in the plane or forced to lie on any specified fixed line in the plane.

Displacements of the nodal points are produced. All the non-zero stress components for both elements and nodes are obtained at the latter by taking arithmetic means over the surrounding elements. Additionally FLAP-5 provides the principal stresses and the second invariant of stress for the elements and nodes.

The finite-element mesh was made as fine as possible within the limitations of the program and the available computer core store. The mesh (Fig. 5.5.1) was defined uniformly along

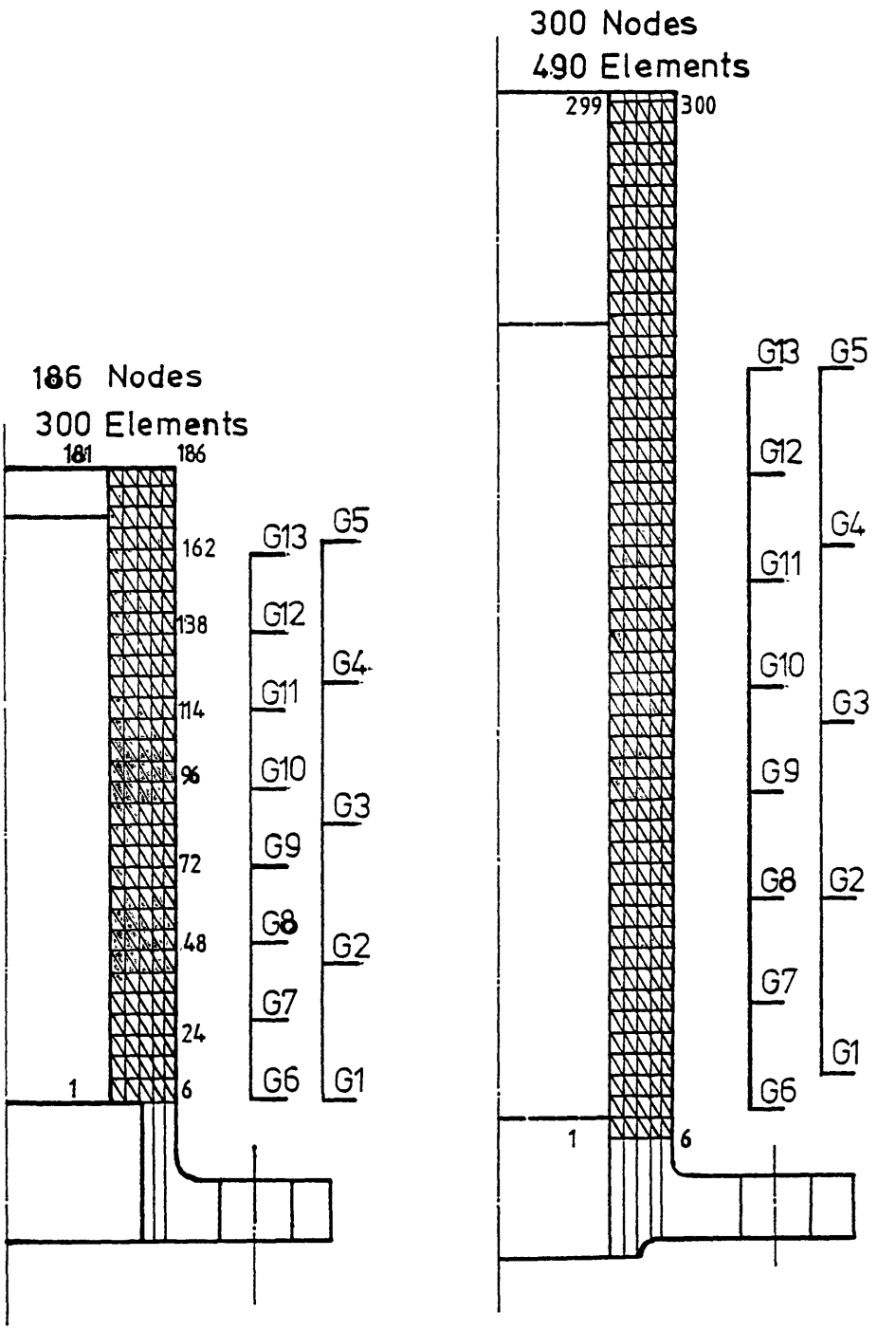


Fig. 5.5.1 Finite element meshes for containers.

the length of the specimen. This was considered preferable to the alternative of a coarser mesh away from stress concentrations and a finer mesh around the stress concentrations themselves. Because of geometrical symmetry about the centre sections of both backward and forward extrusion containers, it is sufficent to consider only half section of each container, as illustrated in Fig. 5.5.1. The loading condition was unit internal pressure applied uniformly to a fixed length of the bore. The dimensions of the mitre and O-ring used in the calibrations of containers were 1/8 in (3.175 mm),(45^{o} cone angle), and 1/8 in (3.175 mm) diameter respectively. Thus, the assumption made in the finite-element analysis loading was that the pressure drop occurred (in calibration) mainly in the mitre ring, and that the seals themselves transmitted pressure hydrostatically for a good proportion of their length. These assumptions seem reasonable, although there is no direct evidence to support them.

FLAP-5 was also used to compute elastic stress-strain distributions in the forward extrusion container, while the commercially pure aluminium and pure lead specimens were extruded into rods. The results of this finite-element analyses are summarised in Chapter 6.

6. RESULTS AND DISCUSSION

6.1 Results for forward extrusion

6.1.1 Velocity, strain rate, strain and stress fields computed from semi-empirical method

The steady state flow lines in the axisymmetric lubricated forward extrusion of commercially pure aluminium through a conical die of semi-angle of 25^{o}, at the extrusion ratio of 2 were obtained by the semi-empirical method. Fig. 5.1.1 (in section 5.1) shows a photograph of the grid pattern of aluminium after extrusion at a punch speed of 0.47"/min ($\sim$ 0.02 cm/sec) with castor oil as a lubricant. From Fig. 5.1.1, it can be seen that there is no sharp change of slope of the flow line at the contact between the billet and the die. The deformation of the billet before the die is reached is not pronounced but is, nevertheless present. It is also apparent that the flow in the deformation zone does not follow either the radial or parallel flow paths normally assumed in upper-bound approaches. The above figure confirms that a line, which is initially mid-way between the centre line and the surface, deforms as follows. There is an initial region with a fairly sharp change of slope as the deformation zone is entered. Next, there is a portion in which the line is nearly straight, then, the slope of the flow line decreases slightly at a point about one third of the way along the die. The slope again increases and the line is once more approximately straight, until exit from the deformation region.

In Fig. 5.1.1, lines are shown which were scribed on the billet initially perpendicular to the axis of flow. After extrusion, these lines are isochronous lines and are an indication of the position reached along each flow line in a given time. In the same figure, it is also clear that the line just inside the deformation zone is curved, so that the distance covered by the material along a line near the surface during a particular time interval is smaller than along the centre line.

Attempts were made to estimate the deformation boundaries (entry, exit and die/billet boundaries) by following the flow lines in Fig. 5.1.1 from the billet and product until they deviated from straight lines parallel with the axis, which was very difficult to observe especially near the centre where the change of curvature is smallest. Therefore, a polynomial curve fitting with the 7th order was used to estimate the entry and exit boundaries (detailed procedure is given in SUBROUTINE SMOOTH in Appendix B).

When the data (the coordinates of the observed points along the flow lines shown in Fig. 5.1.3 in section 5.1 constitute the data input for the computer program described in Appendix B) were used in the computer program , and smoothing (described in section 5.1) was carried out between the deformation boundaries, it was found that the results near these boundaries were erratic. This was due to the inaccuracy of the estimated boundaries forcing a deformation pattern on the flow which had not occurred in practice. It was found necessary to smooth the

flow function throughout the entire calculations. Much effort has been concentrated on smoothing the flow function between two K sections (Fig. 5.1.2, in section 5.1), one in the billet and one in the product.

From the input data, the absolute velocities (defined in section 5.4.6), strain rates and the total strains were calculated by using the computer program (given in Appendix B). For the stress calculation with the method of weighted residuals (described in Chapter 3), the flow stress of the material must be known in terms of the strain and temperature. Quantitative data of this kind can be obtained from simple tests. Fig. 2.3 in Chapter 2 shows the stress-strain curve of commercially pure aluminium obtained at room temperature in a plane strain compression test by Johnson and Mellor {63}, used in the calculations.

The results of the semi-empirical method are given in Figs 6.1.1 to 6.1.4 for the lubricated rod extrusion of aluminium at the extrusion ratio of 2, for die semi-angle of 25°, with a constant-friction factor of 0.12 (assumed value for the castor oil lubricated rod extrusion of aluminium). The contour drawings were plotted by using a contouring package available from the Imperial College computer library (D.M. MONRO), which interpolates irregular data into a fine regular grid and then proceed to contour in the same way as with regular data.

From Fig. 6.1.1, it can be seen that the distribution of the absolute velocity is not uniform because of the uncertainty of the deformation boundaries. Furthermore, a block of material

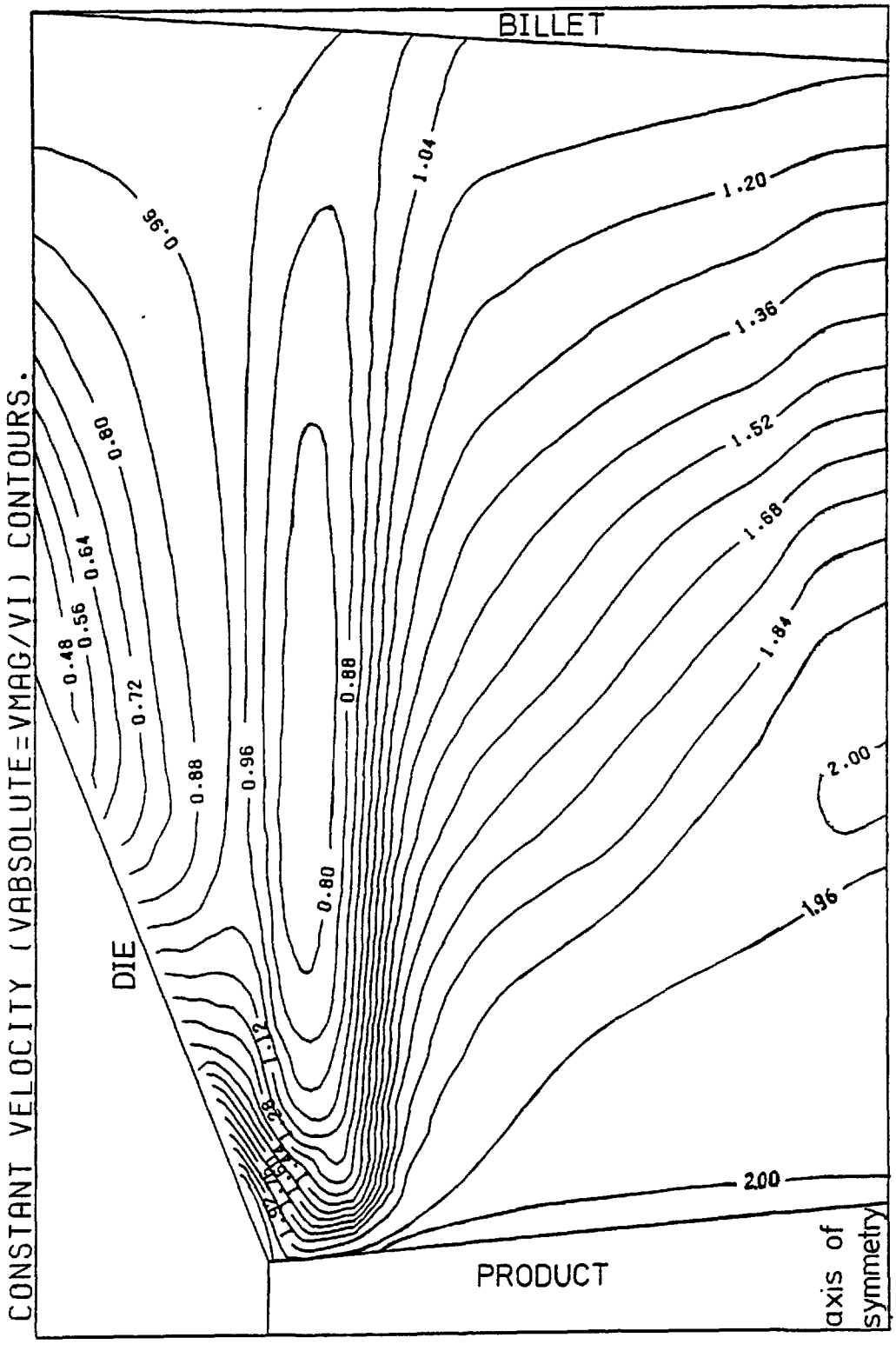


Fig. 6.1.1 Absolute velocity distribution in the deformation zone, Aluminium, R = 2, die semi-angle of 25°, constant-friction factor Q = 0.12.

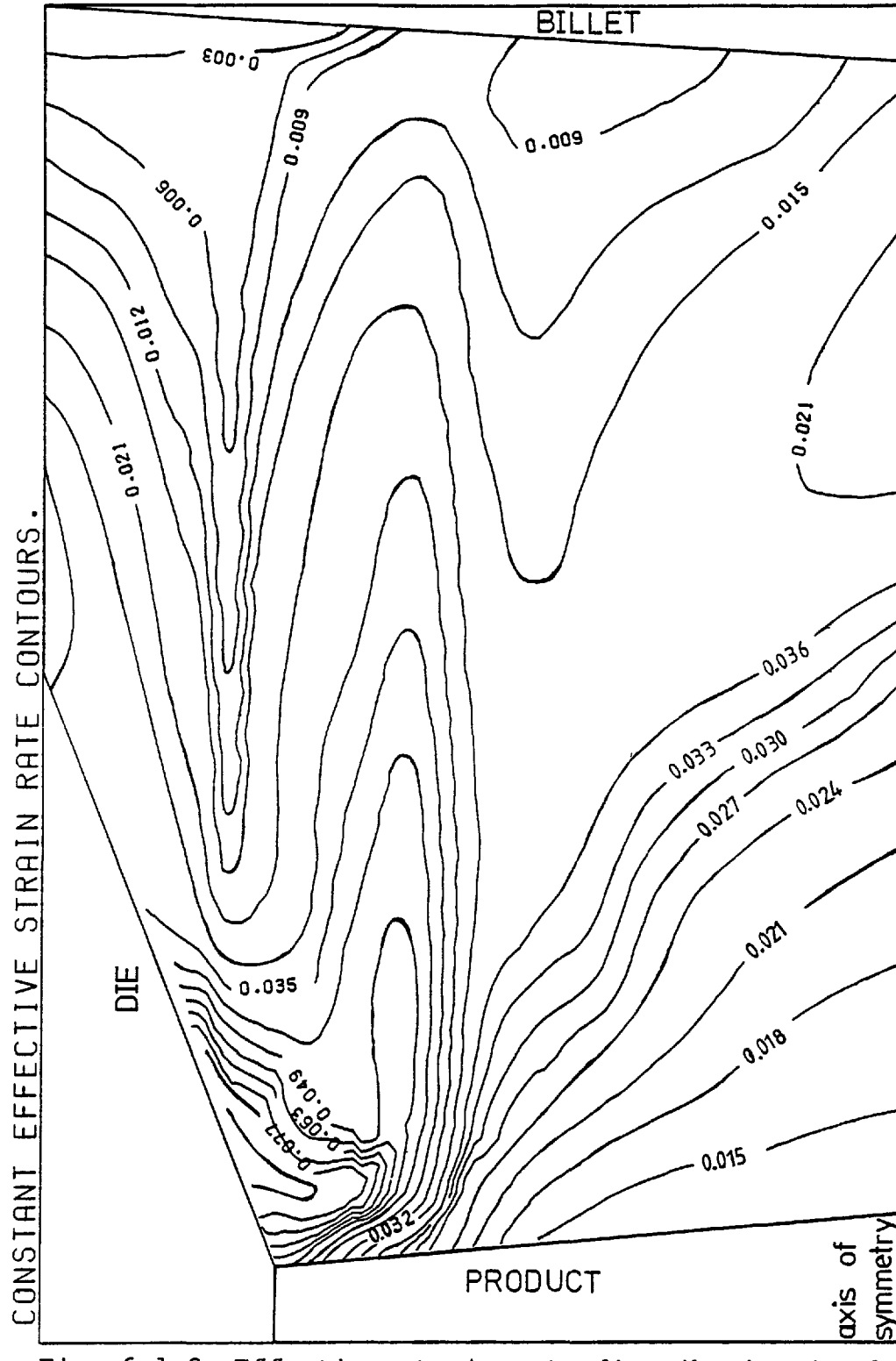


Fig. 6.1.2 Effective strain rate distribution in the deformation zone, Aluminium, R = 2, die semi-angle of 25°, constant-friction factor; Q = 0.12.

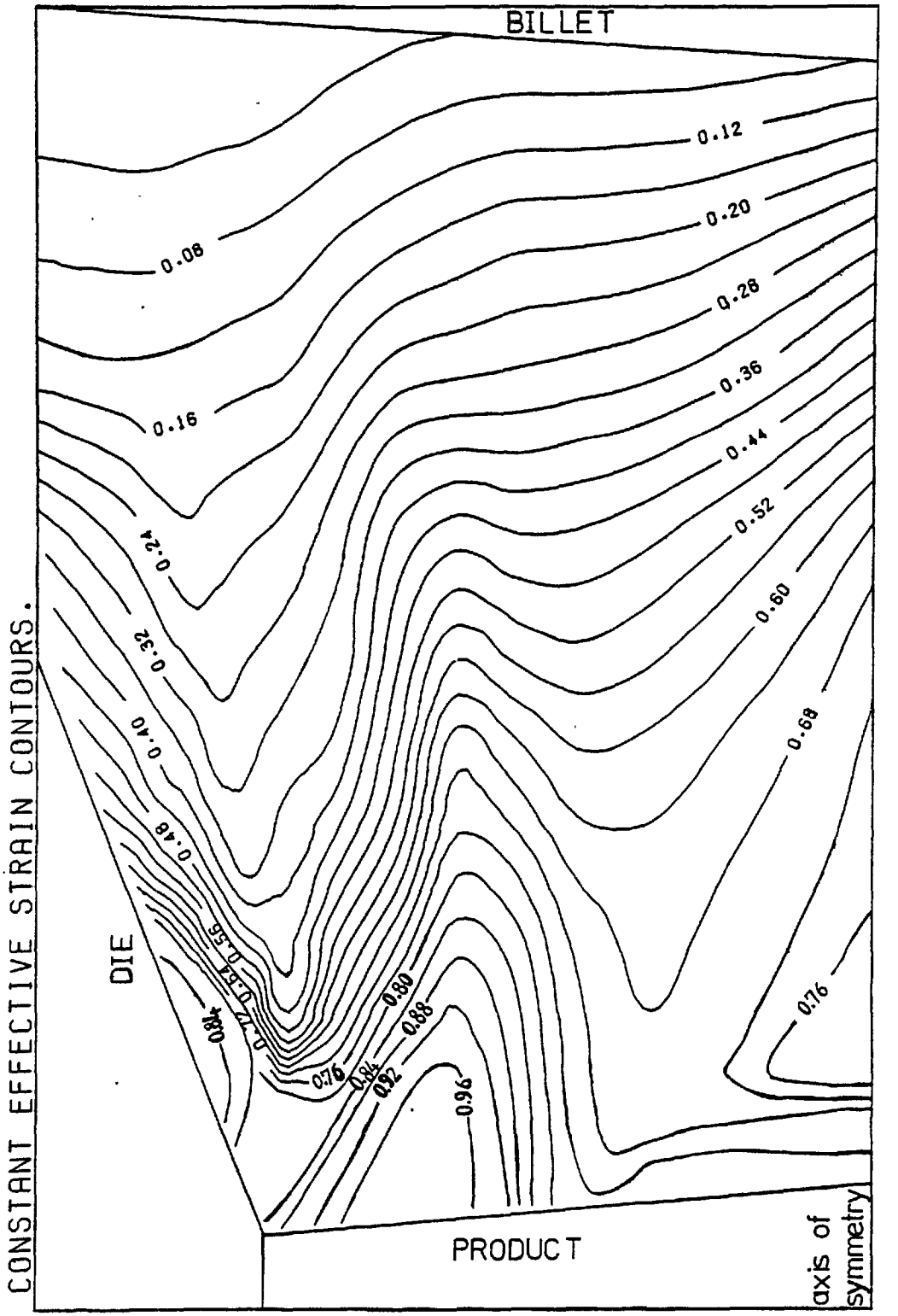


Fig. 6.1.3 Effective strain distribution in the deformation zone, Aluminium, R = 2, die semi-angle of 25°, constant-friction factor Q = 0.12.

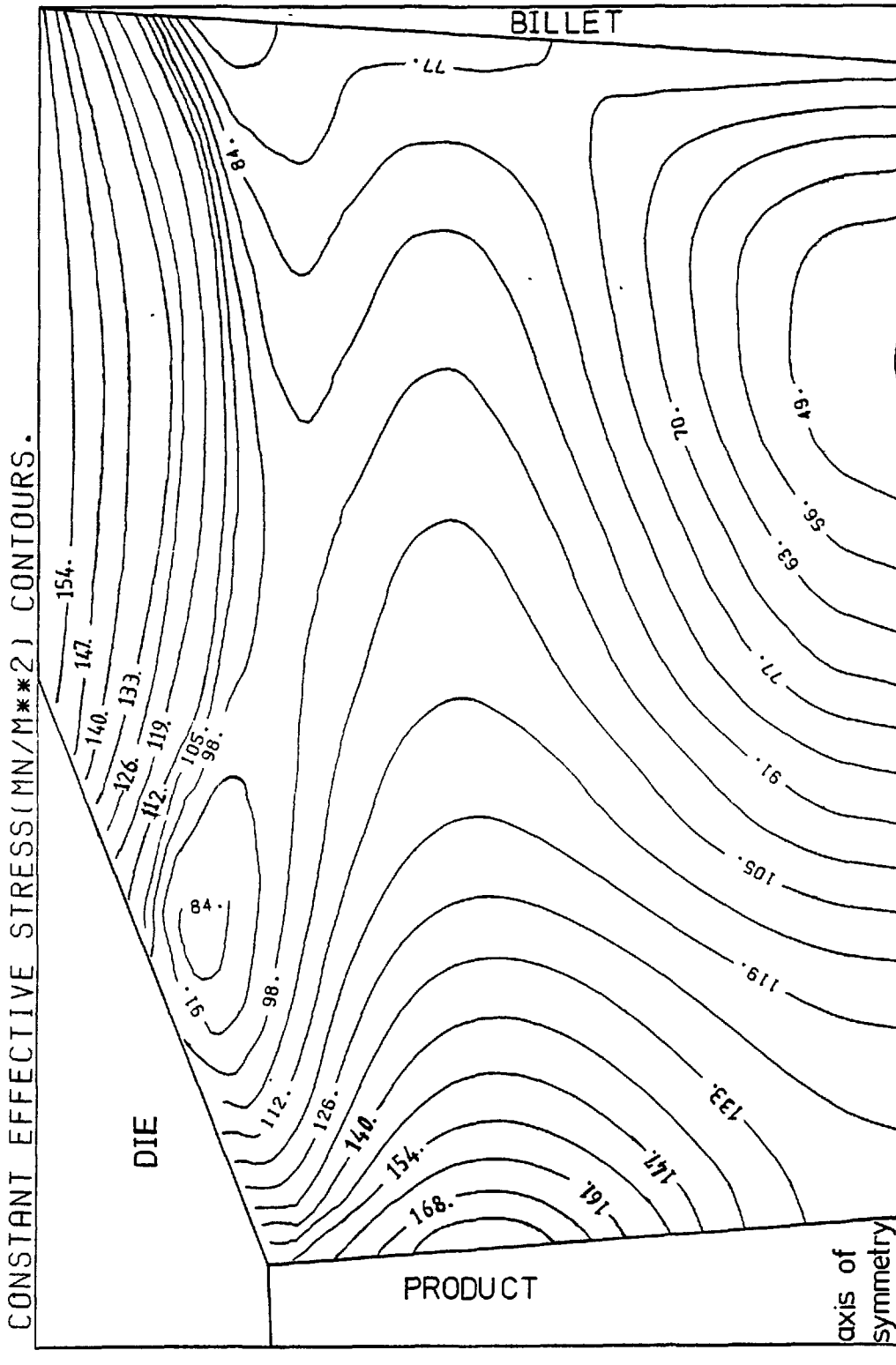


Fig. 6.1.4 Effective stress distribution in the deformation zone, Aluminium, R = 2, die semi-angle of 25°, constant-friction factor Q = 0.12.

in the deformation zone appears to be moving towards the exit section with an absolute velocity of about 0.80, which is once more due to the inaccuracies of the estimated boundaries forcing a deformation pattern on the flow which had not occurred in practice. From the same figure, it can be also noted that, for commercially pure aluminium, the absolute velocity along the die/billet boundary drops to a minimum at the die corner (the intersection between the die and container wall at the die entry). This is in agreement with the observation in recent studies of flow in conventional extrusion processes using the visioplasticity method {111}, that the absolute velocity of an element of the material moving along the die/billet boundary, from right to left (in Fig. 5.1.3, in section 5.1) first decreases. The absolute velocity is minimum at the stagnation point (the die corner), but subsequently increases from the stagnation point and reaches the absolute exit velocity at the die exit. It is evident, therefore, that interface friction affects both the boundary velocities and the velocities in the deformation region, higher friction decreasing the interface velocities.

Since the velocity components v_r and v_z (defined in section 5.1) are known, the strain rate components $\dot{\varepsilon}_r$, $\dot{\varepsilon}_z$ and $\dot{\varepsilon}_{rz}$ are calculated according to eq. (2.31), while $\dot{\varepsilon}_\theta$ is obtained directly from v_r by $\dot{\varepsilon}_\theta = v_r/r$. The incompressibility condition $\dot{\varepsilon}_r + \dot{\varepsilon}_\theta + \dot{\varepsilon}_z = 0$ was checked and found to be satisfied. From the strain rate components

(not presented here, for brevity) the effective strain rate can be obtained, eq. (2.26), and the distribution is shown in Fig. 6.1.2.

It must be noted that in the effective strain rate distribution, the shear strain rate appears to be more sensitive to changing conditions than any of the other parameters. The first calculations were unsuccessful and produced erratic results. The shear strain rate was therefore smoothed both in the radial and axial directions. This did not alter the shape of the effective strain rate contours but it did reduce the range of these across any section (K sections shown in Fig. 5.1.2, in section 5.1). After numerical differentiations, small errors in the velocity field are magnified in the strain rate field, especially in the shear strain rate which is equal to the change of axial velocity in the radial direction plus the change of the radial velocity in the axial direction, both small quantities.

The total effective strain was evaluated by integrating the effective strain rate along the flow lines according to eq. (2.27). The total effective strain contours are shown in Fig. 6.1.3. The results of the effective strain distribution indicate that the work-hardening is more or less uniform across the section except around the exit boundary. This uniformity is due to the small reduction and the small cone angle which result in a flow whose direction changes gradually.

Fig. 6.1.4 indicates the effective stress contours calculated from the strain rates and total strains by the method

of weighted residuals. Similarly, the stress components (not presented here, for brevity) have also been calculated. It was found that the Haar-Von Kármán hypothesis (defined in section 2.6, the assumption that, if the radial and hoop strain rates are the same at any point, then the radial and hoop stresses will also be the same) is approximately true over the majority of the deformation region but large differences occur near the surface and near the exit region.

Examination of Fig. 6.1.4 shows that the effective stress increases gradually to a maximum value at about the exit section. Furthermore, around the die corner where the absolute velocities are at a minimum, the effective stress steeply increases.

6.1.2 Velocity, strain rate, strain and stress fields computed from the assumed velocity field

As an alternative to the semi-empirical method described in the preceeding section, distributions of the absolute velocity, effective strain rate and effective strain were calculated from the assumed velocity field (Fig. 5.3.1 in section 5.3) and the effective stress computed by the method of weighted residuals simulating the plastic deformation of commercially pure aluminium at room temperature, at the extrusion ratio of 2, for die semi-angle of 25^{o}, constant friction factor of 0.12, the assumed value for the castor oil lubricated rod extrusion. The results are given in Figs 6.1.5 to 6.1.8 together with the flow lines (shown in Fig. 5.4.1, in section 5.4). From these

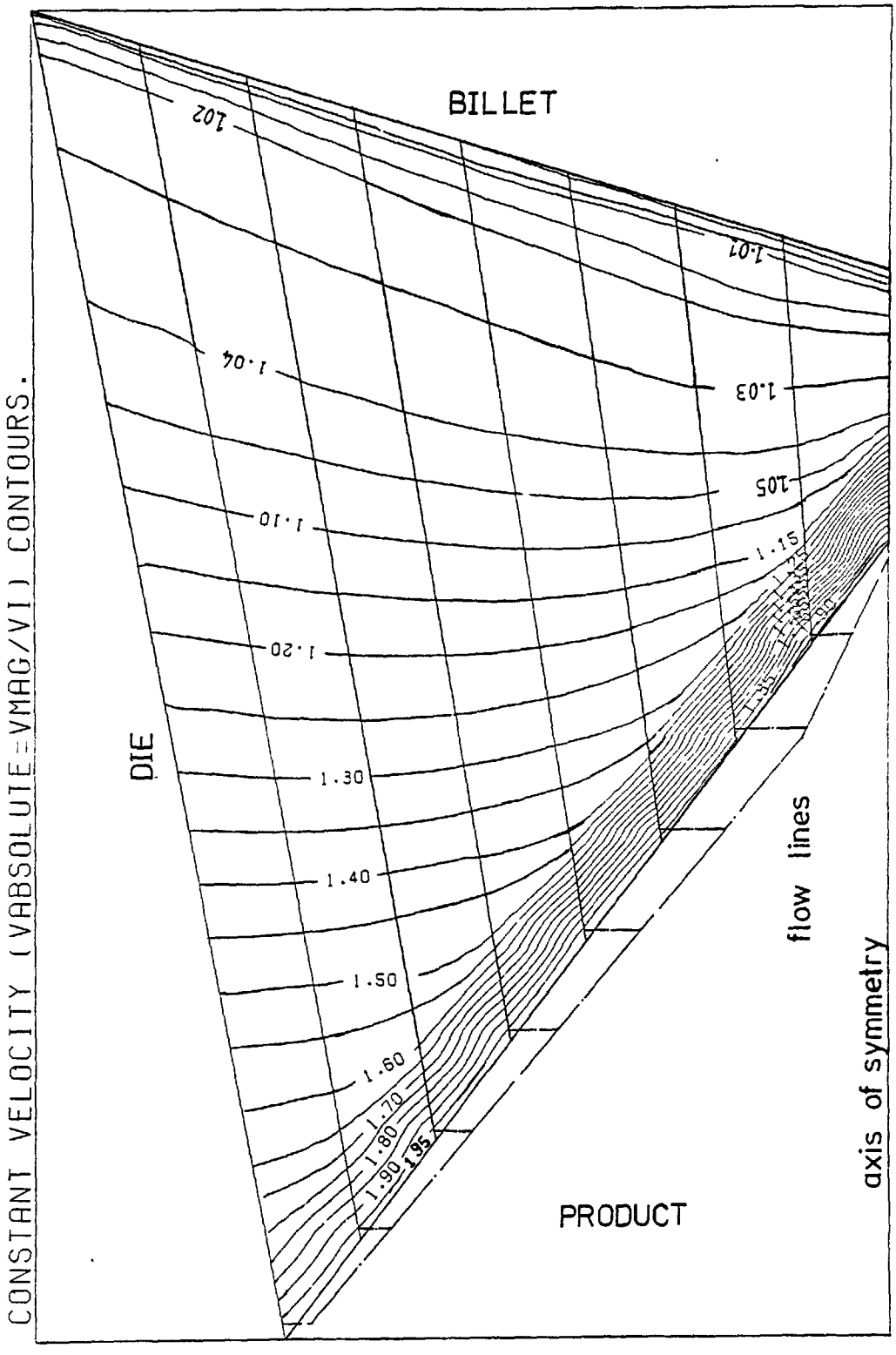


Fig. 6.1.5 Absolute velocity distribution, in the deformation zone, Aluminium, R = 2, die semi-angle of 25° constant-friction factor Q = 0.12.

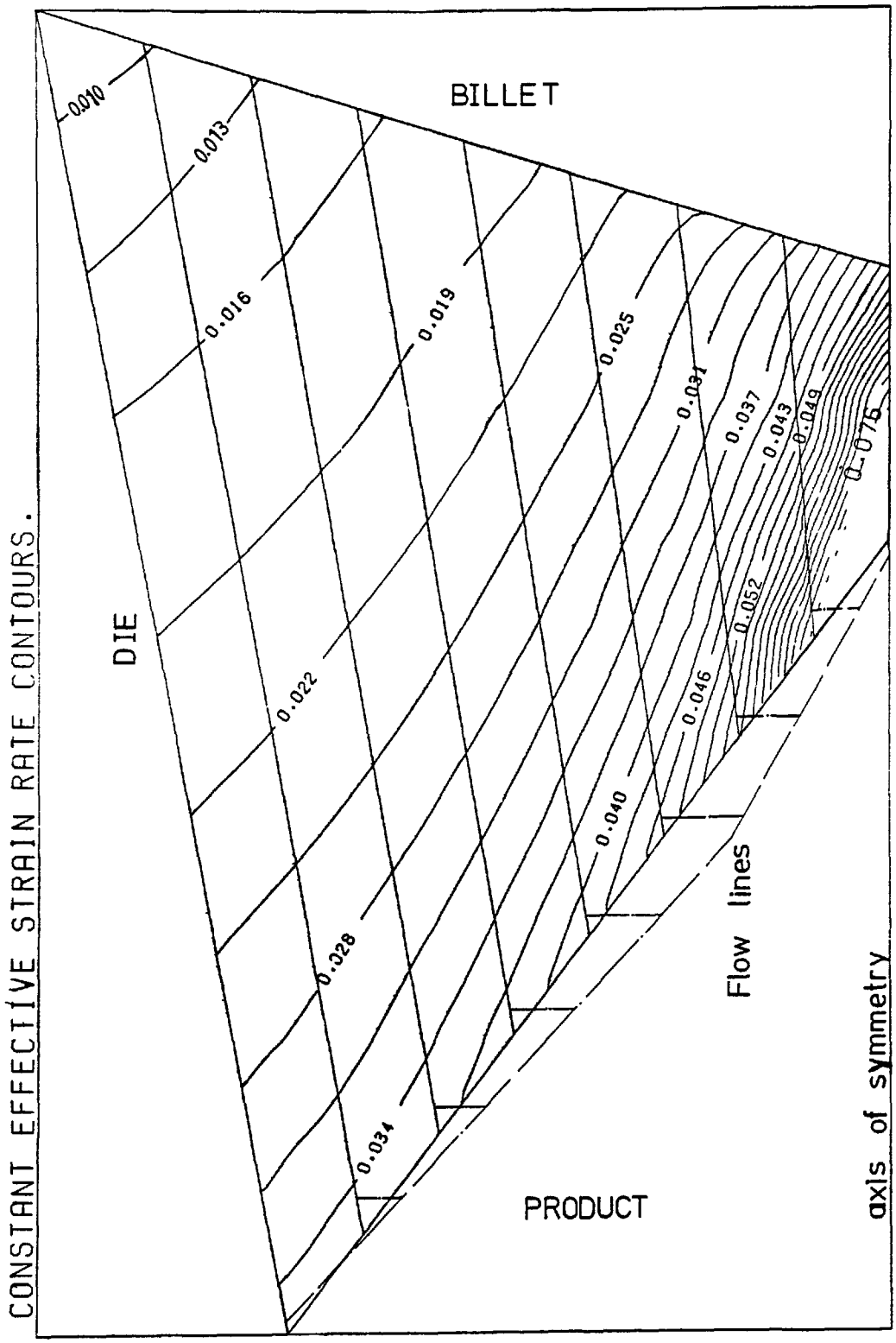


Fig. 6.1.6 Effective strain rate distribution in the deformation zone, Aluminium, R = 2, semi-angle of 25°, constant-friction factor Q = 0.12.

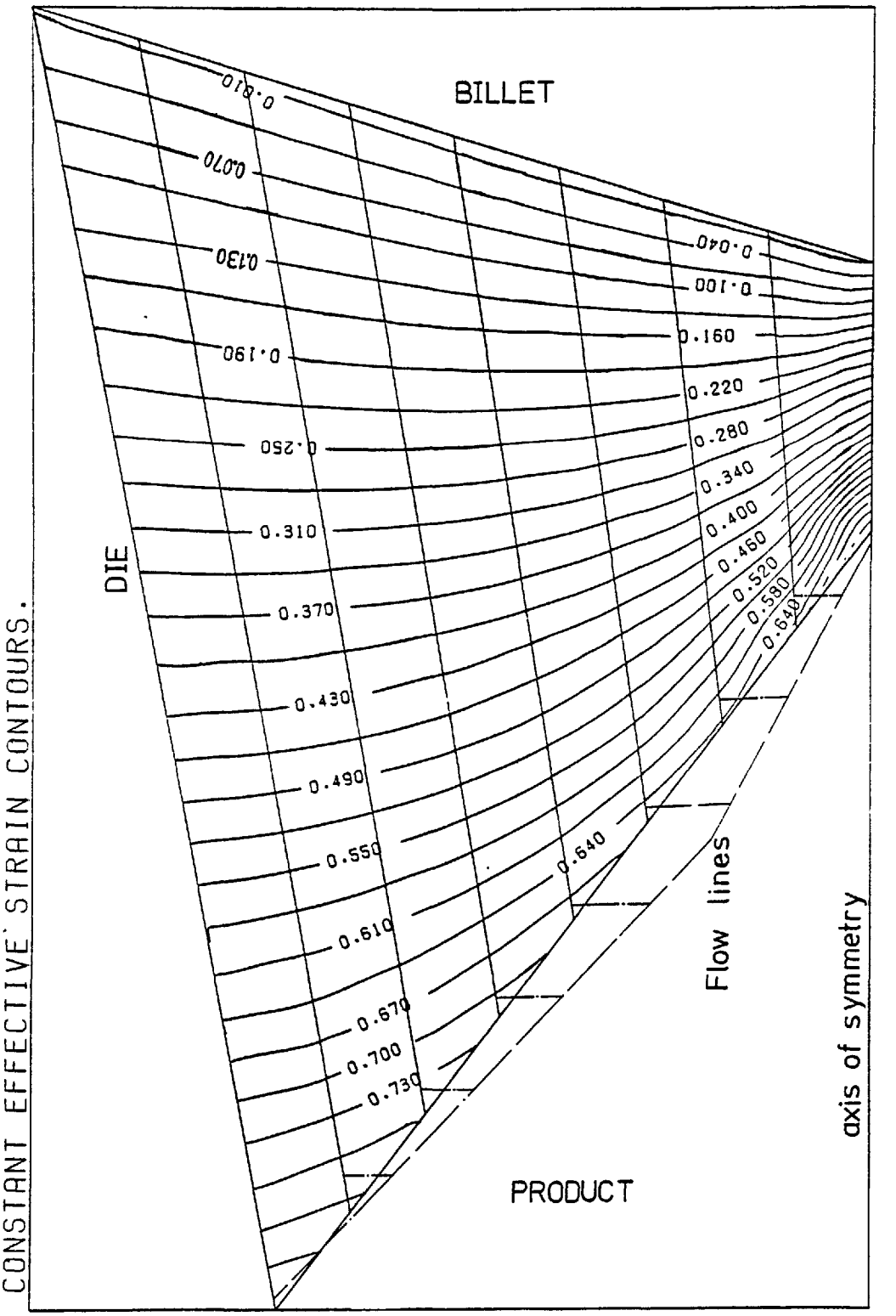


Fig. 6.1.7 Effective strain distriubtion in the deformation zone, Aluminium, R = 2, die semi-angle of 25^{o}, constant friction factor Q = 0.12.

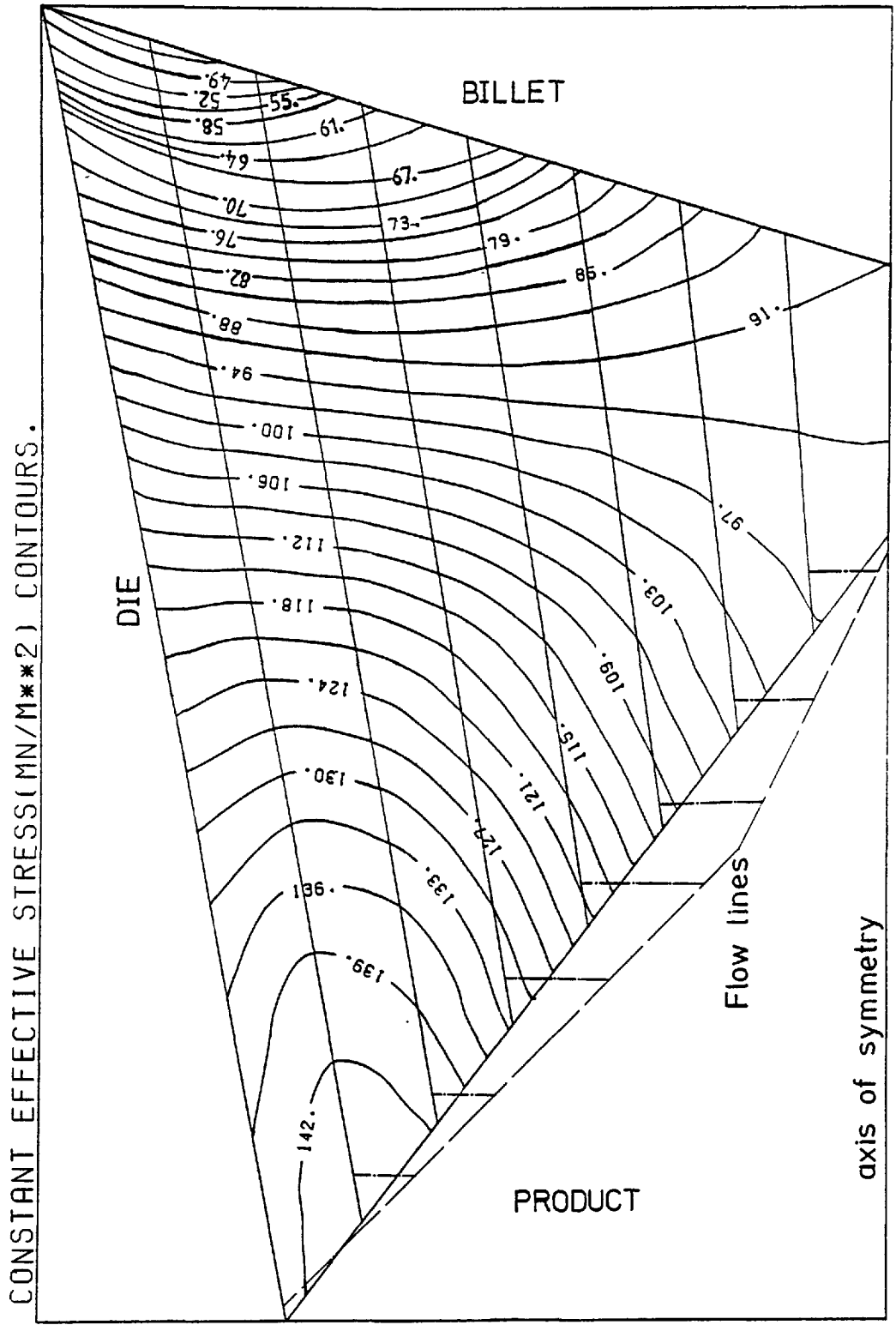


Fig. 6.1.8 Effective stress distribution in the deformation zone, Aluminium, R = 2, die semi-angle of 25°, constant-friction factor Q = 0.12.

figures the absolute velocity, effective strain rate, strain and effective stress contours with the straight flow lines drawn are uniform throughout the continuum and their values increase toward the exit.

From Fig. 6.1.1 and Fig. 6.1.5, absolute velocities at the entry and exit sections had a value of approximately 1 and 2 respectively, indicating that a block of material moved into the deformation zone with a constant velocity (punch or billet velocity) at the entry, and left the deformation zone with the constant product velocity at the exit. It can be seen, in Fig. 6.1, that the absolute velocities are increasing gradually towards the exit section. On the other hand, the absolute velocities in Fig. 6.1.1, as mentioned previously were decreasing considerably at the die corner (the intersection between the die and container wall at the die entry).

It is interesting to note that the experimentally observed deformation zone in Fig. 6.1.1 is larger than that shown in Fig. 6.1.5. This is because deformation in practice starts before the die corner is reached (clearly seen in Fig. 5.1.1 in section 5.1), while the deformation, in Fig. 6.1.5, was assumed to begin at the entry section which includes the die corner. Furthermore, from Fig. 6.1.5, it is clear that the absolute velocities obtained from the kinematically admissible velocity field are uniform. However, it must be emphasised that this figure was a product of eq. (5.3.14) in section 5.3. On the other hand,

Fig. 6.1.1 gives an insight into the nature of the velocities which were produced from the experimentally observed data.

It is of interest to observe that the effective strain rate in Fig. 6.1.6 reaches its largest value on the centre line (denoted as the axis of symmetry in the figure), while the largest effective strain rate values in Fig. 6.1.2 are close to the die/billet boundary around the exit section. The latter is in the semi-empirical method where overestimating the numerical differentiations is involved in calculating the strain rate components as previously mentioned.

It is confirmed by Fig. 6.1.3 and Fig. 6.1.7 that the distribution of effective strains is increasing gradually to a maximum at about the exit section. The main difference is that in Fig. 6.1.3 the effective strains are shown to be larger near the boundaries, depending on the numerical integration of the effective strain rate along a flow line with respect to time (previously described in section 5.1).

The effective stresses in Fig. 6.1.4 steeply increase around the die corner, while they are at a minimum around the entry section in Fig. 6.1.8. This is mainly, in Fig. 6.1.4 due to inaccuracies in estimating the boundaries imposing a a deformation pattern on the flow that had not occurred in practice.

Fig. 6.1.9 to Fig. 6.1.16 show the effect of varying the semi-angle of the die on the velocity and stress fields in axisymmetric dry rod extrusion of pure lead at the extrusion ratios of 3 and 4, for die semi-angles of 30^{o} and 35^{o} respectively.

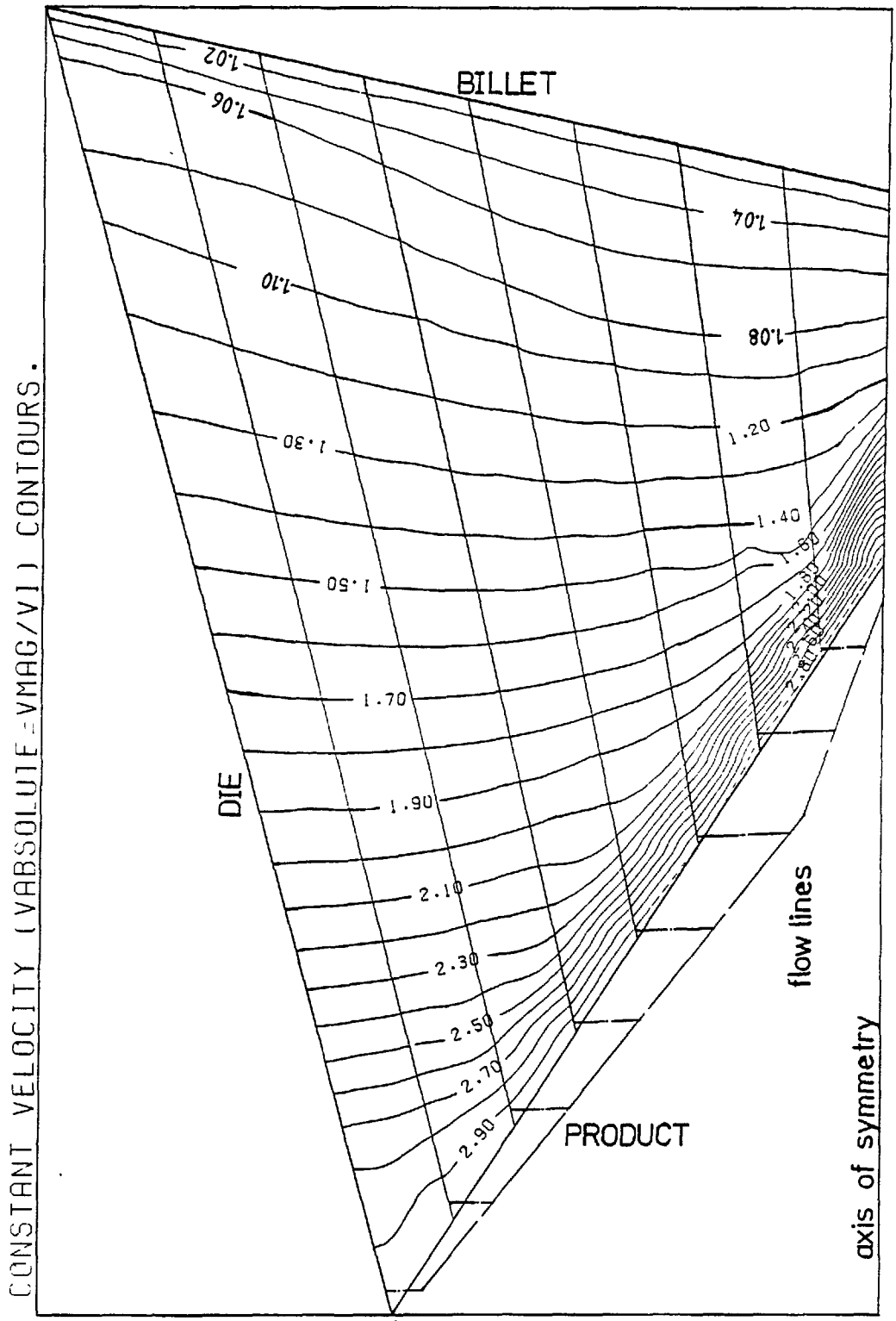


Fig. 6.1.9 Absolute velocity distribution in the deformation zone, Lead, R = 3, die semi-angle of 30^{o}, constant friction factor Q = 0.75.

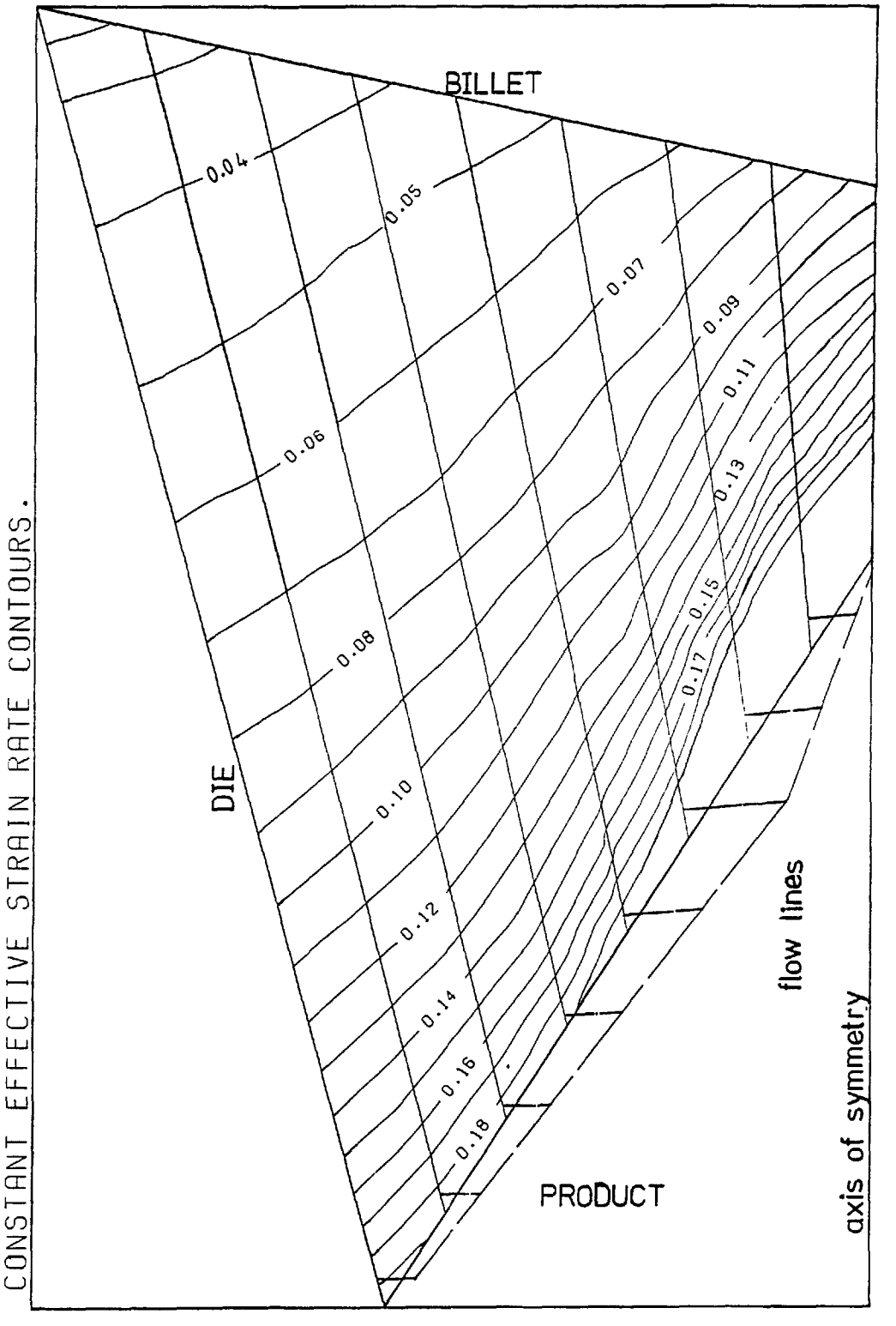


Fig. 6.1.10 Effective strain rate distribution in the deformation zone, Lead, R = 3, die semi-angle of 30^{o}, constant-friction factor Q = 0.75.

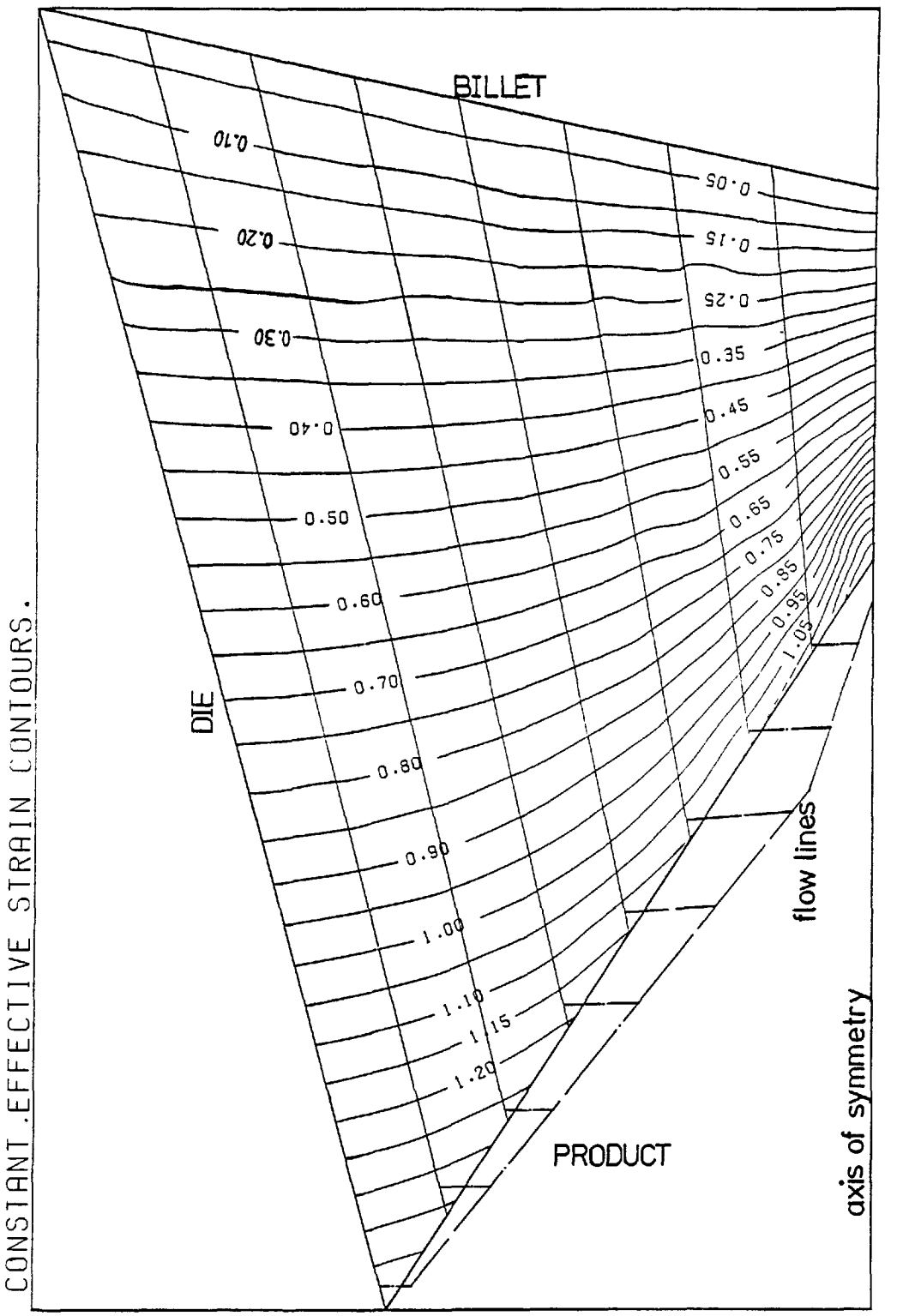


Fig. 6.1.11 Effective strain distribution in the deformation zone, Lead, R = 3, die semi-angle of 30°, constnat friction factor Q = 0.75.

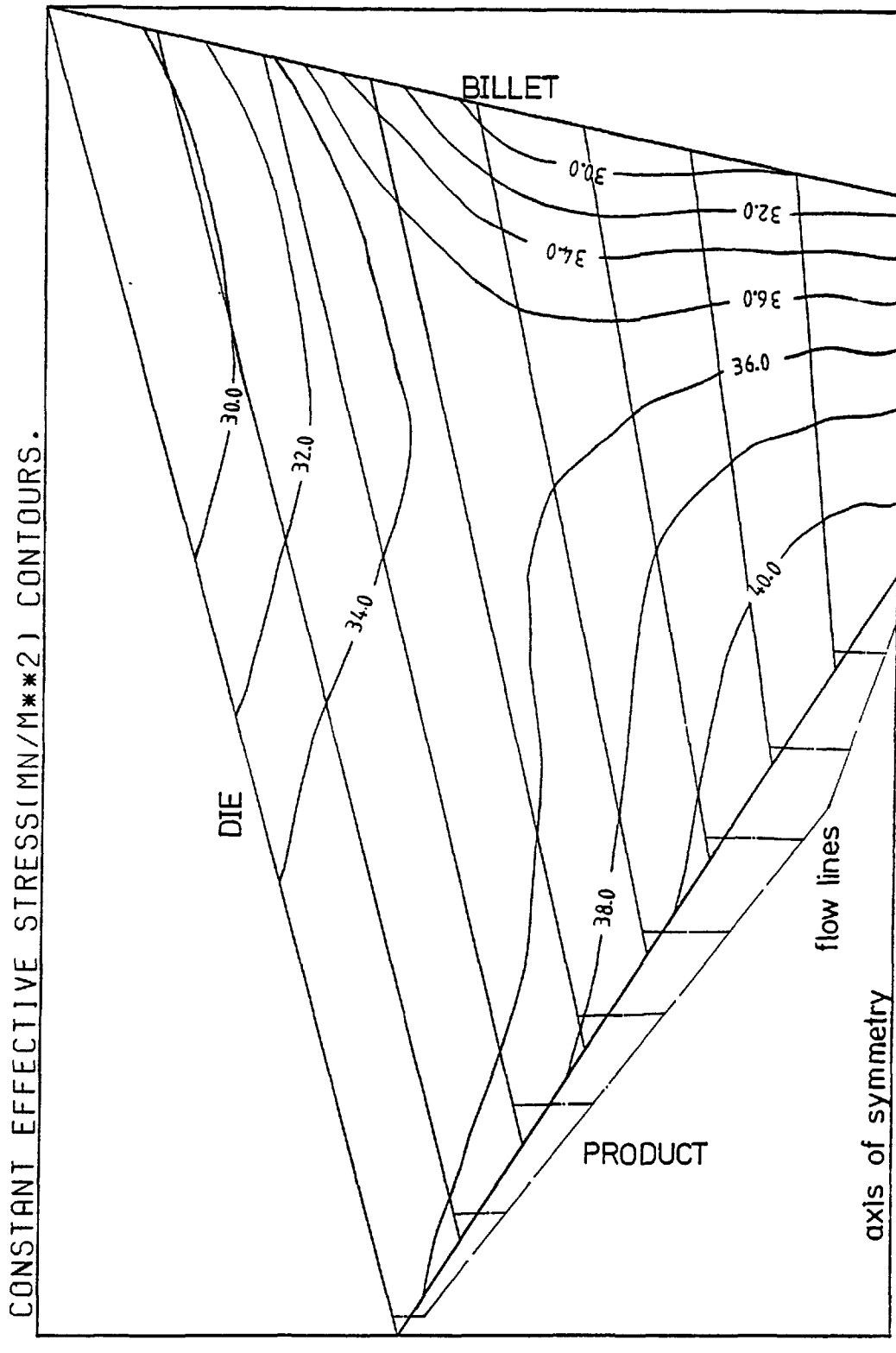


Fig. 6.1.12 Effective stress distribution in the deformation zone, Lead, R = 3, die semi-angle of 30°, constant-friction factor Q = 0.75.

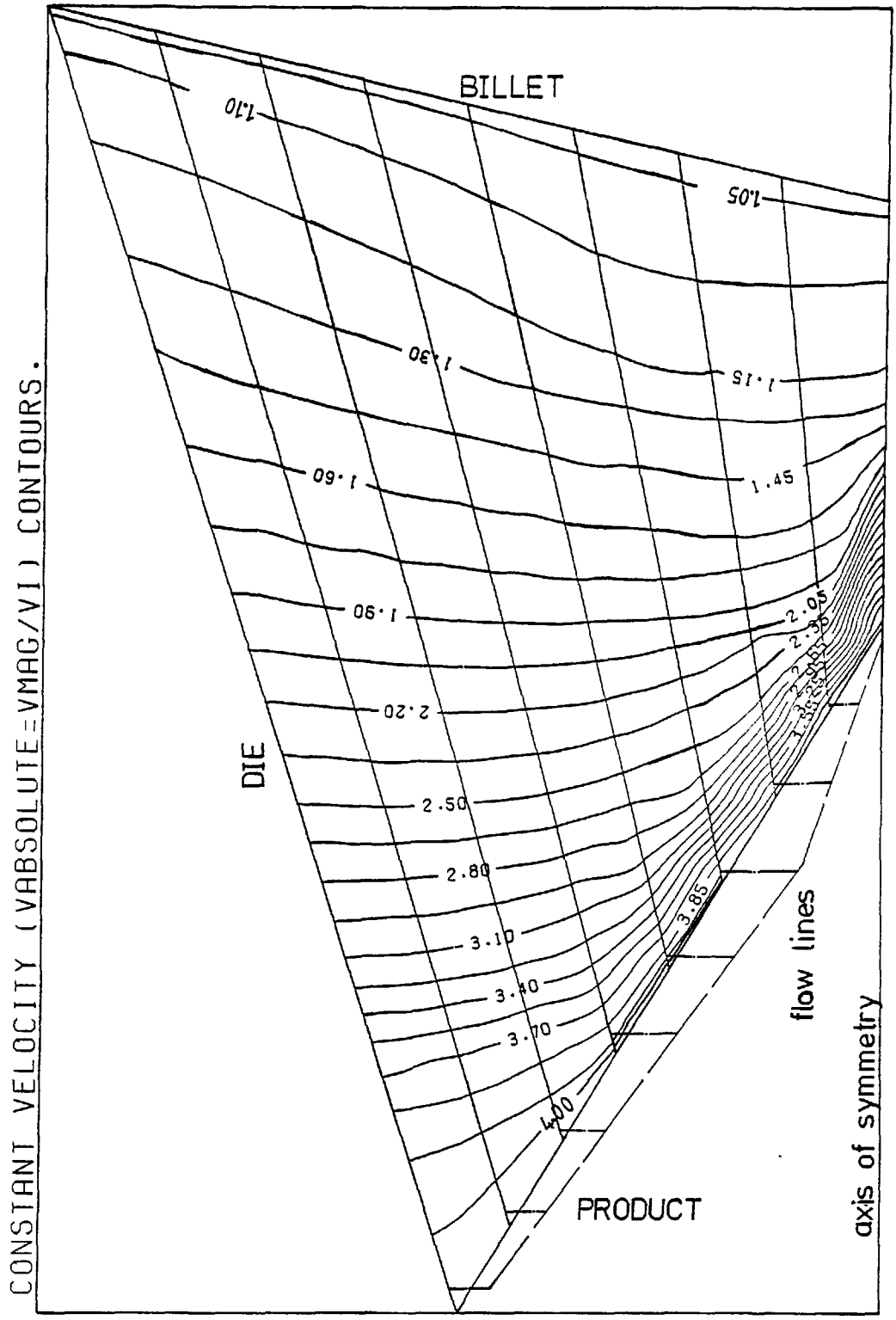


Fig. 6.1.13 Absolute velocity distribution in the deformation zone, Lead, R = 4, die semi-angle of 35°, constant friction factor Q = 0.75.

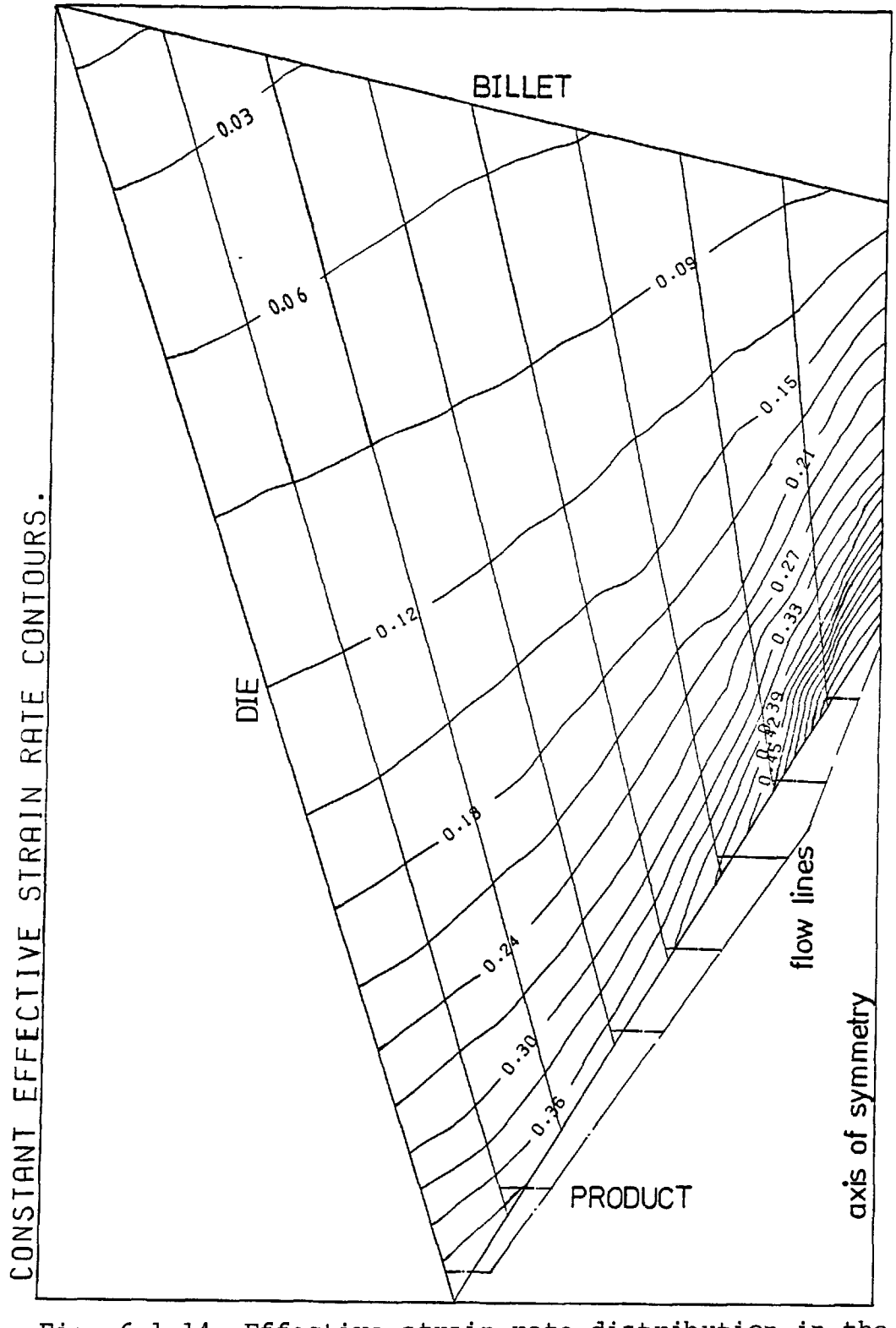


Fig. 6.1.14 Effective strain rate distribution in the deformation zone, Lead, R = 4, die semi-angle of 35°, constant friction factor Q = 0.75.

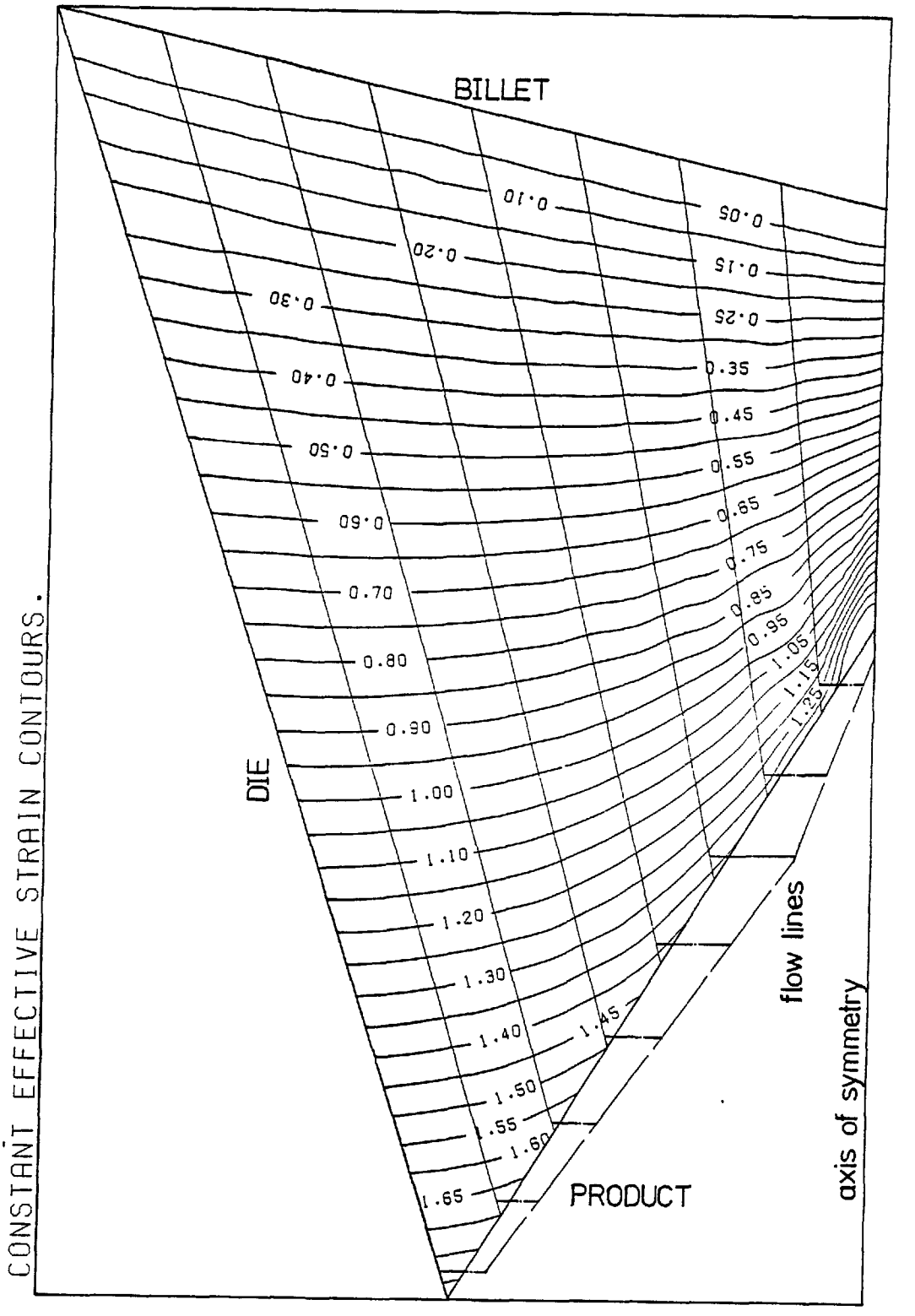


Fig. 6.1.15 Effecitve strain distribution in the deformation zone, Lead, R = 4, die semi-angle of 35°, constant-friction factor Q = 0.75.

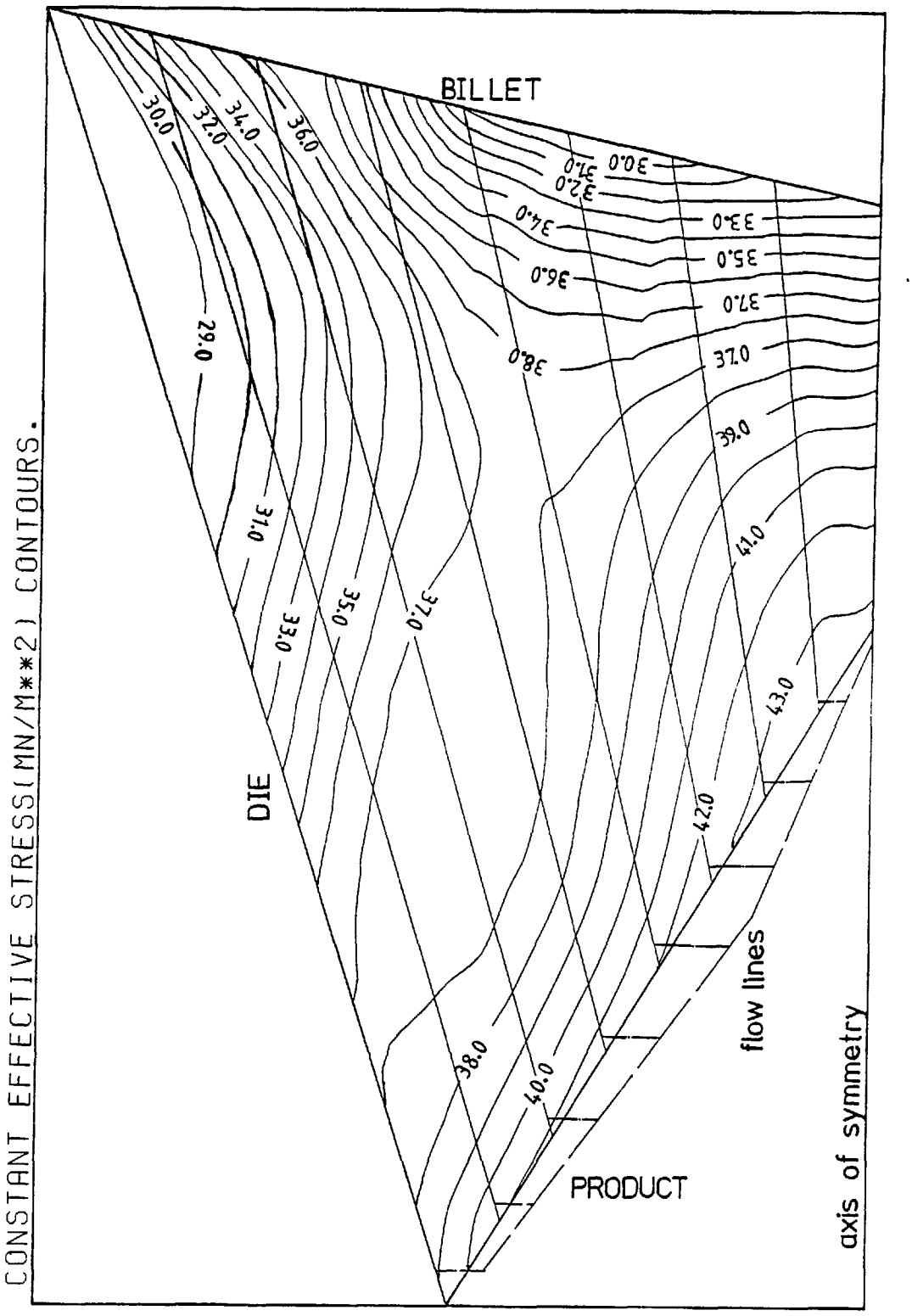


Fig. 6.1.16 Effective stress distribution in the deformation zone, Lead, R = 4, die semi-angle of 35^{o}, constant friction factor Q = 0.75.

An examination of these figures reveals that the absolute velocity, the effective strain rate and the effective strain fields are qualitatively similar to those of forward extrusion of aluminium (Fig. 6.1.5 to Fig. 6.1.7) but they increase towards the exit section as the semi-angle of the die increases.

For a lead specimen, the stress-strain property is available only for a limited range of strain and strain rate. Therefore, the flow stress $\bar{\sigma}$ in the present calculation of the stress components is assumed constant as 2.3 Tonf/in^2 ($\sim$ 35.52 MN/m^2) {112}.

It is of interest to note that the effective stress distributions in the deformation zone, as seen in Fig. 6.1.12 and Fig. 6.1.16 remain more or less constant during extrusion. This is because of constant flow stress assumption for a non-work hardening material, i.e. pure lead.

A final comment on the above figures (from Fig. 6.1.5 to 6.1.16) is that the flow lines drawn are similar but not identical. The slopes of the flow lines (as described in section 5.3) are dependent upon the extrusion ratio and the semi-angles of the entry and exit boundaries (these are β and λ defined in section 5.3) respectively.

6.1.3 Pressure distribution in the forward extrusion container

Fig. 6.1. 17 indicates the normal (σ) and frictional shear (τ) stresses in the bore of the forward extrusion container,

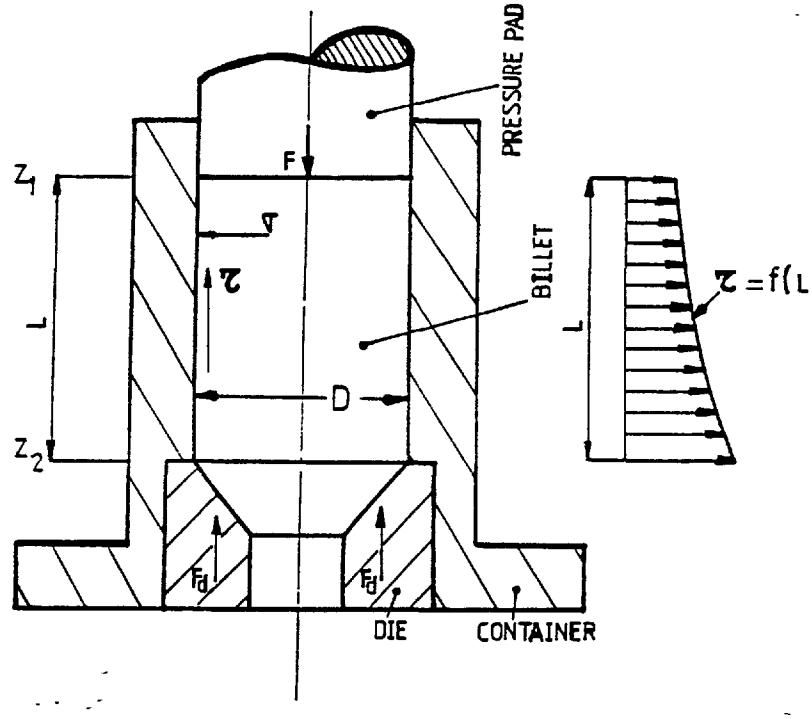


Fig. 6.1.17 Normal (σ) and frictional shear (τ) stresses in the bore of the forward extrusion container.

together with loads on the pressure pad (F) and die (F_d).

If the frictional drag on the container wall is

$$F_c = \pi D \int_{z_1}^{z_2} \tau \, dz$$

then the load on the pressure pad becomes

$$F = F_d + F_c$$

For the lubricated forward extrusion of lead at an extrusion ratio of 16, the pressure pad and die loads are shown in Fig. 6.1.28, reproduced here for ease of reference. In the steady state these loads are almost equal, indicating that the frictional drag on the container wall is small, $F_c \sim 0$. The same conclusion can be drawn from several other experimental findings, which will be discussed in the next section. Billet/container friction could lead to higher bore pressures away from the die, conversely small container friction must signify an approximately constant bore pressure along the container length. Consequently, it was assumed in the calculations that the normal stress is constant along the container and is equal to the value obtained theoretically for the die corner.

Fig. 6.1.18 a, b and c show the strain and wall pressure distributions together with the finite element mesh used in the computations, all as a function of the strain

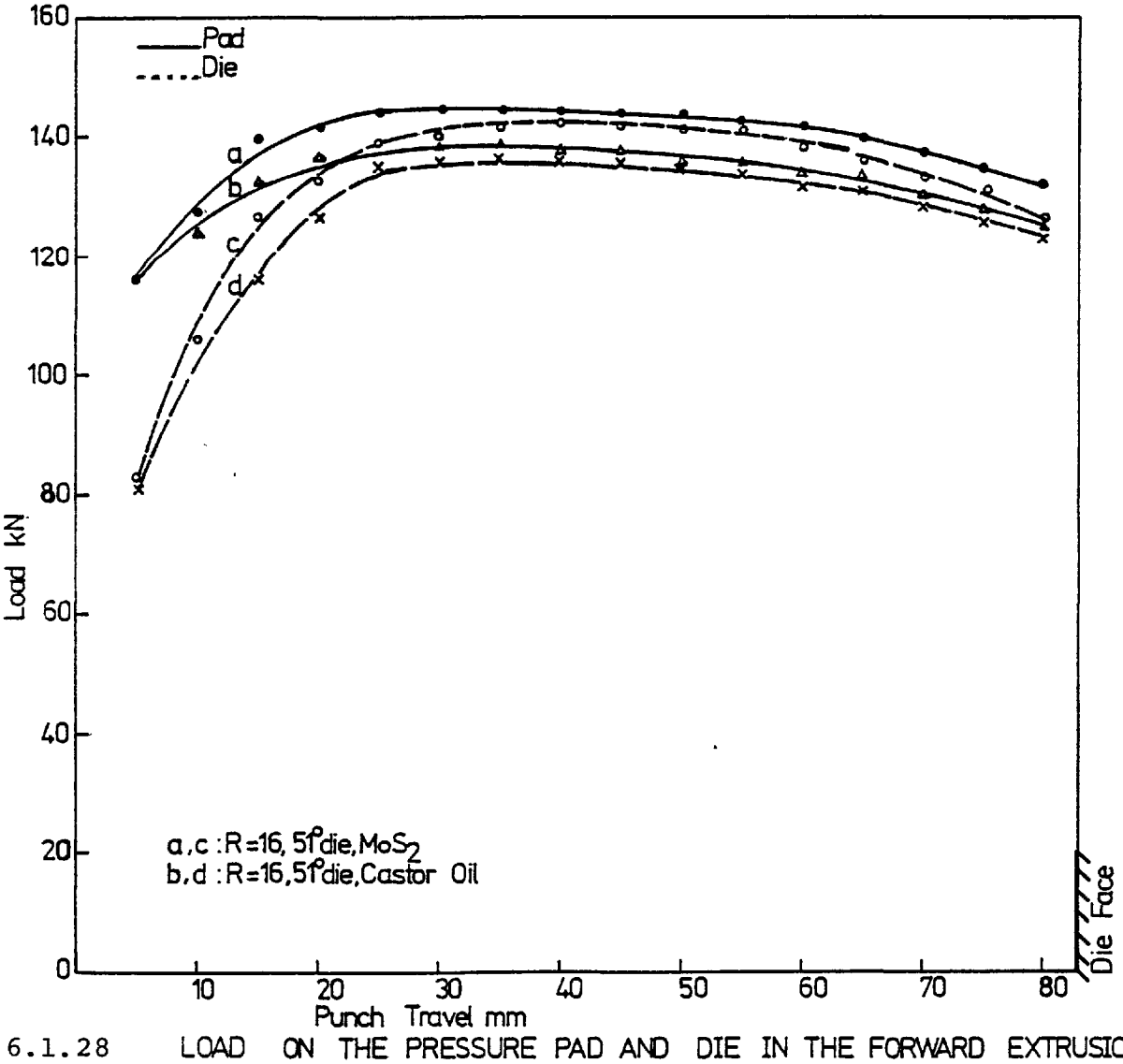


Fig. 6.1.28 LOAD ON THE PRESSURE PAD AND DIE IN THE FORWARD EXTRUSION OF LEAD

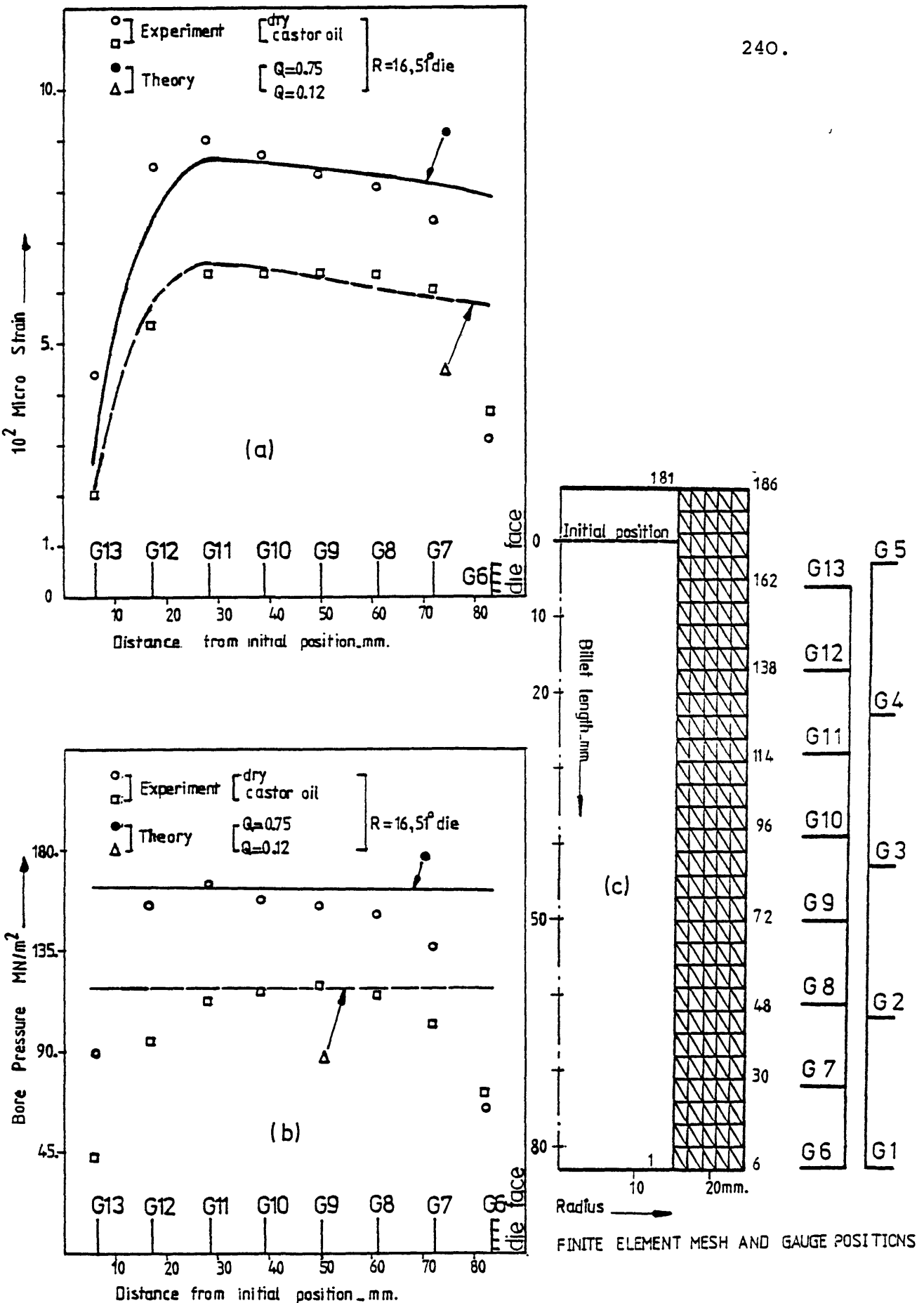


Fig. 6.1.18 Hoop strains and pressure distributions on the container wall in the forward extrusion of lead (After 20 mm punch travel).

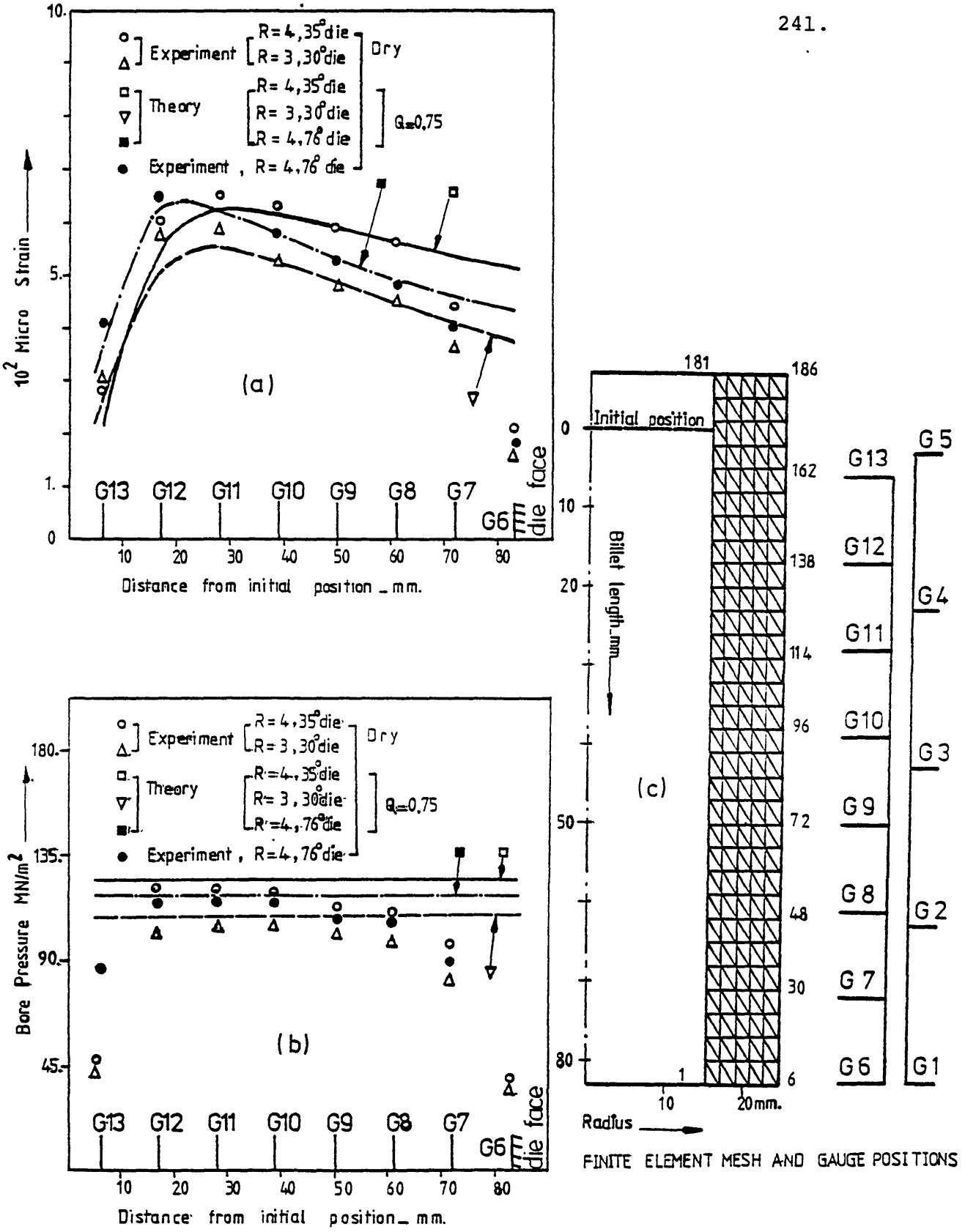


Fig. 6.1.19 Hoop strains and pressure distributions on the container wall in the forward extrusion of lead (After 20 mm punch travel).

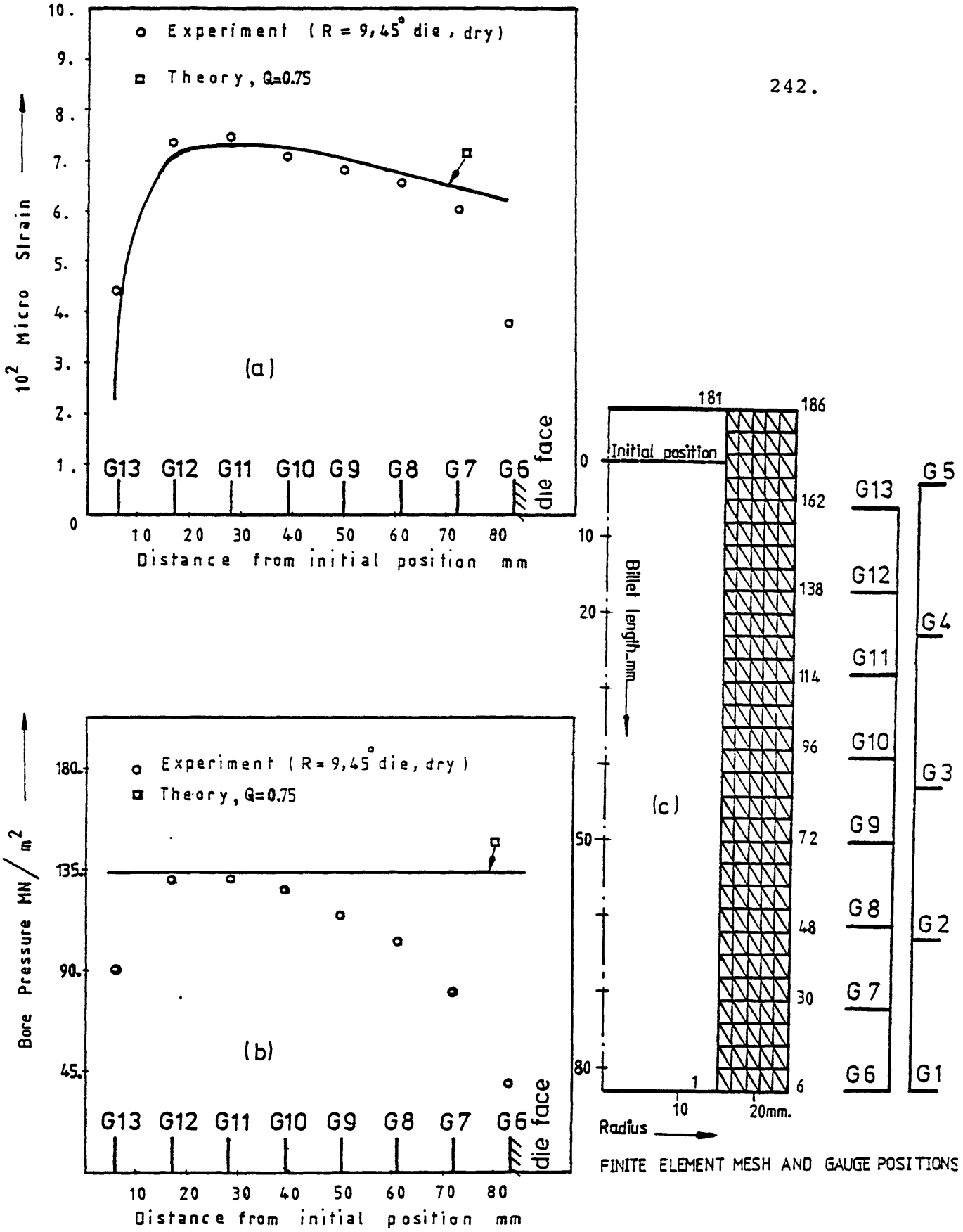


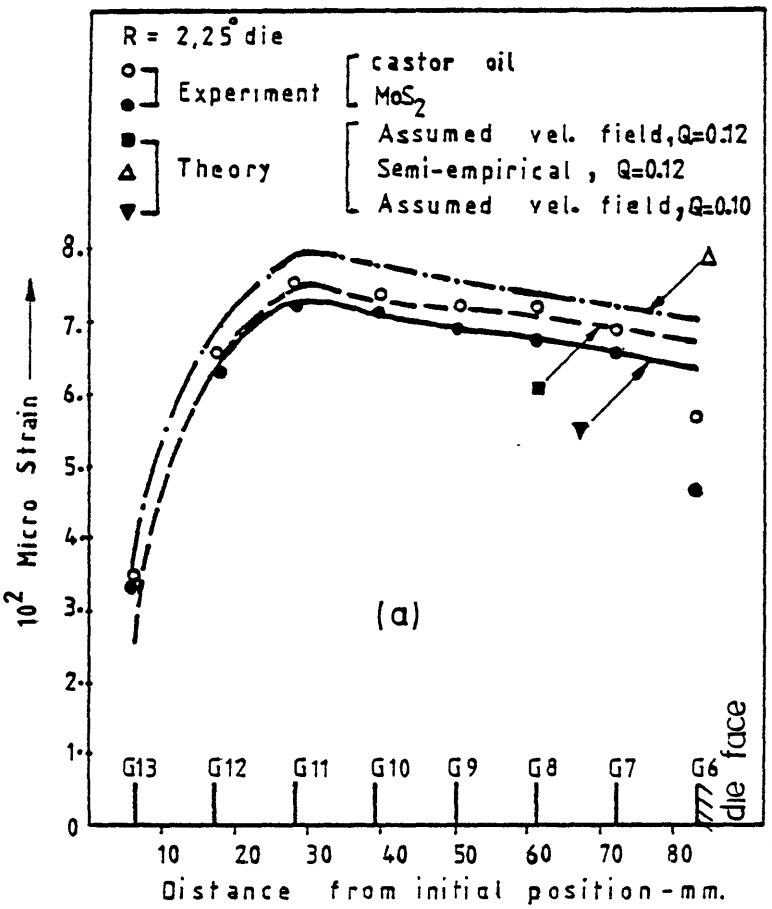
Fig. 6.1.20 Hoop strains and pressure distributions on the container wall in the forward extrusion of lead (After 20 mm punch travel).

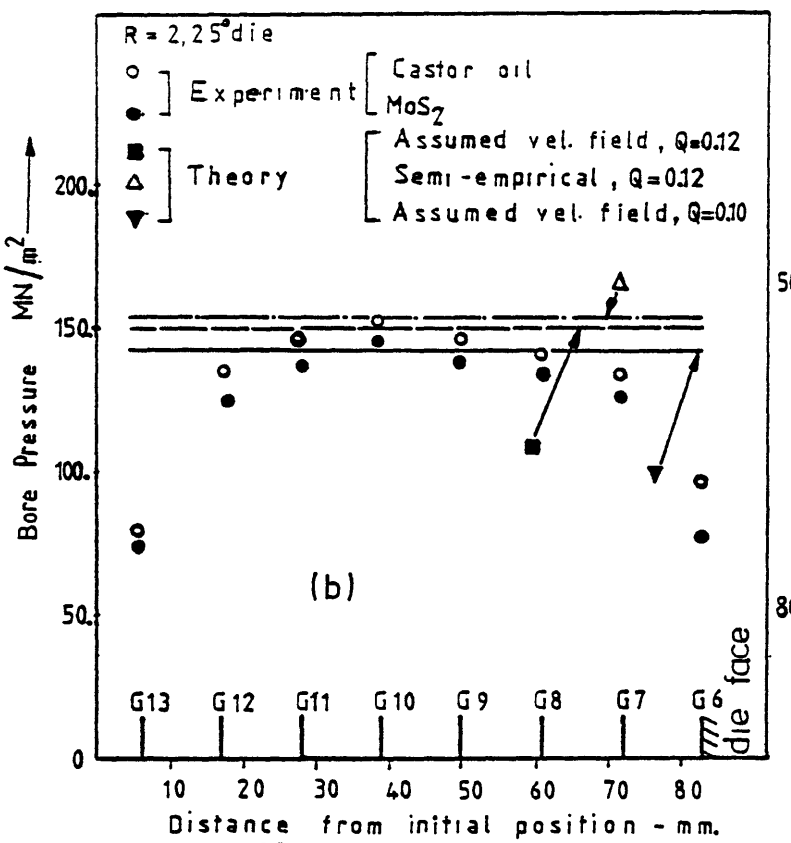
gauge positions along the container for lead extrusion of ratio 16 with lubricant.

In Fig. 6.1.18 b, the theoretically obtained pressure at the die corner is shown, assumed constant along the container. A friction factor of Q = 0.12 was used in the calculations for the lubricated case, while Q = 0.75 to simulate extrusion without a lubricant, taken from {17}, {21}.

The theoretical pressures shown in Fig. 6.1.18 b have been used as input data in the finite element program and hoop strains on the outside diameter of the container calculated, which are shown in Fig. 6.1.18 b together with the experimentally obtained strains. The agreement between the experimental and calculated values is good, particularly for the lubricated case. The exceptions are the experimental strains recorded by the guages close to the die, where the die and the flange on the outside of the container must have affected the strain gauge readings, factors which could not be taken into account in the finite element calculations.

The correlation between the theoretical strains calculated with a friction factor 0.75 and the strains measured in extrusion without a labricant are also reasonably good. Indeed, the same could be said for the results for the lubricated extrusion of aluminium, Fig. 6.1.21, despite the fact that the variation in bore pressure along the container wall must be significant, judging by the differences between





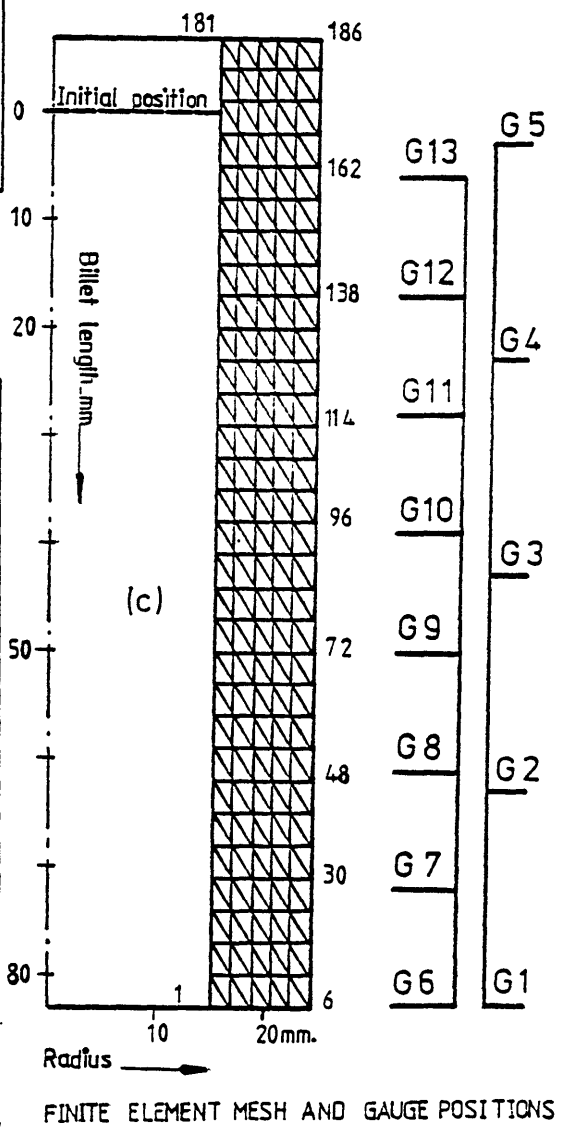


Fig. 6.1.21 Hoop strains and pressure distrubtions on the container wall in the forward extrusion of aluminium (After 20 mm punch travel).

the pressure pad and die loads shown in Fig. 6.1.29 (reproduced here for ease of reference). This is a clear indication that hoop strains do not provide a sensitive indication of pressure distribution in the container bore.

Approximate bore pressure distributions have been obtained by MUTLU {113} from the experimental hoop strains, on the assumption that the strain measured by a particular strain gauge is produced by a band of pressure facing that gauge and that pressures away from that strain gauge have no effect on the readings. The calculations give a step-wise pressure distribution along the container wall, which was smoothed to give the approximate pressures.

Similar calculations have been carried out in the present case and the results are shown in Fig. 6.1.18 b by the experimental points. The bore pressures so calculated deviate from the theoretical line at both ends of the container, where pressure and geometric discontinuities caused the measured strains to fall even though there was no appropriate change in the bore pressure. It could thus be concluded that, while finite element calculations give strains in close agreement with experiments for the theoretical constant pressure distribution, to the extent that even the drop in the strains near the container can be predicted accurately, the reverse approximate method gives realistic bore pressures only away from the container ends and grossly underestimates the pressures elsewhere.

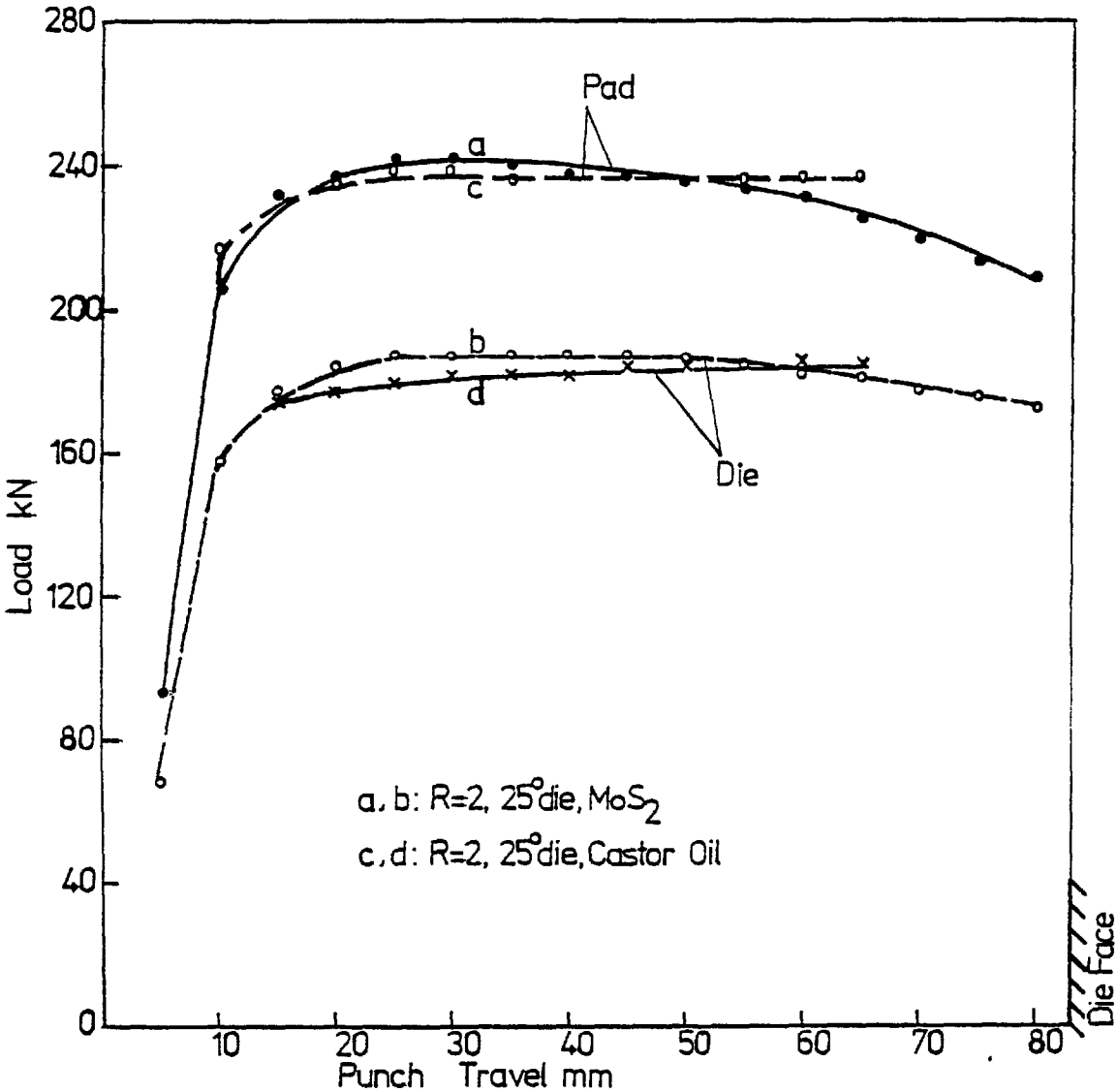


Fig. 6.1.29 LOAD ON THE PRESSURE PAD AND DIE IN THE FORWARD EXTRUSION OF ALUMINIUM

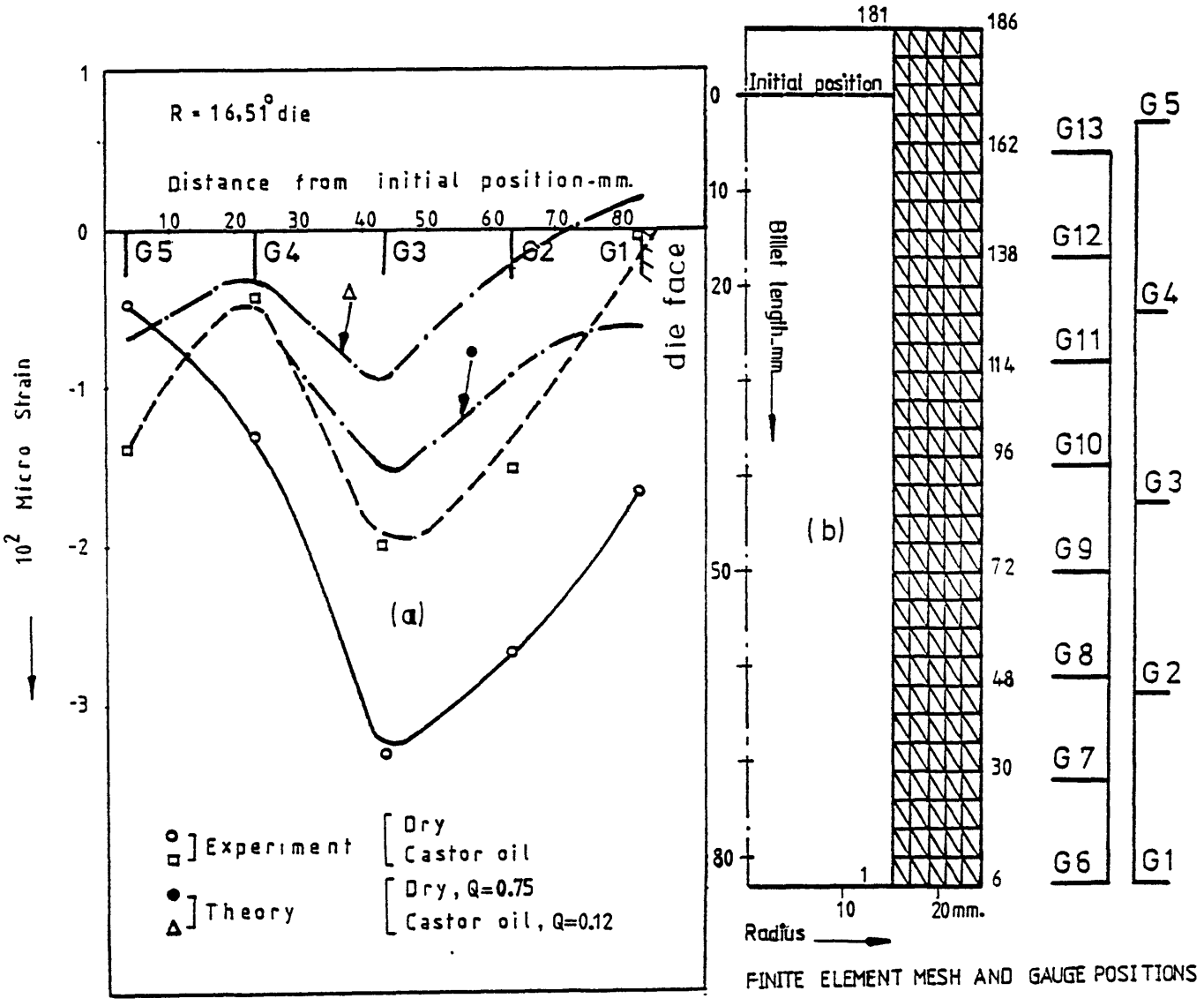


Fig. 6.1.22 Axial strain distributions on the container wall in the forward extrusion of lead (After 20 mm punch travel).

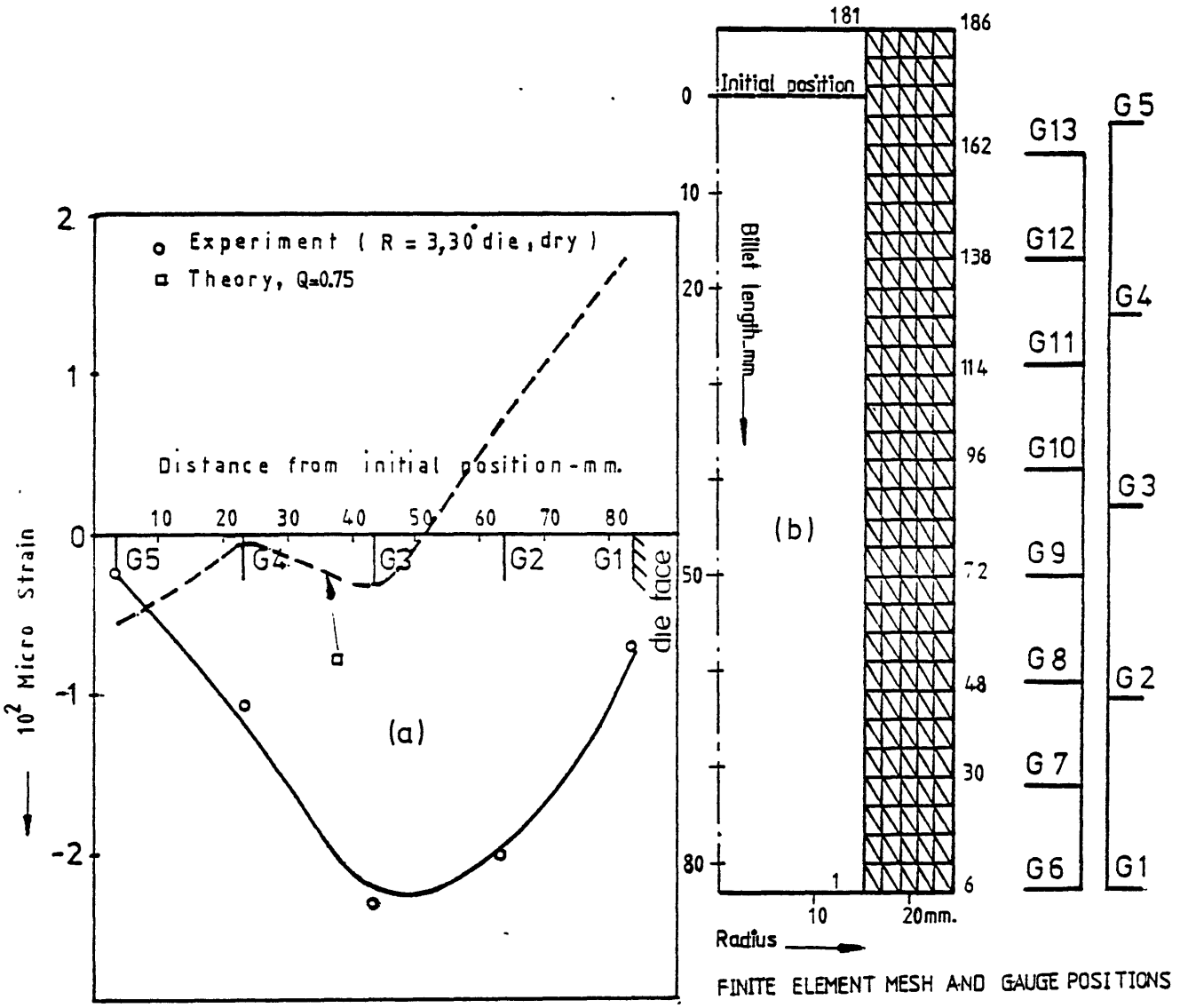


Fig. 6.1.23 Axial strain distributions on the container wall in the forward extrusion of lead (After 20 mm punch travel).

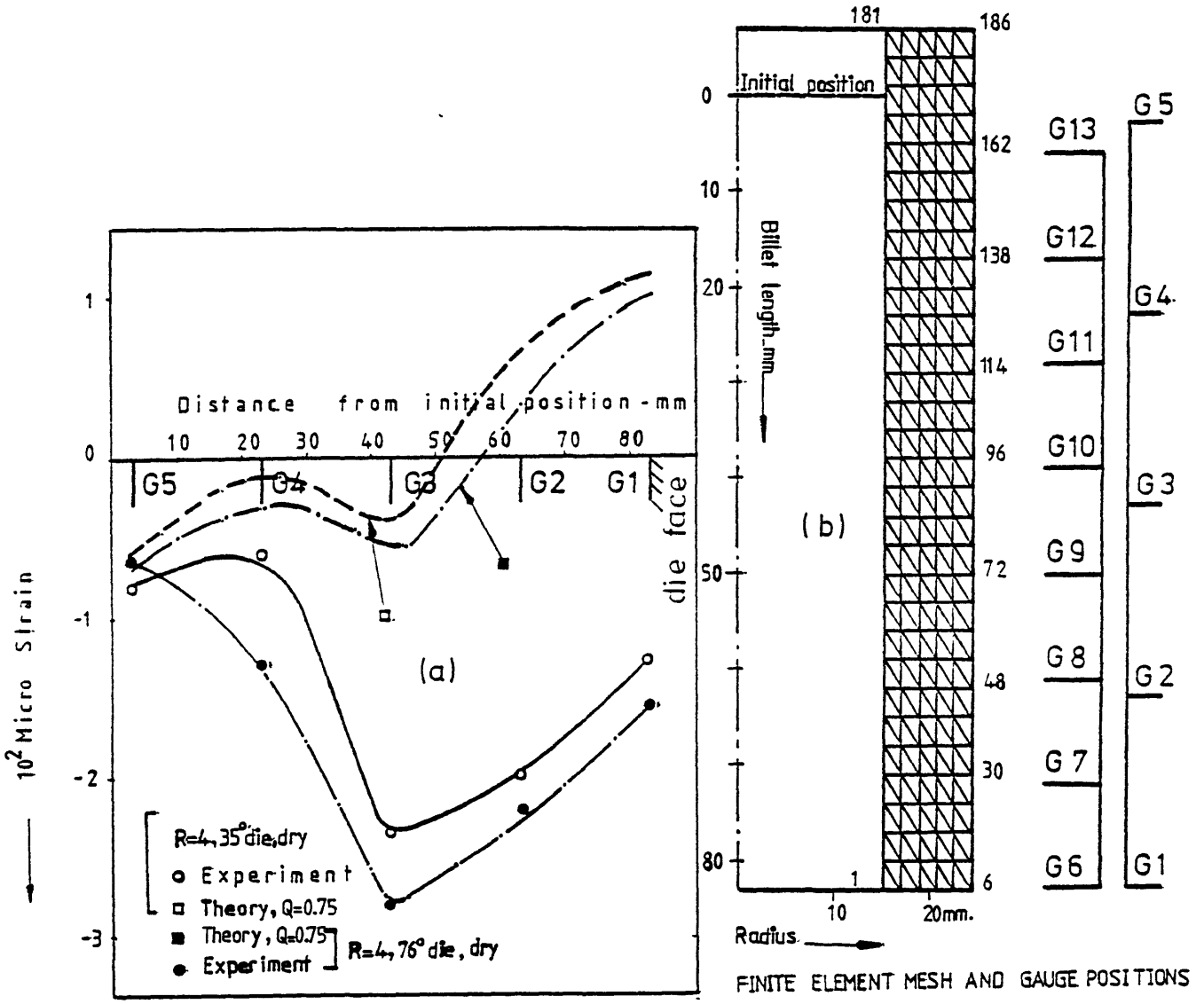


Fig. 6.1.24 Axial strain distributions on the container wall in the forward extrusion of lead (After 20 mm punch travel).

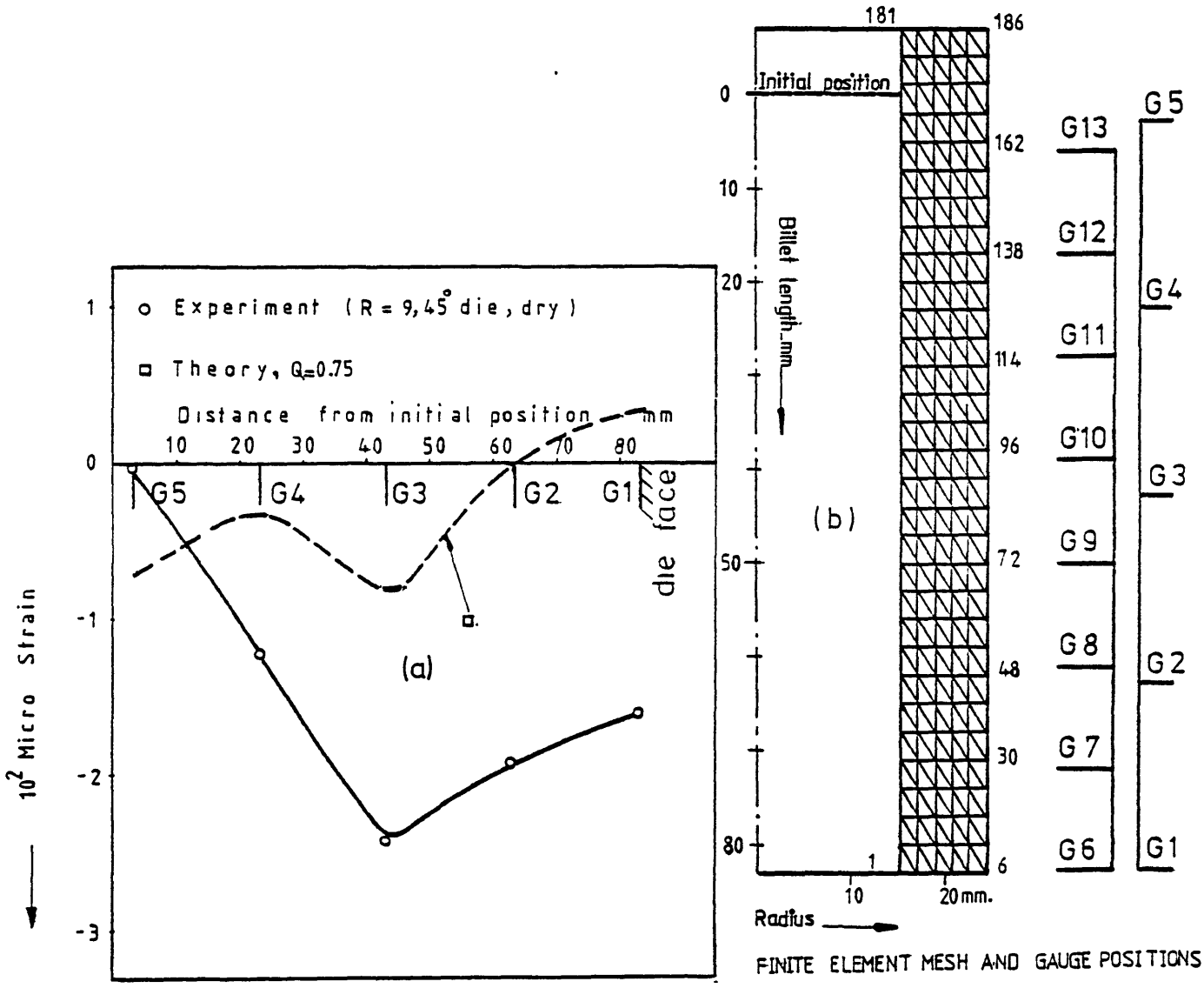


Fig. 6.1.25 Axial strain distributions on the container wall in the forward extrusion of lead (After 20 mm punch travel).

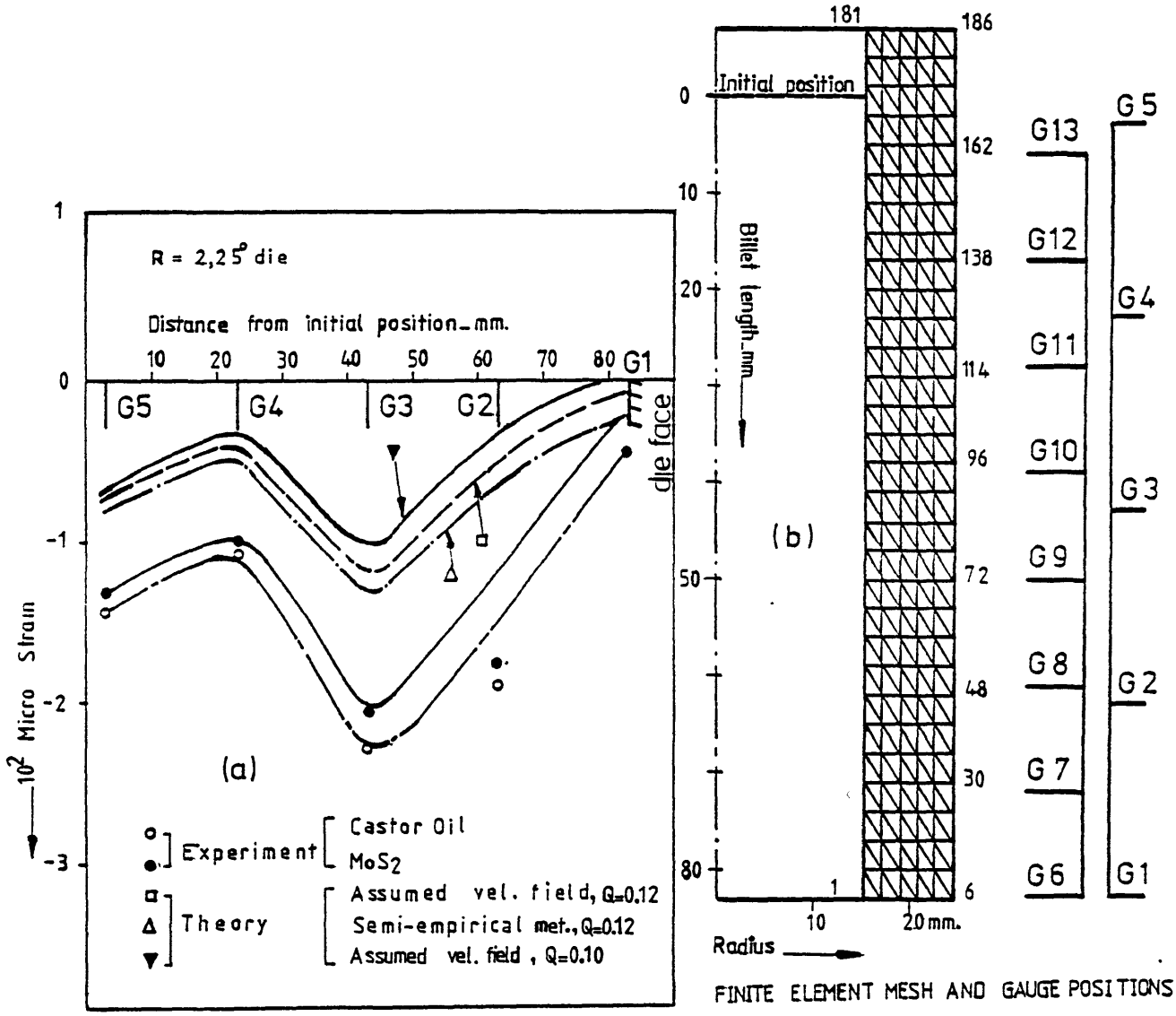


Fig. 6.1.25/A Axial strain distributions on the container wall in the forward extrusion of aluminium (After 20 mm punch travel).

Fig. 6.1.22 compares the axial strains calculated from theory with those obtained experimentally, for the conditions shown in Fig. 6.1.18. For lubricated extrusion, the theoretical and experimental strains are once more in good agreement, but the same is not true for dry conditions. The theory, which assumes that the bore pressure distribution is constant and equals the value calculated for the die corner, underestimates the axial stresses, which imply that bore pressures away from the die must be higher for dry conditions, as would be expected. The dry conditions also represent larger axial stresses on the container wall due to increased frictional shear stresses, which must have more noticeable effect on the axial than on the hoop strain readings.

Similar conclusions can be drawn from Fig. 6.1.23, 6.1.24 and 6.1.25 which show comparisons between experimental and theoretical axial strains for various die angles and extrusion ratios, all for dry conditions for lead and from Fig. 6.1.25/A with results for the lubricated extrusion of aluminium at a ratio of 2. These results indicate that axial strains are far more indicative of the normal and shear stress distributions in the extrusion container bore than are hoop strains.

6.1.4 Further experimental results in forward extrusion {113}

The experiments were carried out on one hand to check the computed results and to verify the suitability of the assumed

velocity field and the semi-empirical method. To produce the illustrations of the previous section, a vast number of experimental data were needed, which will now be presented in full. Furthermore, it was decided to obtain additional information not only in the forward extrusion of rod, but also in the backward extrusion of cans, under various extrusion conditions. Owing to the experimental limitations explained in earlier, the main experimental billet material was lead, but a limited number of experiments have been carried out with commercial purity aluminium also.

In the following, the full set of experimental result will be presented. Fig. 6.1.26 illustrates the load on the pressure pad in the dry rod extrusion of pure lead at various extrusion ratios, as a function of punch travel. The loads on the die for the dry forward extrusion of pure lead for the same extrusion ratios are shown in Fig. 6.1.27. It is interesting to note that, for lubricated extrusion, the load on the die remains constant in the steady state, for each extrusion condition as extrusion proceeds, reinforcing the assumption of negligible friction and uniform bore pressure. The opposite is true for unlubricated extrusion:load on the pressure pad falls steeply with reducing billet length, indicating significant frictional shear stress in the bore. Fig. 6.1.26 and Fig. 6.1.27, show that using a conical die with die semi-angle of 76^{o}, insteand of 51^{o}, has a considerable effect on loads on the pressure pad and the die respectively.

Fig. 6.1.28 shows the loads on the pressure pad and the die in the lubricated forward extrusion of lead, for the

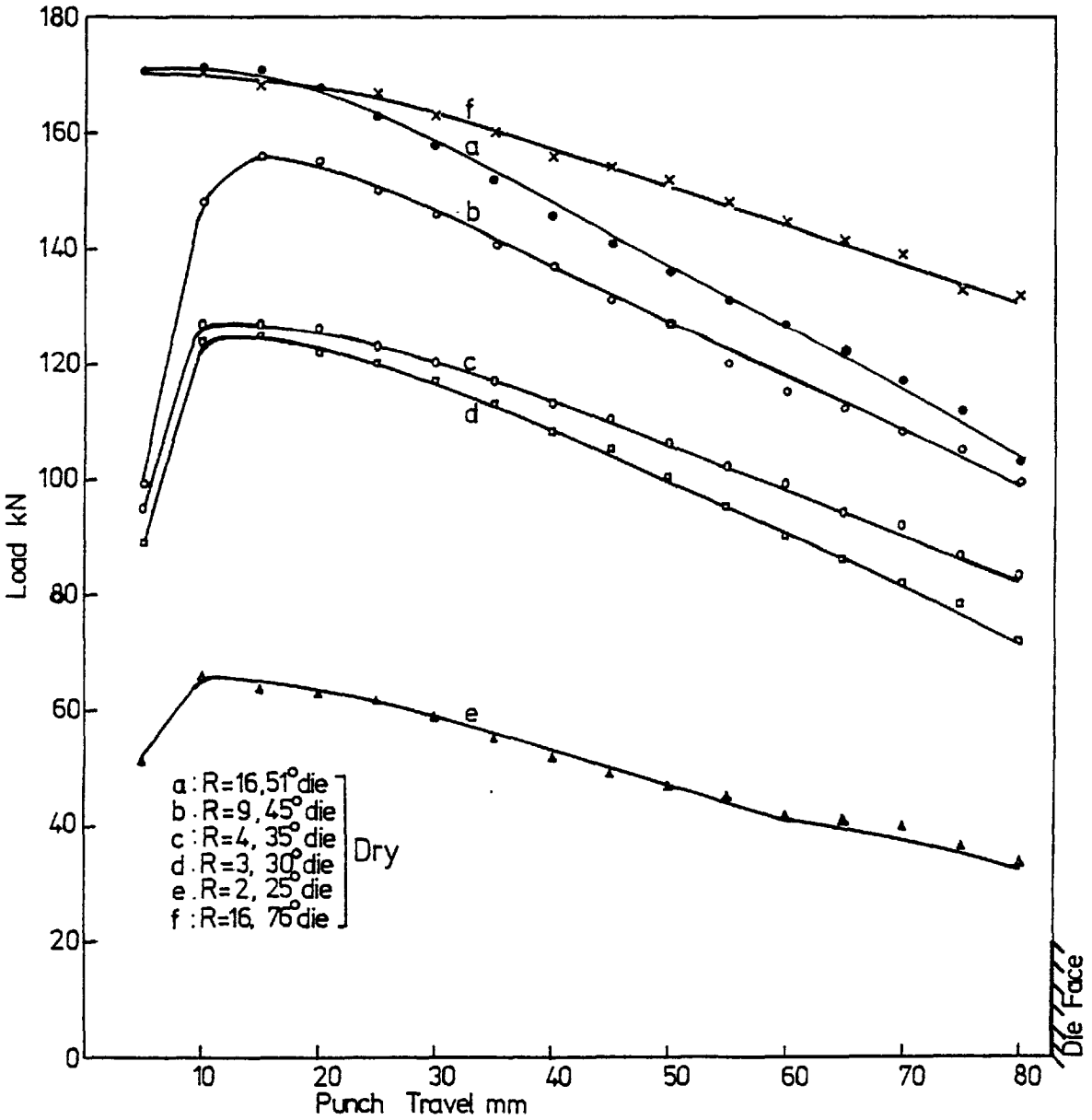


Fig. 6.1.26 LOAD ON THE PRESSURE PAD IN THE FORWARD EXTRUSION OF LEAD.

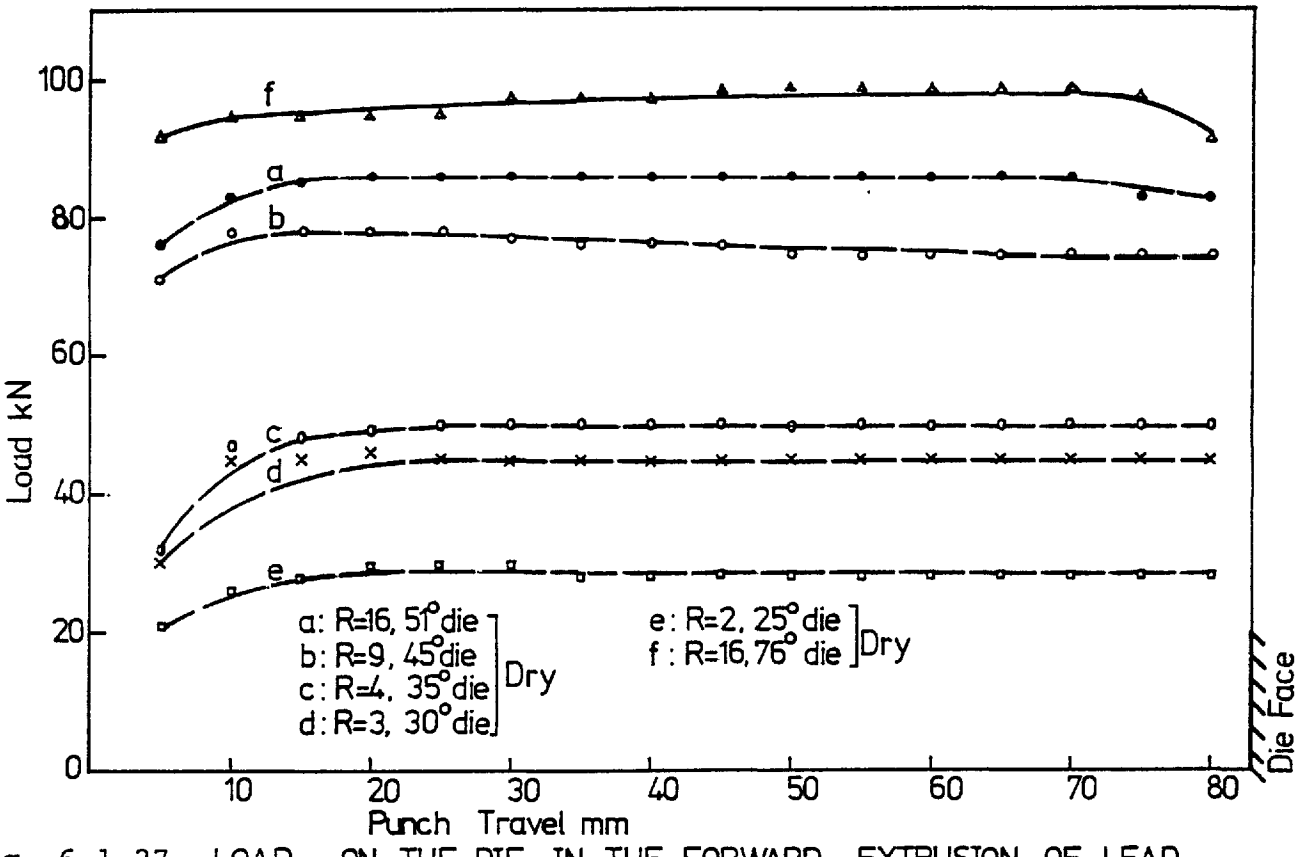


Fig. 6.1.27 LOAD ON THE DIE IN THE FORWARD EXTRUSION OF LEAD.

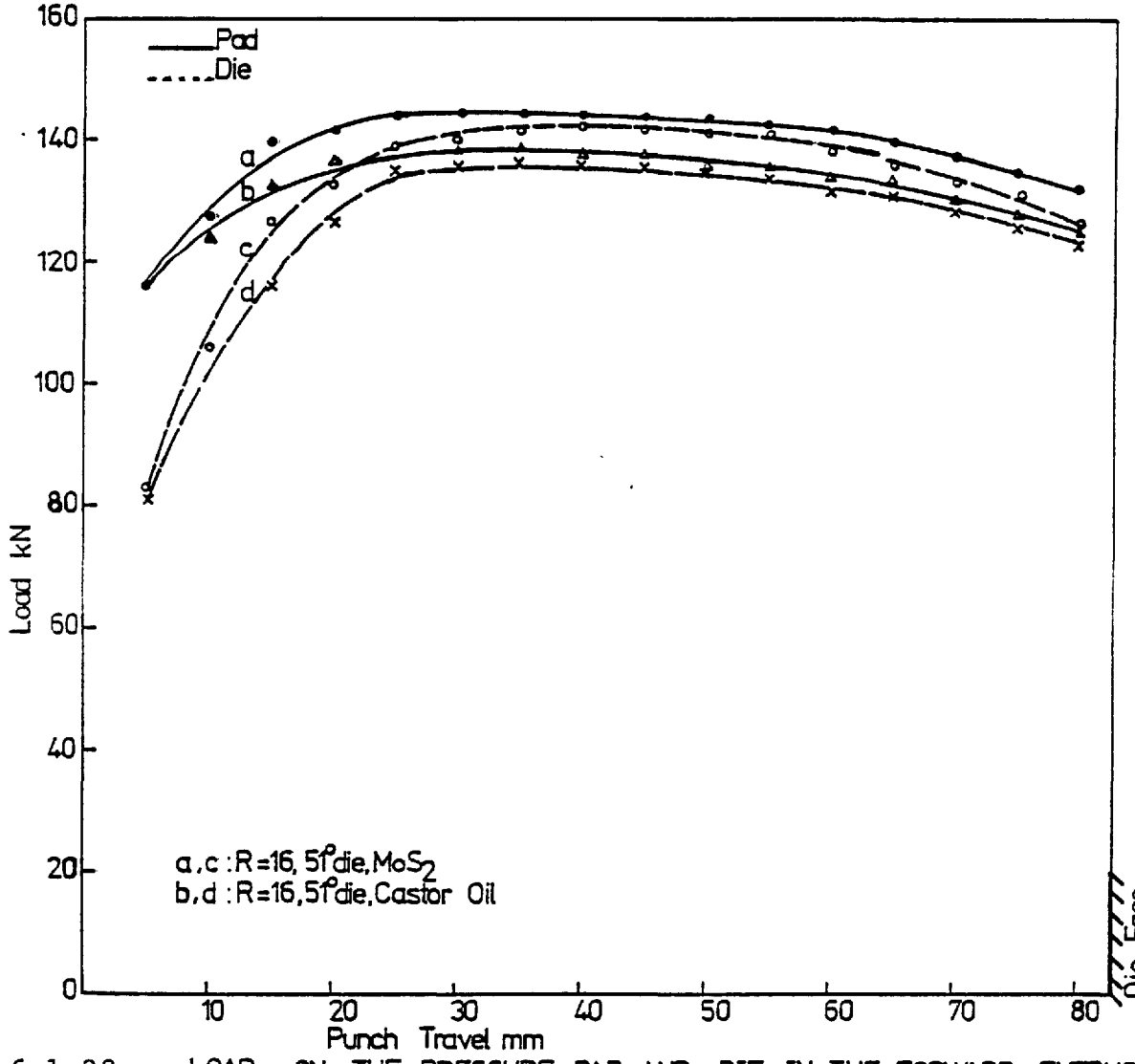


Fig. 6.1.28 LOAD ON THE PRESSURE PAD AND DIE IN THE FORWARD EXTRUSION OF LEAD.

extrusion ratio of 16 and die semi-angle of 51^{o}. Friction is small at the container/billet interface so that loads on the pressure pad and die remain constant and there is little difference between them in the steady state. For the lubricated rod extrusion of aluminium at the extrusion ratio of 2 and die semi-angle of 25^{o}, the loads on the pressure pad and the die are shown in Fig. 6.1.29. This figure clearly illustrates that, despite the presence of lubricants, container/billet friction results in considerably higher initial loads on the pressure pad than on the die and, as the unextruded billet length decreases, the difference becomes smaller as would be expected but still remains significant. Friction accounts for a considerable proportion of the total load so that theoretical predictions of the type described earlier would be less useful than for lead.

Typical hoop strain distribution recorded by the various strain gauges as a function of punch travel, for the dry forward extrusion of lead through a conical die at the extrusion ratio of 4, for die semi-angle of 35^{o} is shown in Fig. 6.1.30, which is also an implication of stresses and pressures in the container bore. Similar results are shown for various other conditions in Figs 6.1.31 to 6.1.34. At the beginning of process, the strains are much higher further away from the die (gauges No. 10, 11 and 12) than nearer the exit (gauges No. 6 and 7) while in lubricated forward extrusion of lead at the extrusion ratios of 4 and 16 and die semi-angle of 76^{o} and 51^{o} (Figs 6.1.35 to 6.1.38) the strains are largest close to the die,

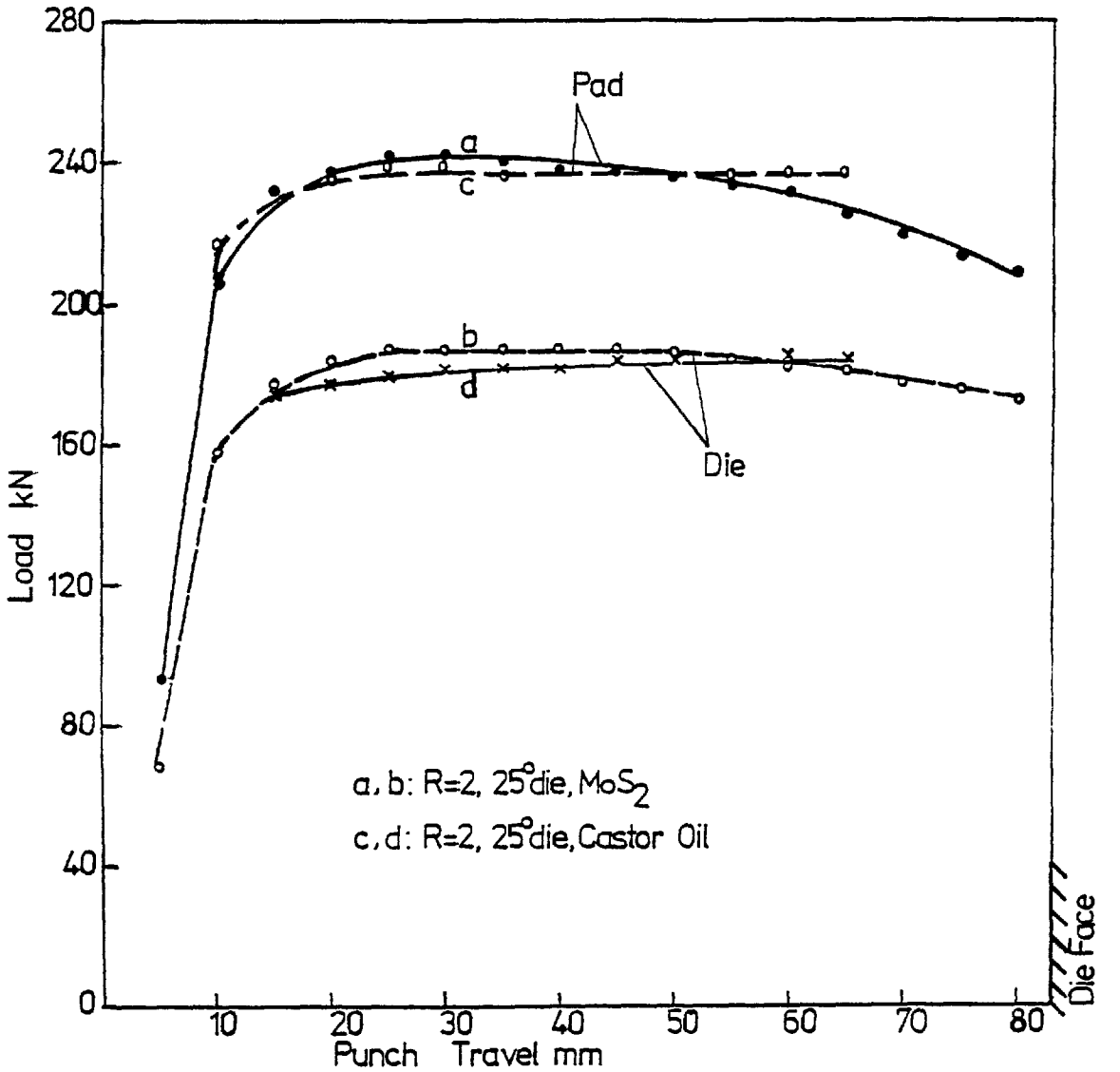
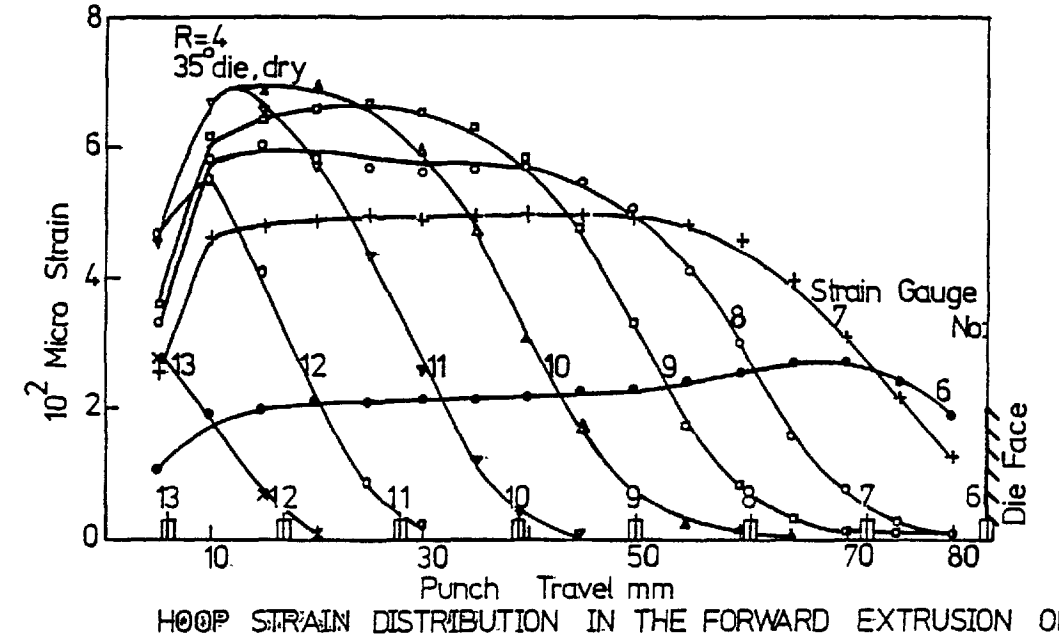


Fig. 6.1.29 LOAD ON THE PRESSURE PAD AND DIE IN THE FORWARD EXTRUSION OF ALUMINIUM.



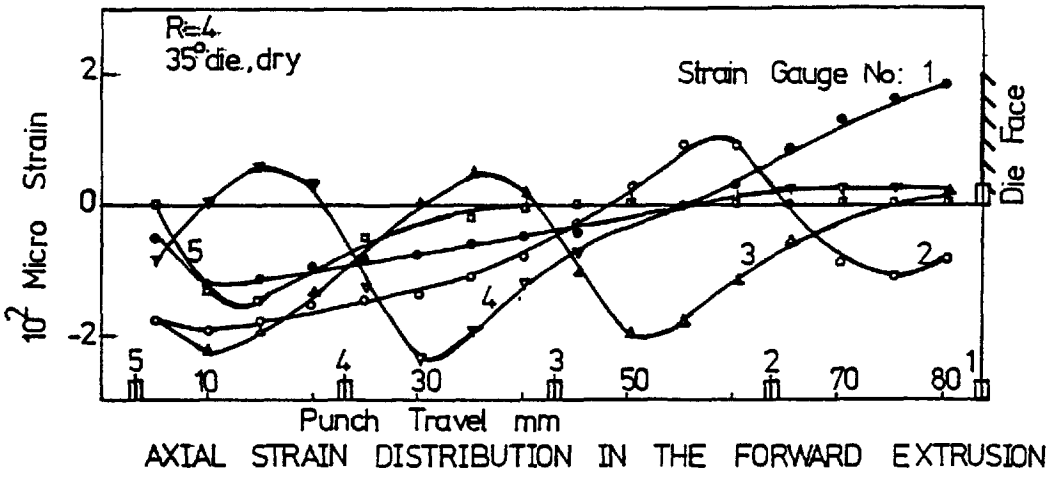
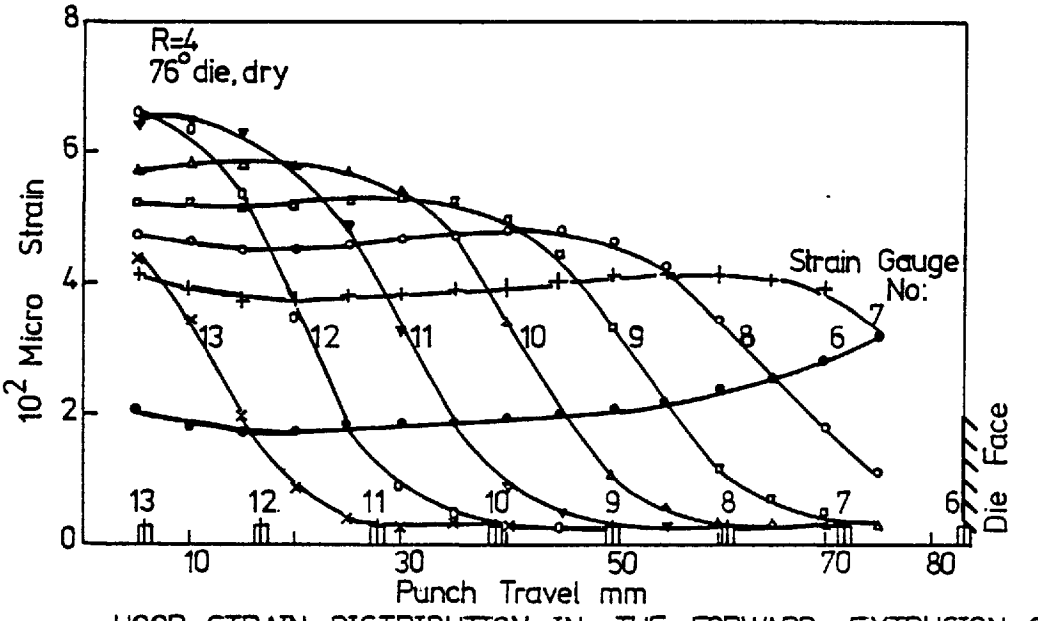
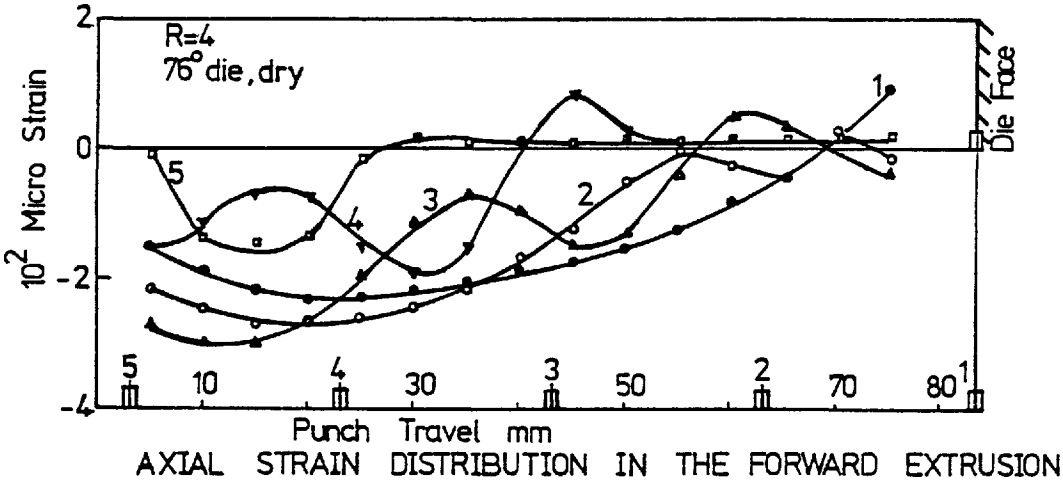


Fig. 6.1.30 Hoop and axial strain distributions.

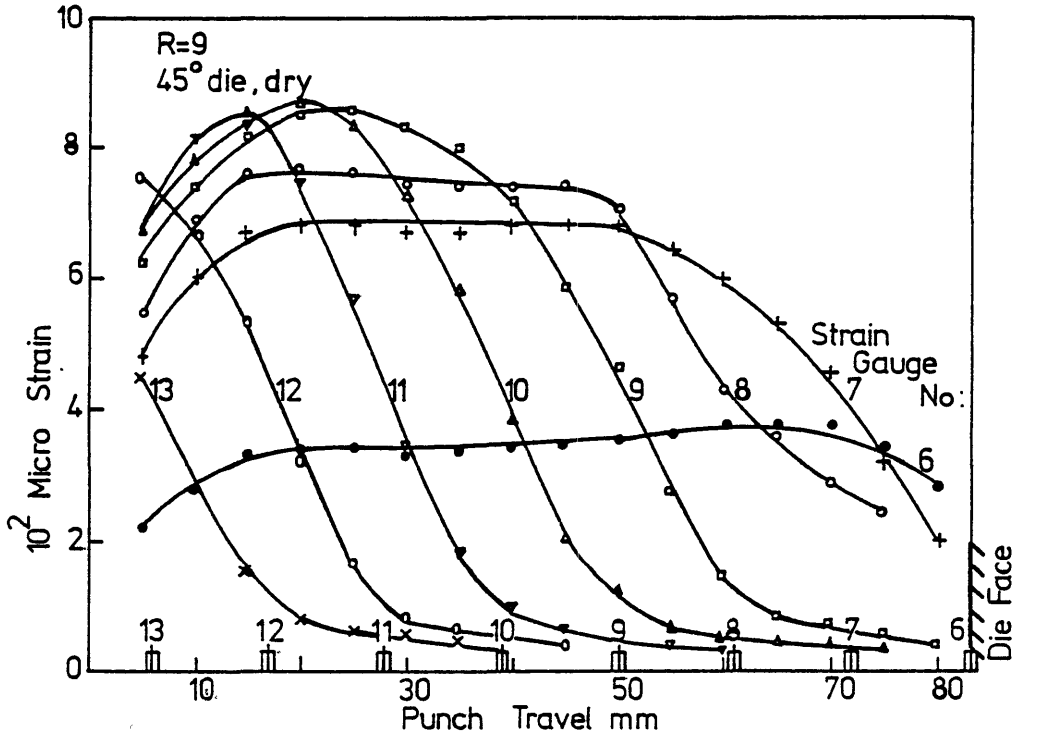


HOOP STRAIN DISTRIBUTION IN THE FORWARD EXTRUSION OF LEAD



AXIAL STRAIN DISTRIBUTION IN THE FORWARD EXTRUSION OF LEAD

Fig. 6.1.31 Hoop and axial strain distributions.



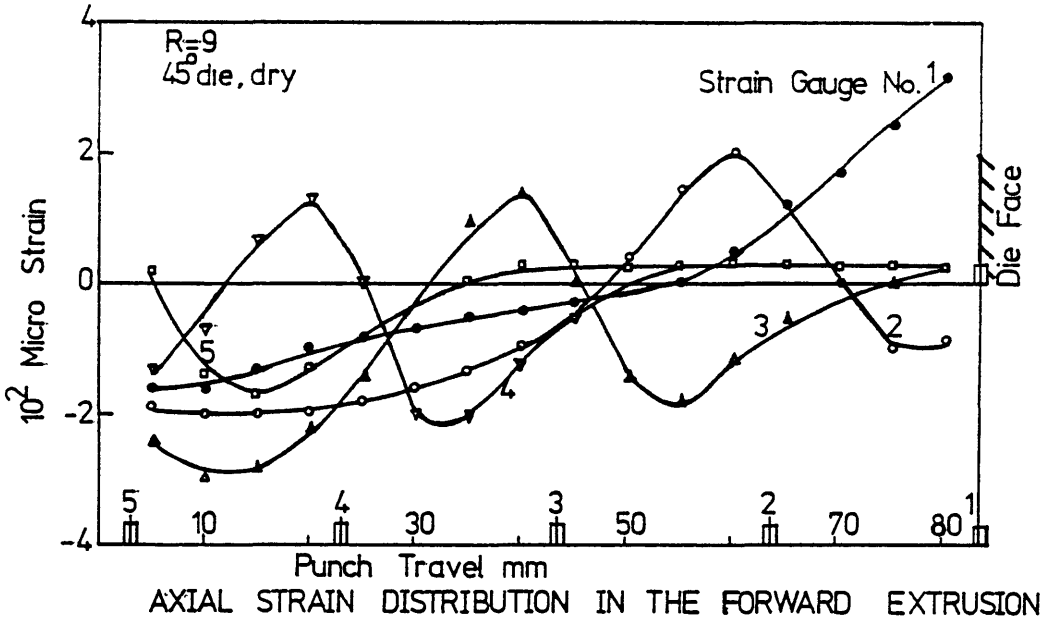
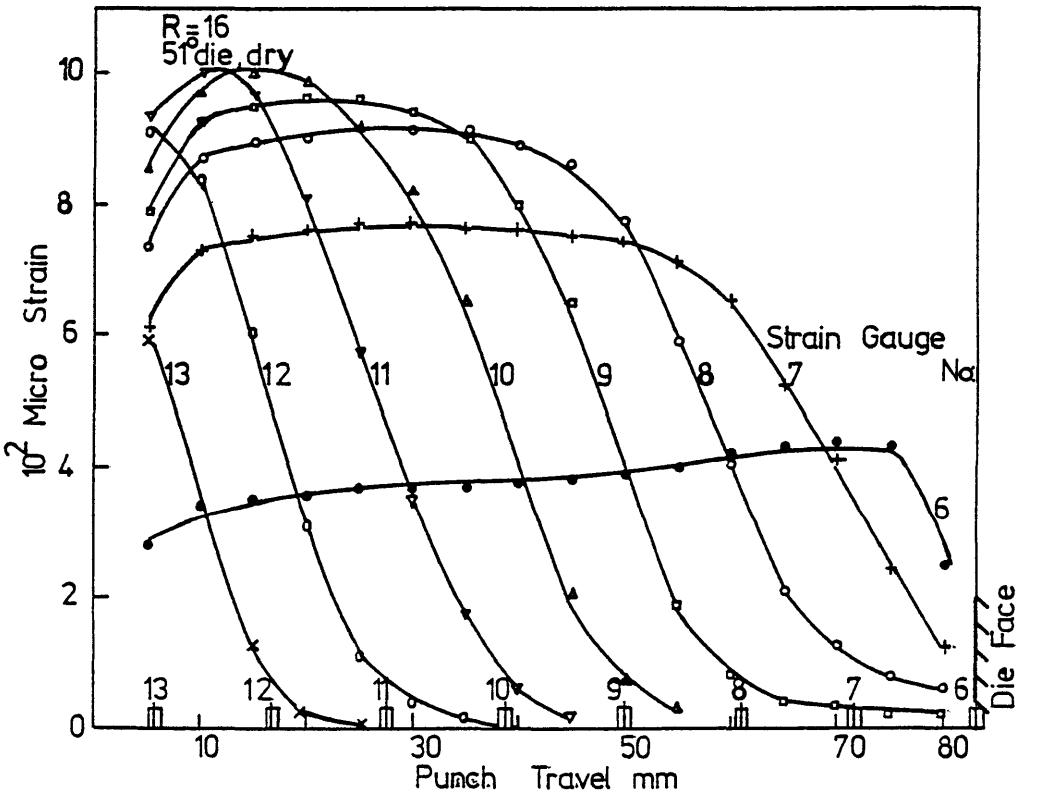


Fig. 6.1.32 Hoop and axial strain distributions.



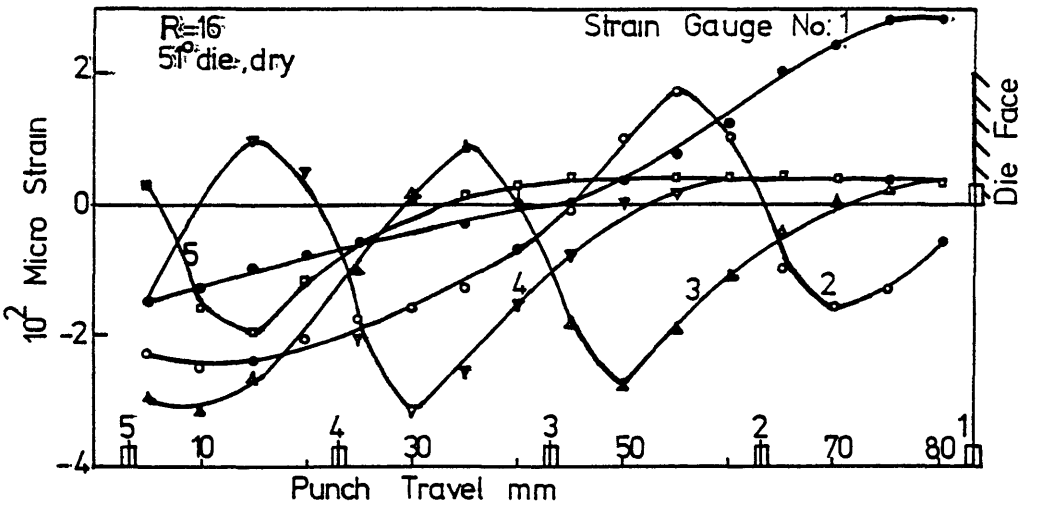
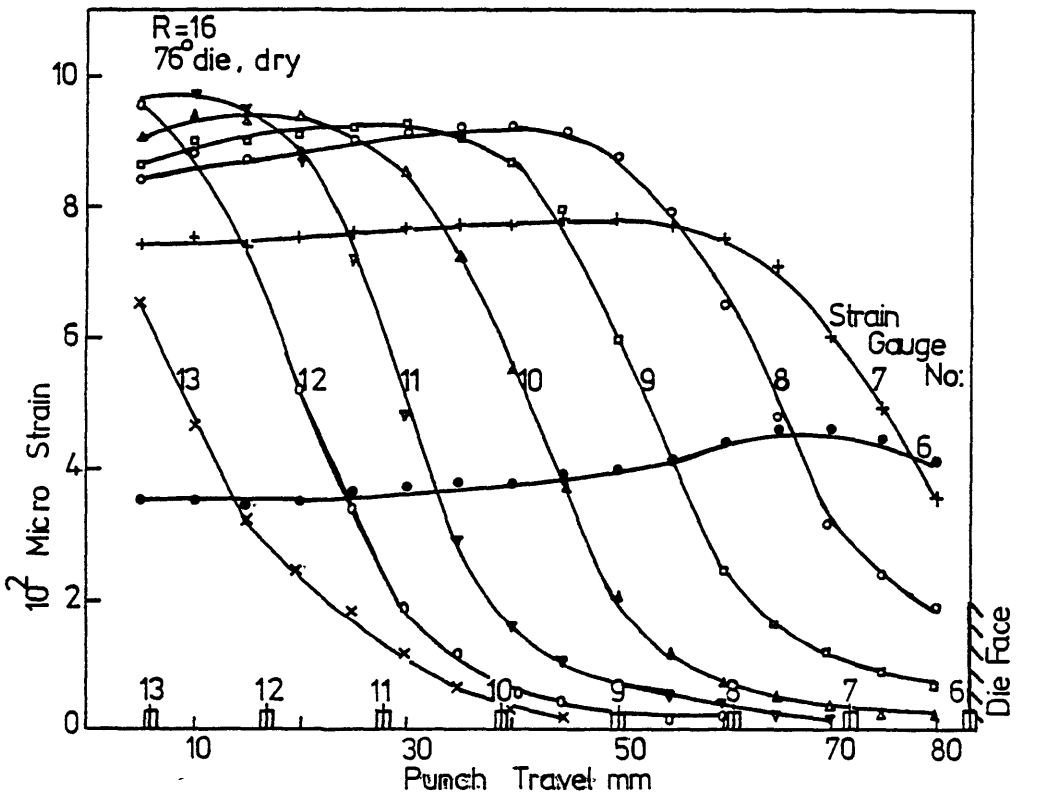
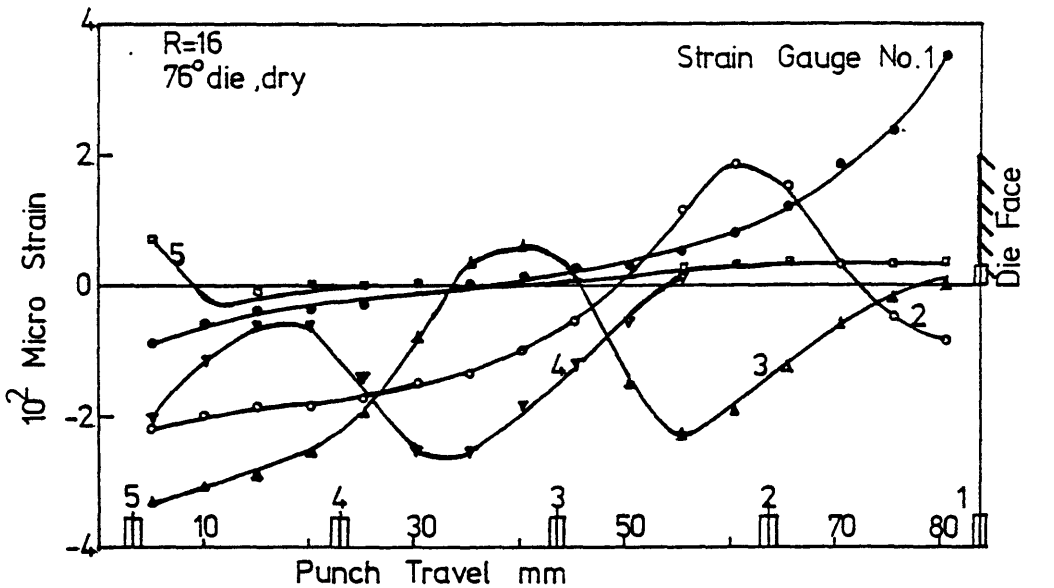


Fig. 6.1.33 Hoop and axial strain distributions.

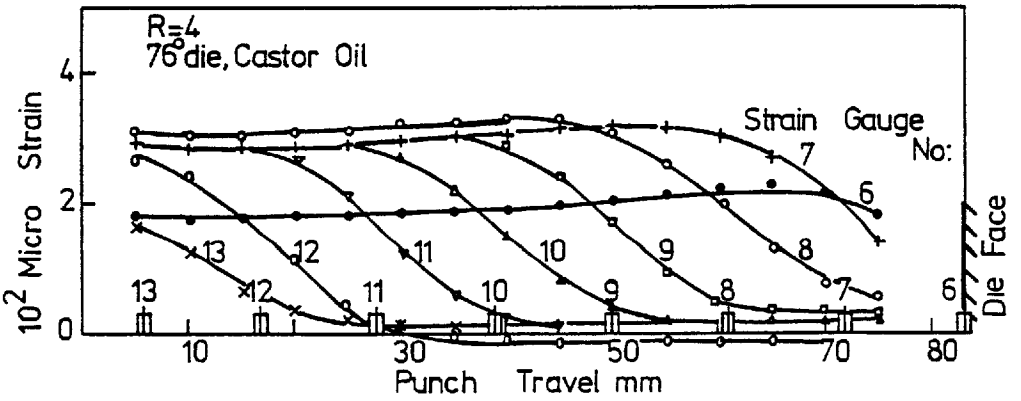


HOOP STRAIN DISTRIBUTION IN THE FORWARD EXTRUSION OF LEAD



AXIAL STRAIN DISTRIBUTION IN THE FORWARD EXTRUSION OF LEAD

Fig. 6.1.34 Hoop and axial strain distributions.



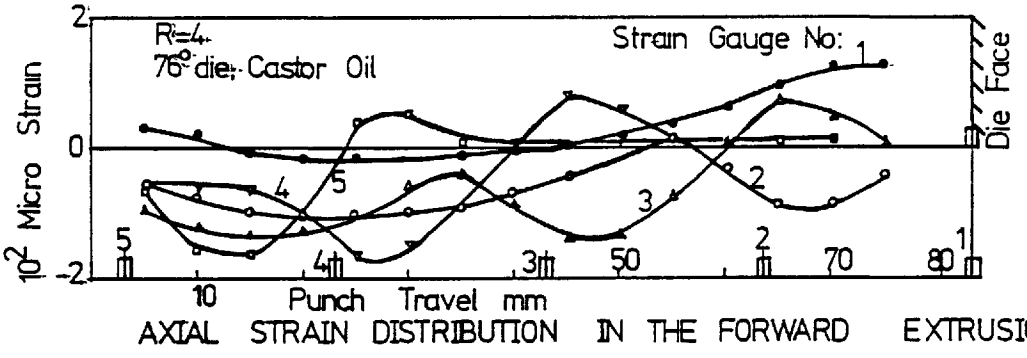
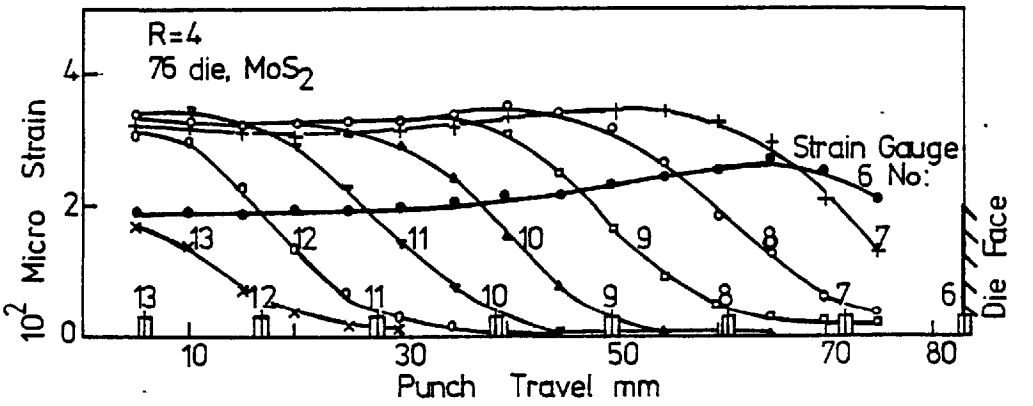
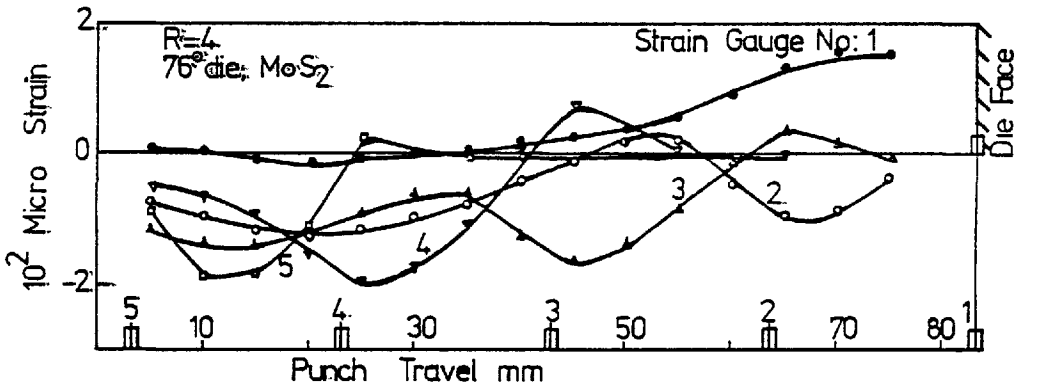


Fig. 6.1.35 Hoop and axial strain distributions.

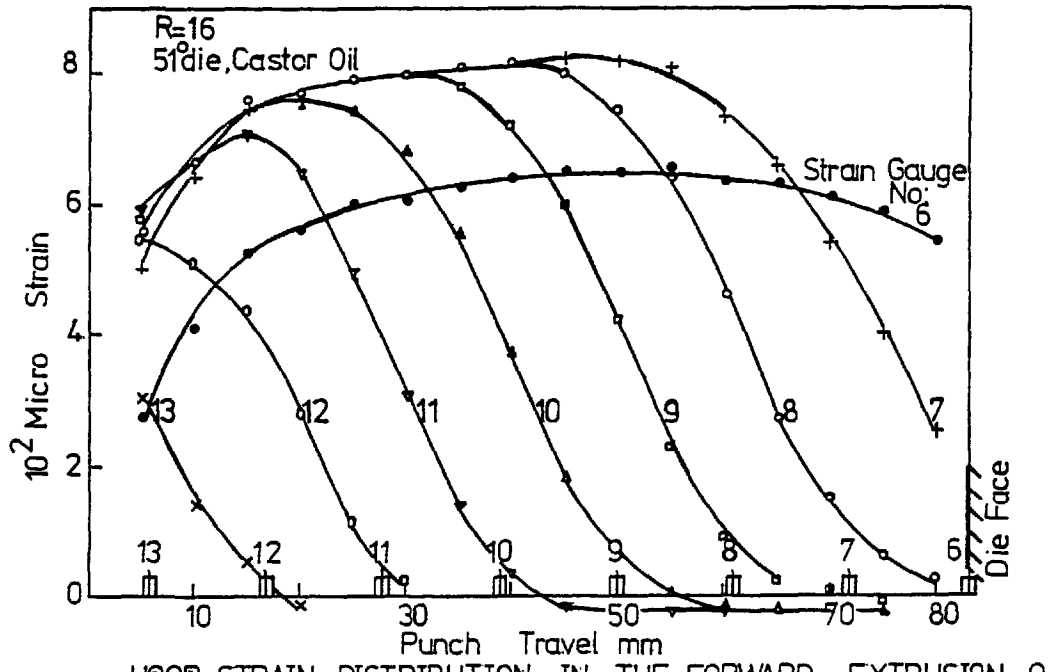


HOOP STRAIN DISTRIBUTION IN THE FORWARD EXTRUSION OF LEAD

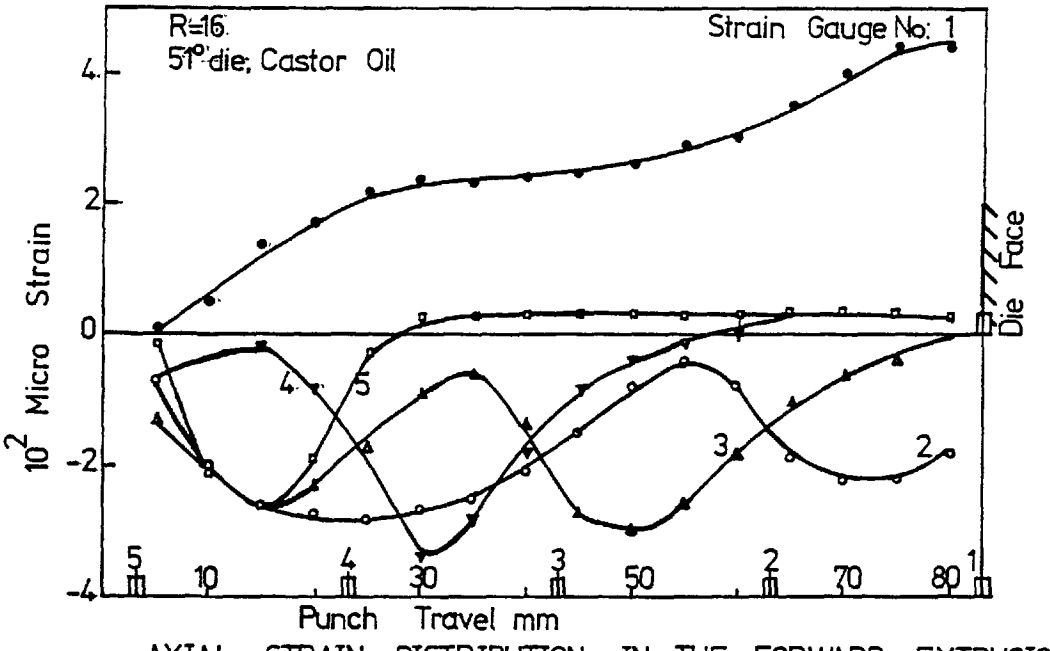


AXIAL STRAIN DISTRIBUTION IN THE FORWARD EXTRUSION OF LEAD

Fig. 6.1.36 Hoop and axial strain distributions.

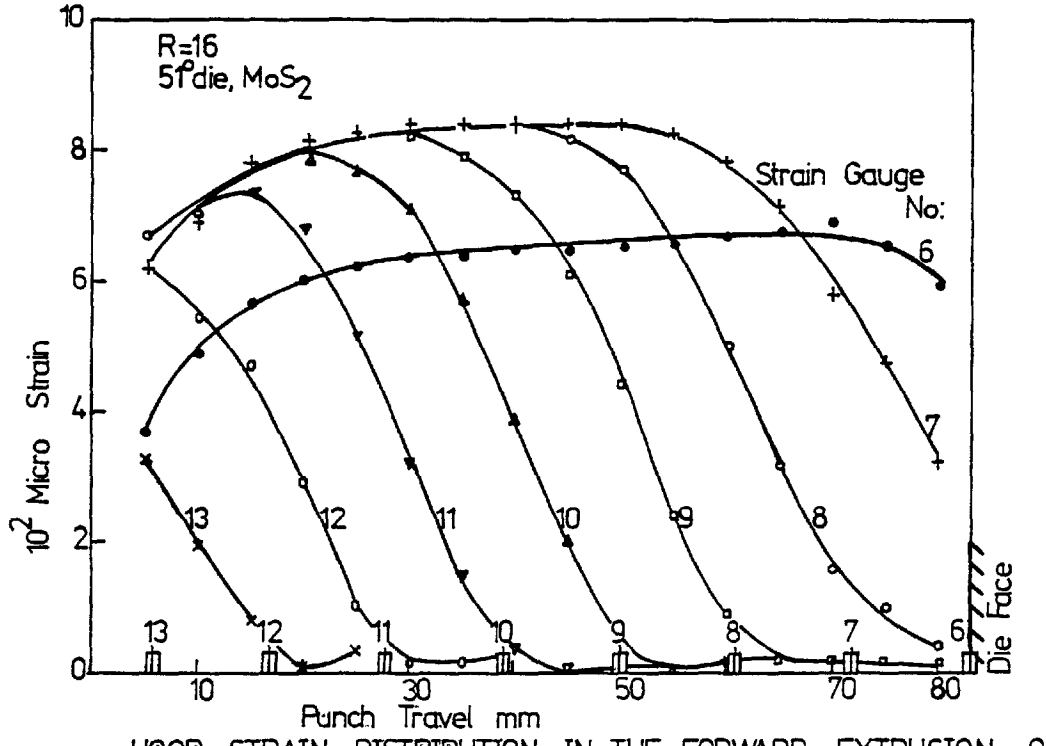


HOOP STRAIN DISTRIBUTION IN THE FORWARD EXTRUSION OF LEAD



AXIAL STRAIN DISTRIBUTION IN THE FORWARD EXTRUSION OF LEAD

Fig. 6.1.37 Hoop and axial strain distributions.



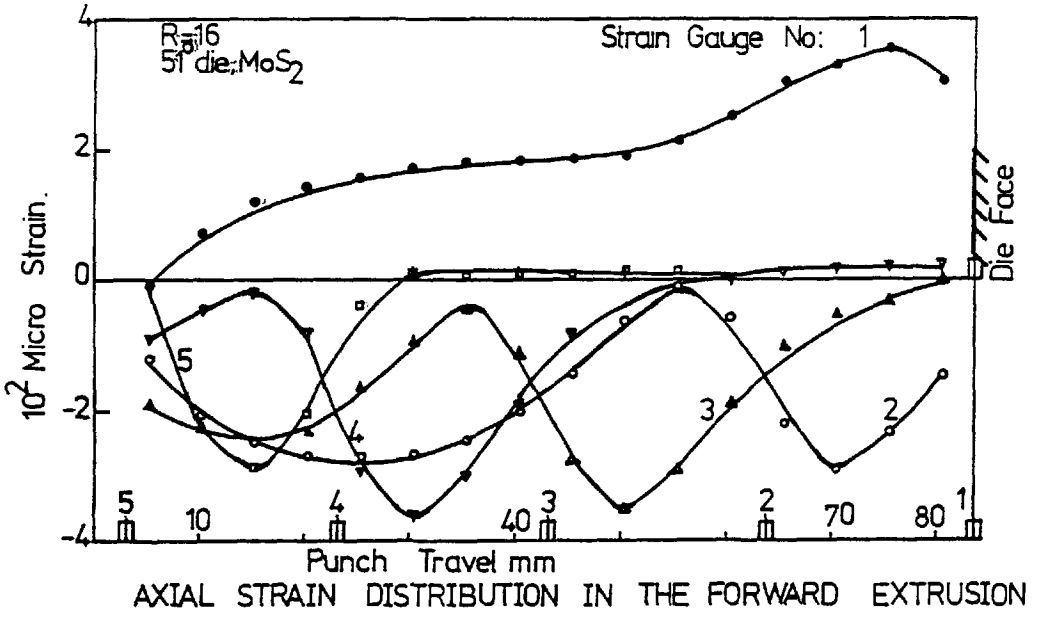
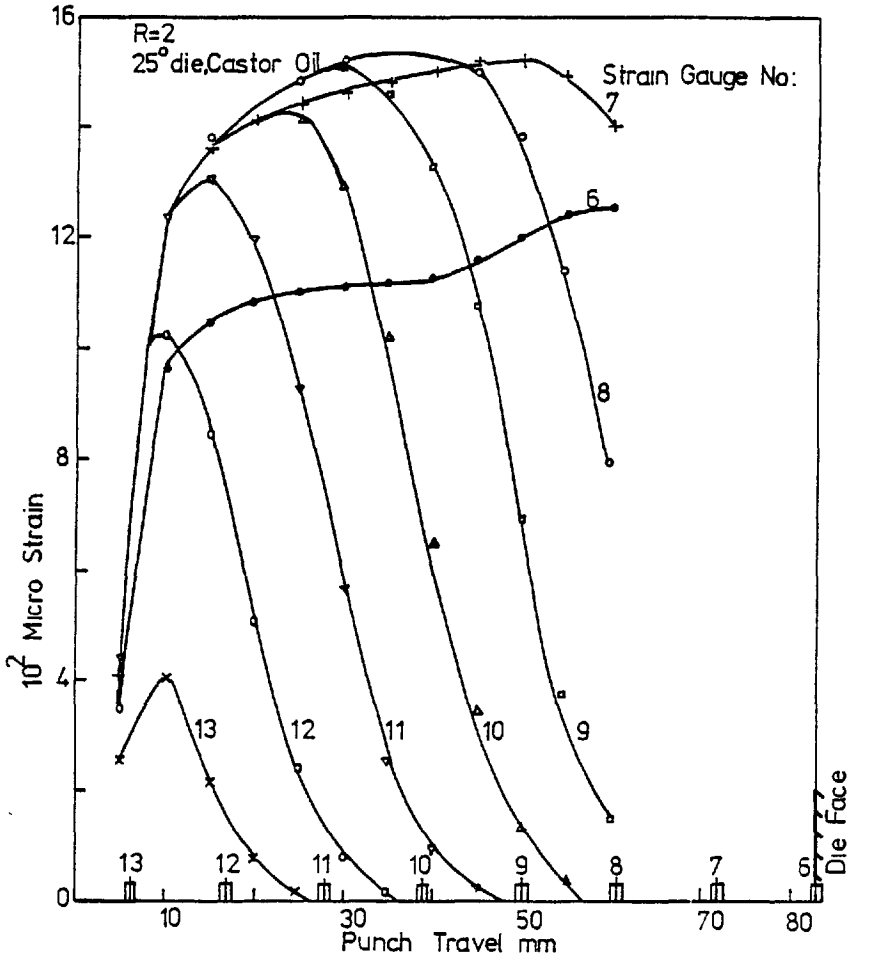


Fig. 6.1.38 Hoop and axial strain distributions.

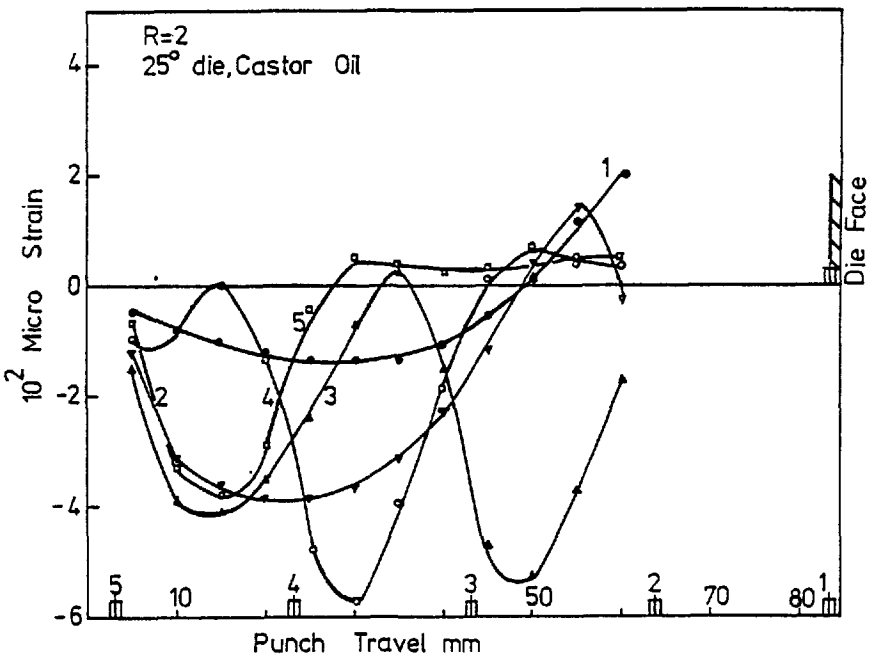
clearly indicating the effect of lubrication in minimising pressure build-up with increasing billet length. While the peak strain (thus bore pressure) drops significantly with punch travel in dry forward extrusion through a conical die with semi-angle of 51^{o} (Fig. 6.1.33), the peak is still near the billet/pressure pad interface, consistent with the effect of friction. It is interesting to note that the strains in dry forward extrusion through a conical die with semi-angle of 35^{o} stay much higher than in lubricated forward extrusion through a die with semi-angle of 76^{o} (Fig. 6.1.30 and Fig. 6.1.35), indicating a significant effect of lubrication conditions on bore pressures in this particular case.

The hoop strains illustrated in Fig. 6.1.39 and Fig. 6.1.40 on the outside diameter of the container for lubricated forward extrusion of aluminium at the extrusion ratio of 2, for die semi-angle of 25^{o} are qualitatively similar to those of dry and lubricated forward extrusion of lead, with the hoop strains at a particular strain gauge falling to zero as the pressure pad passes it.

With punch travel strains (Figs 6.1.30 to 6.1.40) near the die face remain constant (gauges No. 7 and 8) which shows that pressures in this region are independent of billet length but not of lubrication conditions. After about 60 mm punch travel when strains recorded by gauges No. 9 to 13 are much reduced, in dry forward extrusion largest strains were recorded by gauges No. 8 and 7, while in lubricated forward extrusion

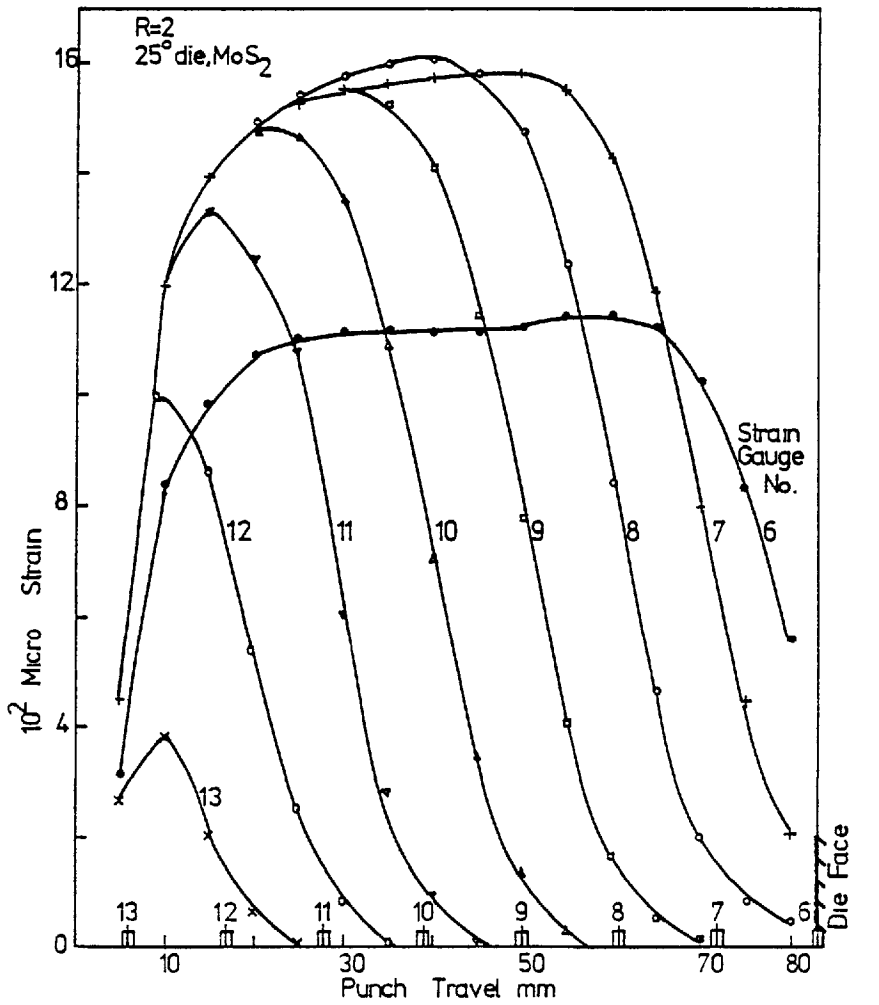


HOOP STRAIN DISTRIBUTION IN THE FORWARD EXTRUSION OF ALUMINIUM

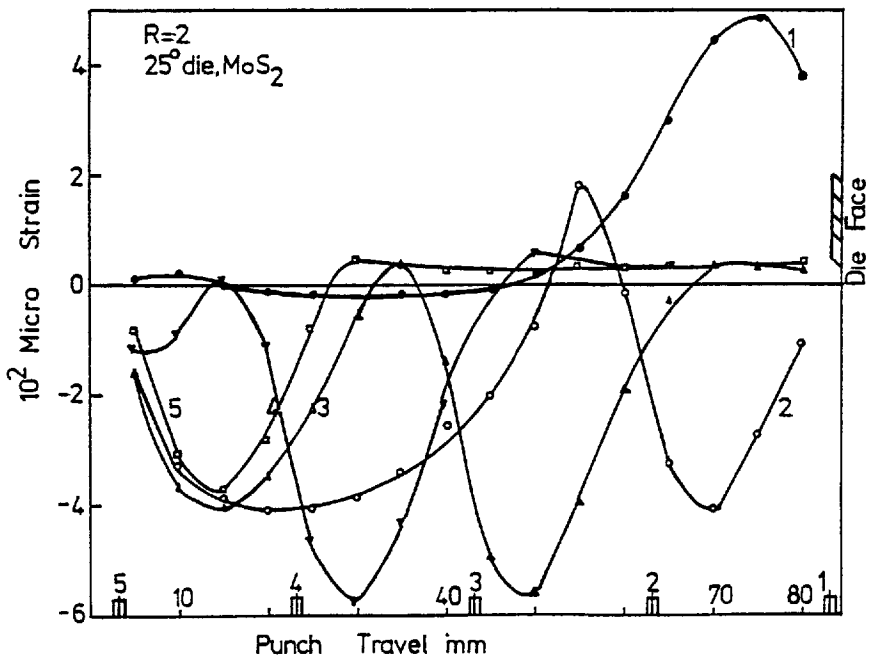


AXIAL STRAIN DISTRIBUTION IN THE FORWARD EXTRUSION OF ALUMINIUM

Fig. 6.1.39 Hoop and axial strain distributions.



HOOP STRAIN DISTRIBUTION IN THE FORWARD EXTRUSION OF ALUMINIUM



AXIAL STRAIN DISTRIBUTION IN THE FORWARD EXTRUSION OF ALUMINIUM

Fig. 6.1.40 Hoop and axial strain distributions.

the largest strain was recorded by gauges 6 and 7. As would be expected, strains recorded by a particular strain gauge drop steeply as the billet/pressure pad interface passes that gauge, in some cases to negative values indicating stress cycles between extremes of tension and compression. The range of hoop strains in dry forward extrusion is much smaller near the die face than away from the die, while in lubricated forward extrusion strains close to the die face are larger, so that the critical conditions affecting container life could be expected at different cross-sections according to extrusion conditions.

The axial strain distributions in forward extrusion of lead and aluminium at the extrusion ratios of 4, 9, 16 and 2, for die semi-angles of 35^{o}, 76^{o}, 45^{o}, 51^{o} and 25^{o} are shown in Figs. 6.1.30 to 6.1.40. The axial strains (gauge No. 3) as seen in Fig. 6.1.30 rise to a maximum and then begins to decrease as extrusion becomes steady. The decrease continues as the punch travels nearer the gauge position. The strain value reaches a maximum value (negative) and then starts increasing again as the punch passes. This increase reaches a maximum again, and again decreases gradually to zero. This almost forms one and half cycles of a sine curve. The explanation of this strain variation is that the axial strain is produced by both shear and normal stress (wall pressure) in the container bore, which causes bulging out of the container and thus tensile strains on the container surface, and the axial frictional force

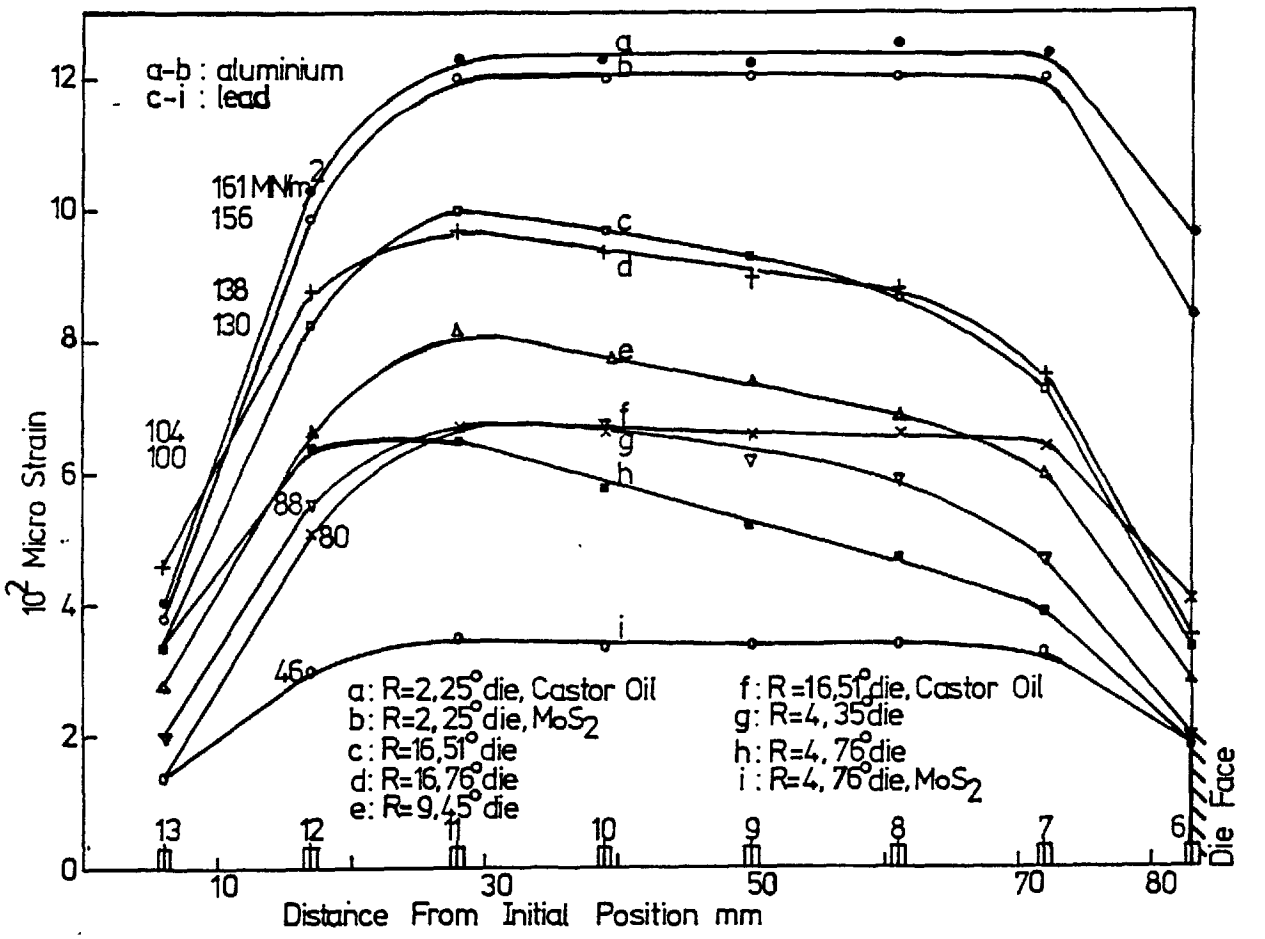


Fig. 6.1.41 Hoop strains on the container wall in the forward extrusion (After 10 mm punch travel).

on the container, which causes compression of the container and thus compressive strains on the container surface. As the punch approaches a position of an axial gauge the compressive strain increases. When the punch passes the position, the compressive effect is relaxed and the effects of the normal wall pressure increase. These bulging out effects decrease gradually as the punch moves far away from the strain gauge position.

Fig. 6.1.41 shows the hoop strains in both dry and lubricated forward extrusion of lead at various extrusion ratios and die semi-angles and lubricated rod extrusion of aluminium at the extrusion ratio of 2, for die semi-angle of 25^{o}, with the pressure pad at 10 mm from its initial position (after 10 mm travel of the punch). This figure indicates that the distribution of hoop strains are qualitatively similar for the dry and lubricated extrusion of aluminium and lead.

6.2 Experimental results of backward extrusion {113}

In backward extrusion, the load on the punch (Figs 6.2.1 to 6.2.3) is higher than on the pressure pad throughout the process. But for the friction at the container/extruded can interface, the difference between the forces at the two ends of the unextruded billet would be negligible. The fact that the frictional force is considerable relative to the total extrusion load indicates that it should be feasible to design clamps of reasonable lengths for continuous extrusion, which agrees with earlier experiments {114} and with the findings of Alexander and Said {11}.

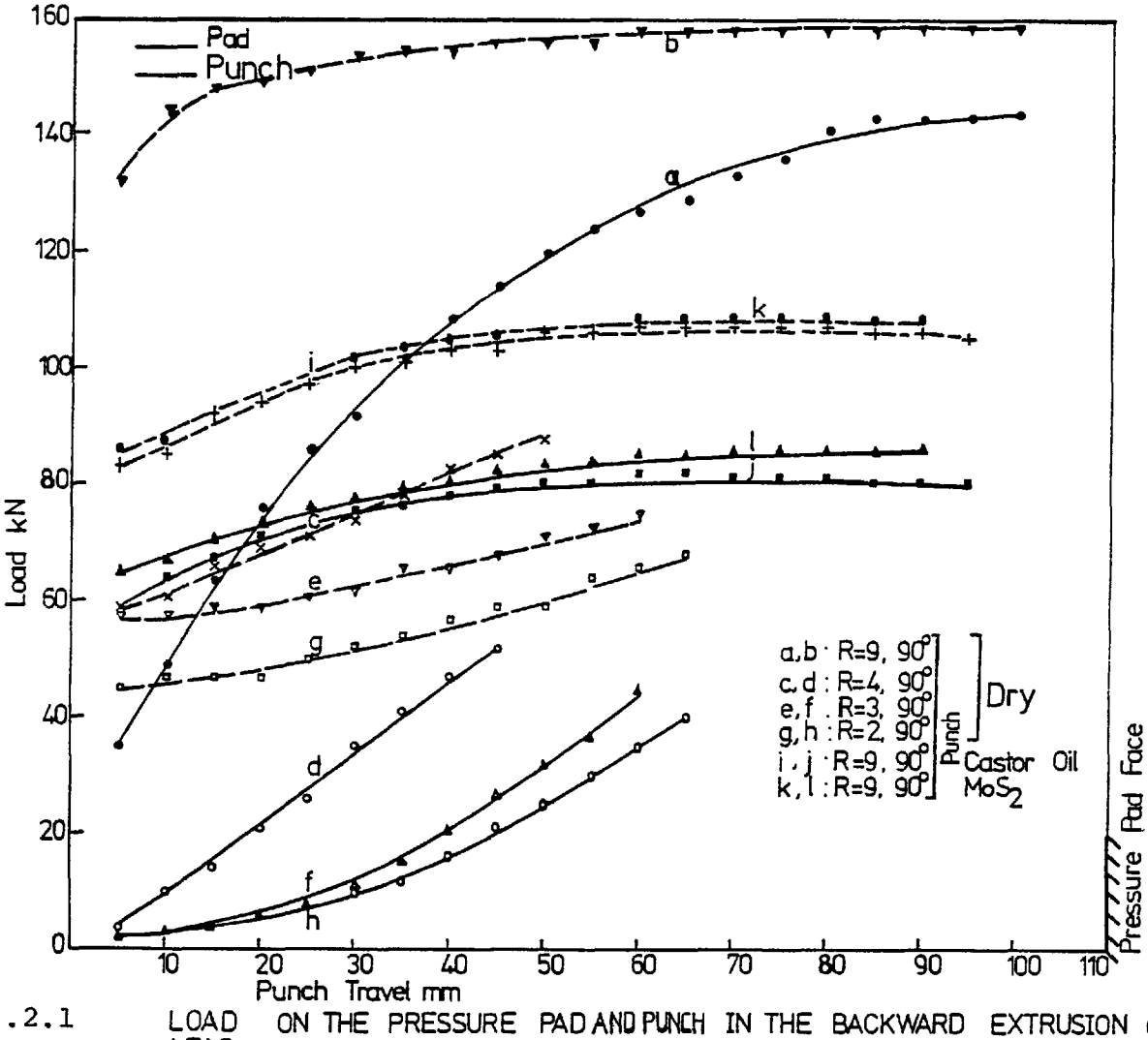


Fig. 6.2.1 LOAD ON THE PRESSURE PAD AND PUNCH IN THE BACKWARD EXTRUSION OF LEAD.

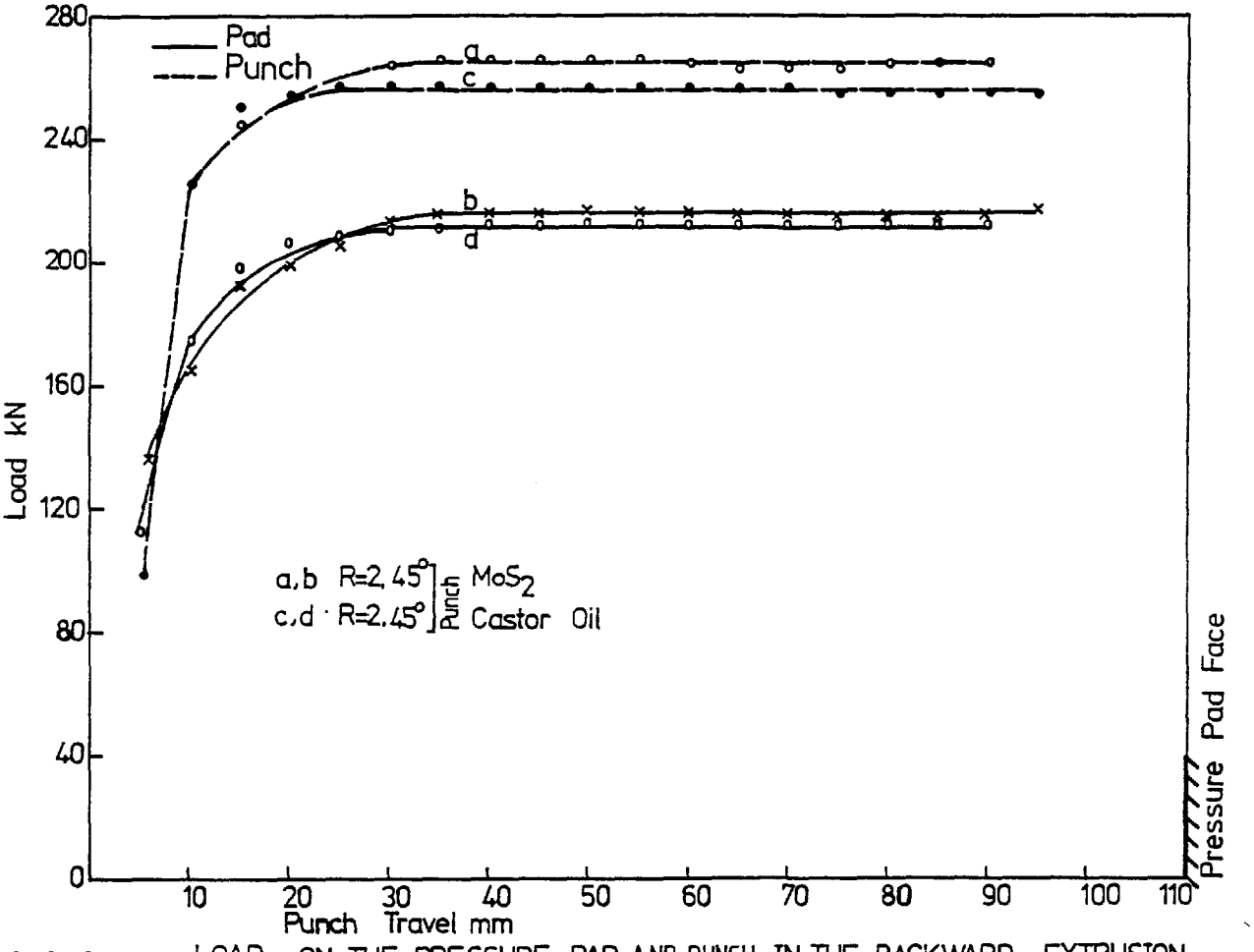


Fig. 6.2.2 LOAD ON THE PRESSURE PAD AND PUNCH IN THE BACKWARD EXTRUSION OF ALUMINIUM.

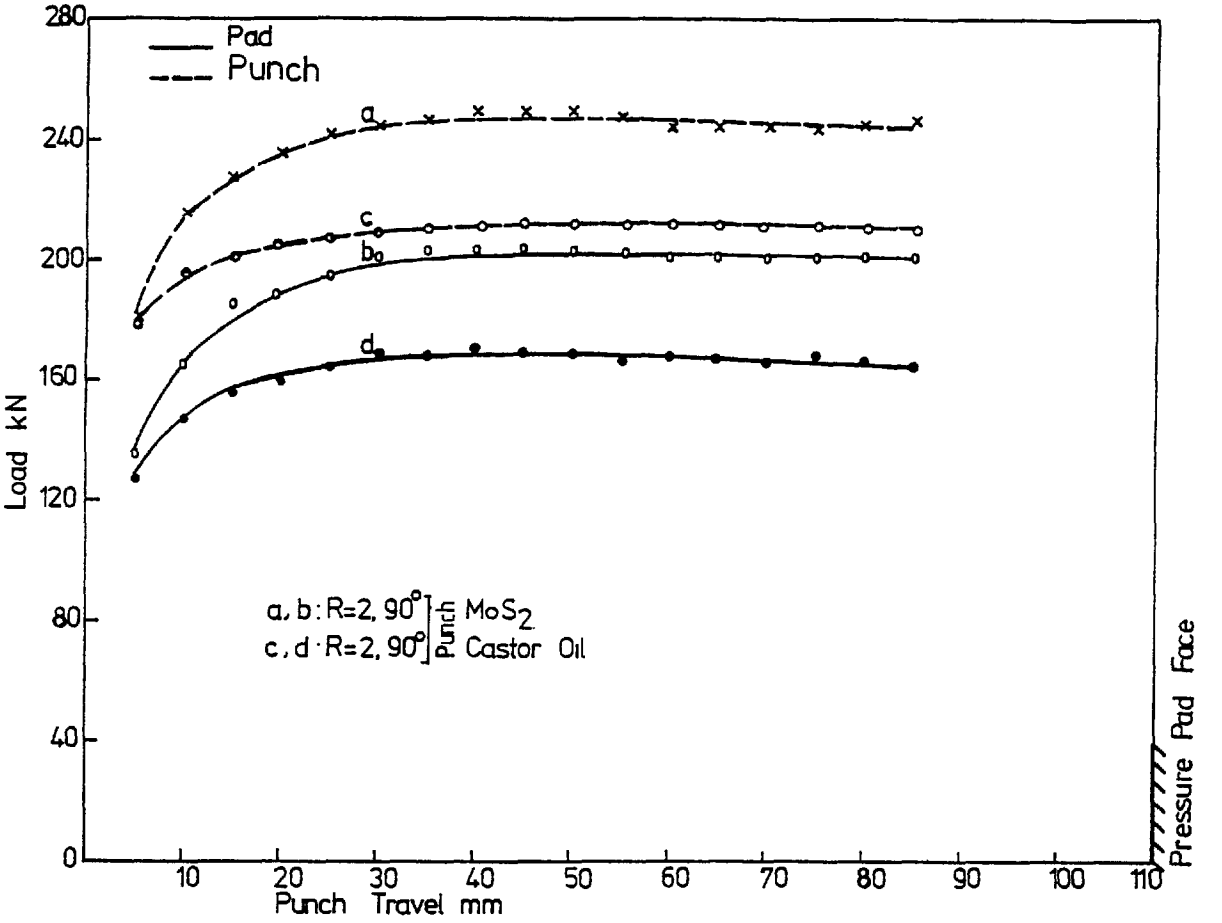


Fig. 6.2.3 LOAD ON THE PRESSURE PAD AND PUNCH IN THE BACKWARD EXTRUSION OF ALUMINIUM.

Fig. 6.2.2 and Fig. 6.2.3 indicate that the load on the pressure pad remains more or less constant for lubricated can extrusion of aluminium at the extrusion ratio of 2 and punch insert semi-angles of 90^{o} and 45^{o}.

Tensile hoop strains and axial strain variations in can extrusion as seen in Figs 6.2.4 to 6.2.13 are qualitatively similar to those for rod extrusion, with the hoop strains at a particular strain gauge falling to zero as the punch passes it.

The hoop strain distributions as seen in Figs 6.2.10 to 6.2.13 were recorded along the full container length even after the billet was fully extruded, except for a short discard. This is a clear indication that the outside diameter of the extruded can is larger than the bore diameter of the depressurised container, a fact well know in practice. The resultant pressure on the container wall produces friction, which is in turn responsible for the often significant forces needed for the ejection of the extruded can. The hoop strains also indicate the presence of pressure between the container and the extruded can, which could form the basis of predicting the forces necessary for ejecting the extruded can from the container, an aspect of some practical significance.

When the billet end is approached by the punch in the backward extrusion of cans, frictional forces increase as the material flows radially outwards between the punch face and pressure pad. This increased frictional restraint must

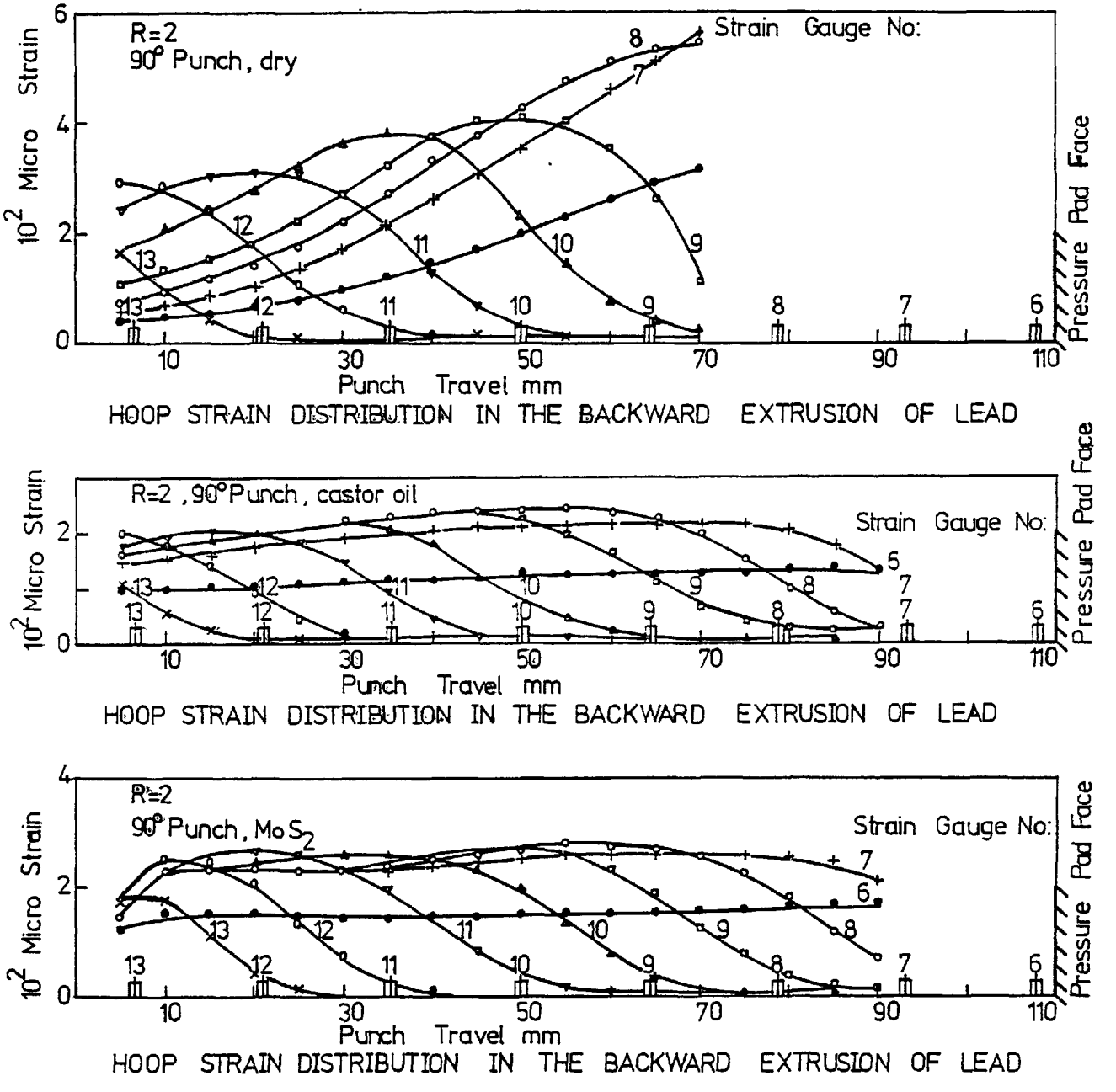


Fig. 6.2.4 Hoop strain distributions.

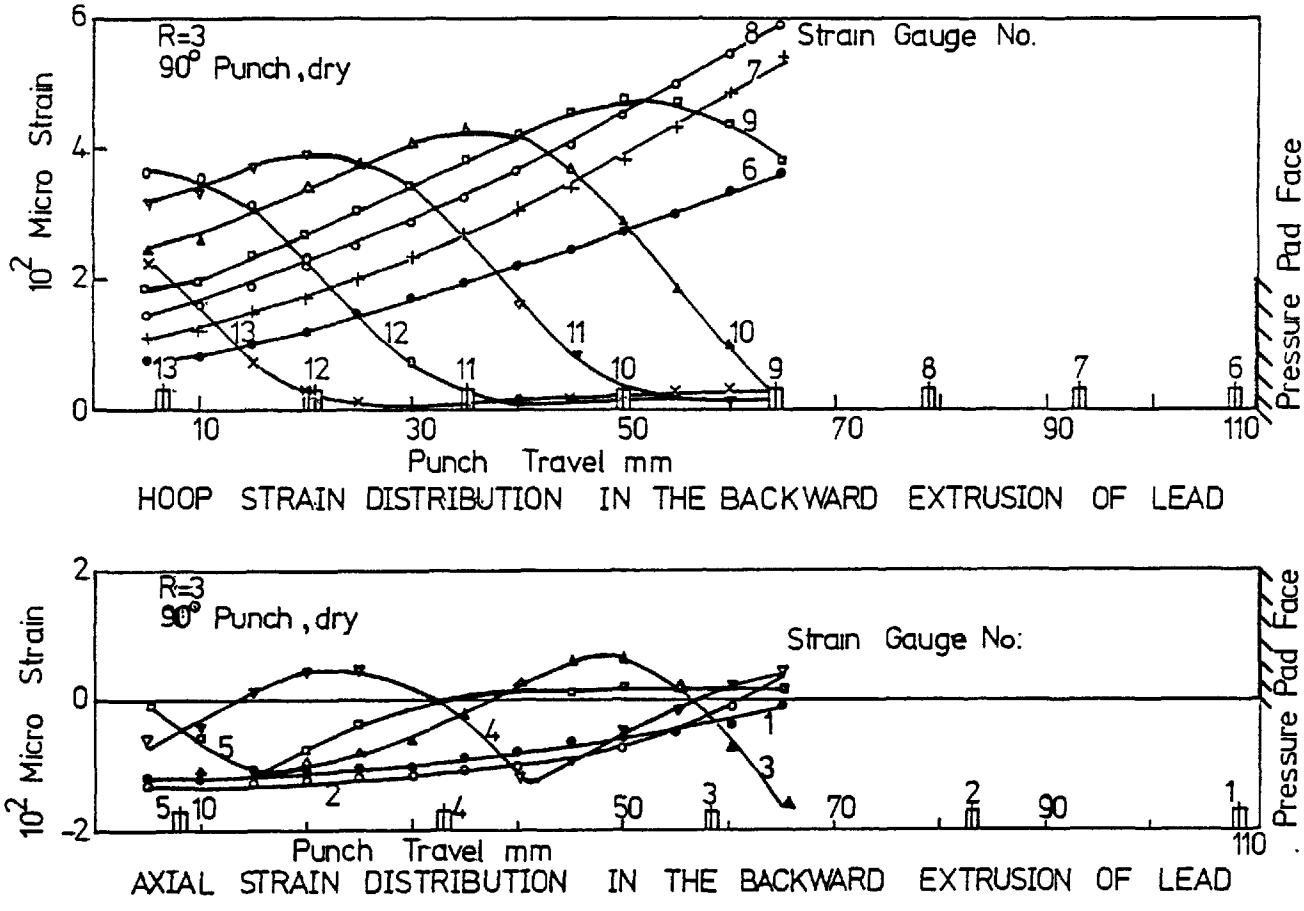


Fig. 6.2.5 Hoop and axial strain distributions.

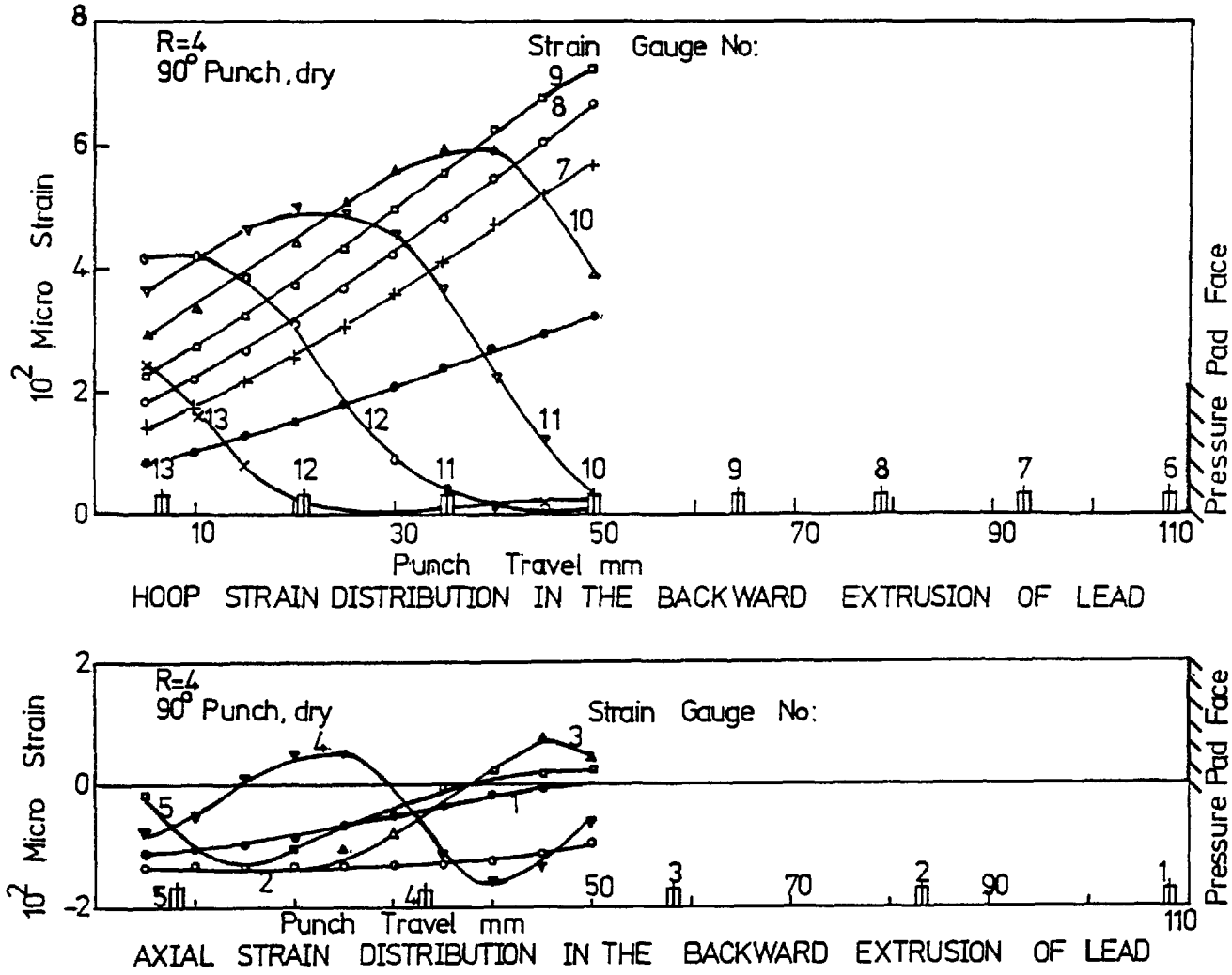


Fig. 6.2.6 Hoop and axial strain distributions.

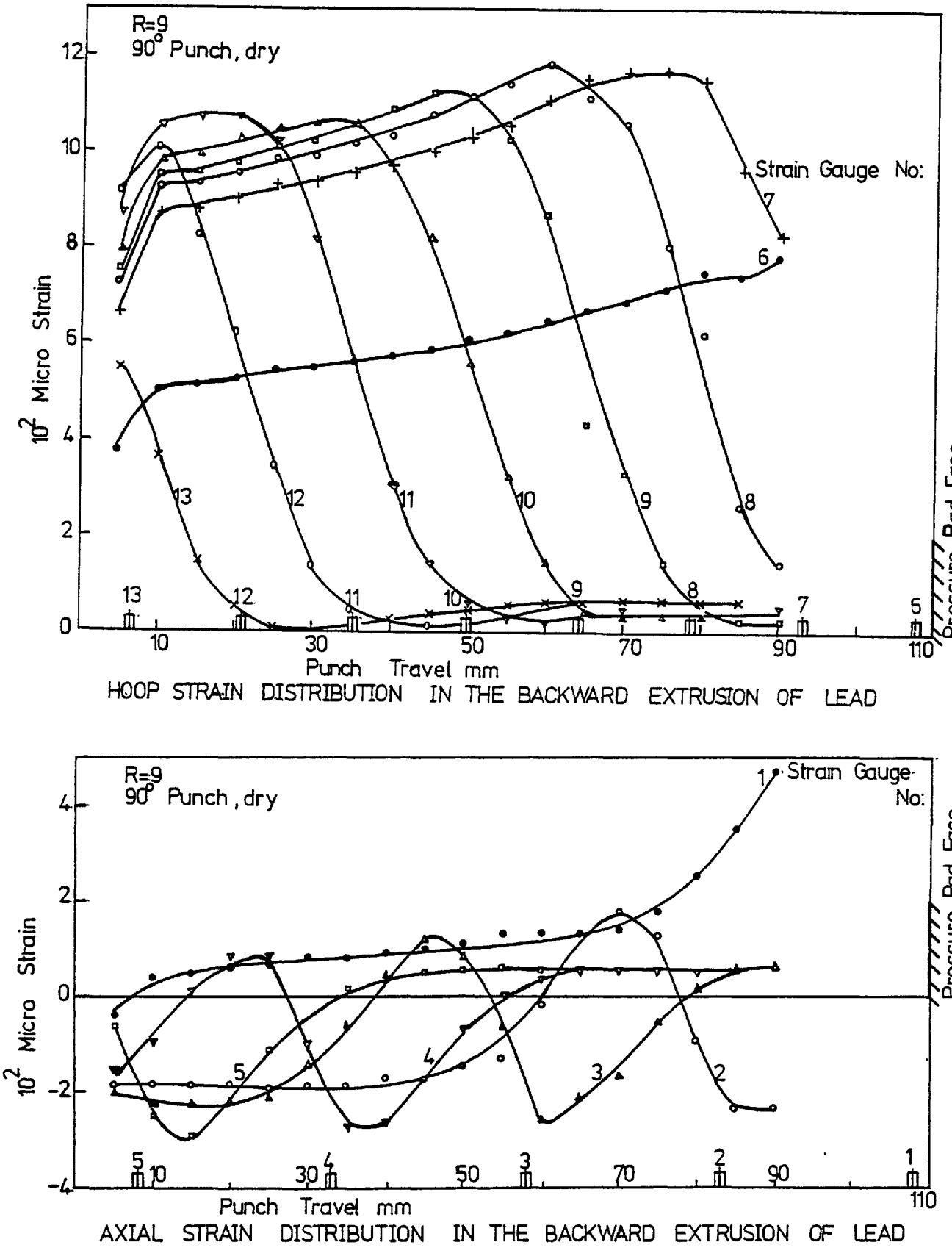


Fig. 6.2.7 Hoop and axial strain distributions.

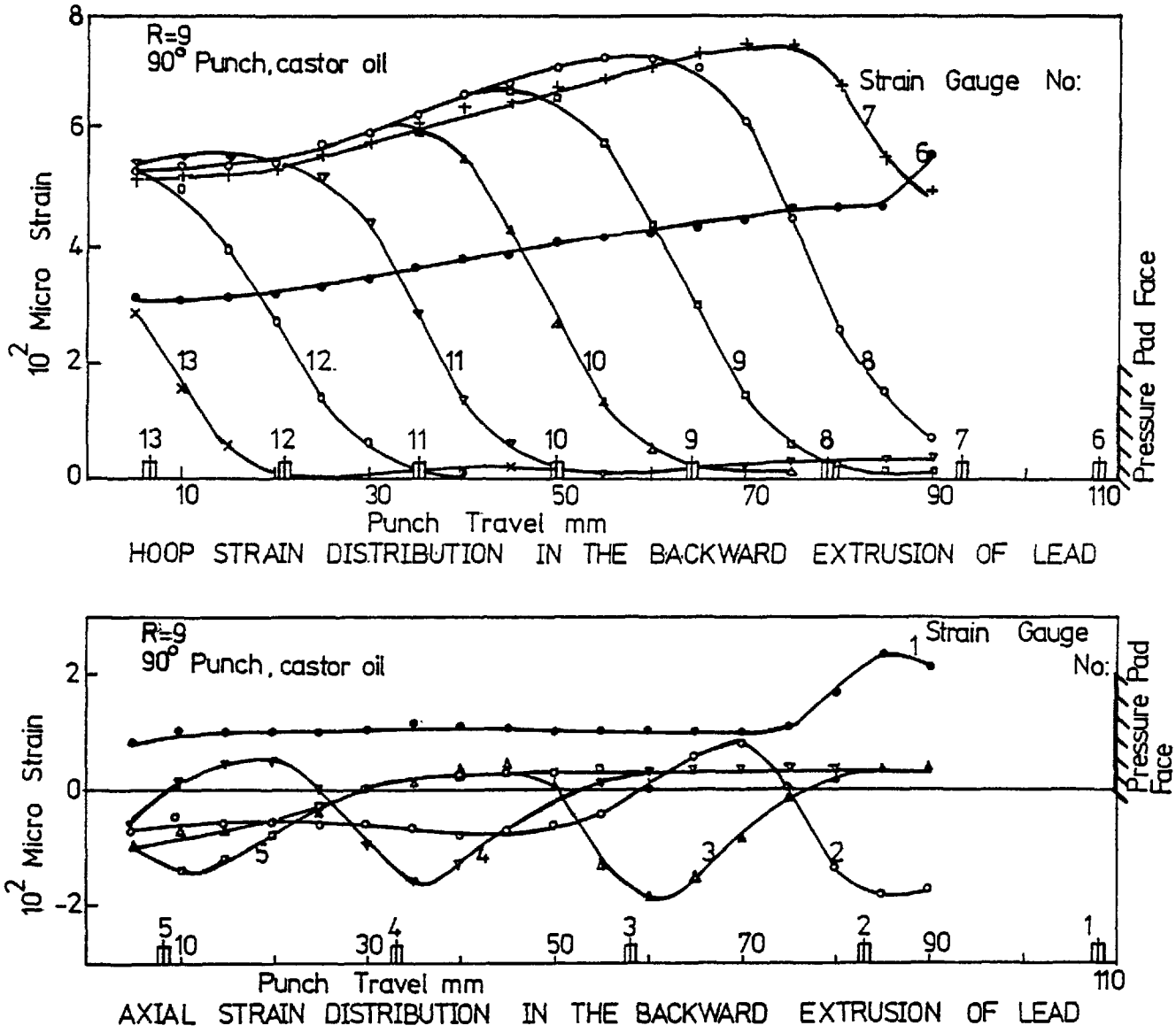


Fig. 6.2.8 Hoop and axial strain distributions.

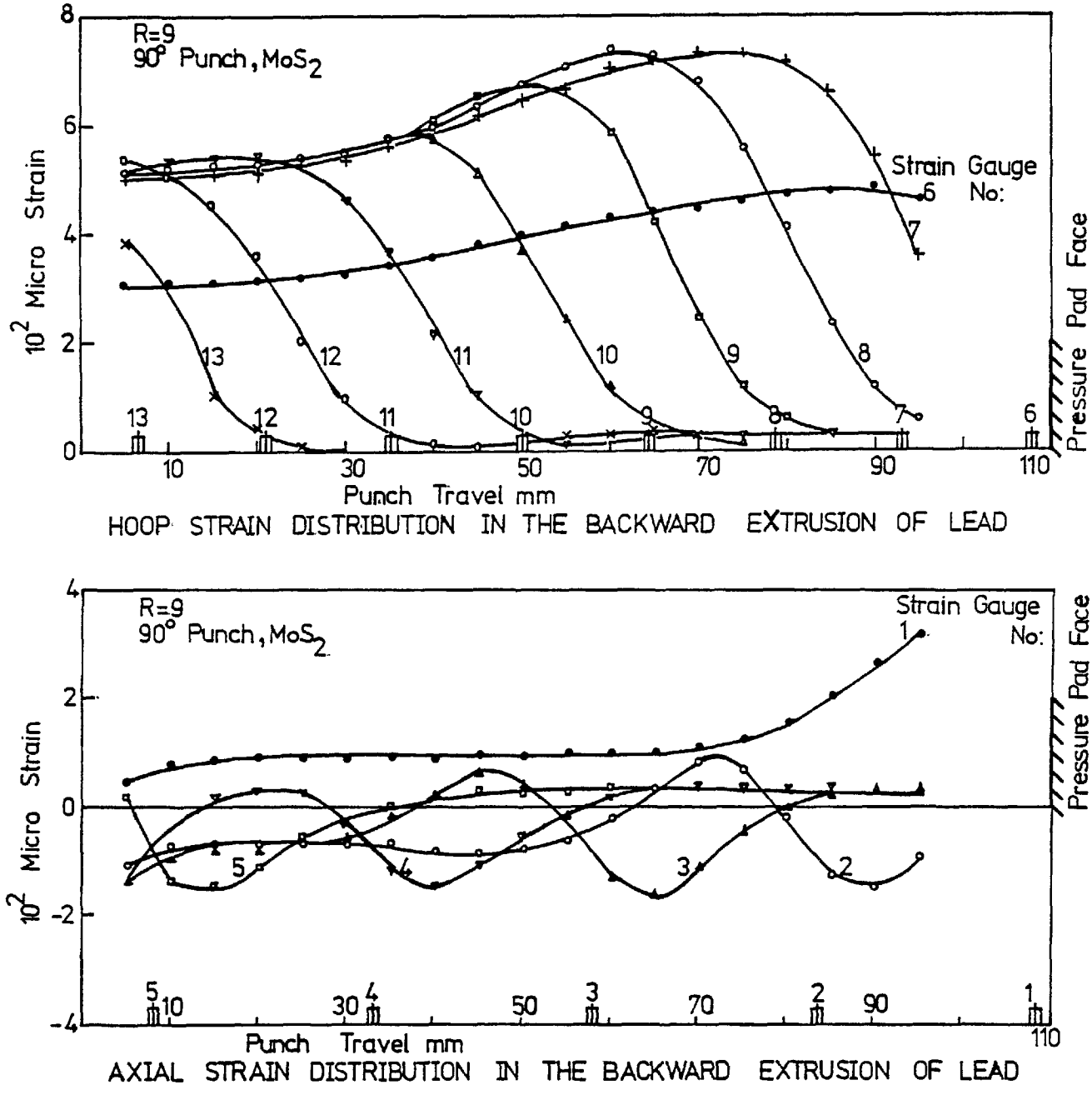
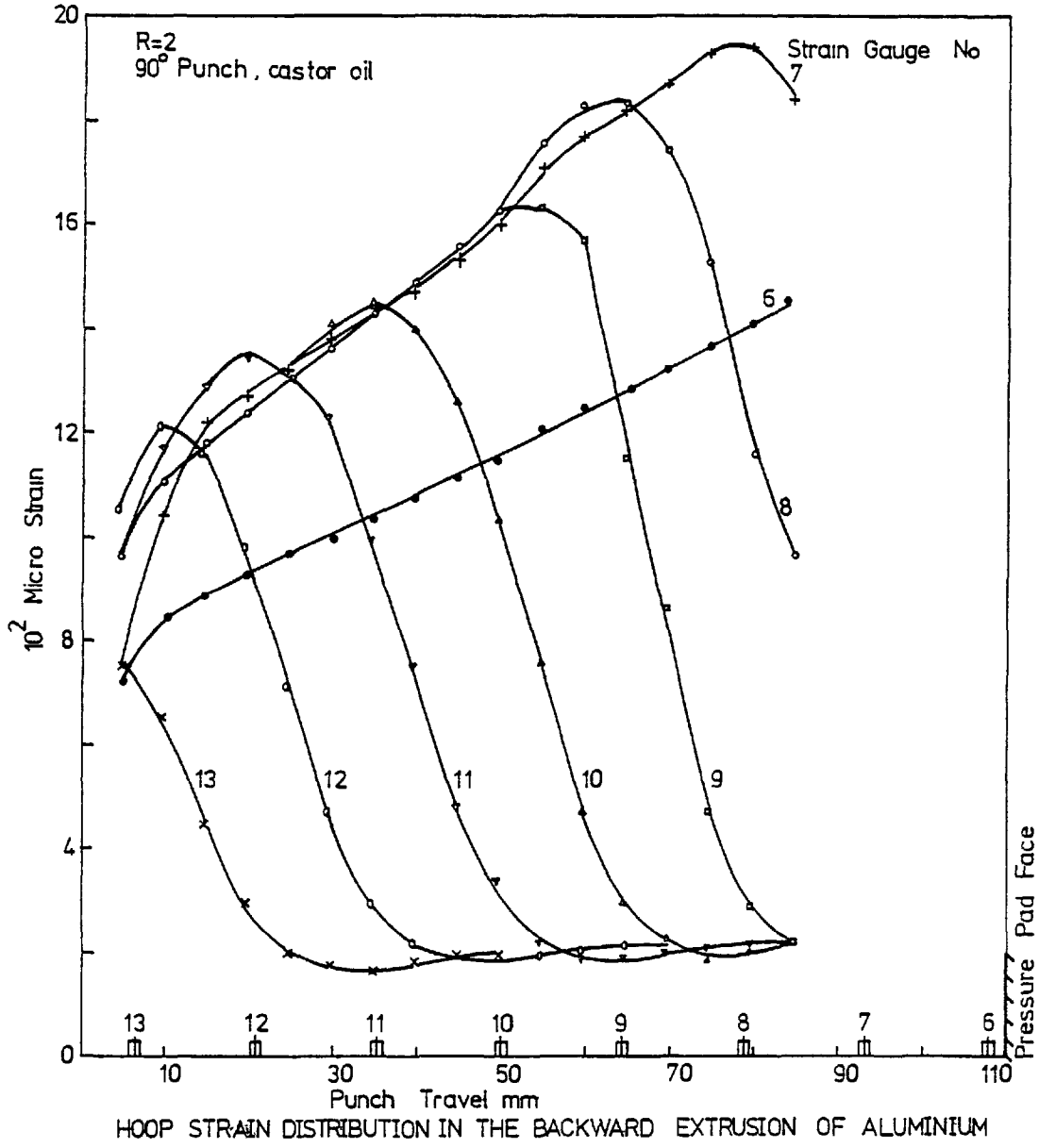
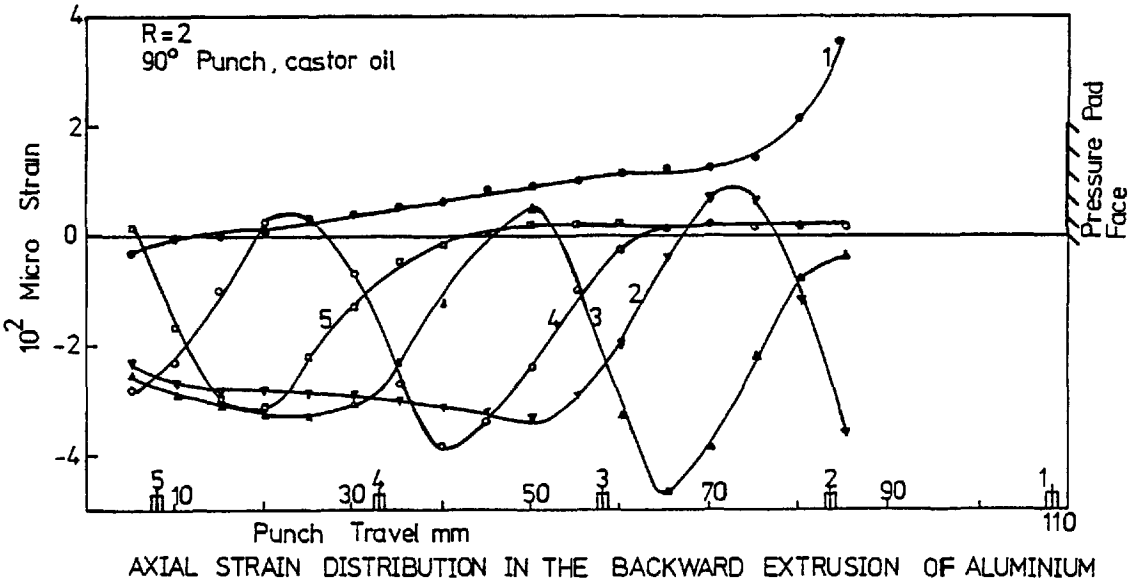


Fig. 6.2.9 Hoop and axial strain distributions.



HOOP STRAIN DISTRIBUTION IN THE BACKWARD EXTRUSION OF ALUMINIUM



AXIAL STRAIN DISTRIBUTION IN THE BACKWARD EXTRUSION OF ALUMINIUM

Fig. 6.2.10 Hoop and axial strain distributions.

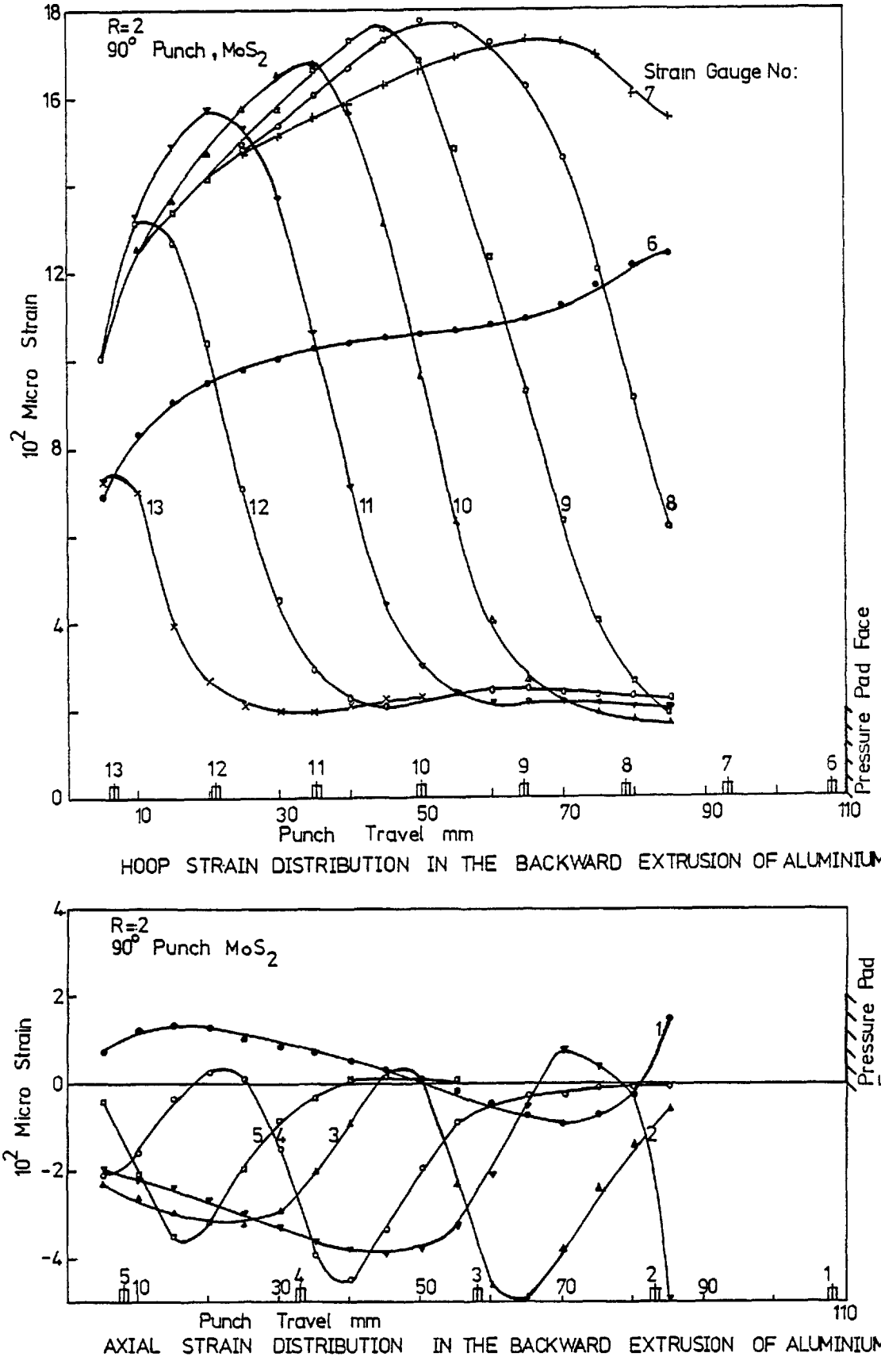


Fig. 6.2.11 Hoop and axial strain distributions.

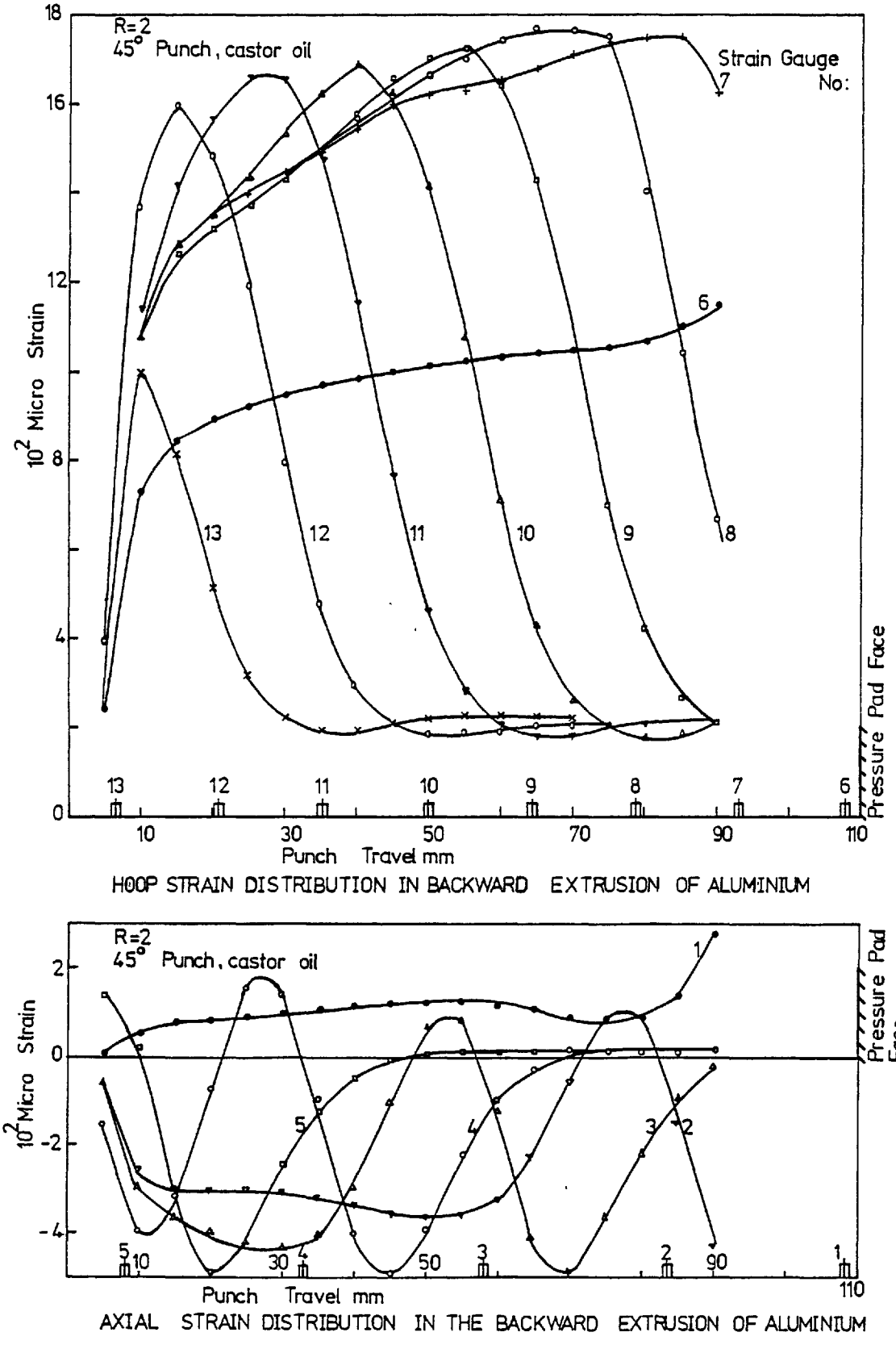
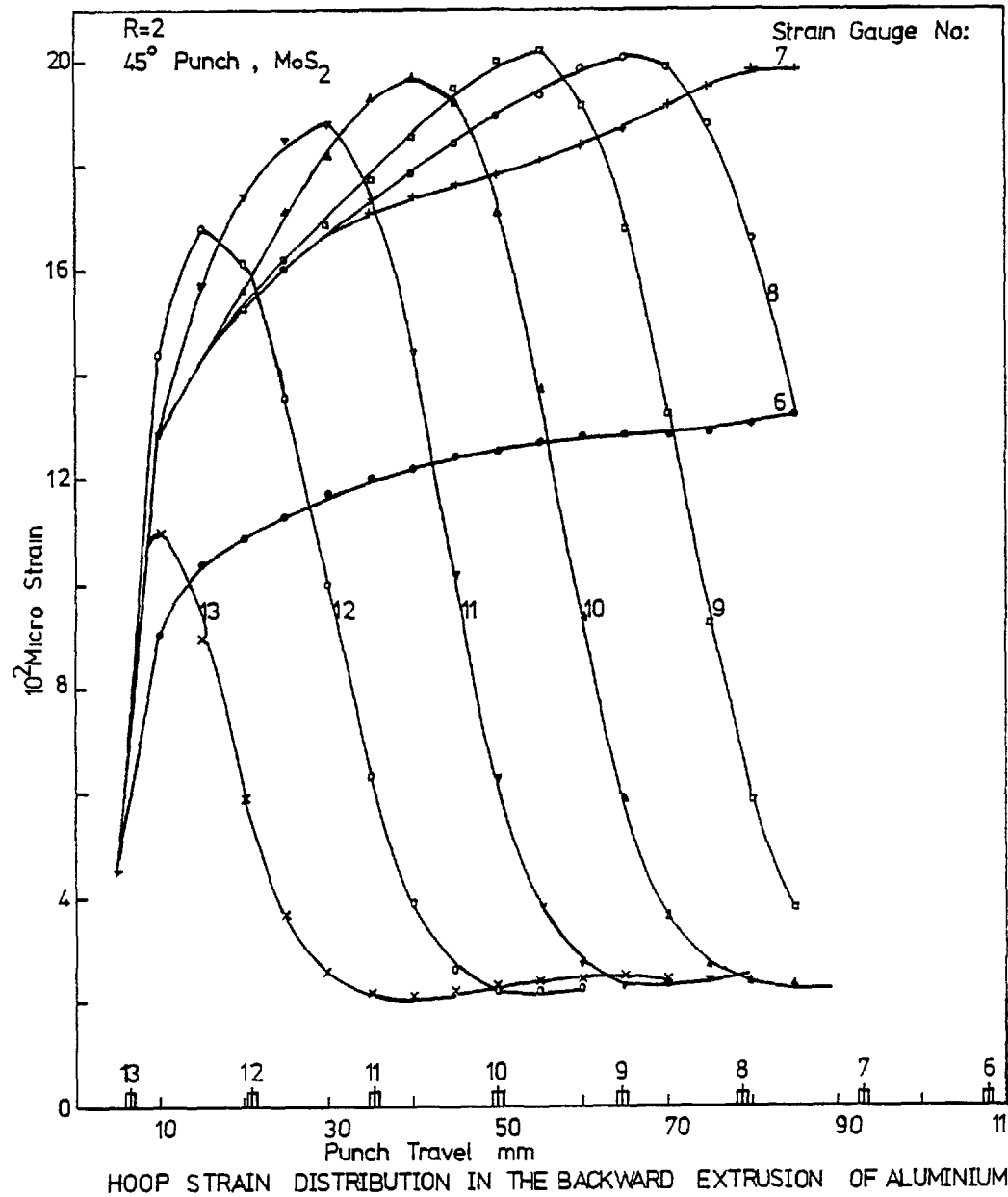
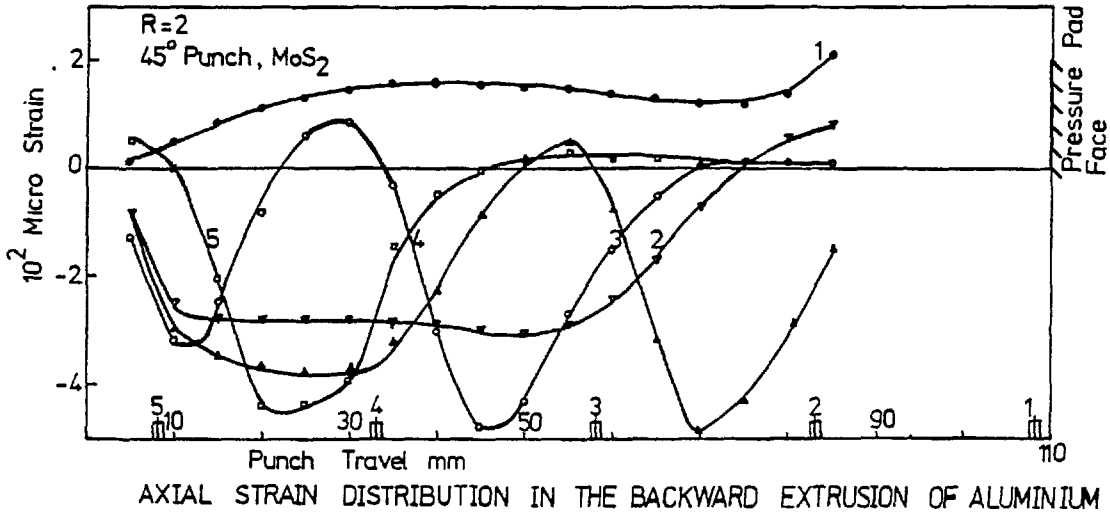


Fig. 6.2.12 Hoop and axial strain distributions.



HOOP STRAIN DISTRIBUTION IN THE BACKWARD EXTRUSION OF ALUMINIUM



AXIAL STRAIN DISTRIBUTION IN THE BACKWARD EXTRUSION OF ALUMINIUM

Fig. 6.2.13 Hoop and axial strain distributions.

lead to higher local bore pressures, particularly significant in unlubricated extrusion. This is clearly indicated by the steeply increasing hoop strains shown by the gauges adjacent to to the discard, Fig. 6.2.4 to 6.2.7.

The hoop strains after 10 mm travel of the punch at various extrusion ratios and lubrication conditions are given in Fig. 6.2.14. The trend is similar to those for forward extrusion, which indicates that the bore pressure distribution must also be similar in the two cases in the steady state.

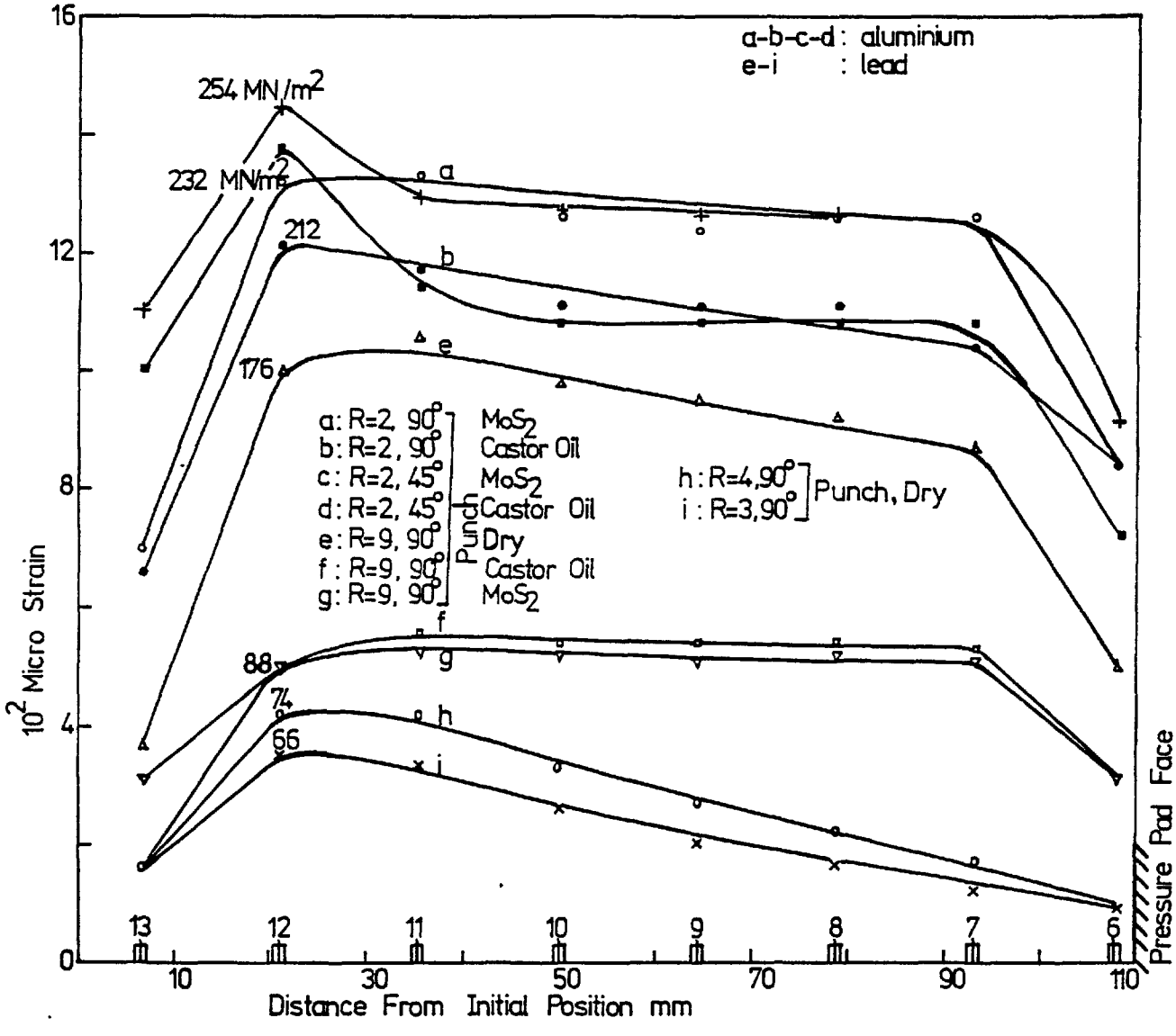


Fig. 6.2.14 Hoop strains on the container wall in backward extrusion (After 10 mm punch travel).

7. Conclusions

7.1 Forward Extrusion

As stated in Chapter 1, the basic aim of this work was to define a method by which the pressure distribution could be evaluated for use in the design of containers for metal-working processes, with particular reference to conventional rod extrusion. To be successful, the method should be able to distinguish between small changes of frictional conditions. The various measurement which have been taken during the experiments will now be considered and their sensitivity to changes of friction discussed.

The metals were assumed to obey the Von-Mises yield criterion, an empirical equation (2.45) for the strain-hardening characteristics and Prandtl-Reuss stress-strain relationship. A kinematically admissible velocity field for the upper-bound solution was assumed to characterise the flow of metals through the dies. A semi-empirical method was also considered to analyse the flow of pure aluminium through a conical die.

As the metal-working process is far too complex to be solved in closed analytical form, numerical solutions have been employed to determine the velocity and stress fields. Numerical methods that are in common use require much effort and computational facilities and often the effort needed is out of proportion to the advantages that maybe gained by applying these sophisticated methods. It is therefore necessary to develop relatively simple,

less demanding and sufficiently accurate methods. The chosen method of weighted residuals has proved easy to handle and suitable to solve the Prandtl-Reuss equations encountered in this work. It is also much less demanding in terms of computation and consequently less expensive in comparison with the method of finite elements. About four seconds of processing time (on CDC 6400) was required to obtain the stress distribution from the assumed velocity field described in section 5.3, whereas the central processing time required to obtain the same information by the method of finite elements would probably be several orders of magnitude higher. Furthermore, whenever a solution to a system of partial differential equations (or tensor differential equations) approximated by a polynomial as in the method of weighted residuals to within an acceptable level of accuracy, it is usually necessary to use high order expansions. This condition could lead to high rounding errors and excessive computing time. On account of simplicity of the method of weighted residuals this complex problem could be formulated and handled with relative ease.

Analysis of Steck's work {75-76}, and more recently Helman {115} and Ravindranath {116}, the only other known application of the method of weighted residuals to metal working problems, reveals that it is necessary to assume a velocity field to obtain reliable solutions. The assumed velocity field based on the upper-bound solution and constant friction factor throughout the deformation describes the process adequately.

Theoretical and experimental results of rod extrusion presented for different conditions provide adequate information regarding the effects of extrusion speed, extrusion ratios and lubrication conditions on the pressure distribution in the extrusion container. Results may be summarised as follows: The semi-empirical method can be used to provide a more sensitive indication of changes of frictional conditions than has previously been possible.

The flow patterns found by experiment and used for the semi-empirical method (lubricated rod extrusion of aluminium at the extrusion ratio of 2 for die semi-angle of 25^{o}) show that the flow is not radial towards the apex of the conical surface of the die, as the flow lines are not straight, even in the region removed from the deformation boundaries.

Of all the parameters considered to judge the quality of different lubricants the velocity, strain rate and strain fields are by far the most sensitive to variations of frictional conditions. The fields obtained from the semi-empirical method (for one particular case as castor oil lubricated rod extrusion of aluminium) and given in section 6.1.1 can be used to assess the dependence of the operative friction on the other conditions of extrusion. Interface friction also causes non-uniform deformation resulting in increase in stress and variation of stresses within the continuum.

As stated in section 6.1.1 the change of stress across any K section (defined in Fig. 5.1.2) is too large, resulting

in unreliable stress components near the surface.

Velocity and stress fields have been obtained from the assumed velocity field for the castor oil lubricated rod extrusion of aluminium at the extrusion ratio of 2, for die semi-angle of 25^{o}, with the constant-friction of 0.12 and for the dry forward extrusion of lead at the extrusion ratios of 3 and 4, for die semi-angles of 30^{o} and 35^{o} respectively, with the constant friction factor of 0.75. These results indicated that the distributions of velocity and stress fields are uniform throughout the continuum.

Theoretically obtained hoop strains (from the finite element analysis with the semi-empirical method and the assumed velocity field for commerically pure lead and aluminium) in forward extrusion container were in good agreement with the experimental results, i.e. the hoop strains measured along the length of the container during the rod extrusions of aluminium and lead had a magnitude of about 5% smaller than that obtained, from the finite element analysis of the forward extrusion at the same extrusion condition.

The axial strain (produced by the shear stress and the normal wall pressure on the container bore) obtained from the finite element analysis had a magnitude of about 20% and 30% smaller than that measured along the length of container during extrusion.

The apparatus developed and used in the experiments for measuring the strains on the container surface, functioned

satisfactorily and proved suitable for the experimental work. The experiments for the commericially pure aluminium specimens with the extrusion ratio of 2 and die semi-angle of 25° and pure lead specimens with the extrusion ratios of 2, 3, 4, 9 and 16 and the semi-die angles of 25°, 30°, 35°, 45°, 51° respectively were carried out mainly to check the computed results and to verify the suitability of the assumed velocity field and the semi-empirical method (used for one particular case of lubricated rod extrusion of aluminium).

The load on the pressure pad increases with increase in extrusion ratio at a decreasing rate. In the dry rod extrusion, the container/billet friction result in considerably higher initial loads on the pressure pad than on the die. This difference becomes smaller depending on the decrease of the unextruded billet length.

The harder material (e.g. aluminium compared with lead) needs more applied pressure pad load in forward extrusion of aluminium to build up similar strains and pressures in the container walls.

Hoop strain distributions in forward extrusion on the outside diameter of the container obtained gave a clear indication of the stress conditions in the container wall. In the lubricated rod extrusion, results showed that the greatest surface strains and thus maximum wall pressures occur next to the die face. The experimental results also indicate that, in the well lubricated forward extrusion of lead, the steady state pressure pad and die loads are identical within the accuracy of the experiments. This

in turn shows low friction and constant pressure distribution along the container wall, so that the theoretically obtained stresses at the die corner could be assumed to represent the predicted container bore stresses. But the same is not true for dry conditions. The theory, which assumes that the bore pressure distribution is constant and equals the value calculated for the die corner, underestimates the axial stresses, which imply that bore pressures away from the die must be higher for dry conditions, as would be expected. The dry conditions also represent larger axial stresses on the container wall due to increased frictional shear stresses, which must have considerable effect on the axial than on the hoop strain readings.

Strains and pressure distributions remain similar for different extrusion ratios though their magnitudes increase with the increase in extrusion ratios.

7.2 Backward extrusion

It is hoped that the theoretical analysis for the forward extrusion container (finite element analysis with the assumed velocity field and the semi-empirical method) will provide basic data for the design of extrusion containers and for the design of clamps in conventional extrusion. Therefore, theoretical analysis of backward extrusion, which in this respect is very similar to forward extrusion (the experimental results for both processes presented in Chapter 6 are very much alike) has not been carried out.

Experiments were performed for the commercially pure aluminium specimens with the extrusion ratio of 2 and punch insert

semi-angle of 90^{o} and 45^{o} and for pure lead specimens with the extrusion ratios of 2, 3, 4, and 9 and punch insert semi-angle of 90^{o} respectively.

The hoop strains and the corresponding pressure distributions could be experimentally evaluated together with the coefficient of friction at the container/metal interface. In can extrusion, hoop strains indicate the presence of pressures between the container and the extruded can, which could form the basis of predicting the forces necessary for ejecting the extruded can from the container, an aspect of some practical significance. Wall hoop strains were smaller ahead of the moving tool than nearer to it, once more indicating the presence of significant frictional forces.

Finally, it would be interesting to note that, since pressure is either constant in the bore or increases monotonously towards the pressure pad (in forward extrusion) and the punch insert (in backward extrusion) due to friction, so that there are no "peaks" or sudden drops, the methods used in the design of pressure vessels under high bore pressure, as recommended by Crossland {2}, {3}, {4}, Morrison {2} and others, could be used with confidence.

The suggestions for future work are as follows:

It is thought that this work will lay the basis for any further work directed at the application and development of this method.

New methods of smoothing in the semi-empirical method could be tried in the computer program to see if more accurate values of stresses can be calculated without loosing the characteristics of the flow fields.

It would be interesting to use the proposed kinematically admissible velocity field for evaluating the stress distribution and hence pressure distribution in the backward extrusion container.

The computer programs (for the semi-empirical method and the assumed velocity field) could also be extended to calculate the temperature distribution during extrusion.

Finally, further extrusion experiments could be carried out at higher speed with different lubricants.

REFERENCES

1. HARVEY, D.C., and LENGYEL, B. (1968). Pressure vessels under cyclic loading; test rig and initial results. Advances in Machine Tool Design and Research. Pergamon Press, Oxford.

2. MORRISON, J.L.M., CROSSLAND, B., and PARRY, J.S.C. (1960). Strength of thick cylinders subjected to repeated internal pressure. Proc. Inst. Mech. Engrs., 174, p. 95.

3. AUSTIN, B.A., and CROSSLAND, B. (1965-1966). Law endurance fatigue strength of thick-walled cylinders: development of a testing machine and preliminary results. Proc. Inst. Mech. Engrs., 180, p. 43.

4. CROSSLAND, B. and SKELTON, W.J. (1967). Effect of varying hardness on the fatigue strength of thick-walled cross-bore cylinders of EN25. Proc. Inst. Mech. Engrs., 182, p. 106.

5. AUSTIN, B.A., REINER, A.N. and DAVIDSON, T.E. (1967). Low cycle fatigue strength of thick-walled pressure vessels. Proc. Inst. Mech. Engrs., 182, p. 91.

6. TERAO, M. and YAMASHITA, Y. (1973). Low cycle fatigue strength of thick-walled cylinders. Proc. 2nd Int. Conf. Pressure Vessel Technology, Pt. 2, p. 835.

7. BLASS, J.J., and FINDLEY, W.N. (1967). The influence of the intermediate principal stress on fatigue under triaxial stress. Materials Research and Standards, 7, p. 254.

8. LENGYEL, B. and HARVEY, D.C. (1972). Elastic stresses at seals in plain and necked open-ended cylinders under internal and external pressures. Proc. 12th MTDR Conf., p. 573.

9. KUDO, H. and MATSUBARA, S. (1968). Stress analysis in cylindrical dies of finite length subjected to a band of internal pressure. J. Jap. Soc. for Techn. and Plast.

10. LENGYEL, B. (1968). A semi-continuous hydrostatic extrusion process. Metals and Materials, January 1968.

11. ALEXANDER, J.M. and SAID, M.E. (1975). Design of clamping devices for semi-continuous hydrostatic extrusion. North American Metalworking Research Conference, May 1975.

12. LENGYEL, B. and KAMYAB-TEHRANI, S. (1976). Investigations into continuous extrusion. Proc. 17th MTDR Conference.

13. BOWDEN, E.P. and TABOR, D. (1958). The friction and lubrication of solids. Clarendon Press.

14. SHAW, M.C. (1964). Surface conditions in deformation processes. Proc., 9th Sagamore Army Matr. Res. Conf. 1962. Syracase University Press 1964.

15. LAUTERBACH, R., LIRA , F. and THOMSEN, E.G. (1967). Friction under high normal pressures. Wear, 10, p. 469.

16. KASUGA, Y. and YAMAGUCHI, K. (1968). Friction and, lubrication in the deformation processing of metals. Bulletin of J.S.M.E. 11, No. 44, p. 344.

17. MALE, A.T. and COCKROFT, M.G. (1964-65). A method for the determination of the coefficient of friction of metals under conditions of bulk plastic deformation. J. Inst. Metals, 93, p. 38.

18. KUNOGI, M.J. (1956). Sci. Research Inst. (Tokyo), 50, p. 215.

19. SCHROEDER, W. and WEBSTER, D.A. (1949). Press-forging thin sections: effect of friction, area and thickness on pressures required. ASME J. Appl. Mechs., p. 289.

20. ALEXANDER, J.M. (1955). The effects of Coulomb friction in the plane strain compression of plastic-rigid material. J. Mech. Phys. Solids, 3, p. 233.

21. TAKAHASHI, H. and ALEXANDER, J.M. (1962). Friction in the plane-strain compression test. J. Metals, 90, p. 72.

22. EVANS, W. and AVITZUR, B. (1968). Measurement of friction in drawing, extrusion and rolling. Trans. ASME, J. Lub. Tech., p. 72.

23. AVITZUR, B. (1964). Analysis of wire drawing and extrusion through dies of large cone angle. Trans. ASME, J. Engng. Ind., 86, p. 305.

24. SIEBEL, E. and LUEG, W. (1933). Untersuchungen über die Spannungsverteilung im Walzspalt. Mitteilungen aus dem Kaiser Wilhelm Institut für Eisenforschung, 15, p. 1.

25. FRISCH, J. and THOMSEN, E.G. (1954). An experimental study of metal extrusions at various strain rates. Trans. ASME, 76, p. 599.

26. FRISCH, J. (1955). Contribution to the knowledge of pressure measurements during metal deformation. Trans. ASME, 77, p. 509.

27. VAN ROOYEN, G.T. and BACKOFEN, W.A. (1957). Friction in cold rolling. J. Iron and Steel Inst., 186, p. 235.

28. EL-BEHERY, A.M., LAMBLE, J.H. and JOHNSON, W. (1963). The measurement of container wall pressure and friction coefficient in axi-symmetric extrusion. 4th Conference M.T.D.R. Manchester, p. 319.

29. JOHNSON, W. and COLLINS, A.G. (1957). The plane strain extrusion of lead and aluminium through wedge-shaped dies. B.I.S.R.A. Report, MW/E/54/54.

30. MAJORS, H.R.J. (1955). Studies in cold drawing, determination of the coefficient of friction. Trans. ASME, 78, p. 79.

31. PEARSALL, G.W. and BACKOFEN, W.A. (1963). Frictional boundary conditions in plastic compression. Trans. ASME, 85, p. 68.

32. NAGAMATSU, A., MUROTA, T. and JIMMA, T. (1971). On the non-uniform deformation of material in axially symmetric compression caused by friction. Bulletin of the J.S.M.E., 14, No. 70, p. 331.

33. KUDO, H. (1961). Some analytical and experimental studies of axi-symmetric cold forging and extrusion-II. Int. J. Mech. Sci., 3, p. 91.

34. THOMSEN, E.G. (1955). A new approach to metal forming problems-experimental stress analysis of tubular extrusion. Trans. ASME, 75, p. 515.

35. WHITTON, P.W. and FORD, H. (1955). Surface friction and lubrication in cold strip rolling. Proc. Inst. Mech. Engrs., 169, p. 123.

36. WISTREICH, J.G. (1955). Investigation of the mechanics of wire drawing. Proc. Inst. Mech. Engrs., 169, p. 654.

37. MACLELLAN, G.D.S. (1948). J. Iron Steel Inst., 158, p. 347.

38. YANG, C.T. (1961). On the mechanics of wire drawing. Trans. ASME, J. Engng. Ind., 83, p. 523.

39. BLAZYNSKI, T.Z. and COLE, I.M. (1960). An investigation of plug drawing process. Proc. Inst. Mech. Engrs., 174, p. 797.

40. PARSONS, B., BRETHERTON, D. and COLE, N.B. (1968). A preliminary investigation of the combined hydrostatic extrusion and drawing process. 9th Conference M.T.D.R.

41. KAMYAB, S. and ALEXANDER, J.M. (1972). Pressure distribution in hydrostatic extrusion dies. J. Strain Analysis, 7, No. 3.

42. LENGYEL, B. and MUSUVA, J.K. (1976). Strain and pressure distribution in extrusion containers. Proc. 17th MTDR Conference, p. 429.

43. COOK, P.M. and WISTREICH, J.G. (1952). Measurements of die pressures in wire drawing by photo-elastic methods Brit, J. App. Phys., 3.

44. OHASHI, Y. and NISHITANI, T. (1967). On a method for analysing the effect of back tension in strip drawing through wedge-stopped die. J.S.M.E. Semi Int. Symp., p. 129.

45. EL-BEHERY, A.M. and LAMBLE, J.H. (1969). Stress distribution in an extrusion container found by the sandwich technique. J. Strain, p. 209.

46. THOMSEN, E.G. and LAPSLEY, J.T. (1954). Experimental stress determination within a metal during plastic flow. Proc. Soc. Expt. Stress Analysis, 11, p. 59.

47. THOMSEN, E.G., YANG, C.T. and BIERBOWER, J.B. (1954). Experimental investigation of the mechanics of plastic deformation of metals. University of California Press, Berkeley.

48. SHABAIK, A. and KOBAYASHI, S. (1967). Computer application to the visioplasticity method. Trans. ASME, J. Engng. Ind., 89, p. 339.

49. SHABAIK, A. and THOMSEN, E.G. (1968). Friction studies by the visioplasticity method. 9th MTDR Conference.

50. DUNN, P. and LENGYEL, B. (1972). Lubrication and friction in hydrostatic extrusion/drawing. J. Inst. Metals, 100, p. 317.

51. FUNG, Y.C. (1965). Foundations of solid mechanics. Prentice Hall.

52. MALVERN, L.E. (1969). Introduction to the mechanics of a continuous medium. Englewood Cliffs, Prentice Hall.

53. FORD, H. (1963). Advanced mechanics of materials. Longmans.

54. AVITZUR, B. (1968). Metal forming: processes and analysis. McGraw-Hill.

55. MENDELSON, A. (1968). Plasticity: theory and application. MacMillan Co.

56. THOMSEN, E.G., YANG, C.T. and KOBAYASHI, S. (1965). Mechanics of plastic deformation in metal processing. MacMillan Co., New York.

57. DRUCKER, D.C. (1951). A more fundamental approach to plastic stress strain relations. Proc. 1st U.S. National Congr. Appl. Mech., ASME, p. 487.

58. DRUCKER, D.C. (1950). Some applications of work hardening and ideal plasticity. Quart. Appl. Math., 7, p. 411.

59. OLSZAK, W., MROZ, T. and PERZYNA, P. (1963). Recent trends in the development of the theory of plasticity. Pergamon Press.

60. NAGHDI, P.M. (1960). Proc. 2nd Symp. on Naval Structural Mechanics. Ed. Lee and Symonds. New York, Pergamon.

61. DRUCKER, D.C. (1956). On uniqueness in the theory of plasticity. Quart. App. Math., 14, p. 35.

62. SWIFT, H.W. (1952). Plastic instability under plane stress. J. Mech. Phys. Solids 1, p. 1.

63. JOHNSON, W. and MELLOR, P.B. (1973). Engineering plasticity. Van Nostrand Reinhold Comp. London, p. 253.

64. CRANDALL, S.H. (1956). Engineering analysis. McGraw-Hill.

65. ZIENKIEWICZ, D.C. and TAYLOR, C. (1973). Weighted residual process in finite element with particular reference to some transient and coupled problems. In lectures on finite element methods in continuum mechanics, Univ. of Alabama Press, p. 415.

66. KANTOROVICH, L.V. and KRYLOV, N.M. (1958). Approximate methods of higher analysis. Netherlands, P. Noordhoff.

67. FINLAYSON, B.A. and SCRIVEN, L.E. (1966). The method of weighted residuals, a review. Appl. Mech. Rev., 19, (9), p. 735.

68. FINLAYSON, B.A. (1972). The method of weighted residuals and variational principles. Academic Press.

69. KAPLAN, S. (1963). On the best method for choosing the weighting functions in the methods of weighted residuals. Trans. American Nuclear Society, 6, p. 3.

70. NEUMAN, C.P. (1974). Recent developments in discrete weighted residual methods. Computational methods in non-linear mechanics. Ed. J.T. Oden Proc. Int. Conf. on Computational Methods, Univ. Texas, Austin.

71. HIRST, S. and URSELL, D.H. (1958). Some limiting factors in the extrusion of metals. Proc. Conf. Techn. Engng. Mf., No. 32 (Ins Mech. Engrs).

72. ALEXANDER, J.M. and LENGYEL, B. (1971). Hydrostatic extrusion. M & B Technical Library.

73. PEARSON, C.E. and PARKINS, R.N. (1961). The extrusion of metals. Chapman and Hall Ltd.

74. MURRAY, M.W. and STEIN, P.K. (1950). Strain gauge techniques. Massachusetts Institute of Technology, Cambridge, Mass.

75. STECK, E. (1969). Ein Verfahren zur näherungsweisen Berechnung des Spannungs und Verformungsanders bei Umformvorgängen. Annals of the CIRP, XVIII, p. 251.

76 STECK, E. (1971). Numerische Behandlung von Verfahren der Umformtechnik. Berichte aus dem Institut für Umformtechnik, Stuttgart University, Essen.

77. HILL, R. (1951). On the state of stress in a plastic-rigid body at the yield point. Phil. Mag. 42, p. 868.

78. DRUCKER, D.C., GREENBERG, H.J. and PRAGER, W. (1951). The safety factor of an elastic-plastic body in plane strain. J. Appl. Mech., 18, p. 371.

79. PRAGER, W. (1959). Introduction to plasticity. Addison-Wesley, Massachusetts.

80. JOHNSON, W. (1959). Estimation of upper bound loads for extrusion and coining operations. Proc. Inst. Mech. Eng., 173, p. 61.

81. KUDO, H. (1959). Study on forging and extrusion processes part III - Analysis on axisymmetric problems, Koku-Kenkyu-sho Shuho, Tokyo University, Tokyo, Japan, 1: No. 3, p. 212.

82. DRUCKER, D.C. (1954). Coulomb friction, plasticity and limit loads. J. Apply. Mech., p. 2171.

83. KOBAYASHI, S. (1963). Upper bound solution of axisymmetric forming problems-I, presented at the ASME Prod. Eng. Conf., Cincinnati, Ohio.

84. KOBAYASHI, S. (1964). Upper bound solutions of axi-symmetric forming problems-II. Trans. ASME, p. 326.

85. ALEXANDER, J.M. (1959). Remarks on extrusion and coining and communication on extrusion and coining. Proc. Ins Mech. Eng., 173, p. 85.

86. JOHNSON, W. and KUDO, H. (1962). The mechanics of metal extrusion. Manchester Univ. Press.

87. KOBAYASHI, S. and THOMSEN, E.G. (1965). Upper and lower bound solutions of axisymmetric compression and extrusion problems. J. Mech. Sci., 7, p. 127.

88. ALEXANDER, J.M. and LENGYEL, B. (1964). On the cold extrusion of flanges against high hydrostatic pressure. J. Ins. Metals, 93, p. 137.

89. HALLING, J. and MITCHELL, L.A. (1965). An upper-bound solution for axisymmetric extrusion. Int. J. Mech. Sci. Pergamon Press, 7, p. 277.

90. HADDOW, J.B. (1966). Comment on an upper-bound solution for axisymmetric extrusion. Ins. J. Mech. Sci., 8, p. 145.

91. LANGE, K. and STECK, E. (1966). Some recent results of investigations in rod, hooker and can extrusion and upsetting. Sheet Metal Ind., 43, p. 205.

92. STEPANSKII, L.G. (1963). The boundaries of the area of plastic deformation in extrusion. J. Russian Engr., 9, p. 40.

93. ZIMERMAN, Z. and AVITZUR, B. (1970). Metal flow through conical converging dies - a lower upper bound approach using generalized boundaries of the plastic zone. J. Ind. Eng., Trans. ASME, p. 119.

94. PUGH, H. Ll.D. (1964). Redundant work and friction in the hydrostatic extrusion of pure aluminium and an aluminium alloy. J. Mech. Eng. Sci., 6, p. 362.

95. OSAKADA, K. and NIIMI, Y. (1975). A study on radial flow field for extrusion through conical dies. Int. J. Mech. Sci., 17, p. 241.

96. LAMBERT, E.R. and KOBAYASHI, S. (1968). A theory on the mechanics of axisymmetric extrusion through conical dies. J. Mech. Eng. Sci., 10, p. 367.

97. TIROSH, J. (1971). On the dead-zone formation in plastic axially-symmetric converging flow. J. Mech. Phys. Solids, 19, p. 39.

98. CHEN, P.C.T. and LING, F.F. (1968). Upper bound solutions to axisymmetric extrusion problems. Int. J. Mech. Sci., 10, p. 863.

99. CHANG, K.T. and CHOI, J.C. (1971). Upper bound solutions to extrusion problems, through curved dies. Proc. 12th Midwestern Mechanics Conf., University of Notre Dame, 6, p. 383.

100. NAGPAL, V. (1974). General kinematically admissible velocity fields for some axisymmetric metal forming problems. J. Ind. Eng., Trans. ASME, p. 1197.

101. "Thick-Walled Cylinder Handbook" Report No. WAL 893/172, 1954, Watertown Arsenal Laboratory.

102. TIMOSHENKO, S. and GOODIER, J.N. (1951). Theory of elasticity McGraw-Hill, p. 388.

103. BARTON, M.V. (1941). The circular cylinder with a band of uniform pressure on a finite length of the surface. J. Appl. Mech., Trans. ASME, 8, A-97.

104. MOHAUPT, U.H., PICK, R.J. and BURNS, D.J. (1969). Bending stresses in elastic thick-walled cylindrical pressure vessels. First Intern. Conf. Pressure Vessel Technology, Delft, p. 195.

105. SIMONEN, F.A., MEYER, G.E., FIORENTINO, R.J. and SABROFF, A.M. (1969). Design of containers for large scale hydrostatic extrusion. 25th National Conf. of Fluid Power.

106. HULBERT, L.E. and SIMONEN, F.A. (1969). On the solution of axisymmetric elastic stress problems by the boundary point least squares technique. First Intern. Conf. Pressure Vessel Technology, Delft.

107. ARGYRIS, J.H. (1955). Energy theorems and structural analysis. Aircraft Eng., 27, p. 80, 125, 145.

108. TURNER, M.J., CLOUGH, R.W., MARTIN, H.C. and TOPP, L.J. (1956). Stiffness and deflection analysis of complex structures. J. Aeron. Sci., 23, p. 805.

109. ZIENKIEWICZ, O.C. (1971). The finite element method in engineering science. MacGraw-Hill, London.

110. DESAI, C.S. and ABEL, J.F. (1972). Introduction to the finite element method. Van Nostrand/Reinhold, New York.

111. SOHRABPOUR, S., SHABAIK, A.H. and THOMSEN, E.G. (1970). Local friction coefficients in axisymmetric extrusion of aluminium. J. Ind. Eng., Trans. ASME, p. 461.

112. LOIZOU, N. and SIMS, R.B. (1953). The yield stress of pure lead in compression. J. Mech. Phys. Solids, 1, p. 234.

113. LENGYEL, B. and MUTLU, D. (1978). Pressure distribution and friction in extrusion containers. 19th MTDR Conference, p. 265.

114. LENGYEL, B. and ASHFORD, P.G. (1967). An experimental pre-production unit for semi-continuous hydrostatic extrusion. Proc. 8th MTDR Conference.

115 HELMAN, H. (1976). Ph.D. Thesis, London University.

116 RAVINDRANATH, T. (1976). Ph.D. Thesis, London University.

APPENDIX A

A1. Symbols used in computer programs (semi-empirical method and assumed velocity field).

A	Radius at entry.
AA(I,J)	Corresponds to equation.
ALPHA	Semi-die angle.
AK(J,K)	Shear yield stress at a node.
B	Radius at exit.
BB(I)	Corresponds to equation.
BETA,GAMMA	Semi-angles of exit and entry boundaries.
C	Constant for stress-strain curve.
CPSI	Flow function.
CR(L,N),CZ(L,N)	Input data coordinates.
CR1,CZ1	Transformed data coordinates.
CFR	Coefficient of friction.
CX	Free parameters.
D1,D2	Coordinates for determining geometry of flow lines.
DBIL	Diameter of the billet.
DELTA	Angle of inclination of flow line.
DPROD	Diameter of product.
EFFSTN	Effective strain.
EFFSTR	Effective strain rate.
EFFSTS	Efficient stress.
ERZ	Shear strain on RZ plane.
ETR,ETH,ETZ	Strains in radial, hoop and axial directions.
ETRR, ETHH, ETZZ	Strain rates in radial, hoop and axial directions.

ETRZ	Shear strain rate on RZ plane.
G	Weighting factors.
I,K	Mesh parameters in radial and axial directions.
IMAX(K),KMIN(I)	Reference arrays characterising the mesh.
L	Flow line reference number.
NERFN	Number of error functions (stress).
NI,NK	Number of mesh points in radial and axial directions.
NII	Number of lines in product.
NTRM1	Maximum power in R.
NTRM2	Maximum power in Z.
Q	Constant friction factor.
R,Z	Radial and axial coordinates of point (I,K).
RREF,ZREF	Reference points for input data.
RPSI(L,K)	Radius of flow line L at section K.
SGRA,SGRB,SGTB,SGZA,SGRZA	Coefficients of free parameters.
SIGR,SIGT,SIGZ	Stresses in radial, hoop and axial directions.
SIGNR,SIGS	Normal and shear stresses on the die/billet boundary.
SIGRZ	Shear stress on the RZ plane.
SINVAR	Second invariant of strain rate tensor.
TEFST	Total effective strain.
TIME(L,K)	Time to reach section K along flow line L.
VBIL(VI)	Billet velocity.
VPROD(VF)	Product velocity.
VZ, VR	Axial and radial velocities.
VZL	Axial component of velocity on flow line L.
XKDIV	Step length in axial direction.

A2 THE VARIABLE DATA NAMES FOR THE FINITE ELEMENT PROGRAM

ALPHA	Coefficients of thermal expansion.
ANGLEL	Angle of the major principal in plane stress on an element, counter-clockwise from the r-axis.
ANGLEN	Angle of the major principal in plane stress at a node, counter-clockwise from the r-axis.
ANP	Indices of the forced node and of the displaced nodes adjacent to it.
AREA	Area of an element.
B	The B-matrix in the compatibility or in the equilibrium equation for an element.
BI,BJ,BM	For the elements.
BODYF	Gravitational body force per unit thickness on an element taken to be in the - z direction.
CASCTL	Constant with the value NFCASE used for testing for the termination of the job.
CI,CJ,CM	For the elements.
COND	Specified conditions of restraint for boundary nodes with the three possible values.
D	The Elasticity D-matrix for an element.
DELTAT	Temperature rise in the elements above their initial constant value.
DELTAU	r-component of the cyclic increment in the iteration to the displacement of a node.
DELTAV	z-component of the cyclic increment in the iteration to the displacement of a node.

E	Moduli of elasticity in the elements.
EETT	Linear total strain in the θ-direction in an element.
EERR	Linear total strain in the r-direction in an element.
EERZ	Total shear strain in the plane of an element.
EEZZ	Linear total strain in the z-direction in an element.
ETH	Thermal strain in an element.
ETT	Linear elastic strain in the θ direction in an element.
ERR	Linear elastic strain in the r-direction in an element.
ERZ	Elastic shear strain in the plane of an element.
EZZ	Linear elastic strain in the z-direction in an element.
FRR	Components for each node of flexibility times thickness in the r-direction due to a force per unit thickness on itself in the r-direction.
FRZ	Components for each node of flexibility times thickness in the r-direction due to a force per unit thickness on itself in the z-direction.
FZR	Components for each node of flexibility times thickness in the z-direction due to a force per unit thickness on itself in the r-direction.
FZZ	Components for each node of flexibility times thickness in the z-direction due to a force per unit thickness on itself in the z-direction.
I,J	Working indices of the first or second node of an element.

K	Matrix of stiffness per unit thickness for an element.
KRR	Components for each node of stiffness per unit thickness in the r-direction due to displacements in the r-direction of itself and of nodes adjacent to it.
KRZ	Compcnents for each node of stiffness per unit thickness in the r-direction due to displacements in the z-direction of itself and of nodes adjacent to it.
KZR	Components for each node of stiffness per unit thickness in the z-direction due to displacements in the r-direction of itself and of nodes adjacent to it.
KZZ	Components for each node of stiffness per unit thickness in the z-direction due to displacements in the z-direction of itself and of nodes adjacent to it.
L	Running Index of the elements.
L1,L2,L3	Working variables used in the output of element data.
LE	Index of particular element.
LN	Working indices of the three nodes of an element.
M	Working index of the third node of an element.
MAT	Indices of materials specified for the elements.
MATN	Index of a particular material.
N	Running index of the nodes.
N1,N2,N3	Working variables in the output of node displacements.
NAP	Numbers of nodes adjacent to each node plus one added for itself.

NAP1	Number of nodes adjacent to a particular node plus one added for itself.
NB	Indices of the restrained boundary nodes with values corresponding to those of NP.
NBR	Number of restrained boundary nodes.
NC	Cycle count in the iteration.
NCC	Cycle interval for writing the iteration progress.
NCY	Maximum number of cycles for the case.
NEL	Number of elements.
NM	Running index of materials.
NMAT	Number of materials.
NNP	Number of nodes.
NP	Index of a particular node.
NPI,NPJ,NPM	Indices of the nodes of the elements.
NR	Running index of restrained boundary nodes with values 1, 2, ...
NU	Poisson's ratios in the elements.
O	Working row or column index used in matrix multiplication.
OMEGA	Over-relaxation factor.
P	Working row index of a matrix.
Q	Working column index of a matrix.
QA	Running index of a reference node and the nodes adjacent to it.
RBAR	Radial abscissa of the centroid of an element.
RELDIF	Relative sum of absolute cyclic component increments in displacements.
R	Abscissa of the nodes.

RHO	Densities in the elements.
RR	r-components of forces per unit thickness acting on the nodes, external or total.
RR1	r-component of an out-of-balance force per unit thickness acting on a node plus the force per unit thickness acting on the node due to its own displacement.
RZ	z-component of forces per unit thickness acting on the nodes, external or total.
RZ1	z-component of an out-of-balance force per unit thickness acting on a node plus the force per unit thickness acting on the node due to its own displacement.
SD	Sum of the absolute components of displacements.
SDD	Sum of the absolute components of cyclic displacement increments.
SIGLM	The second invariant of stress in an element.
SIGLRR	Normal stress in the r-direction in the elements.
SIGLRZ	Shear in plane components of stress in the elements.
SIGLZZ	Normal stress in the z-direction in the elements.
SIGL$\theta\theta$	Normal stress in the θ-direction in the elements.
SIGL1,SIGL2	Maximum and minimum principle in plane stress on an element.
SIGL3	Principal anti-plane stress on an element.
SIGNM	The second invariant of stress at a node.
SIGNRR	Normal stress in the r-direction at a node.
SIGNRZ	Shear in plane component of stress at a node.
SIGNZZ	Normal stress in the z-direction at a node.

SIGNθθ	Normal stress component in the θ - direction at a node.
SIGN1,SIGN2	Maximum and minimum principals in plane stress at a node.
SIGN3	Principal anti-plane stress at a node.
SLOPE	Tan ϕ for the condition COND = 2 at the restrained boundary, nodes (in plane angle ϕ measured counter-clockwise from the r-axis).
SR	Control parameter specifying stresses to be output , with the four possible values 0 none 1 elements only 2 nodes only 3 both elements and nodes.
STRAIN-R	Strain in the r-direction at a node.
STRAIN-T	Strain in the θ-direction at a node.
STRAIN-Z	Strain in the z-direction at a node.
STRAIN-RZ	Shear strain at a node.
TITLE	Input text being the case title.
TOLER	Cyclic convergence test constant.
U,V	r and z components of displacements of the nodes, the input guessed values or the solution values.
W	Working matrix.
WI	Control parameter specifying how much of the input data is to be output, with the two possible values 0 case title and control parameters only. 1 all input data.
W1,W2,W3,W4,W5	Working variables.
Z	Ordinates of the nodes.

APPENDIX B

B1. Listing of the computer programme for the semi-empirical method.

```
      PROGRAM DATARD (INPUT,OUTPUT,TAPE5=INPUT,TAPE6=OUTPUT,TAPE11,
     1TAPE12,TAPE13,TAPE14)
      COMMON /VAR/ PIE,ALPHA,ALPHAD,DBIL,DPROD,VBIL,VPROD,NFL,NPFL(25),
     1CR(10,25),CZ(10,25),KI(30),KF(30),ZI(30),RI(30),ZF(30),RF(30)
      COMMON /ZONE/ NI,NII,NK,NKK,IMAX(30),KMIN(30)
      COMMON /PAR1/ R(25,25),Z(25,25),RPSI(25,25),CPSI(25,25),PSI(20)
      COMMON /PAR2/ VZ(25,25),VR(25,25),VA(25,25),ETRR(25,25),ETHH(25,25
     1),ETZZ(25,25),ETRZ(25,25)
      COMMON /PAR3/ TEFST(25,25),EFFSTR(25,25)
      COMMON /PAR4/ SIGNR(25,25),SIGS(25,25),CFR(25,25)
      COMMON /STRES/ SIGR(25,25),SIGT(25,25),SIGZ(25,25),SIGRZ(25,25),
     1EFFSTS(25,25),CX(20)
      DO 10 L=1,9
      DO 10 M=1,23
      CR(L,M)=0.
   10 CZ(L,M)=0.
      PIE=3.1415926536
      NTRM1=3
      NTRM2=3
      NPARAM=NTRM1*NTRM2*2
C     READ IN DIMENSIONS OF PROBLEM AND BILLET VELOCITY.
C     ALPHAD IS DIE HALF ANGLE.
      READ(5,101) ALPHAD,DBIL,DPROD,VBIL
      WRITE(6,101) ALPHAD,DBIL,DPROD,VBIL
  101 FORMAT(4F10.5)
      VPROD=VBIL*(DBIL/DPROD)**2
      ALPHA=ALPHAD*PIE/180.
C     READ COORDINATES OF FLOW LINES.
C     POINT RREF,ZREF ARE ON THE AXIS IN THE PLANE OF THE DIE EXIT.
      READ(5,105) NI,NII,NK,NKK
      WRITE(6,105) NI,NII,NK,NKK
  105 FORMAT(4I5)
      READ(5,102) NFL,RREF,ZREF
      WRITE(6,102) NFL,RREF,ZREF
  102 FORMAT(I5,2F10.5)
      RREF=RREF*2.54
      ZREF=ZREF*2.54
      DO 20 L=1,NFL
      READ(5,103) NPFL(L)
  103 FORMAT(I5)
      NPFLL=NPFL(L)
      READ(5,104) (CZ(L,J),CR(L,J),J=1,NPFLL)
  104 FORMAT(6F10.5)
      DO 20 J=1,NPFLL
      CR(L,J)=CR(L,J)*2.54
      CZ(L,J)=CZ(L,J)*2.54
      CR1=CR(L,J)-RREF
      CZ1=ZREF-CZ(L,J)
      CR(L,J)=CR1
   20 CZ(L,J)=CZ1
      READ(5,106) ((ZF(L),RF(L),ZI(L),RI(L)),L=1,NFL)
  106 FORMAT(4F10.5)
      DO 15 L=1,NFL
      RI(L)=RI(L)*2.54
```

```
      ZI(L)=ZI(L)*2.54
      RF(L)=RF(L)*2.54
      ZF(L)=ZF(L)*2.54
      R1=RI(L)-RREF
      Z1=ZREF-ZI(L)
      R2=RF(L)-RREF
      Z2=ZREF-ZF(L)
      RI(L)=R1
      ZI(L)=Z1
      RF(L)=R2
   15 ZF(L)=Z2
      CALL MESH
      CALL FLOW
      CALL STRATE
      CALL TSTRAIN
      CALL STRESS
      WRITE(6,1004) (I,CX(I),I=1,NPARAM)
 1004 FORMAT(6X,29H  FREE PARAMETER (STRESS) A -,I3,7H.......,E12.4/)
      WRITE(6,1003)
 1003 FORMAT(2X,1HI,3X,1HK,4X,9HSIGR(I,K),3X,9HSIGT(I,K),3X,9HSIGZ(I,K),
     13X,10HSIGRZ(I,K)//)
      DO 1200 K=1,NK
      IM=IMAX(K)
      DO 1200 I=1,IM
      IF(K.GT.19) GO TO 1200
      IF(K.EQ.1.AND.I.EQ.1) GO TO 1200
      WRITE(6,1002) (I,K,SIGR(I,K),SIGT(I,K),SIGZ(I,K),SIGRZ(I,K))
 1002 FORMAT(1X,I3,1X,I3,4E12.4)
      II=0
      KK=0
      DZ=0.
      DR=0.
      WRITE(11,1210) II,KK,Z(I,K),R(I,K),VA(I,K),DZ,DR
      WRITE(12,1210) II,KK,Z(I,K),R(I,K),EFFSTR(I,K),DZ,DR
      WRITE(13,1210) II,KK,Z(I,K),R(I,K),TEFST(I,K),DZ,DR
      WRITE(14,1210) II,KK,Z(I,K),R(I,K),EFFSTS(I,K),DZ,DR
 1210 FORMAT(2I5,5F10.5,1X,A4)
 1200 CONTINUE
      WRITE(6,1006)
 1006 FORMAT(//2X,1HI,3X,1HK,4X,10HSIGNR(I,K),3X,9HSIGS(I,K),3X,8HCFR(I,
     1K)//)
      DO 35 K=2,(NK-4)
      IM=IMAX(K)
      I=IM
      WRITE(6,1007) (I,K,SIGNR(I,K),SIGS(I,K),CFR(I,K))
 1007 FORMAT(1X,I3,1X,I3,3E12.4)
   35 CONTINUE
      STOP
      END
      SUBROUTINE MESH
      DIMENSION XX(30),YY(30),W(50),SI(11),WR1(3,30),WR2(2,8),AC(8,8),
     1PO(8)
      COMMON /VAR/ PIE,ALPHA,ALPHAD,DBIL,DPROD,VBIL,VPROD,NFL,NPFL(25),
     1CR(10,25),CZ(10,25),KI(30),KF(30),ZI(30),RI(30),ZF(30),RF(30)
      COMMON /ZONE/ NI,NII,NK,NKK,IMAX(30),KMIN(30)
```

```
      COMMON /PAR1/ R(25,25),Z(25,25),RPSI(25,25),CPSI(25,25),PSI(20)
C     CALCULATE COORDINATES OF MESH POINTS.
C     Z SECTIONS ARE EQUI-SPACED.
C     R(IMAX,K) IS CHOSEN SO IT LIES ON BOUNDING STREAMLINE.
      XKDIV=(DBIL-DPROD)/(FLOAT(NKK-2)*TAN(ALPHA)*2.)
      XIDIV=DPROD/(FLOAT(NII-1)*2.)
      NIO=NI-NII
      XIODIV=(DBIL-DPROD)/(FLOAT(NIO)*2.)
      TDIV=DPROD/2.
      DO 290 I=1,NI
      DO 290 K=1,NK
      R(I,K)=0.
  290 Z(I,K)=0.
      DO 45 I=1,NII
      DO 45 K=1,NK
      R(I,K)=XIDIV*FLOAT(I-1)
   45 KMIN(I)=1
      DO 40 I=1,NII
      DO 40 K=1,NK
      Z(I,K)=XKDIV*FLOAT(K-1)
   40 CONTINUE
      IMAX(1)=NII
      IMAX(2)=NII
C     TRANSFORM INPUT DATA TO MESH COORDINATES.
      DO 50 L=1,NFL
      NPFLL=NPFL(L)
      DO 50 J=1,NPFLL
   50 CZ(L,J)=CZ(L,J)+XKDIV
C     FIND R COORDINATES OF THE FLOW LINES AT EACH K SECTION USING
C     POLYNOMIAL FIT.
      DO 60 L=1,NFL
      NPFLL=NPFL(L)
      DO 70 J=1,NPFLL
      XX(J)=CZ(L,J)
      YY(J)=CR(L,J)
   70 W(J)=1.
      KKOR=7
      K1=KKOR+1
      LL=K1
      IFAIL=0
      IF(L.EQ.1) GO TO 61
      CALL E02ADF (NPFLL,K1,LL,XX,YY,W,WR1,WR2,AC,SI,IFAIL)
      IF(IFAIL.NE.0) PRINT,"NAG ROUTINE FAILURE"
   61 DO 80 K=1,NK
      XMN=Z(1,1)
      XMX=Z(1,NK)
      DD=XMX-XMN
      IF(Z(1,K).GT.CZ(L,NPFLL)) GO TO 81
      IF(Z(1,K).LT.CZ(L,1)) GO TO 82
      IF(L.EQ.1) GO TO 83
      DO 75 IP=1,K1
   75 PO(IP)=AC(K1,IP)
      XCAP=((Z(1,K)-XMN)-(XMX-Z(1,K)))/DD
      IFAIL=0
      CALL E02AEF (K1,PO,XCAP,CP,IFAIL)
```

```
      IF(IFAIL.EQ.1) PRINT,"NAG ROUTINE FAILURE"
      RPSI(L,K)=CP
      GO TO 80
   81 RPSI(L,K)=CR(L,NPFLL)
      GO TO 80
   82 RPSI(L,K)=CR(L,1)
      GO TO 80
   83 RPSI(L,K)=0.0
   80 CONTINUE
   60 CONTINUE
C     RPSI IS SMOOTHED USING METHOD OF MEANS.
      NK2=NK-2
      DO 250 L=1,NFL
      DO 250 K=3,NK2
      IF(L.EQ.1) GO TO 250
      SM=(RPSI(L,K-1)+2.*RPSI(L,K)+RPSI(L,K+1))/4.
      RPSI(L,K)=SM
  250 CONTINUE
C     FIND POSITION OF MESH POINTS.
      N1=NII+1
      DO 200 K=3,NK
      MM=0
      DO 210 I=N1,NI
      MM=MM+1
      R(I,K)=TDIV+FLOAT(MM)*XIODIV
      IF(R(I,K).GE.RPSI(NFL,K)) GO TO 211
  210 CONTINUE
  211 IMAX(K)=I
      IF(K.EQ.3) IMAX(K)=I-1
      IF(IMAX(K).GT.NI) IMAX(K)=NI
      IM=IMAX(K)
      R(IM,K)=RPSI(NFL,K)
      Z(IM,K)=Z(1,K)
  200 CONTINUE
      DO 220 I=N1,NI
      DO 230 K=1,NK
      IF(R(I,K).NE.0.) GO TO 231
  230 CONTINUE
  231 KMIN(I)=K
      KM=KMIN(I)
      DO 240 K=KM,NK
      IF(R(I,K).EQ.R(I,K+1)) GO TO 241
  240 Z(I,K)=XKDIV*FLOAT(K-1)
  241 KMIN(I)=K
      DO 220 K=KM,NK
  220 Z(I,K)=XKDIV*FLOAT(K-1)
      RETURN
      END
      SUBROUTINE FLOW
      DIMENSION X(10),Y(10),C(10),KC(10)
      DIMENSION CHE(25,25)
      COMMON /VAR/ PIE,ALPHA,ALPHAD,DBIL,DPROD,VBIL,VPROD,NFL,NPFL(25),
     1CR(10,25),CZ(10,25),KI(30),KF(30),ZI(30),RI(30),ZF(30),RF(30)
      COMMON /ZONE/ NI,NII,NK,NKK,IMAX(30),KMIN(30)
      COMMON /PAR1/ R(25,25),Z(25,25),RPSI(25,25),CPSI(25,25),PSI(20)
```

```
C     FIND VALUE OF FLOW FUNCTION AT EACH MESH POINT.
C     NON ZERO COEFFICIENTS DEFINED IN KC.
      DO 300 L=1,NFL
      IF (L.EQ.1) GO TO 301
      NPFLL=NPFL(L)
      PSI(L)=PIE*ABS(VBIL)*CR(L,NPFLL)**2
      GO TO 300
  301 PSI(L)=0.
  300 CONTINUE
C     POLYNOMIAL LEAST SQUARES FIT.
      DO 310 K=1,NK
      DO 320 L=1,NFL
      IF (K.EQ.1.AND.L.EQ.1) GO TO 321
      X(L)=RPSI(L,K)
      Y(L)=PSI(L)
      GO TO 320
  321 X(L)=RPSI(L,K)=0.
      Y(L)=PSI(L)=0.
  320 CONTINUE
      KTOT=0
      KOR=8
      DO 350 M=1,(KOR-1),2
  350 KC(M)=0
      DO 360 M=2,KOR,2
  360 KC(M)=M
      DO 330 M=1,KOR
      IF(KC(M).EQ.0) GO TO 330
      KTOT=KTOT+1
  330 CONTINUE
      KCOEF=KTOT+1
      CALL POLFIT(X,Y,NFL,KOR,KCOEF,KC,CO,C)
      IM1=IMAX(K)-1
      DO 340 I=2,IM1
      L=1
      CPSI(I,K)=CO
      DO 340 M=1,KOR
      IF(KC(M).EQ.0) GO TO 340
      L=L+1
      CPSI(I,K)=CPSI(I,K)+C(L)*R(I,K)**KC(M)
  340 CONTINUE
      IM=IMAX(K)
      CPSI(IM,K)=PSI(NFL)
      CPSI(1,K)=0.0
  310 CONTINUE
      CALL SMOOTH(NI,NK,IMAX,KMIN,NII,R,Z,CPSI,CHE,1)
      RETURN
      END
      SUBROUTINE POLFIT (X,Y,NN,KOR,KCOEF,KC,CO,C)
      DIMENSION X(10),Y(10),KC(10),C(10),A(10,10),B(10),AB(10,10),WRKS1(
     110),WRKS2(10)
      DIMENSION SUMX(30),SMYX(30)
C     KTOT=TOTAL NO.NON-ZERO TERMS.
      KTOR=2*KOR
      DO 400 J=1,KOR
  400 SMYX(J)=0.0
```

```
      DO 410 J=1,KTOR
  410 SUMX(J)=0.0
      SUMY=0.0
C     FORMULATION OF NORMAL EQATIONS.
      DO 420 J=1,(KTOR-1),2
  420 SUMX(J)=0.
      DO 490 J=2,KTOR,2
      SUMX(J)=0.
      DO 490 I=1,NN
      SUMX(J)=SUMX(J)+X(I)**J
  490 CONTINUE
      DO 430 I=1,NN
  430 SUMY=SUMY+Y(I)
      DO 440 J=1,(KOR-1),2
  440 SMYX(J)=0.
      DO 445 J=2,KOR,2
      SMYX(J)=0.
      DO 445 I=1,NN
      SMYX(J)=SMYX(J)+Y(I)*X(I)**J
  445 CONTINUE
C     A(KTOT+1,KTOT+1) IS MATRIX OF COEFFICIENT.
C     B(KTOT+1) IS MATRIX OF CONSTANTS.
      B(1)=SUMY
      L=1
      DO 450 I=1,KOR
      IF(KC(I)) 451,450,451
  451 L=L+1
      J=KC(I)
      B(L)=SMYX(J)
  450 CONTINUE
      I1=1
      K=KOR+1
      DO 460 I=1,K
      IF(I.EQ.1) GO TO 461
      IF(KC(I-1)) 462,460,462
  462 I1=I1+1
  461 L1=1
      DO 480 L=1,K
      IF(I.EQ.1.AND.L.EQ.1) GO TO 463
      IF(L.EQ.1) GO TO 464
      IF(KC(L-1)) 465,480,465
  465 L1=L1+1
      A(I1,L1)=SUMX(I+L-2)
      GO TO 480
  464 A(I1,1)=SUMX(I-1)
      GO TO 480
  463 A(1,1)=NN
  480 CONTINUE
  460 CONTINUE
      KK=KCOEF
      IA=10
      IAB=10
      IFAIL=0
      CALL F04ATF(A,IA,B,KK,C,AB,IAB,WRKS1,WRKS2,IFAIL)
      IF(IFAIL.NE.0) PRINT,"NAG ROUTINE FAILURE"
```

```
      CO=C(1)
      RETURN
      END
      SUBROUTINE STRATE
      DIMENSION DERZ(25,25),DERR(25,25)
      COMMON /VAR/ PIE,ALPHA,ALPHAD,DBIL,DPROD,VBIL,VPROD,NFL,NPFL(25),
     1CR(10,25),CZ(10,25),KI(30),KF(30),ZI(30),RI(30),ZF(30),RF(30)
      COMMON /ZONE/ NI,NII,NK,NKK,IMAX(30),KMIN(30)
      COMMON /PAR1/ R(25,25),Z(25,25),RPSI(25,25),CPSI(25,25),PSI(20)
      COMMON /PAR2/ VZ(25,25),VR(25,25),VA(25,25),ETRR(25,25),ETHH(25,25
     1),ETZZ(25,25),ETRZ(25,25)
C     FIND VZ AND VR VELOCITIES AT EACH MESH POINTS
      DO 910 K=1,NK
      DO 910 I=1,NI
      VZ(I,K)=VR(I,K)=0
  910 ETRR(I,K)=ETHH(I,K)=ETZZ(I,K)=ETRZ(I,K)=0.
      CUT=1.0E-10
      CALL DIFFR(R,NI,NK,IMAX,CPSI,DERR,3,3,CUT)
      DO 900 K=1,NK
      IM=IMAX(K)
      DO 905 I=2,IM
  905 VZ(I,K)=-DERR(I,K)/(2.*PIE*R(I,K))
      VZ(1,K)=(4.*VZ(2,K)-VZ(3,K))/3.
  900 CONTINUE
      CALL DIFFZ(R,Z,NI,NK,NII,IMAX,KMIN,CPSI,DERZ,3,3,CUT)
      DO 915 K=1,NK
      IM=IMAX(K)
      DO 915 I=1,IM
      IF(I.EQ.1) GO TO 916
      VR(I,K)=DERZ(I,K)/(2.*PIE*R(I,K))
      GO TO 915
  916 VR(1,K)=0
  915 CONTINUE
      DO 920 I=1,NI
      IF(I.GT.NII) GO TO 921
      VZ(I,1)=VZ(I,2)=-ABS(VPROD)
      VR(I,1)=VR(I,2)=0.
  921 VZ(I,NK)=VZ(I,NK-1)=-ABS(VBIL)
  920 VR(I,NK)=VR(I,NK-1)=0.
      DO 925 K=2,(NK-2)
      IM=IMAX(K)
      DO 925 I=1,IM
      IF(ABS(VZ(I,K)).GT.ABS(VPROD))VZ(I,K)=-ABS(VPROD)
  925 IF(VR(I,K).GT.0.) VR(I,K)=0.
      DO 970 I=1,NII
      KFF=KF(I)-1
      DO 970 K=1,KFF
      VR(I,K)=0.
  970 VZ(I,K)=-ABS(VPROD)
      DO 980 I=1,NI
      KII=KI(I)+1
      DO 980 K=KII,NK
      VR(I,K)=0.
  980 VZ(I,K)=-ABS(VBIL)
      DO 985 K=1,NK
```

```
      IM=IMAX(K)
      DO 985 I=1,IM
      V1=VR(I,K)**2
      V2=VZ(I,K)**2
      V3=SQRT(V1+V2)
  985 VA(I,K)=V3/VBIL
C     FIND STRAIN RATES.
      CALL DIFFR(R,NI,NK,IMAX,VR,ETRR,3,3,CUT)
      DO 930 K=1,NK
      IM=IMAX(K)
      DO 930 I=1,IM
      IF(ABS(VZ(I,K)).LT.ABS(VBIL))VZ (I,K)=-ABS(VBIL)
      IF(I.EQ.1) GO TO 931
      ETHH(I,K)=VR(I,K)/R(I,K)
      GO TO 930
  931 ETHH(I,K)=ETRR(I,K)
  930 CONTINUE
      CALL DIFFZ(R,Z,NI,NK,NII,IMAX,KMIN,VZ,ETZZ,3,3,CUT)
      CALL DIFFR(R,NI,NK,IMAX,VZ,DERR,3,3,CUT)
      CALL DIFFZ(R,Z,NI,NK,NII,IMAX,KMIN,VR,ETRZ,3,3,CUT)
      DO 935 K=1,NK
      IM=IMAX(K)
      DO 935 I=1,IM
      ETRZ(I,K)=ETRZ(I,K)+DERR(I,K)
  935 DERR(I,K)=ETRR(I,K)+ETHH(I,K)+ETZZ(I,K)
      DO 950 I=1,NII
      KFF=KF(I)-1
      DO 950 K=1,KFF
  950 ETRR(I,K)=ETHH(I,K)=ETZZ(I,K)=ETRZ(I,K)=0.
      DO 960 I=1,NI
      KII=KI(I)+1
      DO 960 K=KII,NK
  960 ETRR(I,K)=ETHH(I,K)=ETZZ(I,K)=ETRZ(I,K)=0.
      RETURN
      END
      SUBROUTINE TSTRAIN
      DIMENSION FESTR(10,25),TIME(10,25),TFEFST(10,25),UF(10,25)
      COMMON /VAR/ PIE,ALPHA,ALPHAD,DBIL,DPROD,VBIL,VPROD,NFL,NPFL(25),
     1CR(10,25),CZ(10,25),KI(30),KF(30),ZI(30),RI(30),ZF(30),RF(30)
      COMMON /ZONE/ NI,NII,NK,NKK,IMAX(30),KMIN(30)
      COMMON /PAR1/ R(25,25),Z(25,25),RPSI(25,25),CPSI(25,25),PSI(20)
      COMMON /PAR2/ VZ(25,25),VR(25,25),VA(25,25),ETRR(25,25),ETHH(25,25
     1),ETZZ(25,25),ETRZ(25,25)
      COMMON /PAR3/ TEFST(25,25),EFFSTR(25,25)
C     CALCULATE EFFECTIVE STRAIN RATE + TOTAL EFFECTIVE STRAIN.
      DO 595 K=1,NK
      DO 595 I=1,NI
  595 EFFSTR(I,K)=TEFST(I,K)=0.
      DO 500 K=1,NK
      IM=IMAX(K)
      DO 510 I=1,IM
      E1=ETRR(I,K) -ETHH(I,K)
      E2=ETHH(I,K)- ETZZ(I,K)
      E3=ETZZ(I,K)- ETRR(I,K)
      E4=ETRZ(I,K)**2
```

```
      E=E1**2+E2**2+E3**2
      EFFSTR(I,K)=SQRT(2.)/3.*SQRT(E+1.5*E4)
  510 CONTINUE
  500 CONTINUE
      DO 505 I=1,NII
      KFF=KF(I)-1
      DO 505 K=1,KFF
  505 EFFSTR(I,K)=0.
      DO 515 I=1,NI
      KII=KI(I)+1
      DO 515 K=KII,NK
  515 TEFST(I,K)=0.
      DO 520 K=1,NK
      IM=IMAX(K)
      DO 525 L=1,NFL
      DO 530 I=1,IM
      IF(RPSI(L,K)-R(I,K)) 521,522,530
  530 CONTINUE
  522 FESTR(L,K)=EFFSTR(I,K)
      VZL(L,K)=VZ(I,K)
      GO TO 525
  521 FESTR(L,K)=EFFSTR(I-1,K)+(EFFSTR(I,K)-EFFSTR(I-1,K))*(RPSI(L,K)-R(
     1I-1,K))/(R(I,K)-R(I-1,K))
      VZL(L,K)=VZ(I-1,K)+(VZ(I,K)-VZ(I-1,K))*(RPSI(L,K)-R(I-1,K))/(R(I,K
     1)-R(I-1,K))
  525 CONTINUE
  520 CONTINUE
C     FIND TIME TO REACH EACH K  SECTION ON EACH FLOW LINE.
      DO 540 L=1,NFL
      TFEFST(L,NK)=0.
      TIME(L,NK)=0.
      DO 540 KD=1,(NK-1)
      K=NK-KD
      TIME(L,K)=TIME(L,K+1)+2.*(Z(1,K+1)-Z(1,K))/(VZL(L,K+1)+VZL(L,K))
  540 CONTINUE
      DO 550 L=1,NFL
      DO 550 KD=1,(NK-1)
      K=NK-KD
      TFEFST(L,K)=TFEFST(L,K+1)+(TIME(L,K)-TIME(L,K+1))*.5*(FESTR(L,K)+
     1FESTR(L,K+1))
  550 CONTINUE
      DO 560 K=1,NK
      IM=IMAX(K)
      M1=IM-1
      TEFST(IM,K)=TFEFST(NFL,K)
      TEFST(1,K)=TFEFST(1,K)+RPSI(1,K)*(TFEFST(2,K)-TFEFST(1,K))/(RPSI(2
     1,K)-RPSI(1,K))
      DO 560 I=2,M1
      DO 570 L=1,NFL
      IF(RPSI(L,K)-R(I,K)) 570,571,572
  570 CONTINUE
      GO TO 560
  571 TEFST(I,K)=TFEFST(L,K)
      GO TO 560
  572 TEFST(I,K)=TFEFST(L-1,K)+(TFEFST(L,K)-TFEFST(L-1,K))*(R(I,K)-RPSI(
```

```
     1L-1,K))/(RPSI(L,K)-RPSI(L-1,K))
  560 CONTINUE
      DO 580 I=1,NII
      KFF=KF(I)
      KFI=KF(I)-1
      DO 580 K=1,KFI
  580 TEFST(I,K)=0.
      DO 590 I=1,NI
      KII=KI(I)+1
      DO 590 K=KII,NK
  590 TEFST(I,K)=0.
      DO 585 K=1,NK
      IM=IMAX(K)
      DO 585 I=1,IM
  585 TEFST(I,K)=ABS(TEFST(I,K))
      RETURN
      END
      SUBROUTINE DIFFZ(R,Z,NI,NK,NII,IMAX,KMIN,D,DERZ,NNC,NNB,CUT)
      DIMENSION R(25,25),Z(25,25),IMAX(30),KMIN(30),D(25,25),DERZ(25,25)
      DIMENSION XX(10),YY(10),E(10),C(10)
C     DIFFERENTIATION OF ARRAY D W.R.T. Z.
C     NNC POINTS ARE USED IN THE CENTRE OF THE FIELD.
C     NNB POINTS ARE USED ALONG THE BOUNDARY.
      DO 700 I=1,NI
      DO 700 K=1,NK
  700 DERZ(I,K)=0.
      IF(NNC.NE.2) GO TO 701
      DO 705 I=1,NI
      KM=KMIN(I)
      DO 705 K=KM,NK
      IF(K.EQ.KM) GO TO 706
      DERZ(I,K)=(D(I,K)-D(I,K-1))/(Z(I,K)-Z(I,K-1))
      GO TO 705
  706 DERZ(I,K)=(D(I,K+1)-D(I,K))/(Z(I,K+1)-Z(I,K))
  705 CONTINUE
      NK1=NK-1
      DO 710 K=1,NK1
      IM=IMAX(K)
      DO 715 M=1,NI
      IF(R(IM,K).EQ.R(M,K+1)) GO TO 716
      IF(R(IM,K).LT.R(M,K+1)) GO TO 717
  715 CONTINUE
  716 D1=D(M,K+1)
      GO TO 718
  717 D1=D(M-1,K+1)+(D(M,K+1)-D(M-1,K+1))*(R(IM,K)-R(M-1,K+1))/(R(M,K+1)
     1-R(M-1,K+1))
  718 DERZ(IM,K)=(D1-D(IM,K))/(Z(1,K+1)-Z(IM,K))
  710 CONTINUE
      IF(NNB.EQ.2) RETURN
      GO TO 739
  701 NF=NNC/2
      NK1=NK-1
      DO 720 I=1,NI
      KM1=KMIN(I)+1
      NM1=KM1+NF-1
```

```
      NM2=NK-NF
      IF(KM1.GT.NK1) KM1=NK1
      DO 720 K=KM1,NK1
      IF(K.LT.NM1) GO TO 721
      IF(K.GT.NM2) GO TO 722
      DO 725 M=1,NNC
      M1=K-NF+M-1
      XX(M)=Z(I,M1)
  725 YY(M)=D(I,M1)
      CALL FIT (XX,YY,NNC,C)
      GO TO 726
  721 DO 730 M=1,NNC
      M1=KM1+M-2
      XX(M)=Z(I,M1)
  730 YY(M)=D(I,M1)
      CALL FIT (XX,YY,NNC,C)
      GO TO 726
  722 DO 735 M=1,NNC
      M1=NK-NNC+M
      XX(M)=Z(I,M1)
  735 YY(M)=D(I,M1)
      CALL FIT (XX,YY,NNC,C)
  726 DERZ(I,K)=0.
      IF(ABS(D(I,K)-D(I,K-1)).LT.CUT.OR.ABS(D(I,K)-D(I,K+1)).LT.CUT) GO
     1TO 720
      DO 740 M=2,NNC
  740 DERZ(I,K)=DERZ(I,K)+C(M)*Z(I,K)**(M-2)*FLOAT(M-1)
  720 CONTINUE
  739 DO 745 I=1,NI
      DO 750 M=1,NNB
      M1=NK-NNB+M
      XX(M)=Z(I,M1)
  750 YY(M)=D(I,M1)
      CALL FIT (XX,YY,NNB,C)
      IF(D(I,NK).EQ.D(I,NK1)) GO TO 745
      DO 755 M=2,NNB
  755 DERZ(I,NK)=DERZ(I,NK)+C(M)*Z(I,NK)**(M-2)*FLOAT(M-1)
  745 CONTINUE
      DO 760 I=1,NII
      KM=KMIN(I)
      DO 765 M=1,NNB
      M1=KM+M-1
      XX(M)=Z(I,M1)
  765 YY(M)=D(I,M1)
      CALL FIT (XX,YY,NNB,C)
      DERZ(I,1)=C(2)
      IF(ABS(D(I,1)-D(I,2)).LT.CUT) DERZ(I,1)=DERZ(I,2)=0.
  760 CONTINUE
      N1=NII+1
      NF=NNB/2
      NI1=NI-1
      DO 770 I=N1,NI1
      KM=KMIN(I)
      DO 775 M=1,NF
      KA=KM-NF+M-1
```

```
      IMAXK=IMAX(KA)
      IMIN=IMAXK-NNB+1
      IMAXK1=IMAXK-1
      IMAXK2=IMAXK-2
      T1=(R(IMAXK,KA)-R(IMAXK1,KA))/(R(IMAXK1,KA)-R(IMAXK2,KA))
      IF(T1.LT.0.55) IMIN=IMIN-1
      IMA=IMIN+NNB-1
      DO 780 M1=IMIN,IMA
      M2=M1-IMIN+1
      XX(M2)=R(M1,KA)
  780 YY(M2)=D(M1,KA)
      XX(NNB)=R(IMAXK,KA)
      YY(NNB)=D(IMAXK,KA)
      CALL FIT (XX,YY,NNB,C)
      E(M)=C(1)
      DO 775 M1=2,NNB
  775 E(M)=E(M)+C(M1)*R(I,KM)**(M1-1)
      DO 785 M1=1,NF
      KA=KM-NF+M1-1
      XX(M1)=Z(1,KA)
  785 YY(M1)=E(M1)
      XX(NF+1)=Z(I,KM)
      YY(NF+1)=D(I,KM)
      M2=NF+2
      DO 786 M1=M2,NNB
      M3=KM+M1-NF-1
      XX(M1)=Z(I,M3)
  786 YY(M1)=D(I,M3)
      CALL FIT (XX,YY,NNB,C)
      DERZ(I,KM)=0.
      IF(ABS(D(I,KM)-D(I,KM+1)).LT.CUT) GO TO 770
      DO 787 M=2,NNB
  787 DERZ(I,KM)=DERZ(I,KM)+C(M)*Z(I,KM)**(M-2)*FLOAT(M-1)
  770 CONTINUE
      KM=KMIN(NI)
      DERZ(NI,KM)=0.
      KM=KM-1
      DO 789 K=2,KM
      IM=IMAX(K)
      DO 790 M=1,NNB
      KA=K-NF+M-1
      IMAXK=IMAX(KA)
      IMIN=IMAXK-NNB+1
      IMAXK1=IMAXK-1
      IMAXK2=IMAXK-2
      T1=(R(IMAXK,KA)-R(IMAXK1,KA))/(R(IMAXK1,KA)-R(IMAXK2,KA))
      IF(T1.LT.0.55) IMIN=IMIN-1
      IMA=IMIN+NNB-1
      DO 791 M1=IMIN,IMA
      M2=M1-IMIN+1
      XX(M2)=R(M1,KA)
  791 YY(M2)=D(M1,KA)
      XX(NNB)=R(IMAXK,KA)
      YY(NNB)=D(IMAXK,KA)
      CALL FIT (XX,YY,NNB,C)
```

```
      E(M)=C(1)
      DO 790 M1=2,NNB
  790 E(M)=E(M)+C(M1)*R(IM,K)**(M1-1)
      DO 792 M=1,NNB
      M1=K-NF+M-1
      XX(M)=Z(1,M1)
  792 YY(M)=E(M)
      CALL FIT (XX,YY,NNB,C)
      DERZ(IM,K)=0.
      DO 795 M=2,NNB
  795 DERZ(IM,K)=DERZ(IM,K)+C(M)*Z(IM,K)**(M-2)*FLOAT(M-1)
  789 CONTINUE
      RETURN
      END
      SUBROUTINE DIFFR(R,NI,NK,IMAX,D,DERR,NNC,NNB,CUT)
      DIMENSION R(25,25),IMAX(30),D(25,25),DERR(25,25)
      DIMENSION XX(10),YY(10),C(10)
C     DIFFERENTIATION OF ARRAY D W.R.T. R.
C     NNC POINTS ARE USED IN THE CENTRE OF THE FIELD.
C     NNB POINTS ARE USED ALONG THE BOUNDARY.
      DO 800 I=1,NI
      DO 800 K=1,NK
  800 DERR(I,K)=0.
      IF(NNC.NE.2) GO TO 801
      DO 805 K=1,NK
      IM=IMAX(K)
      DO 805 I=1,IM
      IF(I.EQ.1) GO TO 806
      DERR(I,K)=(D(I,K)-D(I-1,K))/(R(I,K)-R(I-1,K))
      GO TO 805
  806 DERR(I,K)=(D(I+1,K)-D(I,K))/(R(I+1,K)-R(I,K))
  805 CONTINUE
      IF(NNB.EQ.2) RETURN
      GO TO 807
  801 NF=NNC/2
      DO 810 K=1,NK
      IM1=IMAX(K)-1
      NM=IM1-NF+1
      DO 810 I=2,IM1
      IF(I.LT.NF) GO TO 811
      IF(I.GT.NM) GO TO 812
      DO 815 M=1,NNC
      M1=I-NF+M-1
      XX(M)=R(M1,K)
      YY(M)=D(M1,K)
  815 CONTINUE
      CALL FIT (XX,YY,NNC,C)
      GO TO 816
  811 DO 820 M=1,NNC
      XX(M)=R(M,K)
  820 YY(M)=D(M,K)
      CALL FIT (XX,YY,NNC,C)
      GO TO 816
  812 DO 825 M=1,NNC
      M1=IM1-NNC+M+1
```

```
      XX(M)=R(M1,K)
  825 YY(M)=D(M1,K)
      CALL FIT (XX,YY,NNC,C)
  816 DERR(I,K)=0.
      IF(ABS(D(I,K)-D(I-1,K)).LT.CUT.OR.ABS(D(I,K)-D(I+1,K)).LT.CUT) GO
     1TO 810
      DO 830 M=2,NNC
  830 DERR(I,K)=DERR(I,K)+C(M)*R(I,K)**(M-2)*FLOAT(M-1)
      IF(I.EQ.2) GO TO 810
      IF(ABS(D(I-1,K)-D(I-2,K)).GT.CUT) GO TO 810
      DERR(I,K)=(D(I+1,K)-D(I,K))/(R(I+1,K)-R(I,K))
  810 CONTINUE
  807 DO 835 K=1,NK
      DO 840 M=1,NNB
      XX(M)=R(M,K)
  840 YY(M)=D(M,K)
      CALL FIT (XX,YY,NNB,C)
      DERR(1,K)=C(2)
      IF(ABS(D(1,K)-D(2,K)).LT.CUT) DERR(1,K)=0.
      IM=IMAX(K)
      IM1=IMAX(K)-1
      IM2=IMAX(K)-2
      T1=(R(IM,K)-R(IM1,K))/(R(IM1,K)-R(IM2,K))
      IN=0
      IF(T1.LT.0.55) IN=1
      INB=NNB-1
      DO 845 M=1,INB
      M1=IM+M-NNB-IN
      XX(M)=R(M1,K)
  845 YY(M)=D(M1,K)
      XX(NNB)=R(IM,K)
      YY(NNB)=D(IM,K)
      CALL FIT (XX,YY,NNB,C)
      DERR(IM,K)=0.
      DO 850 M=2,NNB
  850 DERR(IM,K)=DERR(IM,K)+C(M)*R(IM,K)**(M-2)*FLOAT(M-1)
      DO 855 M=1,NNB
      M1=IM1+M-NNB-IN+1
      XX(M)=R(M1,K)
  855 YY(M)=D(M1,K)
      CALL FIT (XX,YY,NNB,C)
      DERR(IM1,K)=0.
      DO 860 M=2,NNB
  860 DERR(IM1,K)=DERR(IM1,K)+C(M)*R(IM1,K)**(M-2)*FLOAT(M-1)
  835 CONTINUE
      RETURN
      END
      SUBROUTINE FIT(X,Y,NPT,C)
      DIMENSION X(10),Y(10),A(10,10),B(10),C(10),AB(10,10),WRKS1(10),
     1WRKS2(10)
      DO 2000 KROW=1,NPT
 2000 A(KROW,1)=1.
      DO 2010 KROW=1,NPT
      DO 2020 KCOL=2,NPT
 2020 A(KROW,KCOL)=X(KROW)**(KCOL-1)
```

```
 2010 B(KROW)=Y(KROW)
      KCOEF=NPT
      KK=KCOEF
      IA=10
      IAB=10
      IFAIL=0
      CALL F04ATF(A,IA,B,KK,C,AB,IAB,WRKS1,WRKS2,IFAIL)
      IF(IFAIL.NE.0) PRINT,"NAG ROUTINE FAILURE"
      RETURN
      END
      SUBROUTINE SMOOTH(NI,NK,IMAX,KMIN,NII,R,Z,CPSI,CHECK,IT)
      DIMENSION XX(10),YY(10),W(10),SI(10),WR1(3,10),WR2(2,6),AC(6,6),
     1PO(6)
      DIMENSION IMAX(30),KMIN(30),R(25,25),Z(25,25),CPSI(25,25),CHECK(25
     1,25)
      COMMON /VAR/ PIE,ALPHA,ALPHAD,DBIL,DPROD,VBIL,VPROD,NFL,NPFL(25),
     1CR(10,25),CZ(10,25),KI(30),KF(30),ZI(30),RI(30),ZF(30),RF(30)
      IF(IT.GT.1) GO TO 3101
C     DEFINE DEFORMATION ZONE.
      KKOR=5
      IF(ZI(1).NE.0.) GO TO 3100
      DO 3105 I=1,NI
      KF(I)=KMIN(I)
      IF(KF(I).LT.2) KF(I)=2
 3105 KI(I)=NK-2
      GO TO 3157
 3100 DO 3110 L=1,NFL
      ZI(L)=ZI(L)+Z(1,2)
 3110 ZF(L)=ZF(L)+Z(1,2)
      DO 3115 L=1,NFL
      XX(L)=RF(L)
      YY(L)=ZF(L)
 3115 W(L)=1.
      K1=KKOR+1
      LL=K1
      IFAIL=0
      CALL E02ADF(NFL,K1,LL,XX,YY,W,WR1,WR2,AC,SI,IFAIL)
      IF(IFAIL.NE.0) PRINT,"NAG ROUTINE FAILURE"
      DO 3120 I=1,NII
      XMN=R(1,1)
      XMX=R(NII,1)
      DD=XMX-XMN
      DO 3125 IP=1,K1
 3125 PO(IP)=AC(K1,IP)
      XCAP=((R(I,1)-XMN)-(XMX-R(I,1)))/DD
      IFAIL=0
      CALL E02AEF(K1,PO,XCAP,CP,IFAIL)
      IF(IFAIL.EQ.1) PRINT,"NAG ROUTINE FAILURE"
      ZF(I)=CP
      DO 3130 K=1,NK
      IF(Z(I,K).GT.ZF(I)) GO TO 3131
 3130 CONTINUE
 3131 KF(I)=K
 3120 CONTINUE
      DO 3135 I=(NII+1),NI
```

```
 3135 KF(I)=KMIN(I)
      DO 3140 L=1,NFL
      XX(L)=RI(L)
      YY(L)=ZI(L)
 3140 W(L)=1.
      CALL E02ADF(NFL,K1,LL,XX,YY,W,WR1,WR2,AC,SI,IFAIL)
      IF(IFAIL.NE.0) PRINT,"NAG ROUTINE FAILURE"
      DO 3145 I=1,NI
      XMN=R(1,NK)
      XMX=R(NI,NK)
      DD=XMX-XMN
      DO 3150 IP=1,K1
 3150 PO(IP)=AC(K1,IP)
      XCAP=((R(I,NK)-XMN)-(XMX-R(I,NK)))/DD
      IFAIL=0
      CALL E02AEF(K1,PO,XCAP,CP,IFAIL)
      IF(IFAIL.EQ.1) PRINT,"NAG ROUTINE FAILURE"
      ZI(I)=CP
      DO 3155 K=1,NK
      IF(Z(I,K).GT.ZI(I)) GO TO 3156
 3155 CONTINUE
 3156 KI(I)=K-1
 3145 CONTINUE
 3157 CONTINUE
 3101 CONTINUE
C     CHECK CPSI IN ZONE BEFORE DEFORMATION.
      DO 3190 K=1,NK
      IM=IMAX(K)
      DO 3190 I=1,IM
 3190 CHECK(I,K)=CPSI(I,K)
      DO 3160 I=1,(NI-1)
      CON=PIE*ABS(VBIL)*R(I,NK)**2
      K1=KI(I)+1
      DIF=CON-CPSI(I,K1)
      DO 3165 K=K1,NK
 3165 CPSI(I,K)=CON
      K1=KI(I)
      K2=KF(I)
      DO 3170 K=K2,K1
      CPSI(I,K)=CPSI(I,K)+DIF*FLOAT(K-K2+1)/FLOAT(K1-K2+2)
 3170 CONTINUE
 3160 CONTINUE
C     CHECK CPSI IN ZONE AFTER DEFORMATION.
      DO 3175 I=1,NII
      CON=PIE*ABS(VBIL)*(R(I,1)*DBIL/DPROD)**2
      K1=KF(I)-1
      DIF=CON-CPSI(I,K1)
      DO 3180 K=1,K1
 3180 CPSI(I,K)=CON
      K1=KF(I)
      K2=KI(I)
      DO 3185 K=K1,K2
      CPSI(I,K)=CPSI(I,K)+DIF*FLOAT(K2-K+1)/FLOAT(K2-K1+2)
 3185 CONTINUE
 3175 CONTINUE
```

```
      RETURN
      END
      SUBROUTINE SMOTHZ(NI,NK,IMAX,KMIN,NII,R,Z,PSI,CPSI,CHECK)
      DIMENSION IMAX(30),KMIN(30),R(25,25),Z(25,25),PSI(20),CPSI(25,25),
     1DERZ(25,25),CHECK(25,25),ERRZ(25,25),XX(30)
      COMMON /VAR/ PIE,ALPHA,ALPHAD,DBIL,DPROD,VBIL,VPROD,NFL,NPFL(25),
     1CR(10,25),CZ(10,25),KI(30),KF(30),ZI(30),RI(30),ZF(30),RF(30)
      CUT=1.0E-10
      CALL DIFFZ(R,Z,NI,NK,NII,IMAX,KMIN,CPSI,DERZ,3,3,CUT)
C     SMOOTH DERZ IN Z DIRECTION BY AVERAGING.
      CALL AVZ(DERZ,NI,KI,KF,KMIN,XX)
      CALL AVR(DERZ,R,NK,KI,KF,IMAX,XX)
      CALL AVZ(DERZ,NI,KI,KF,KMIN,XX)
      CALL AVR(DERZ,R,NK,KI,KF,IMAX,XX)
      DO 3200 I=1,(NI-1)
      KM=KMIN(I)
 3200 CALL IZA(NK,I,KM,CPSI,DERZ,Z)
      DO 3205 I=1,(NI-1)
      CON=PIE*ABS(VBIL)*R(I,NK)**2
      K1=KI(I)+1
      DIF=CON-CPSI(I,K1)
      DO 3210 K=K1,NK
 3210 CPSI(I,K)=CON
      K1=KI(I)
      K2=KF(I)
      DO 3215 K=K2,K1
 3215 CPSI(I,K)=CPSI(I,K)+DIF*FLOAT(K-K2+1)/FLOAT(K1-K2+2)
 3205 CONTINUE
      DO 3220 K=1,NK
      IM=IMAX(K)
      CPSI(IM,K)=PSI(NFL)
      DO 3220 I=1,IM
 3220 ERRZ(I,K)=CHECK(I,K)-CPSI(I,K)
C     AVERAGE ERRZ IN Z DIRECTION.
      CALL AVZ(ERRZ,NI,KI,KF,KMIN,XX)
      CALL AVR(ERRZ,R,NK,KI,KF,IMAX,XX)
      CALL AVZ(ERRZ,NI,KI,KF,KMIN,XX)
      DO 3225 I=1,NI
      KM=KMIN(I)
      DO 3225 K=KM,NK
 3225 CPSI(I,K)=CPSI(I,K)+ERRZ(I,K)
      CALL DIFFZ(R,Z,NI,NK,NII,IMAX,KMIN,CPSI,DERZ,3,3,CUT)
C     CHECK CPSI(I,K) LESS THAN CPSI(I,K-1) FOR ALL I+K.
      DO 3230 ITER=1,20
      DO 3230 I=1,NI
      KFI=KF(I)
      KII=KI(I)
      KF1=KF(I)+1
      IF(KF1.GT.KII) KF1=KII
      DO 3235 K=KF1,KII
      IF(CPSI(I,K).GT.CPSI(I,K-1)) GO TO 3236
 3235 CONTINUE
      GO TO 3230
 3236 KK=K-1
      IF(KK.EQ.KFI) GO TO 3237
```

```
      IF(CPSI(I,KK+1).GT.CPSI(I,KK-1)) GO TO 3237
      CPSI(I,KK)=(CPSI(I,KK-1)+CPSI(I,KK+1))/2.
      GO TO 3230
 3237 CPSI(I,KK+1)=(CPSI(I,KK)+CPSI(I,KK+2))/2.
 3230 CONTINUE
      RETURN
      END
      SUBROUTINE SMOTHR (NI,NK,IMAX,KMIN,R,PSI,CPSI)
      DIMENSION IMAX(30),KMIN(30),R(25,25),Z(25,25),PSI(20),CPSI(25,25),
     1DERR(25,25),D(25,25),DERR1(25,25),DERR2(25,25),XX(30)
      COMMON /VAR/ PIE,ALPHA,ALPHAD,DBIL,DPROD,VBIL,VPROD,NFL,NPFL(25),
     1CR(10,25),CZ(10,25),KI(30),KF(30),ZI(30),RI(30),ZF(30),RF(30)
C     FIND FIRST + SECOND DIFFERENCES OF CPSI W.R.T.R.
      CUT=1.0E-10
      CALL DIFFR(R,NI,NK,IMAX,CPSI,DERR,3,3,CUT)
      CALL DIFFR(R,NI,NK,IMAX,DERR,DERR1,3,3,CUT)
C     SMOOTH DERR1 IN Z + R DIRECTIONS.
      IT=2
      DO 3600 ITER=1,IT
      CALL AVR(DERR1,R,NK,KI,KF,IMAX,XX)
 3600 CONTINUE
      DO 3605 K=1,NK
      IM=IMAX(K)
      DO 3605 I=1,IM
      IF(DERR1(I,K).GT.DERR1(1,1)) DERR1(I,K)=DERR1(1,1)
 3605 CONTINUE
      CALL AVR(DERR1,R,NK,KI,KF,IMAX,XX)
      CALL AVR(DERR1,R,NK,KI,KF,IMAX,XX)
      CALL AVZ(DERR1,NI,KI,KF,KMIN,XX)
      CALL AVZ(DERR1,NI,KI,KF,KMIN,XX)
      DO 3610 K=1,NK
      IM=IMAX(K)
      D(1,K)=0.
      DERR(1,K)=0.
      CALL IRA(K,IM,DERR,DERR1,R)
 3610 CALL IRA(K,IM,D,DERR,R)
C     SMOOTHING DERR2 IN R DIRECTION.
      CALL DIFFR(R,NI,NK,IMAX,DERR1,DERR2,3,3,CUT)
      DO 3615 K=1,NK
 3615 DERR2(1,K)=0.
      CALL AVR(DERR2,R,NK,KI,KF,IMAX,XX)
      DO 3620 K=1,NK
      IM=IMAX(K)
      CPSI(1,K)=0.
      DERR(1,K)=0.
      CALL IRA(K,IM,D,DERR,R)
      CALL IRA(K,IM,D,DERR,R)
      CALL IRA(K,IM,D,DERR,R)
      IF(CPSI(IM,K).EQ.PSI(NFL)) GO TO 3620
      DIF=(PSI(NFL)-CPSI(IM,K))/R(IM,K)**2
      DO 3625 I=2,IM
 3625 CPSI(I,K)=CPSI(I,K)+DIF*R(I,K)**2
 3620 CONTINUE
      RETURN
      END
```

```
      SUBROUTINE AVZ(AK,NI,KI,KF,KMIN,XY)
      DIMENSION AK(25,25),KI(30),KF(30),KMIN(30),XY(30)
C     AVZ SMOOTHS ARRAY IN Z DIRECTION BY AVERAGING.
      DO 3700 I=1,(NI-1)
      KII=KI(I)
      KFI=KF(I)
      KI1=KI(I)+1
      IF(KFI.EQ.KMIN(I)) KFI=KFI+1
      DO 3705 K=KFI,KI1
 3705 XY(K)=(AK(I,K-1)+AK(I,K))/2.
      DO 3710 K=KFI,KII
 3710 AK(I,K)=(XY(K)+XY(K+1))/2.
 3700 CONTINUE
      RETURN
      END
      SUBROUTINE AVR(AK,R,NK,KI,KF,IMAX,XY)
      DIMENSION AK(25,25),R(25,25),KI(30),KF(30),IMAX(30),XY(30),RX(30)
C     AVR SMOOTHS ARRAY AK IN R DIRECTION BY AVERAGING.
      DO 3825 I=1,(NK-4)
      XY(I)=AK(I,3)
 3825 RX(I)=R(I,NK)
      DO 3800 K=1,NK
      IM=IMAX(K)
      DO 3805 I=1,IM
      IF(K.GE.KF(I).AND.K.LE.KI(I)) GO TO 3806
 3805 CONTINUE
      GO TO 3800
 3806 ISS=I
      DO 3810 I=ISS,IM
      IF(K.GT.KI(I)) GO TO 3811
 3810 CONTINUE
      IFF=IM-1
      GO TO 3812
 3811 IFF=I
 3812 IF(ISS.GT.1) ISS=ISS-1
      IS1=ISS+1
      DO 3815 I=ISS,IFF
      RX(I)=(R(I,K)+R(I+1,K))/2.
 3815 XY(I)=(AK(I,K)+AK(I+1,K))/2.
      IF(IS1.GT.IFF) IS1=IFF
      DO 3820 I=IS1,IFF
 3820 AK(I,K)=XY(I-1)+(XY(I)-XY(I-1))*(R(I,K)-RX(I-1))/(RX(I)-RX(I-1))
 3800 CONTINUE
      RETURN
      END
      SUBROUTINE IZA(NK,I,KM,D,DERZ,Z)
      DIMENSION D(25,25),DERZ(25,25),Z(25,25)
      KM1=KM+1
      DO 3300 K=KM1,NK
      QQ=(DERZ(I,K)-DERZ(I,K-1))/(2.*(Z(I,K)-Z(I,K-1)))
      QA=DERZ(I,K)-2.*QQ*Z(I,K)
      QB=D(I,K-1)-QA*Z(I,K-1)-QQ*Z(I,K-1)**2
 3300 D(I,K)=QB+QA*Z(I,K)+QQ*Z(I,K)**2
      RETURN
      END
```

```
      SUBROUTINE IRA(K,IM,D,DERR,R)
      DIMENSION D(25,25),DERR(25,25),R(25,25)
      DO 3500 I=2,IM
      QQ=(DERR(I,K)-DERR(I-1,K))/(2.*(R(I,K)-R(I-1,K)))
      QA=DERR(I,K)-2.*QQ*R(I,K)
      QB=D(I-1,K)-QA*R(I-1,K)-QQ*R(I-1,K)**2
 3500 D(I,K)=QB+QA*R(I,K)+QQ*R(I,K)**2
      RETURN
      END
      SUBROUTINE STRESS
      DIMENSION G(10),AK(25,25),SINVAR(25,25),EF(5,20),AA(20,20),BB(20)
      DIMENSION AB(20,20),WRKS1(20),WRKS2(20)
      COMMON /VAR/ PIE,ALPHA,ALPHAD,DBIL,DPROD,VBIL,VPROD,NFL,NPFL(25),
     1CR(10,25),CZ(10,25),KI(30),KF(30),ZI(30),RI(30),ZF(30),RF(30)
      COMMON /ZONE/ NI,NII,NK,NKK,IMAX(30),KMIN(30)
      COMMON /PAR1/ R(25,25),Z(25,25),RPSI(25,25),CPSI(25,25),PSI(20)
      COMMON /PAR2/ VZ(25,25),VR(25,25),VA(25,25),ETRR(25,25),ETHH(25,25
     1),ETZZ(25,25),ETRZ(25,25)
      COMMON /PAR3/ TEFST(25,25),EFFSTR(25,25)
      COMMON /PAR4/ SIGNR(25,25),SIGS(25,25),CFR(25,25)
      COMMON /STRES/ SIGR(25,25),SIGT(25,25),SIGZ(25,25),SIGRZ(25,25),
     1EFFSTS(25,25),CX(20)
      Q=0.12
      C=1560.88
      CVF=.09807
      NTRM1=3
      NTRM2=3
      NPARAM=NTRM1*NTRM2*2
      KP=NPARAM+1
      NERFN=4
      DO 1055 J=1,KP
      DO 1055 I=1,KP
      BB(J)=0.
 1055 AA(I,J)=0.
      DO 1000 I=1,NERFN
 1000 G(I)=.1000E+01
C     CALCULATE THE SECOND PRINCIPAL DEVIATORIC INVARIANT.
      DO 1025 K=1,NK
      DO 1025 I=1,NI
 1025 SINVAR(I,K)=AK(I,K)=0.
      DO 1010 K=1,NK
      IM=IMAX(K)
      DO 1020 I=1,IM
      IF(K.EQ.1.AND.I.EQ.1) GO TO 1020
      SINVAR(I,K)=ABS(ETRZ(I,K)**2-ETRR(I,K)*ETHH(I,K)-ETHH(I,K)*ETZZ(I,
     1K)-ETZZ(I,K)*ETRR(I,K))
      SIG=C*TEFST(I,K)**0.25
      AK(I,K)=SIG/SQRT(3.)
 1020 CONTINUE
 1010 CONTINUE
      DO 1005 I=1,NII
      KFF=KF(I)-1
      DO 1005 K=1,KFF
 1005 SINVAR(I,K)=AK(I,K)=0.
```

```
      DO 1015 I=1,NI
      KII=KI(I)+1
      DO 1015 K=KII,NK
 1015 SINVAR(I,K)=AK(I,K)=0.
      DO 1040 K=2,(NK-4)
      IM=IMAX(K)
      DO 1040 I=1,IM
      IF(SINVAR(I,K).EQ.0.) GO TO 1061
      NERR=NERFN-1
      STK=AK(I,K)/SQRT(SINVAR(I,K))
      FCT=1.
      IF(I.EQ.IM) FCT=0.05
      DO 1050 NL=1,NTRM1
      DO 1050 NM=1,NTRM2
      INDN=NM
      INDM=NL-1
      INDQ=NM-1
      INDP=NL-1
      NT=NM+(NL-1)*NTRM1
      NTT=NT+(NTRM1*NTRM2)
      SGRA=FLOAT(INDN*(INDN-1))*(R(I,K)**(2*INDM+2))*Z(I,K)**(INDN-2)
      SGRB=R(I,K)**(2*INDP)*Z(I,K)**INDQ
      SGTB=FLOAT(2*INDP+1)*R(I,K)**(2*INDP)*Z(I,K)**INDQ
      SGZA=FLOAT((2*INDM+3)*(2*INDM+2))*R(I,K)**(2*INDM)*Z(I,K)**INDN
      SGRZA=FLOAT(-(2*INDM+3)*INDN)*R(I,K)**(2*INDM+1)*Z(I,K)**(INDN-1)
C     CHOOSE ERROR FUNCTIONS.
      EF(1,NT)=(2./3.)*SGRA-SGZA/3.
      EF(1,NTT)=(2./3.)*SGRB-SGTB/3.
      EF(2,NT)=-SGRA/3.-SGZA/3.
      EF(2,NTT)=(2./ 3.)*SGTB-SGRB/ 3.
      EF(3,NT)=SGRZA
      EF(3,NTT)=0.
      IF(I.NE.IM) GO TO 1050
      EF(4,NT)=(SGRA-SGZA)*SIN(2.*ALPHA)/2.+SGRZA*COS(2.*ALPHA)
      EF(4,NTT)=SGRB*SIN(2.*ALPHA)/2.
 1050 CONTINUE
      EF(1,KP)=-STK*ETRR(I,K)
      EF(2,KP)=-STK*ETHH(I,K)
      EF(3,KP)=-STK*ETRZ(I,K)
      IF(I.NE.IM) GO TO 1052
      EF(4,KP)=-Q*AK(I,K)
 1052 IF(I.EQ.IM) NERR=NERFN
      DO 1060 LT=1,NERR
      DO 1070 J=1,KP
      DO 1075 N=1,KP
      AA(N,J)=AA(N,J)+EF(LT,N)*EF(LT,J)*G(LT)*FCT
 1075 CONTINUE
 1070 CONTINUE
 1060 CONTINUE
 1061 SINVAR(I,K)=.1000E-10
 1040 CONTINUE
      DO 1080 I=1,NPARAM
 1080 BB(I)=-AA(I,KP)
C     SOLVE EQUATIONS AND DETERMINE UNKNOWNS.
      IA=20
```

```
      IAB=20
      IFAIL=0
      CALL F04ATF(AA,IA,BB,NPARAM,CX,AB,IAB,WRKS1,WRKS2,IFAIL)
      IF(IFAIL.NE.0) PRINT,"NAG ROUTINE FAILURE"
      DO 1100 K=1,NK
      DO 1100 I=1,NI
 1100 SIGR(I,K)=SIGT(I,K)=SIGZ(I,K)=SIGRZ(I,K)=EFFSTS(I,K)=0.
      DO 1125 K=2,NK
      IM=IMAX(K)
      DO 1125 I=1,IM
      SIGR(I,K)=SIGT(I,K)=SIGZ(I,K)=SIGRZ(I,K)=0.
      IT=1
      DO 1120 NL=1,NTRM1
      DO 1120 NM=1,NTRM2
      INDN=NM
      INDM=NL-1
      INDQ=NM-1
      INDP=NL-1
      NT=NM+(NL-1)*NTRM1
      NTT=NT+(NTRM1*NTRM2)
      IF(IT.NE.1) GO TO 1121
      SGRA=FLOAT(INDN*(INDN-1))*(R(I,K)**(2*INDM+2))*Z(I,K)**(INDN-2)
      SGRB=R(I,K)**(2*INDP)*Z(I,K)**INDQ
      SGTB=FLOAT(2*INDP+1)*R(I,K)**(2*INDP)*Z(I,K)**INDQ
      SGRZA=FLOAT(-(2*INDM+3)*INDN)*R(I,K)**(2*INDM+1)*Z(I,K)**(INDN-1)
 1121 SGZA=FLOAT((2*INDM+3)*(2*INDM+2))*R(I,K)**(2*INDM)*Z(I,K)**INDN
      IF(IT.NE.1) GO TO 1122
      SIGR(I,K)=SIGR(I,K)+CX(NT)*SGRA+CX(NTT)*SGRB
      SIGT(I,K)=SIGT(I,K)+CX(NTT)*SGTB
      SIGRZ(I,K)=SIGRZ(I,K)+CX(NT)*SGRZA
 1122 SIGZ(I,K)=SIGZ(I,K)+CX(NT)*SGZA
 1120 CONTINUE
 1125 CONTINUE
      DO 1130 K=1,NK
      IM=IMAX(K)
      DO 1140 I=1,IM
C     CONVERT STRESS COMPONENTS INTO (MN/M**2).
      SIGR(I,K)=CVF*SIGR(I,K)
      SIGT(I,K)=CVF*SIGT(I,K)
      SIGZ(I,K)=CVF*SIGZ(I,K)
      SIGRZ(I,K)=CVF*SIGRZ(I,K)
 1140 EFFSTS(I,K)=SQRT(.5*((SIGR(I,K)-SIGT(I,K))**2+(SIGT(I,K)-SIGZ(I,K)
     1)**2+(SIGZ(I,K)-SIGR(I,K))**2)+3.*SIGRZ(I,K)**2)
 1130 CONTINUE
      DO 25 K=2,(NK-1)
      IM=IMAX(K)
      I=IM
      IF(K.GT.(NKK+1)) GO TO 26
      SIGNR(I,K)=SIGZ(I,K)*SIN(ALPHA)**2+SIGR(I,K)*COS(ALPHA)**2-SIGRZ(I
     1,K)*SIN(2.*ALPHA)
      SIGS(I,K)=SIGRZ(I,K)*COS(2.*ALPHA)+(SIGR(I,K)-SIGZ(I,K))*SIN(2.*
     1ALPHA)/2.
      CFR(I,K)=ABS(SIGS(I,K)/SIGNR(I,K))
      GO TO 25
   26 SIGNR(I,K)=SIGR(I,K)
```

```
      SIGS(I,K)=SIGRZ(I,K)
      CFR(I,K)=ABS(SIGS(I,K)/SIGNR(I,K))
   25 CONTINUE
      RETURN
      END
```

B2. Listing of the computer programme for the assumed velocity field.

```
      PROGRAM WRESIDU(INPUT,OUTPUT,TAPE5=INPUT,TAPE6=OUTPUT,TAPE7,TAPE8,
     1TAPE9,TAPE10)
      DIMENSION F(3),F1(3),F2(3)
      COMMON CP,CQ,CS,CT,CN,Z1,ZK(15,25),RK(15,25),RKK(15,25)
      COMMON PIE,D1,D2,A,B,VI,VF,DBIL,ALPHA,BETA,GAMMA,DELTA(15,25),
     1NPARAM
      COMMON NI,NK,NK1,NK2,R(15,25),Z(15,25),IMAX(25),KMIN(25)
      COMMON VR(15,25),VZ(15,25),VA(15,25),ETRR(15,25),ETHH(15,25),ETZZ(
     115,25),ETRZ(15,25),EFFSTR(15,25)
      COMMON ERR(15,25),EHH(15,25),EZZ(15,25),ERZ(15,25),EFFSTN(15,25)
      COMMON SIGR(15,25),SIGT(15,25),SIGZ(15,25),SIGRZ(15,25),EFFSTS(15,
     125),CX(20)
      COMMON SIGNR(15,25),SIGS(15,25),CFR(15,25)
      PIE=3.1415926536
      EXRAT=2.
      READ(5,1001) NI,NK,ALPHAD,BET,GAM,VI
      WRITE(6,1001) NI,NK,ALPHAD,BET,GAM,VI
 1001 FORMAT(2I5,4F10.5//)
      NK1=9
      NK2=11
      COF=2./SQRT(3.)
      ALPHA=ALPHAD*PIE/180.
      BETA=BET*PIE/180.
      GAMMA=GAM*PIE/180.
      DBIL=3.
      A=DBIL/2.
      B=A/SQRT(EXRAT)
      EK=SQRT(B)
      VF=VI*(A/B)**2
      D1=B*(1./TAN(ALPHA)+1./TAN(BETA))
      D2=A*(1./TAN(ALPHA)-1./TAN(GAMMA))
      CALL MESH
      LL=3
      MI=0
      DO 300 K=1,NK
      IF(K.LE.NK1) MI=MI+1
      IF(K.GT.NK1.AND.K.LE.NK2) MI=NI
      IF(K.GT.NK2) MI=MI-1
      DO 300 I=1,MI
      Z3=ZK(I,K)
      RR=R(I,K)
      ZZ=Z(I,K)
C     VELOCITY FIELD.
      CC=VI/(4.*CN**2*RR*ZZ*TAN(ALPHA))
      CC=CC*EK
      C1=CP*RR-CQ*ZZ-CS
      X=SQRT(C1**2+4.*CT*CN*RR)
      Y=C1+X
      DYR=CP+(CP*C1+2.*CT*CN)/X
      DYZ=-CQ*(1.+C1/X)
      DXR=(CP*C1+2.*CT*CN)/X
      DXZ=-CQ*C1/X
      DYZR=-CQ*(CP*X-DXR*C1)/X**2
      DYRZ=-(CQ*CP*X+DXZ*(CP*C1+2.*CT*CN))/X**2
      DYZZ=CQ*(CQ*X+DXZ*C1)/X**2
```

```
      DYRR=(CP**2*X-DXR*(CP*C1+2.*CT*CN))/X**2
      VR(I,K)=CC*Y*(DYZ-Y/(2.*ZZ))
      VZ(I,K)=-CC*Y*DYR
      V1=VR(I,K)**2
      V2=VZ(I,K)**2
      V3=SQRT(V1+V2)
      VA(I,K)=V3/VI
C     STRAIN RATE FIELD.
      ETRR(I,K)=CC*(-Y*DYZ/RR+DYR*DYZ+Y*DYZR+Y**2/(2.*ZZ*RR)-Y*DYR/ZZ)
      ETHH(I,K)=CC*Y*(DYZ-Y/(2.*ZZ))/RR
      ETZZ(I,K)=-CC*(DYZ*DYR+Y*DYRZ-Y*DYR/ZZ)
      ETRZ(I,K)=(CC/2.)*(DYZ**2+Y*DYZZ-Y*DYZ/ZZ+Y**2/ZZ**2-Y*DYZ/ZZ-(-Y*
     1DYR/RR+DYR**2+Y*DYRR))
C     EFFECTIVE STRAIN RATE.
      ET1=ETRR(I,K)**2
      ET2=ETHH(I,K)**2
      ET3=ETZZ(I,K)**2
      ET4=ETRZ(I,K)**2
      ET=.5*(ET1+ET2+ET3)
      EFFSTR(I,K)=COF*SQRT(ET+ET4)
C     STRAIN FIELD.
      IF(K.LE.NK1.AND.I.EQ.1) L=NK+1-K
      IF(K.LE.NK1.AND.I.GT.1) L=NK-K+I
      IF(K.GT.NK1.AND.K.LT.NK2.AND.I.EQ.1) L=NK+2-K
      IF(K.GT.NK1.AND.K.LT.NK2.AND.I.GT.1) L=NK-K+I+1
      IF(K.GE.NK2.AND.I.EQ.1) L=K
      IF(K.GE.NK2.AND.I.GT.1) L=K-1+I
      KK=KMIN(L)
      EPT=ALOG(R(I,K)/R(1,KK))
      DO 310 J=1,LL
      IF(J.EQ.1) RJ=Z(I,K)
      IF(J.EQ.2) RJ=(Z(I,K)+Z(1,KK))/2.
      IF(J.EQ.3) RJ=Z(1,KK)
      RZ=(RJ+(CN*RK(I,K)+CS)/CQ)*(1./Z3)
      RR=RZ
      ZZ=RJ
      CC=VI/(4.*CN**2*RR*ZZ*TAN(ALPHA))
      CC=CC*EK
      C1=CP*RR-CQ*ZZ-CS
      X=SQRT(C1**2+4.*CT*CN*RR)
      Y=C1+X
      DYR=CP+(CP*C1+2.*CT*CN)/X
      DYZ=-CQ*(1.+C1/X)
      DXR=(CP*C1+2.*CT*CN)/X
      DXZ=-CQ*C1/X
      DYZR=-CQ*(CP*X-DXR*C1)/X**2
      DYRZ=-(CQ*CP*X+DXZ*(CP*C1+2.*CT*CN))/X**2
      DYZZ=CQ*(CQ*X+DXZ*C1)/X**2
      DYRR=(CP**2*X-DXR*(CP*C1+2.*CT*CN))/X**2
      V=-CC*Y*DYR
      E3=(CC/2.)*(DYZ**2+Y*DYZZ-Y*DYZ/ZZ+Y**2/ZZ**2-Y*DYZ/ZZ-(-Y*DYR/RR+
     1DYR**2+Y*DYRR))
      F1(J)=-(DYZ*DYR+Y*DYRZ-Y*DYR/ZZ)/(Y*DYR)
      F2(J)=-E3/V
  310 CONTINUE
```

```
      EHH(I,K)=EPT
      EZZ(I,K)=(Z(1,KK)-Z(I,K))/6.*(F1(1)+4.*F1(2)+F1(3))
      ERR(I,K)=-(EHH(I,K)+EZZ(I,K))
      ERZ(I,K)=(Z(1,KK)-Z(I,K))/6.*(F2(1)+4.*F2(2)+F2(3))
      ES1=ERR(I,K)**2
      ES2=EZZ(I,K)**2
      ES3=EHH(I,K)**2
      ES4=ERZ(I,K)**2
      ES=0.5*(ES1+ES2+ES3)
      EFFSTN(I,K)=COF*SQRT(ES+ES4)
  300 CONTINUE
      CALL STRESS
      WRITE(6,1002) (I,CX(I),I=1,NPARAM)
 1002 FORMAT(6X,29H  FREE PARAMETER (STRESS) A -,I3,7H.......,E12.4/)
      WRITE(6,1003)
 1003 FORMAT(//2X,1HI,3X,1HK,4X,7HVA(I,K),5X,11HEFFSTR(I,K),1X,11HEFFSTN
     1(I,K),1X,11HEFFSTS(I,K),1X,9HSIGR(I,K),3X,10HSIGRZ(I,K)//)
      MI=0
      DO 30 K=1,NK
      IF(K.LE.NK1) MI=MI+1
      IF(K.GT.NK1.AND.K.LE.NK2) MI=NI
      IF(K.GT.NK2) MI=MI-1
      DO 30 I=1,MI
      WRITE(6,333) Z(I,K)
  333 FORMAT(E12.4)
      WRITE(6,1004) (I,K,VA(I,K),EFFSTR(I,K),EFFSTN(I,K),EFFSTS(I,K),
     1SIGR(I,K),SIGRZ(I,K))
 1004 FORMAT(1X,I3,1X,I3,6E12.4)
      II=0
      KK=0
      DZ=0.
      DR=0.
      WRITE(7,1007) II,KK,Z(I,K),R(I,K),VA(I,K),DZ,DR
      WRITE(8,1007) II,KK,Z(I,K),R(I,K),EFFSTR(I,K),DZ,DR
      WRITE(9,1007) II,KK,Z(I,K),R(I,K),EFFSTN(I,K),DZ,DR
      WRITE(10,1007) II,KK,Z(I,K),R(I,K),EFFSTS(I,K),DZ,DR
 1007 FORMAT(2I5,5F10.5,1X,A4)
   30 CONTINUE
      WRITE(6,1005)
 1005 FORMAT(//2X,1HI,3X,1HK,4X,10HSIGNR(I,K),3X,9HSIGS(I,K),3X,8HCFR(I,
     1K)//)
      DO 40 K=1,NK
      I=IMAX(K)
      WRITE(6,1006) (I,K,SIGNR(I,K),SIGS(I,K),CFR(I,K))
 1006 FORMAT(1X,I3,1X,I3,3E12.4)
   40 CONTINUE
      STOP
      END
      SUBROUTINE MESH
      COMMON CP,CQ,CS,CT,CN,Z1,ZK(15,25),RK(15,25),RKK(15,25)
      COMMON PIE,D1,D2,A,B,VI,VF,DBIL,ALPHA,BETA,GAMMA,DELTA(15,25),
     1NPARAM
      COMMON NI,NK,NK1,NK2,R(15,25),Z(15,25),IMAX(25),KMIN(25)
      COMMON VR(15,25),VZ(15,25),VA(15,25),ETRR(15,25),ETHH(15,25),ETZZ(
     115,25),ETRZ(15,25),EFFSTR(15,25)
```

```
      COMMON ERR(15,25),EHH(15,25),EZZ(15,25),ERZ(15,25),EFFSTN(15,25)
      R1=SIN(GAMMA)
      R2=COS(GAMMA)
      R3=SIN(BETA)
      R4=COS(BETA)
      Z1=R2/R1
      Z2=R4/R3
      CP=Z1+B*Z2/A
      CQ=1.-B/A
      CS=B*D2/A-D1
      CT=D2-D1
      CN=B*(Z1+Z2)/A
      DIVK=(D2-D1)/FLOAT(NK2-NK1)
      MI=0
      DO 200 K=1,NK
      IF(K.LE.NK1) MI=MI+1
      IF(K.GT.NK1.AND.K.LE.NK2) MI=NI
      IF(K.GT.NK2) MI=MI-1
      DO 200 I=1,MI
      IF(I.EQ.MI) IMAX(K)=I
      IF(I.EQ.1.AND.K.GE.NK2) KMIN(K)=K
      IF(K.LE.NK1) J=NI-1-K+I
      IF(K.GT.NK1.AND.K.LT.NK2) J=NI-K+I
      IF(K.GE.NK2) J=K-NK2+I-1
      RK(I,K)=A/FLOAT(NI-1)*FLOAT(J)
      IF(I.EQ.1.AND.K.GE.NK1.AND.K.LE.NK2) RK(I,K)=0.001
      RKK(I,K)=B*RK(I,K)/A
      CC=CP+CT/RK(I,K)
      DELTA(I,K)=ATAN(CQ/CC)
      IF(I.EQ.MI) DELTA(I,K)=ALPHA
      R5=SIN(DELTA(I,K))
      R6=COS(DELTA(I,K))
      Z3=R6/R5
      ZK(I,K)=Z3
      IF(K.GE.NK1.AND.K.LE.NK2) GO TO 201
      IF(K.GT.NK2) GO TO 202
      Z(I,K)=D1-RKK(1,K)*Z2
      R(I,K)=(Z(I,K)+(CN*RK(I,K)+CS)/CQ)*(1./Z3)
      GO TO 200
  201 Z(I,K)=D2-DIVK*FLOAT(NK2-K)
      R(I,K)=(Z(I,K)+(CN*RK(I,K)+CS)/CQ)*(1./Z3)
      GO TO 200
  202 Z(I,K)=D2+RK(1,K)*Z1
      R(I,K)=(Z(I,K)+(CN*RK(I,K)+CS)/CQ)*(1./Z3)
  200 CONTINUE
      RETURN
      END
      SUBROUTINE STRESS
      DIMENSION EF(5,20),AA(20,20),BB(20),WRKS1(20),WRKS2(20),G(5),AB(20
     1,20)
      COMMON CP,CQ,CS,CT,CN,Z1,ZK(15,25),RK(15,25),RKK(15,25)
      COMMON PIE,D1,D2,A,B,VI,VF,DBIL,ALPHA,BETA,GAMMA,DELTA(15,25),
     1NPARAM
      COMMON NI,NK,NK1,NK2,R(15,25),Z(15,25),IMAX(25),KMIN(25)
      COMMON VR(15,25),VZ(15,25),VA(15,25),ETRR(15,25),ETHH(15,25),ETZZ(
```

```
     115,25),ETRZ(15,25),EFFSTR(15,25)
      COMMON ERR(15,25),EHH(15,25),EZZ(15,25),ERZ(15,25),EFFSTN(15,25)
      COMMON SIGR(15,25),SIGT(15,25),SIGZ(15,25),SIGRZ(15,25),EFFSTS(15,
     125),CX(20)
      COMMON SIGNR(15,25),SIGS(15,25),CFR(15,25)
      IT=1
      C=1560.88
      CVF=.09807
      Q=0.12
      NTRM1=3
      NTRM2=3
      NPARAM=NTRM1*NTRM2*2
      KP=NPARAM+1
      NERFN=4
      DO 400 I=1,NERFN
  400 G(I)=.1000E+01
      DO 410 J=1,KP
       DO 410 I=1,KP
  410 AA(I,J)=0.
      MI=0
      DO 420 K=1,NK
      IF(K.LE.NK1) MI=MI+1
      IF(K.GT.NK1.AND.K.LE.NK2) MI=NI
      IF(K.GT.NK2) MI=MI-1
      II=1
      IF(K.GE.NK1.AND.K.LE.NK2) II=2
      DO 420 I=II,MI
      NERR=NERFN-1
      FCT=1.
      IF(I.EQ.MI) FCT=6.75
      SINVAR=ABS(ETRZ(I,K)**2-ETRR(I,K)*ETHH(I,K)-ETHH(I,K)*ETZZ(I,K)-
     1ETZZ(I,K)*ETRR(I,K))
      SIG=C*EFFSTN(I,K)**.25
      IF(IT.EQ.2) SIG=362.25
      AK=SIG/SQRT(3.)
      STK=AK/SQRT(SINVAR)
      DO 430 NL=1,NTRM1
      DO 430 NM=1,NTRM2
      INDN=NM
      INDM=NL-1
      INDQ=NM+2
      INDP=NL-1
      NT=NM+(NL-1)*NTRM2
      NTT=NT+(NTRM1*NTRM2)
      SGRA=FLOAT(INDN*(INDN-1))*(R(I,K)**(2*INDM+2))*Z(I,K)**(INDN-2)
      SGZA=FLOAT((2*INDM+3)*(2*INDM+2))*R(I,K)**(2*INDM)*Z(I,K)**INDN
      SGRZA=FLOAT(-(2*INDM+3)*INDN)*R(I,K)**(2*INDM+1)*Z(I,K)**(INDN-1)
      SGRB=R(I,K)**(2*INDP)*Z(I,K)**INDQ
      SGTB=FLOAT(2*INDP+1)*R(I,K)**(2*INDP)*Z(I,K)**INDQ
C     CHOOSE ERROR FUNCTIONS.
      EF(1,NT)=(2./3.)*SGRA-SGZA/3.
      EF(1,NTT)=(2./3.)*SGRB-SGTB/3.
      EF(2,NT)=-SGRA/3.-SGZA/3.
      EF(2,NTT)=(2./3.)*SGTB-SGRB/3.
      EF(3,NT)=SGRZA
```

```
      EF(3,NTT)=0.
      IF(I.NE.MI) GO TO 430
      EF(4,NT)=(SGRA-SGZA)*SIN(2.*ALPHA)/2.+SGRZA*COS(2.*ALPHA)
      EF(4,NTT)=SGRB*SIN(2.*ALPHA)/2.
  430 CONTINUE
      EF(1,KP)=-STK*ETRR(I,K)
      EF(2,KP)=-STK*ETHH(I,K)
      EF(3,KP)=-STK*ETRZ(I,K)
      EF(4,KP)=-Q*AK
      IF(I.EQ.MI) NERR=NERFN
      DO 440 LT=1,NERR
      DO 450 J=1,KP
      DO 450 N=1,KP
      AA(N,J)=AA(N,J)+EF(LT,N)*EF(LT,J)*G(LT)*FCT
  450 CONTINUE
  440 CONTINUE
  420 CONTINUE
      DO 460 I=1,NPARAM
  460 BB(I)=-AA(I,KP)
C     SOLVE EQUATIONS AND DETERMINE UNKNOWNS.
      IA=20
      IAB=20
      IFAIL=0
      CALL F04ATF(AA,IA,BB,NPARAM,CX,AB,IAB,WRKS1,WRKS2,IFAIL)
      IF(IFAIL.NE.0) PRINT,"NAG ROUTINE FAILURE"
      MI=0
      DO 470 K=1,NK
      IF(K.LE.NK1) MI=MI+1
      IF(K.GT.NK1.AND.K.LE.NK2) MI=NI
      IF(K.GT.NK2) MI=MI-1
      DO 470 I=1,MI
      SIGR(I,K)=0.
      SIGT(I,K)=0.
      SIGZ(I,K)=0.
      SIGRZ(I,K)=0.
      DO 480 NL=1,NTRM1
      DO 480 NM=1,NTRM2
      INDN=NM
      INDM=NL-1
      INDQ=NM+2
      INDP=NL-1
      NT=NM+(NL-1)*NTRM2
      NTT=NT+(NTRM1*NTRM2)
      SGRA=FLOAT(INDN*(INDN-1))*(R(I,K)**(2*INDM+2))*Z(I,K)**(INDN-2)
      SGZA=FLOAT((2*INDM+3)*(2*INDM+2))*R(I,K)**(2*INDM)*Z(I,K)**INDN
      SGRZA=FLOAT(-(2*INDM+3)*INDN)*R(I,K)**(2*INDM+1)*Z(I,K)**(INDN-1)
      SGRB=R(I,K)**(2*INDP)*Z(I,K)**INDQ
      SGTB=FLOAT(2*INDP+1)*R(I,K)**(2*INDP)*Z(I,K)**INDQ
      SIGR(I,K)=SIGR(I,K)+CX(NT)*SGRA+CX(NTT)*SGRB
      SIGT(I,K)=SIGT(I,K)+CX(NTT)*SGTB
      SIGZ(I,K)=SIGZ(I,K)+CX(NT)*SGZA
      SIGRZ(I,K)=SIGRZ(I,K)+CX(NT)*SGRZA
  480 CONTINUE
C     CONVERT STRESS COMPONENTS INTO (MN/M**2).
      SIGR(I,K)=CVF*SIGR(I,K)
```

```
      SIGT(I,K)=CVF*SIGT(I,K)
      SIGZ(I,K)=CVF*SIGZ(I,K)
      SIGRZ(I,K)=CVF*SIGRZ(I,K)
      EFFSTS(I,K)=SQRT(.5*((SIGR(I,K)-SIGT(I,K))**2+(SIGT(I,K)-SIGZ(I,K)
     1)**2+(SIGZ(I,K)-SIGR(I,K))**2)+3.*SIGRZ(I,K)**2)
  470 CONTINUE
      DO 490 K=1,NK
      I=IMAX(K)
      SIGNR(I,K)=SIGZ(I,K)*SIN(ALPHA)**2+SIGR(I,K)*COS(ALPHA)**2-SIGRZ(I
     1,K)*SIN(2.*ALPHA)
      SIGS(I,K)=SIGRZ(I,K)*COS(2.*ALPHA)+(SIGR(I,K)-SIGZ(I,K))*SIN(2.*
     1ALPHA)/2.
      CFR(I,K)=ABS(SIGS(I,K)/SIGNR(I,K))
  490 CONTINUE
      RETURN
      END
```

B3. Listing of the finite element programme.

```
      PROGRAM FLAP 5 (DATA,OUTPUT,TAPE5=DATA,TAPE6=OUTPUT)                5FLP001
C     FLAP 5 IS AN INSTRUCTIONAL PROGRAM IN FINITE ELEMENT METHODS FOR  5FLP0020
C     THE APPLIED MECHANICS POST-GRADUATE COURSE AT IMPERIAL COLLEGE.   5FLP0030
C     IT ANALYSES ELASTICALLY THE DISPLACEMENTS IN AN AXISYMMETRICALLY  5FLP0040
C     LOADED BODY OF REVOLUTION ASSUMING A LINEAR DISPLACEMENT FIELD    5FLP0050
C     ACROSS AND PERFORMING A ONE POINT STIFFNESS INTEGRATION OVER EACH 5FLP0060
C     OF THE TRIANGULAR ELEMENTS INTO WHICH THE REVOLVED PLANE SECTION  5FLP0070
C     HAS BEEN DIVIDED.  WITH A COMPLETE OUT-OF-BALANCE FORCE TACTIC IT5FLP0080
C     PERMITS ALL FIXED AND LINEAR RESTRAINT CONDITIONS.  AS WELL AS    5FLP0090
C     WRITING ALL THE NON-ZERO STRESS COMPONENTS FOR BOTH ELEMENTS AND  5FLP0100
C     NODES - CALCULATED AT THE LATTER BY TAKING ARITHMETIC MEANS OVER  5FLP0110
C     SURROUNDING ELEMENTS - IT ALSO PROVIDES THE PRINCIPAL STRESSES AND5FLP0120
C     A MEAN STRESS FOR THE USER"S COMPARISON WITH THE PLASTIC YIELD    5FLP0130
C     STRESS.  FLAP 5 WAS DEVELOPED IN APRIL 1971 FROM FLAP 4 A FASTER 5FLP0140
C     VERSION WHICH DOES NOT PERMIT ALL RESTRAINT CONDITIONS.           5FLP0150
C                                                                       5FLP0160
C                                                                       5FLP0170
C    0 SPECIFICATION AND DATA INITIALIZATION STATEMENTS.                5FLP0180
      INTEGER  TITLE,   SR,      QA,      O,                           5FLP0190
     1         CASCTL,  WI,      ANP,     P,                           5FLP0200
     2                  COND,             Q                            5FLP0210
      REAL     NU,      K,       KRR,                                  5FLP0220
     1                          KRZ,                                   5FLP0230
     2                          KZR,                                   5FLP0240
     3                          KZZ                                    5FLP0250
      DIMENSION ENRR(350),ENTT(350),ENZZ(350),ENRZ(350)
      COMMON     TITLE (13), NPI (350),     R (200),       NB (100),    5FLP0260
     1           E (5),      NPJ (350),     Z (200),       COND (100),  5FLP0270
     2           NU (5),     NPM (350),     RR (200),      SLOPE (100), 5FLP0280
     3           RHO (5),    MAT (350),     RZ (200),                   5FLP0290
     4           ALPHA (5),  DELTAT (350),  U (200),                    5FLP0300
     5                                      V (200),                    5FLP0310
     1           BI (350),   KRR (200, 9),  ANP (200, 9),  SIGLRR (350),5FLP0320
     2           BJ (350),   KRZ (200, 9),  NAP (200),     SIGLTT (350),5FLP0330
     3           BM (350),   KZR (200, 9),  LN (3),        SIGLZZ (350),5FLP0340
     4           CI (350),   KZZ (200, 9),  B (4, 6),      SIGLRZ (350),5FLP0350
     5           CJ (350),   FRR (200),     D (4, 4),                   5FLP0360
     6           CM (350),   FRZ (200),     W (4, 6),                   5FLP0370
     7                       FZR (200),     K (6, 6),                   5FLP0380
     8                       FZZ (200)                                  5FLP0390
      DATA  CASCTL / 6HNFCASE /                                         5FLP0400
C                                                                       5FLP0410
C                                                                       5FLP0420
C   10 INPUT THE CASE TITLE BUT STOP IF THERE IS NO FURTHER CASE.       5FLP0430
   11 READ (5, 12)  TITLE                                               5FLP0440
   12 FORMAT (13A6)                                                     5FLP0450
      IF (TITLE (1) .EQ. CASCTL)  STOP                                  5FLP0460
C                                                                       5FLP0470
C                                                                       5FLP0480
C   20 INPUT THE CONTROL PARAMETERS AND PREPARE TO INPUT THE ARRAY DATA. 5FLP0490
      READ (5, 21)  NEL, NNP, NBR, NMAT, NCY, NCC, TOLER, OMEGA, SR, WI 5FLP0500
   21 FORMAT (6I5, E13.5, F7.3, 2I3)                                    5FLP0510
      DO 22  NM = 1, NMAT                                               5FLP0520
```

```
   22 E (NM) = -1.                                                          5FLP0530
      DO 23  L = 1, NEL                                                     5FLP0540
   23 NPI (L) = -1                                                          5FLP0550
      DO 24  N = 1, NNP                                                     5FLP0560
   24 R (N) = -0.123456789E35                                               5FLP0570
C                                                                           5FLP0580
C                                                                           5FLP0590
C  30 INPUT AND CHECK THE ARRAY DATA.                                       5FLP0600
      READ (5, 31)  (MATN, E (MATN), NU (MATN),                             5FLP0610
     1               RHO (MATN), ALPHA (MATN),  NM = 1, NMAT)             5FLP0620
   31 FORMAT (I5, 4E13.5)                                                   5FLP0630
      DO 33  NM = 1, NMAT                                                   5FLP0640
      IF (E (NM) .NE. -1.)  GO TO 33                                        5FLP0650
      WRITE (6, 32)  TITLE                                                  5FLP0660
   32 FORMAT (1H1 ////// 5H IN ", 13A6, 1H" /                               5FLP0670
     1        36H THERE IS A MISSING INPUT DATA CARD.,                       5FLP0680
     2        24H   THE JOB IS ABANDONED.)                                  5FLP0690
      STOP                                                                  5FLP0700
   33 CONTINUE                                                              5FLP0710
      READ (5, 34)  (LE, NPI (LE), NPJ (LE), NPM (LE),                     5FLP0720
     1               MAT (LE), DELTAT (LE),  L = 1, NEL)                   5FLP0730
   34 FORMAT (5I5, F10.3)                                                   5FLP0740
      DO 35  L = 1, NEL                                                     5FLP0750
      IF (NPI (L) .NE. -1)  GO TO 35                                        5FLP0760
      WRITE (6, 32)  TITLE                                                  5FLP0770
      STOP                                                                  5FLP0780
   35 CONTINUE                                                              5FLP0790
      READ (5, 36)  (NP, R (NP), Z (NP), RR (NP), RZ (NP),                 5FLP0800
     1               U (NP), V (NP),  N = 1, NNP)                          5FLP0810
   36 FORMAT (I5, 6E12.5)                                                   5FLP0820
      DO 37  N = 1, NNP                                                     5FLP0830
      IF (R (N) .NE. -0.123456789E35)  GO TO 37                             5FLP0840
      WRITE (6, 32)  TITLE                                                  5FLP0850
      STOP                                                                  5FLP0860
   37 CONTINUE                                                              5FLP0870
      READ (5, 38)  (NB (NR), COND (NR), SLOPE (NR),  NR = 1, NBR)         5FLP0880
   38 FORMAT (2I5, F10.5)                                                   5FLP0890
C                                                                           5FLP0900
C                                                                           5FLP0910
C  40 OUTPUT THE TITLE AND THE CONTROL PARAMETERS.                          5FLP0920
      WRITE (6, 41)                                                         5FLP0930
   41 FORMAT (1H1 //////                                                    5FLP0940
     1        45X, 41HTHE CASE TITLE AND THE CONTROL PARAMETERS /           5FLP0950
     2        45X, 41H---------------------------------------- /////)       5FLP0960
      WRITE (6, 42)  TITLE                                                  5FLP0970
   42 FORMAT (1H , 13A6)                                                    5FLP0980
      WRITE (6, 43)  NEL, NNP, NBR, NMAT, NCY, NCC, TOLER, OMEGA            5FLP0990
   43 FORMAT (26HOTHE NUMBER OF ELEMENTS IS, I5, 1H. /                      5FLP1000
     1        30HOTHE NUMBER OF NODAL POINTS IS, I5, 1H. /                  5FLP1010
     2        43HOTHE NUMBER OF RESTRAINED BOUNDARY NODES IS, I5, 1H. /     5FLP1020
     3        37HOTHE NUMBER OF DIFFERENT MATERIALS IS, I5, 1H. /           5FLP1030
     4        23HOTHE ITERATION LIMIT IS, I5, 8H CYCLES. /                  5FLP1040
     5        36HOTHE INTERVAL FOR PROGRESS OUTPUT IS, I5, 8H CYCLES. /     5FLP1050
     6        29HOTHE CONVERGENCE TOLERANCE IS, E13.5, 1H. /                5FLP1060
     7        30HOTHE OVER-RELAXATION FACTOR IS, F7.3, 1H. /                5FLP1070
```

```
     8        23HOSTRESSES ARE FOUND FOR)                                    5FLP1080
      IF (SR .EQ. 0)  WRITE (6, 44)                                          5FLP1090
   44 FORMAT (1H+, 23X, 42HNEITHER THE ELEMENTS NOR THE NODAL POINTS.)       5FLP1100
      IF (SR .EQ. 1)  WRITE (6, 45)                                          5FLP1110
   45 FORMAT (1H+, 23X, 18HTHE ELEMENTS ONLY.)                               5FLP1120
      IF (SR .EQ. 2)  WRITE (6, 46)                                          5FLP1130
   46 FORMAT (1H+, 23X, 22HTHE NODAL POINTS ONLY.)                           5FLP1140
      IF (SR .EQ. 3)  WRITE (6, 47)                                          5FLP1150
   47 FORMAT (1H+, 23X, 39HBOTH THE ELEMENTS AND THE NODAL POINTS.)          5FLP1160
      IF (WI .EQ. 0)  WRITE (6, 48)                                          5FLP1170
   48 FORMAT (37HOTHE INPUT ARRAY DATA ARE NOT OUTPUT.)                      5FLP1180
      IF (WI .EQ. 1)  WRITE (6, 49)                                          5FLP1190
   49 FORMAT (33HOTHE INPUT ARRAY DATA ARE OUTPUT.)                          5FLP1200
C                                                                            5FLP1210
C                                                                            5FLP1220
C  50 OUTPUT THE ARRAY DATA.                                                 5FLP1230
      IF (WI .EQ. 0)  GO TO 61                                               5FLP1240
      WRITE (6, 51)  (NM, E (NM), NU (NM), RHO (NM),                         5FLP1250
     1                ALPHA (NM),  NM = 1, NMAT)                            5FLP1260
   51 FORMAT (1H1 //////                                                     5FLP1270
     1        56X, 19HINPUT MATERIAL DATA /                                  5FLP1280
     2        56X, 19H------------------- /////                              5FLP1290
     3        28X, 42HMATERIAL  ELASTIC MODULUS  POISSON"S RATIO,            5FLP1300
     4             34H      DENSITY      THML EXPN COEFF //                  5FLP1310
     5        (I33, X, 4E17.5))                                              5FLP1320
      WRITE (6, 52)                                                          5FLP1330
   52 FORMAT (1H1 //////                                                     5FLP1340
     1        57X, 18HINPUT ELEMENT DATA /                                   5FLP1350
     2        57X, 18H------------------ /////                               5FLP1360
     3         3X, 48HELMT NPI  NPJ  NPM  MTRL  DELTA T                    , 5FLP1370
     4             48HELMT NPI  NPJ  NPM  MTRL  DELTA T                    , 5FLP1380
     5             33HELMT NPI  NPJ  NPM  MTRL  DELTA T /)                   5FLP1390
      L1 = (NEL + 2) / 3                                                     5FLP1400
      DO 53  L2 = 1, L1                                                      5FLP1410
      L3 = MINO (L2 + 2 * L1, NEL)                                           5FLP1420
   53 WRITE (6, 54)  (L, NPI (L), NPJ (L), NPM (L),                          5FLP1430
     1                MAT (L), DELTAT (L),  L = L2, L3, L1)                 5FLP1440
   54 FORMAT (1H , 5I5, F10.3, 13X, 5I5, F10.3, 13X, 5I5, F10.3)             5FLP1450
      WRITE (6, 55)  (N, R (N), Z (N), RR (N), RZ (N),                       5FLP1460
     1                U (N), V (N),  N = 1, NNP)                            5FLP1470
   55 FORMAT (1H1 //////                                                     5FLP1480
     1        58X, 15HINPUT NODE DATA /                                      5FLP1490
     2        58X, 15H--------------- /////                                  5FLP1500
     3        13X, 49HNODE          R               Z                     ,5FLP1510
     4             31HRR              RZ            ,                       5FLP1520
     5             21H   U               V //                               5FLP1530
     6        (I16, X, 6E17.5))                                              5FLP1540
      WRITE (6, 56)  (NB (NR), COND (NR), SLOPE (NR),  NR = 1, NBR)          5FLP1550
   56 FORMAT (1H1 //////                                                     5FLP1560
     1        48X, 35HINPUT RESTRAINED BOUNDARY NODE DATA /                  5FLP1570
     2        48X, 35H---------------------------------- /////               5FLP1580
     3        33X, 28HRESTND BNDY NODE          ,                            5FLP1590
     4             37HRESTNT CONDITION              SLOPE //                 5FLP1600
     5        (I42, I27, F30.5))                                             5FLP1610
C                                                                            5FLP1620
```

```
C                                                                       5FLP1630
C  60 DO GEOMETRIC CALCULATIONS ON THE ELEMENTS.                        5FLP1640
   61 DO 72  L = 1, NEL                                                 5FLP1650
      I = NPI (L)                                                       5FLP1660
      J = NPJ (L)                                                       5FLP1670
      M = NPM (L)                                                       5FLP1680
      BI (L) = Z (J) - Z (M)                                            5FLP1690
      BJ (L) = Z (M) - Z (I)                                            5FLP1700
      BM (L) = Z (I) - Z (J)                                            5FLP1710
      CI (L) = - R (J) + R (M)                                          5FLP1720
      CJ (L) = - R (M) + R (I)                                          5FLP1730
      CM (L) = - R (I) + R (J)                                          5FLP1740
      AREA = (BJ (L) * CM (L) - BM (L) * CJ (L)) / 2.                   5FLP1750
      IF (AREA .GT. 1.E-35)  GO TO 71                                   5FLP1760
      WRITE (6, 62)  L                                                  5FLP1770
   62 FORMAT (1H1 ////// 8H ELEMENT, I5, 25H HAS A NON-POSITIVE AREA. / 5FLP1780
     1        23H THE CASE IS ABANDONED.)                               5FLP1790
      GO TO 221                                                         5FLP1800
C                                                                       5FLP1810
C                                                                       5FLP1820
C  70 SUM THE TOTAL NODAL POINT FORCES.                                 5FLP1830
   71 MATN = MAT (L)                                                    5FLP1840
      RBAR = (R (I) + R (J) + R (M)) / 3.                               5FLP1850
      W1 = 3.1415926536 * RBAR * E (MATN) * ALPHA (MATN) * DELTAT (L)   5FLP1860
     1                                    / (1. - 2. * NU (MATN))      5FLP1870
      W2 = (2. * AREA) / (3. * RBAR)                                    5FLP1880
      BODYF = 2. * 3.1415926536 * RBAR * AREA * RHO (MATN) / 3.         5FLP1890
      RR (I) = RR (I) + W1 * (BI (L) + W2)                              5FLP1900
      RZ (I) = RZ (I) + W1 *  CI (L)       - BODYF                      5FLP1910
      RR (J) = RR (J) + W1 * (BJ (L) + W2)                              5FLP1920
      RZ (J) = RZ (J) + W1 *  CJ (L)       - BODYF                      5FLP1930
      RR (M) = RR (M) + W1 * (BM (L) + W2)                              5FLP1940
   72 RZ (M) = RZ (M) + W1 *  CM (L)       - BODYF                      5FLP1950
C                                                                       5FLP1960
C                                                                       5FLP1970
C  80 PREPARE TO SUM THE STIFFNESS COEFFICIENTS.                        5FLP1980
      DO 82  N = 1, NNP                                                 5FLP1990
      DO 81  QA = 1, 9                                                  5FLP2000
      KRR (N, QA) = 0.                                                  5FLP2010
      KRZ (N, QA) = 0.                                                  5FLP2020
      KZR (N, QA) = 0.                                                  5FLP2030
      KZZ (N, QA) = 0.                                                  5FLP2040
   81 ANP (N, QA) = 0                                                   5FLP2050
      ANP (N, 1) = N                                                    5FLP2060
   82 NAP (N) = 1                                                       5FLP2070
C                                                                       5FLP2080
C                                                                       5FLP2090
C  90 FORM THE STIFFNESS MATRIX FOR THE ELEMENT.                        5FLP2100
      DO 105  L = 1, NEL                                                5FLP2110
      DO 92  P = 1, 4                                                   5FLP2120
      DO 91  Q = 1, 6                                                   5FLP2130
   91 B (P, Q) = 0.                                                     5FLP2140
      DO 92  Q = 1, 4                                                   5FLP2150
   92 D (P, Q) = 0.                                                     5FLP2160
      B (1, 1) = BI (L)                                                 5FLP2170
```

```
      B (1, 3) = BJ (L)                                                    5FLP2180
      B (1, 5) = BM (L)                                                    5FLP2190
      AREA = (BJ (L) * CM (L) - BM (L) * CJ (L)) / 2.                      5FLP2200
      I = NPI (L)                                                          5FLP2210
      J = NPJ (L)                                                          5FLP2220
      M = NPM (L)                                                          5FLP2230
      RBAR = (R (I) + R (J) + R (M)) / 3.                                  5FLP2240
      W1 = (2. * AREA) / (3. * RBAR)                                       5FLP2250
      B (2, 1) = W1                                                        5FLP2260
      B (2, 3) = W1                                                        5FLP2270
      B (2, 5) = W1                                                        5FLP2280
      B (3, 2) = CI (L)                                                    5FLP2290
      B (3, 4) = CJ (L)                                                    5FLP2300
      B (3, 6) = CM (L)                                                    5FLP2310
      B (4, 1) = CI (L)                                                    5FLP2320
      B (4, 2) = BI (L)                                                    5FLP2330
      B (4, 3) = CJ (L)                                                    5FLP2340
      B (4, 4) = BJ (L)                                                    5FLP2350
      B (4, 5) = CM (L)                                                    5FLP2360
      B (4, 6) = BM (L)                                                    5FLP2370
      MATN = MAT (L)                                                       5FLP2380
      W1 = NU (MATN)                                                       5FLP2390
      W2 = 1. - W1                                                         5FLP2400
      W3 = 1. + W1                                                         5FLP2410
      W4 = 1. - 2. * W1                                                    5FLP2420
      W5 = 3.1415926536 * RBAR * E (MATN) / (2. * AREA * W3 * W4)          5FLP2430
      D (1, 1) = W5 * W2                                                   5FLP2440
      D (1, 2) = W5 * W1                                                   5FLP2450
      D (1, 3) = W5 * W1                                                   5FLP2460
      D (2, 1) = W5 * W1                                                   5FLP2470
      D (2, 2) = W5 * W2                                                   5FLP2480
      D (2, 3) = W5 * W1                                                   5FLP2490
      D (3, 1) = W5 * W1                                                   5FLP2500
      D (3, 2) = W5 * W1                                                   5FLP2510
      D (3, 3) = W5 * W2                                                   5FLP2520
      D (4, 4) = W5 * W4 / 2.                                              5FLP2530
      DO 93  P = 1, 4                                                      5FLP2540
      DO 93  Q = 1, 6                                                      5FLP2550
      W (P, Q) = 0.                                                        5FLP2560
      DO 93  O = 1, 4                                                      5FLP2570
   93 W (P, Q) = W (P, Q) + D (P, O) * B (O, Q)                            5FLP2580
      DO 94  P = 1, 6                                                      5FLP2590
      DO 94  Q = 1, 6                                                      5FLP2600
      K (P, Q) = 0.                                                        5FLP2610
      DO 94  O = 1, 4                                                      5FLP2620
   94 K (P, Q) = K (P, Q) + B (O, P) * W (O, Q)                            5FLP2630
C                                                                          5FLP2640
C                                                                          5FLP2650
C 100 SUM AND STORE FOR EACH (FORCED) NODE THE NON-ZERO STIFFNESS          5FLP2660
C     COEFFICIENTS FOR THE ADJACENT (DISPLACED) NODES.                     5FLP2670
      LN (1) = NPI (L)                                                     5FLP2680
      LN (2) = NPJ (L)                                                     5FLP2690
      LN (3) = NPM (L)                                                     5FLP2700
      DO 105  P = 1, 3                                                     5FLP2710
      NP = LN (P)                                                          5FLP2720
```

```
      DO 105  Q = 1, 3                                                    5FLP2730
      QA = 0                                                              5FLP2740
  101 QA = QA + 1                                                         5FLP2750
      IF (QA .LE. 9)  GO TO 103                                           5FLP2760
      WRITE (6, 102)  NP                                                  5FLP2770
  102 FORMAT (1H1 ////// 5H NODE, I5,                                     5FLP2780
     1        36H HAS MORE THAN EIGHT ADJACENT NODES. /                   5FLP2790
     2        23H THE CASE IS ABANDONED.)                                 5FLP2800
      GO TO 221                                                           5FLP2810
  103 IF (ANP (NP, QA) .EQ. LN (Q))  GO TO 104                            5FLP2820
      IF (ANP (NP, QA) .NE. 0)  GO TO 101                                 5FLP2830
      ANP (NP, QA) = LN (Q)                                               5FLP2840
      NAP (NP) = QA                                                       5FLP2850
  104 KRR (NP, QA) = KRR (NP, QA) + K (2 * P - 1, 2 * Q - 1)              5FLP2860
      KRZ (NP, QA) = KRZ (NP, QA) + K (2 * P - 1, 2 * Q)                  5FLP2870
      KZR (NP, QA) = KZR (NP, QA) + K (2 * P, 2 * Q - 1)                  5FLP2880
  105 KZZ (NP, QA) = KZZ (NP, QA) + K (2 * P, 2 * Q)                      5FLP2890
C                                                                         5FLP2900
C                                                                         5FLP2910
C 110 BY INVERSION OF THE MAIN DIAGONAL STIFFNESS SUBMATRIX, FIND THE     5FLP2920
C     FLEXIBILITY SUBMATRIX AT EACH NODE DISPLACED BY FORCES AT ITSELF.   5FLP2930
      DO 112  N = 1, NNP                                                  5FLP2940
      W1 = KRR (N, 1) * KZZ (N, 1) - KRZ (N, 1) * KZR (N, 1)              5FLP2950
      FRR (N) =   KZZ (N, 1) / W1                                         5FLP2960
      FRZ (N) = - KRZ (N, 1) / W1                                         5FLP2970
      FZR (N) = - KZR (N, 1) / W1                                         5FLP2980
  112 FZZ (N) =   KRR (N, 1) / W1                                         5FLP2990
C                                                                         5FLP3000
C                                                                         5FLP3010
C 120 CALCULATE THE EFFECTIVE SELF FLEXIBILITY SUBMATRICES FOR THE        5FLP3020
C     RESTRAINED BOUNDARY NODES.                                          5FLP3030
      DO 125  NR = 1, NBR                                                 5FLP3040
      NP = NB (NR)                                                        5FLP3050
      IF (COND (NR) - 1)  123, 122, 121                                   5FLP3060
  121 FRR (NP) = (FRR (NP) * FZZ (NP) - FRZ (NP) * FZR (NP))              5FLP3070
     1               / (FRR (NP) * SLOPE (NR) ** 2                        5FLP3080
     2                  - (FRZ (NP) + FZR (NP)) * SLOPE (NR) + FZZ (NP))5FLP3090
      FRZ (NP) = FRR (NP) * SLOPE (NR)                                    5FLP3100
      FZR (NP) = FRZ (NP)                                                 5FLP3110
      FZZ (NP) = FRZ (NP) * SLOPE (NR)                                    5FLP3120
      GO TO 125                                                           5FLP3130
  122 FZZ (NP) = FZZ (NP) - FZR (NP) * FRZ (NP) / FRR (NP)                5FLP3140
      GO TO 124                                                           5FLP3150
  123 FZZ (NP) = 0.                                                       5FLP3160
  124 FRR (NP) = 0.                                                       5FLP3170
      FRZ (NP) = 0.                                                       5FLP3180
      FZR (NP) = 0.                                                       5FLP3190
  125 CONTINUE                                                            5FLP3200
C                                                                         5FLP3210
C                                                                         5FLP3220
C 130 PERFORM A GAUSS - SEIDEL ITERATION ON THE STIFFNESS MATRIX FOR      5FLP3230
C     THE ENTIRE STRUCTURE.                                               5FLP3240
      IF (NCC .GT. NCY)  GO TO 132                                        5FLP3250
      WRITE (6, 131)                                                      5FLP3260
  131 FORMAT (1H1 //////                                                  5FLP3270
```

```
     1        34X, 35HTHE PROGRESS OF THE GAUSS - SEIDEL ,                5FLP3280
     2             28HITERATION TOWARD CONVERGENCE /                      5FLP3290
     3        34X, 35H-----------------------------------,                5FLP3300
     4             28H---------------------------- /////                  5FLP3310
     5        33X, 39HCYCLE              CONVERGENCE CRITERION,           5FLP3320
     6             26H        CURRENT DIFFERENCE)                         5FLP3330
   132 NC = 0                                                              5FLP3340
   133 SD = 0.                                                             5FLP3350
       SDD = 0.                                                            5FLP3360
       DO 136  N = 1, NNP                                                  5FLP3370
       IF (FRR (N) + FZZ (N) .EQ. 0.)  GO TO 136                           5FLP3380
       RR1 = RR (N)                                                        5FLP3390
       RZ1 = RZ (N)                                                        5FLP3400
       NAP1 = NAP (N)                                                      5FLP3410
       DO 134  QA = 1, NAP1                                                5FLP3420
       NP = ANP (N, QA)                                                    5FLP3430
       RR1 = RR1 - KRR (N, QA) * U (NP) - KRZ (N, QA) * V (NP)             5FLP3440
   134 RZ1 = RZ1 - KZR (N, QA) * U (NP) - KZZ (N, QA) * V (NP)             5FLP3450
       IF (FRR (N) .EQ. 0.)  GO TO 135                                     5FLP3460
       DELTAU = FRR (N) * RR1 + FRZ (N) * RZ1                              5FLP3470
       U (N) = U (N) + OMEGA * DELTAU                                      5FLP3480
       SD = SD + ABS (U (N))                                               5FLP3490
       SDD = SDD + ABS (DELTAU)                                            5FLP3500
       IF (FZZ (N) .EQ. 0.)  GO TO 136                                     5FLP3510
   135 DELTAV = FZR (N) * RR1 + FZZ (N) * RZ1                              5FLP3520
       V (N) = V (N) + OMEGA * DELTAV                                      5FLP3530
       SD = SD + ABS (V (N))                                               5FLP3540
       SDD = SDD + ABS (DELTAV)                                            5FLP3550
   136 CONTINUE                                                            5FLP3560
       SD = AMAX1 (SD, 1.E-35)                                             5FLP3570
       RELDIF = SDD / SD                                                   5FLP3580
C                                                                          5FLP3590
C                                                                          5FLP3600
C  140 TEST FOR CONVERGENCE.                                               5FLP3610
       NC = NC + 1                                                         5FLP3620
       IF (NCC .GT. NCY .OR. MOD (NC, NCC) .NE. 0)  GO TO 142              5FLP3630
       WRITE (6, 141)  NC, TOLER, RELDIF                                   5FLP3640
   141 FORMAT (1H0, I36, 3X, 2E27.5)                                       5FLP3650
   142 IF (RELDIF .GT. TOLER)  GO TO 144                                   5FLP3660
       WRITE (6, 143)  NC                                                  5FLP3670
   143 FORMAT (1H1 ////// 28H THE ITERATION HAS CONVERGED,                 5FLP3680
     1        6H AFTER, I5, 8H CYCLES.)                                   5FLP3690
       GO TO 151                                                           5FLP3700
   144 IF (NC .LT. NCY)  GO TO 133                                         5FLP3710
       WRITE (6, 145)  NC, RELDIF, TOLER                                   5FLP3720
   145 FORMAT (1H1 ////// 28H THE ITERATION HAS COMPLETED, I5, 5H THE ,    5FLP3730
     1        52HMAXIMUM NUMBER OF CYCLES WITHOUT CONVERGING, BUT HAS /   5FLP3740
     2        34H ACHIEVED A RELATIVE DIFFERENCE OF, E13.5,               5FLP3750
     3        33H AGAINST A SPECIFIED TOLERANCE OF, E13.5, 1H. /          5FLP3760
     4        43H THE UNCONVERGED RESULTS ARE WRITTEN BELOW.)             5FLP3770
C                                                                          5FLP3780
C                                                                          5FLP3790
C  150 OUTPUT THE NODE DISPLACEMENTS IN THE PLANE SECTION REVOLVED.        5FLP3800
   151 WRITE (6, 152)                                                      5FLP3810
   152 FORMAT (1H1 //////                                                  5FLP3820
```

```
     1        49X, 33HTHE CALCULATED NODE DISPLACEMENTS /                    5FLP3830
     2        49X, 33H---------------------------------- /////               5FLP3840
     3         3X, 47HNODE         U                 V                ,     5FLP3850
     4             47HNODE         U                 V                ,     5FLP3860
     5             30HNODE         U                 V /)                   5FLP3870
      N1 = (NNP + 2) / 3                                                     5FLP3880
      DO 153  N2 = 1, N1                                                     5FLP3890
      N3 = MINO (N2 + 2 * N1, NNP)                                           5FLP3900
  153 WRITE (6, 154)  (N, U (N), V (N),  N = N2, N3, N1)                     5FLP3910
  154 FORMAT (1H , I5, 2E16.5, I15, 2E16.5, I15, 2E16.5)                     5FLP3920
C                                                                            5FLP3930
C                                                                            5FLP3940
C 160 CALCULATE THE ELEMENT STRESS COMPONENTS.                               5FLP3950
      IF (SR .EQ. 0)  GO TO 221                                              5FLP3960
      DO 184  L = 1, NEL                                                     5FLP3970
      I = NPI (L)                                                            5FLP3980
      J = NPJ (L)                                                            5FLP3990
      M = NPM (L)                                                            5FLP4000
      AREA = (BJ (L) * CM (L) - BM (L) * CJ (L)) / 2.                        5FLP4010
      RBAR = (R (I) + R (J) + R (M)) / 3.                                    5FLP4020
      EERR = (BI (L) * U (I) + BJ (L) * U (J)                                5FLP4030
     1                       + BM (L) * U (M)) / (2. * AREA)                 5FLP4040
      EETT = (U (I) + U (J) + U (M)) / (3. * RBAR)                           5FLP4050
      EEZZ = (CI (L) * V (I) + CJ (L) * V (J)                                5FLP4060
     1                       + CM (L) * V (M)) / (2. * AREA)                 5FLP4070
      EERZ = (CI (L) * U (I) + BI (L) * V (I)                                5FLP4080
     1      + CJ (L) * U (J) + BJ (L) * V (J)                                5FLP4090
     2      + CM (L) * U (M) + BM (L) * V (M)) / (2. * AREA)                 5FLP4100
      MATN = MAT (L)                                                         5FLP4110
      W1 = NU (MATN)                                                         5FLP4120
      W2 = 1. - W1                                                           5FLP4130
      W3 = 1. + W1                                                           5FLP4140
      W4 = 1. - 2. * W1                                                      5FLP4150
      W5 = E (MATN) / (W3 * W4)                                              5FLP4160
      ETH = ALPHA (MATN) * DELTAT (L)                                        5FLP4170
      ERR = EERR - ETH                                                       5FLP4180
      ETT = EETT - ETH                                                       5FLP4190
      EZZ = EEZZ - ETH                                                       5FLP4200
      ERZ = EERZ                                                             5FLP4210
      SIGLRR (L) = W5 * (W2 * ERR + W1 * ETT + W1 * EZZ)                     5FLP4220
      SIGLTT (L) = W5 * (W1 * ERR + W2 * ETT + W1 * EZZ)                     5FLP4230
      SIGLZZ (L) = W5 * (W1 * ERR + W1 * ETT + W2 * EZZ)                     5FLP4240
      SIGLRZ (L) = W5 * W4 * ERZ / 2.                                        5FLP4250
C                                                                            5FLP4260
C                                                                            5FLP4270
C 170 CALCULATE THE ELEMENT PRINCIPAL AND MEAN STRESSES IN THE PLANE         5FLP4280
C     SECTION REVOLVED.                                                      5FLP4290
      IF (SR .EQ. 2)  GO TO 184                                              5FLP4300
      W1 = (SIGLRR (L) + SIGLZZ (L)) / 2.                                    5FLP4310
      W2 = (SIGLRR (L) - SIGLZZ (L)) / 2.                                    5FLP4320
      W3 = SIGLRZ (L)                                                        5FLP4330
      W4 = SQRT (W2 ** 2 + W3 ** 2)                                          5FLP4340
      SIGL1 = W1 + W4                                                        5FLP4350
      SIGL2 = W1 - W4                                                        5FLP4360
      IF (ABS (W2) .GT. 1.E-35 .OR. ABS (W3) .GT. 1.E-35)  GO TO 171         5FLP4370
```

```
      ANGLEL = 0.                                                        5FLP4380
      GO TO 172                                                          5FLP4390
  171 ANGLEL = 28.647889756 * ATAN2 (W3, W2)                             5FLP4400
  172 SIGL3 = SIGLTT (L)                                                 5FLP4410
      SIGLM = SQRT ((SIGL1 + SIGL2 + SIGL3) ** 2                         5FLP4420
     1           - 3. * (SIGL2 * SIGL3 + SIGL3 * SIGL1 + SIGL1 * SIGL2))5FLP4430
C 180 OUTPUT THE ELEMENT STRESSES.                                       5FLP4460
      IF (L .NE. 1)  GO TO 182                                           5FLP4470
C                                                                        5FLP4440
C                                                                        5FLP4450
      WRITE (6, 181)                                                     5FLP4480
  181 FORMAT (1H1 //////                                                 5FLP4490
     1         4X, 44HTHE CALCULATED ELEMENT STRESS COMPONENTS AND,      5FLP4500
     2             43H MEAN STRESS IN THE SPACE AND THE PRINCIPAL,       5FLP4510
     3             39H STRESSES IN THE PLANE SECTION REVOLVED /          5FLP4520
     4         4X, 44H----------------------------------------------,    5FLP4530
     5             43H----------------------------------------------,    5FLP4540
     6             39H---------------------------------------- /////    5FLP4550
     7         1X, 45HELEMENT      SIGMRR          SIGMTT          ,     5FLP4560
     8             45HSIGMZZ          SIGMRZ        ANGLE1        ,     5FLP4570
     9             37HSIGM1           SIGM2           SIGMM /)            5FLP4580
  182 WRITE (6, 183)  L, SIGLRR (L), SIGLTT (L), SIGLZZ (L),             5FLP4590
     1                SIGLRZ (L), ANGLEL, SIGL1, SIGL2, SIGLM            5FLP4600
  183 FORMAT (1H , I5, 4E16.5, F12.2, X, 3E16.5)                         5FLP4610
  184 CONTINUE                                                           5FLP4620
      IF (SR .EQ. 1)  GO TO 221                                          5FLP4630
C                                                                        5FLP4640
C                                                                        5FLP4650
C 190 FIND THE NODE STRESS COMPONENTS.                                   5FLP4660
      DO 212  N = 1, NNP                                                 5FLP4670
      SIGNRR = 0.                                                        5FLP4680
      SIGNTT = 0.                                                        5FLP4690
      SIGNZZ = 0.                                                        5FLP4700
      SIGNRZ = 0.                                                        5FLP4710
      QA = 1                                                             5FLP4720
      DO 191  L = 1, NEL                                                 5FLP4730
      IF (NPI (L) .NE. N .AND. NPJ (L) .NE. N .AND. NPM (L) .NE. N)      5FLP4740
     1                                                    GO TO 1915FLP4750
      SIGNRR = SIGNRR + SIGLRR (L)                                       5FLP4760
      SIGNTT = SIGNTT + SIGLTT (L)                                       5FLP4770
      SIGNZZ = SIGNZZ + SIGLZZ (L)                                       5FLP4780
      SIGNRZ = SIGNRZ + SIGLRZ (L)                                       5FLP4790
      QA = QA + 1                                                        5FLP4800
      IF (QA .EQ. NAP (N))  GO TO 192                                    5FLP4810
  191 CONTINUE                                                           5FLP4820
  192 W1 = FLOAT (QA - 1)                                                5FLP4830
      SIGNRR = SIGNRR / W1                                               5FLP4840
      SIGNTT = SIGNTT / W1                                               5FLP4850
      SIGNZZ = SIGNZZ / W1                                               5FLP4860
      SIGNRZ = SIGNRZ / W1                                               5FLP4870
C                                                                        5FLP4880
C     FIND THE NODE STRAIN COMPONENTS.
      W1=1./E(1)
      W2=NU(1)
      W3=2.*(1.+W2)*W1
```

```
      ENRR(N)=W1*(SIGNRR-W2*(SIGNZZ+SIGNTT))
      ENTT(N)=W1*(SIGNTT-W2*(SIGNRR+SIGNZZ))
      ENZZ(N)=W1*(SIGNZZ-W2*(SIGNTT+SIGNRR))
      ENRZ(N)=W3*SIGNRZ
C                                                                      5FLP4890
C 200 CALCULATE THE NODE PRINCIPAL AND MEAN STRESSES IN THE PLANE      5FLP4900
C     SECTION REVOLVED.                                                5FLP4910
  201 W1 = (SIGNRR + SIGNZZ) / 2.                                      5FLP4920
      W2 = (SIGNRR - SIGNZZ) / 2.                                      5FLP4930
      W3 = SIGNRZ                                                      5FLP4940
      W4 = SQRT (W2 ** 2 + W3 ** 2)                                    5FLP4950
      SIGN1 = W1 + W4                                                  5FLP4960
      SIGN2 = W1 - W4                                                  5FLP4970
      IF (ABS (W2) .GT. 1.E-35 .OR. ABS (W3) .GT. 1.E-35)  GO TO 202   5FLP4980
      ANGLEN = 0.                                                      5FLP4990
      GO TO 203                                                        5FLP5000
  202 ANGLEN = 28.647889756 * ATAN2 (W3, W2)                           5FLP5010
  203 SIGN3 = SIGNTT                                                   5FLP5020
      SIGNM = SQRT ((SIGN1 + SIGN2 + SIGN3) ** 2                       5FLP5030
     1           - 3. * (SIGN2 * SIGN3 + SIGN3 * SIGN1 + SIGN1 * SIGN2))5FLP5040
C                                                                      5FLP5050
C                                                                      5FLP5060
C 210 OUTPUT THE NODE STRESSES.                                        5FLP5070
      IF (N .NE. 1)  GO TO 212                                         5FLP5080
      WRITE (6, 211)                                                   5FLP5090
  211 FORMAT (1H1 //////                                               5FLP5100
     1         6X, 41HTHE CALCULATED NODE STRESS COMPONENTS AND,       5FLP5110
     2             43H MEAN STRESS IN THE SPACE AND THE PRINCIPAL,     5FLP5120
     3             39H STRESSES IN THE PLANE SECTION REVOLVED /        5FLP5130
     4         6X, 41H----------------------------------------,        5FLP5140
     5             43H----------------------------------------,        5FLP5150
     6             39H---------------------------------------- /////   5FLP5160
     7         3X, 43HNODE       SIGMRR          SIGMTT          ,     5FLP5170
     8             45HSIGMZZ          SIGMRZ        ANGLE1         ,    5FLP5180
     9             37HSIGM1           SIGM2           SIGMM /)         5FLP5190
  212 WRITE (6, 213)  N, SIGNRR, SIGNTT, SIGNZZ, SIGNRZ,               5FLP5200
     1                ANGLEN, SIGN1, SIGN2, SIGNM                      5FLP5210
  213 FORMAT (1H , I5, 4E16.5, F12.2, X, 3E16.5)                       5FLP5220
C                                                                      5FLP5230
C 300 OUTPUT THE NODE STRAIN COMPONENTS.
      WRITE(6,301)
  301 FORMAT(1H1,///,
     1     47X,37HTHE CALCULATED NODE STRAIN COMPONENTS/,
     2     47X,37H----------------------------------//,
     34X,4HNODE,7X,8HSTRAIN-R,7X,8HSTRAIN-T,7X,8HSTRAIN-Z,6X,
     49HSTRAIN-RZ,1X,4HNODE,7X,8HSTRAIN-R,7X,8HSTRAIN-T,7X,8HSTRAIN-Z,
     56X,9HSTRAIN-RZ//)
      WRITE(6,302) (N,ENRR(N),ENTT(N),ENZZ(N),ENRZ(N),N=1,NNP)
  302 FORMAT(3X,2(I5,4E15.4))
C                                                                      5FLP5240
C 220 RETURN TO THE BEGINNING OF THE PROGRAM FOR THE NEXT CASE.        5FLP5250
  221 GO TO 11                                                         5FLP5260
      END                                                              5FLP5270
```

APPENDIX C

PRESSURE DISTRIBUTION AND FRICTION IN EXTRUSION CONTAINERS

B. LENGYEL and D. MUTLU
Department of Mechanical Engineering, Imperial College, London

SUMMARY

Experiments and apparatus are described to obtain frictional loads in extrusion and pressure distribution in extrusion containers.

Lead and aluminium specimens were extruded into rods by forward extrusion and into cans by backward extrusion, while loads at both ends of the billet, together with hoop and axial strains on the outside diameter of the containers were recorded simultaneously. Experimental frictional loads and pressure distributions in the container bore are presented for various extrusion conditions.

INTRODUCTION

A number of experimental methods have been used in the past to obtain pressure distribution in conventional extrusion containers. A brief survey was given by LENGYEL and MUSUVA [1] which will not be repeated here. They themselves used a foil strain gauge method and presented hoop strains and approximate pressure distributions on the container wall during the direct (forward) extrusion of lead rods at room temperature at slow speeds, at various extrusion ratios and lubrication conditions.

This work has now been extended in several directions. In addition to lead, commercial purity aluminium has also been extruded, so as to obtain experimental results relating to work hardening materials used in industrial production. Furthermore, in addition to the forward extrusion of rods, the backward extrusion of cans has also been investigated, a method widely used in the production of engineering components. Finally, the loads on the pressure pads and dies at each end of the billets have been recorded simultaneously in all cases, which give a good indication of frictional forces on the container wall under various conditions. Selected results of this experimental investigation will be described in what follows.

The significance of pressure distribution on the container wall, as a function of mean punch pressure, has been outlined in reference [1]. The determination of container/billet friction is becoming essential in the design of clamps for semi-continuous hydrostatic extrusion [2] and, more recently, for the various alternatives of continuous extrusion. A common feature of all these processes is that the billet is restrained or moved towards the die by frictional forces between the clamp or container and the plastically deforming billet. Clearly, it is essential to predict these frictional forces before production equipment could be designed with any confidence, which was the aim of the work of ALEXANDER and SAID relating to semi-continuous hydrostatic extrusion [3]. A brief outline of the various friction assisted extrusion processes and a reference list were given by LENGYEL and KAMYAB [4].

Experimental Apparatus

The extrusion tools used in the present work are illustrated in Fig.1. The design pressure for the monobloc containers was kept within the elastic limit at 28 tonf/in^2 (≈ 462 MN/m^2). The tools were fitted to a 50 tonf (500 kN) DENNISON hydraulic compression testing machine and operated at a slow speed. Strain gauge load cells have been used to record loads on the pressure pads and dies simultaneously. The location of the loads cells is indicated in Fig.1.

Thirteen strain gauges were bonded onto the outside diameter of each container, eight to measure hoop strains and five for axial strains. The same number of strain gauges were bonded onto a dummy container in both cases and connected to a strain gauge bridge.

Extrusion ratios of 2, 3, 4, 9 and 16 with die semi-angles of 25°, 30°, 35°, 45°, 51° and 76° were used in forward extrusion while the same extrusion ratios with square and 45° dies were used in backward extrusion.

A variable resistance type displacement transducer to measure punch displacement, the strain gauge load cells to measure loads on the pressure pads and dies and the container strain gauges were connected to a SOLARTRON LP 1029 Digital Data Recorder which could record the output data at speeds of up to 10 samples per second. The extrusion speed was slow

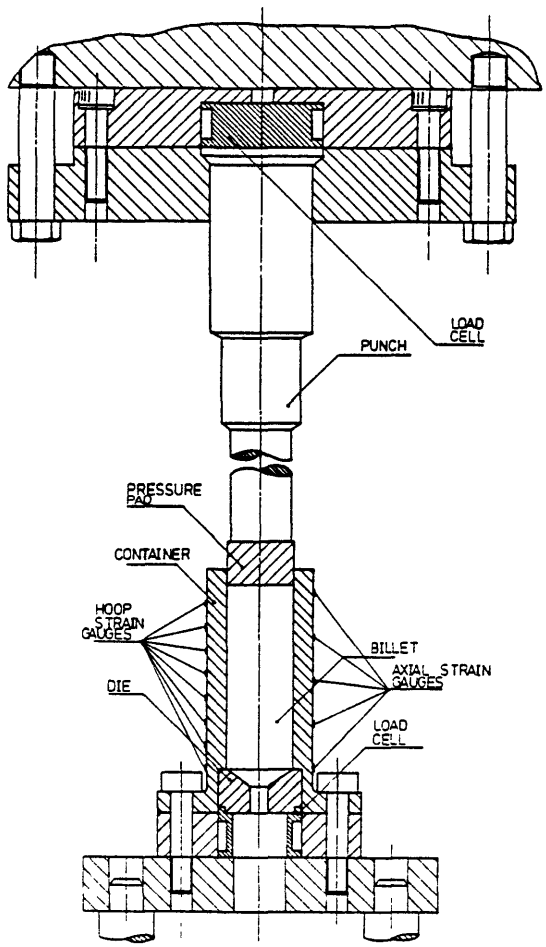


Fig.1a Experimental Apparatus for the Forward Extrusion of Rod

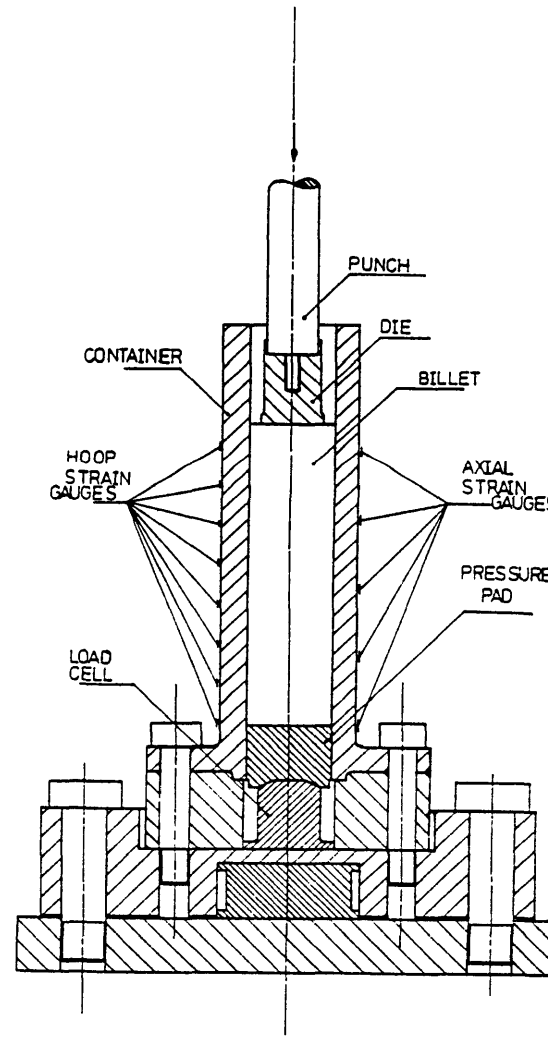


Fig.1b Experimental Apparatus for the Backward Extrusion of Can

so that a single scan of all channels could be considered as the simultaneous recording of the output signals. The recorder converted the signals into digital form and either printed or punched them out onto a paper tape.

The load cells and displacement transducers were calibrated in a high precision testing machine, while known pressures were applied to the bore of the containers in a HARWOOD Controlled Clearance Piston Gauge when calibrating the container strain gauges. All calibrations were carried out by recording the output signals on the SOLARTRON Recorder. The hoop strains were then plotted against pressures at various positions of a sealed plug which simulated the various positions of the pressure pad in forward extrusion and of the die in the backward extrusion experiments. The calibration curves were similar to those given in reference /1/ and they are not shown here.

Results and Discussions

30 mm diameter billets with 83 mm and 110 mm initial lengths were used for forward and backward extrusion respectively. Before each extrusion the tools and billets were carefully cleaned to ensure a good repeatability of the results. Extrusions were carried out either in the dry condition, or the billets and tools were lubricated with molybdenum disulphide in solution or with castor oil.

Fig.2 illustrates that, in forward extrusion, the container/billet friction

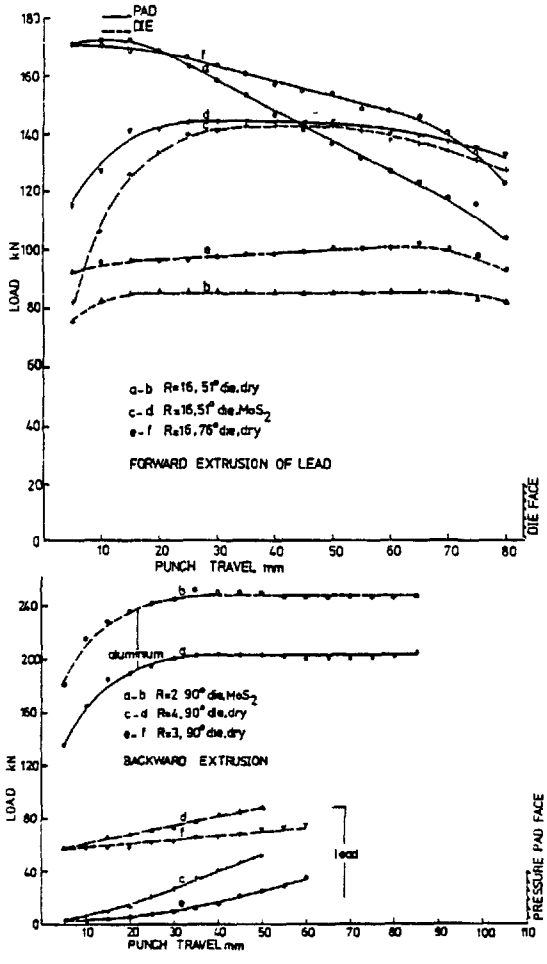


Fig.2 Pressures on the Pressure Pad and Die in Forward Extrusion and in Backward Extrusion

results in considerably higher initial loads on the pressure pad than on the die and, as the unextruded billet length decreases, the difference becomes smaller as would be expected. Initially friction accounts for a considerable proportion of the total load, so that the accuracy of theoretical predictions is likely to be influenced greatly by the assumed frictional conditions.

In backward extrusion the load on the die is higher than on the pressure pad throughout the process. But for the friction at the container/extruded can interface, the difference in the forces at the two ends of the unextruded billet would become once more smaller as extrusion proceeds. The fact that the frictional force is considerable relative to the total extrusion load indicates that it should be feasible to design clamps of reasonable lengths for continuous extrusion, which agrees with earlier experiments [5] and with the findings of ALEXANDER and SAID [3].

Fig.3 illustrates hoop strains on the outside diameter of the container under various conditions. The results for forward extrusion are qualitatively similar to those of LENGYEL and MUSUVA [1], with the hoop strains at a particular strain gauge falling to zero as the pressure pad passes it. In backward extrusion, on the other hand, tensile hoop strains were recorded along the full container length even after the billet was fully extruded, except for a short discard. This is a clear indication that the outside diameter of the extruded can is larger than the bore diameter of the depressurised container, a fact well known in practice. The resultant pressure on the container wall produces friction, which is in turn responsible for the often significant forces needed for the ejection of the extruded can. The present results indicate one possible way of predicting the ejection forces, an important practical aspect in the extrusion of engineering components.

Fig.4 and 5 show the hoop strains and wall pressures in forward and backward extrusion respectively, with the pressure pad in forward extrusion and the die in backward extrusion at 10 mm from their respective initial positions. The wall pressures are considerably smaller upstream ahead of the moving tool, which once more confirm the effect of friction along the container/billet interface.

CONCLUSIONS

By the simultaneous recording of loads at both ends of the deforming billet, information was obtained on the frictional forces at the billet/container interface in the forward extrusion of rods and in the backward extrusion of cans. In the latter process hoop strains indicate the presence of pressures between the container and the extruded can, which could form the basis of predicting the forces necessary for ejecting the extruded can from the container, an aspect of some practical significance. Wall hoop strains were smaller ahead of the moving tool than nearer to it, once more indicating the presence of significant frictional forces.

The results presented here form part of the work at present being carried out and aimed at predicting container wall pressures and friction under various extrusion conditions. It is hoped that the results will give a reasonable assessment of friction and that they will also provide basic data for the design of extrusion containers and ejection devices in conventional extrusion, and for the design of clamps in conventional extrusion.

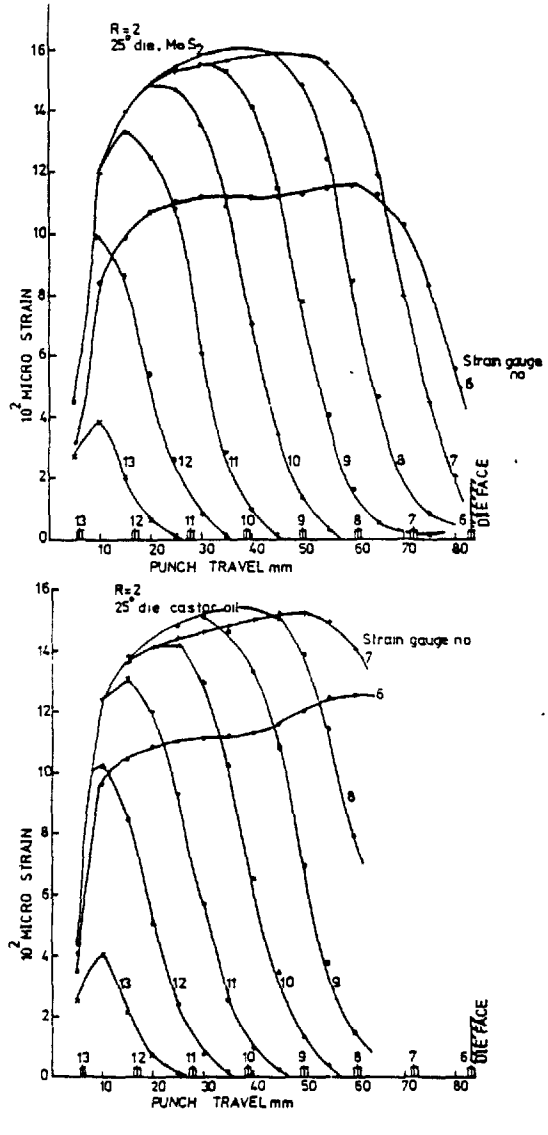


Fig.3a Hoop Strain Distribution in the Forward Extrusion of Aluminium

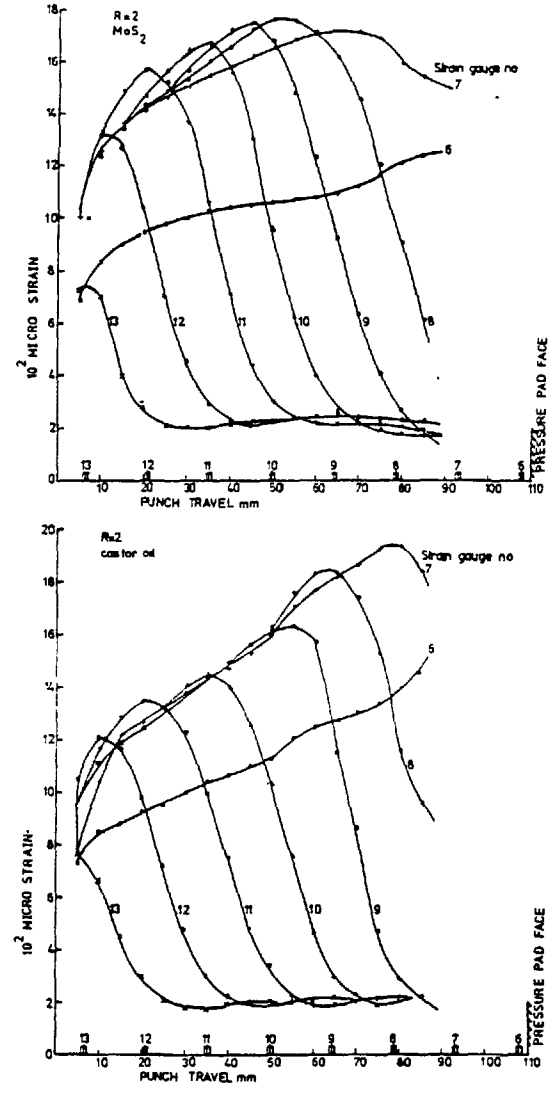


Fig.3b Hoop Strain Distribution in the Backward Extrusion of Aluminium

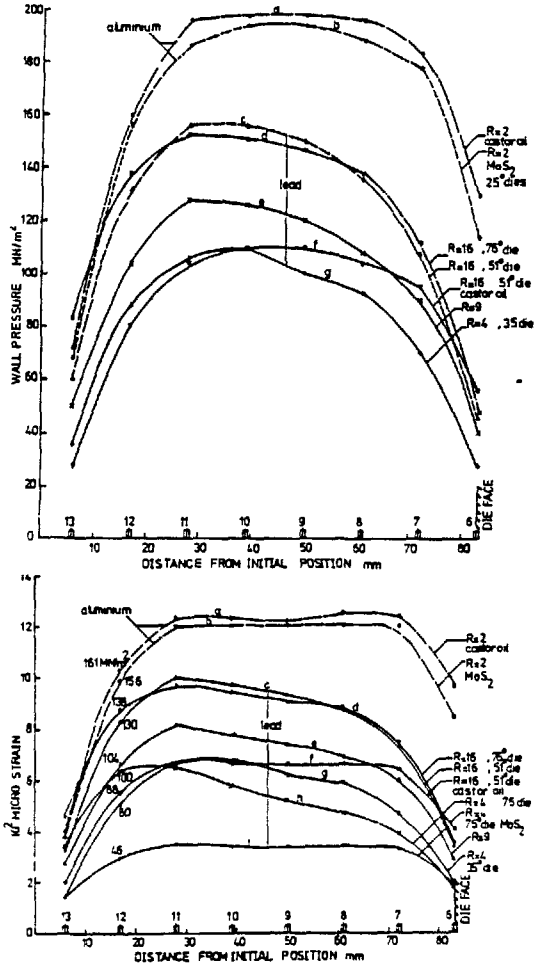


Fig.4 Hoop Strains and Approximate Pressure Distributions on the Container Wall in forward Extrusion

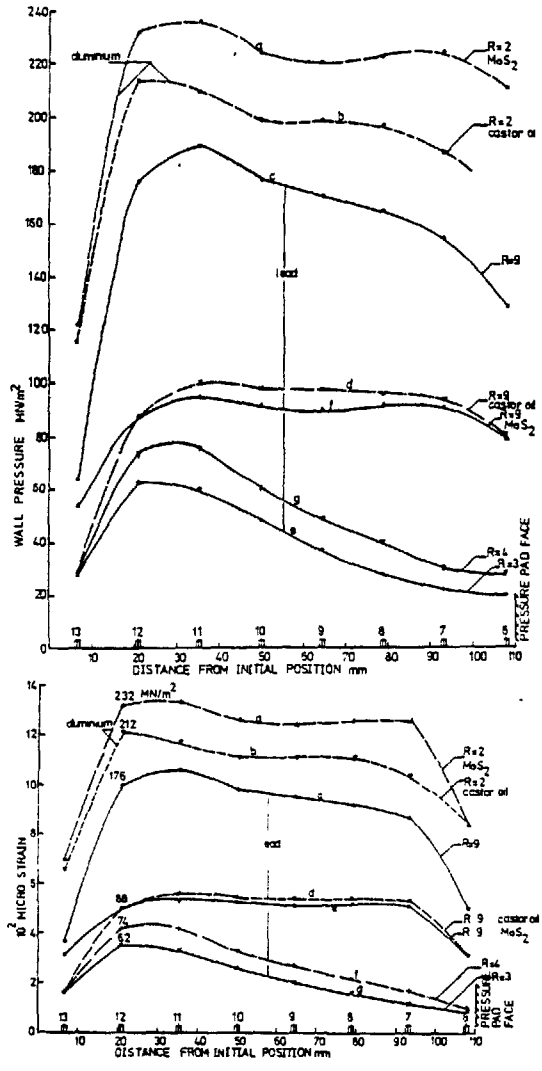


Fig.5 Hoop Strains and Approximate Pressure Distributions on the Container Wall in Backward Extrusion

REFERENCES

1. B. LENGYEL and J.K. MUSUVA (1976) Strain and Pressure Distribution in Extrusion Containers, Proc. 17th MTDR Conference.

2. B. LENGYEL (1968) A Semi-Continuous Hydrostatic Extrusion Process, Metals and Materials, January 1968.

3. J.M. ALEXANDER and M.E. SAID (1975) Design of Clamping Devices for Semi-Continuous Hydrostatic Extrusion, North American Metalworking Research Conference, May 1975.

4. B. LENGYEL and S. KAMYAB-TEHRANI (1976) Investigations into Continuous Extrusion, Proc. 17th MTDR Conference.

5. B. LENGYEL and P.G. ASHFORD (1967). An Experimental Pre-production Unit for Semi-Continuous Hydrostatic Extrusion. Proc. 8th MTDR Conference.

ACKNOWLEDGEMENTS

The authors thank Professor J.M. Alexander for the use of laboratory facilities and the technical staff of the laboratory for assistance in the manufacture of experimental equipment.